Thermophysical characterization of new absorbants based on ionic liquids for natural refrigerant, water

Pablo Breogan Sanchez Vazquez

Universidade Vigo

International Doctoral School

Pablo Breogán Sánchez Vázquez

DOCTORAL DISSERTATION

Thermophysical characterization of new absorbants based on ionic liquids for natural refrigerant, water

Directeur de thèse:

Dr. Josefa García Sánchez
Dr. Agilio A. H. Pádua

thèse soutenue le
16/11/2017

"International Mention"

Universidade Vigo

Universidade Vigo

International Doctoral School

Josefa García Sánchez, Agilio A. H. Pádua

DECLARES that the present work, entitled "Thermophysical characterization of new absorbants based on ionic liquids for natural refrigerant, water", submitted by Pablo Breogán Sánchez Vázquez to obtain the title of Doctor, was carried out under his supervision in the PhD programme "Programa de Doutoramento en Física Aplicada".

Vigo, 15th September 2017

The supervisors,

Dr. Josefa García Sánchez

Dr. Agilio A. H. Pádua

A Fina,
por su cariño y su confianza

Acknowledgements

Firstly, I would like to express my gratitude to my advisors Dr. Josefa García and Prof. Agilio Pádua for their continuous support and valuable advices along these years. It has been a pleasure working under their supervision.

I acknowledge all the entities that have provided financial support to develop this PhD thesis. The Ministerio de Economía y Competitividad (Spain) through the Plan de Investigación Científica y Técnica, the Xunta de Galicia (Spain) through the network REGALIS and the Ministère des Affaires Étrangères (France) through the Bourse d'Excellence Eiffel have contributed with their funds to this work.

I thank the coauthors of the articles included in this PhD, Dr. Josefa Salgado, Dr. María Villanueva and Dr. Juan José Parajó (Universidad de Santiago de Compostela), Dr. Moisés Rios, Dr. Marta Mato, Dr. Elisa González-Romero (Universidad de Vigo), Dr. Alain Dequidt and Dr. Mounir Traikia (Université Clermont-Auvergne), all of them are also contributors to this PhD.

To the people from the FA^2 group in Applied Physics Department of University of Vigo. It has been a pleasure working here during all this time, I have always felt very welcome and I enjoyed very much the time spent in this lab.

To the people from the TIM group in the Institute de Chimie de Clermont-Ferrand. During my stages in Clermont I met great people, we had nice discussions and shared good experiences. Je vous remercie!!

Finally, I would like to thank all the people I have shared my time with along this years. Family and friends, you have also very important to achieve this goal. Thanks for giving me the opportunity to move out from the lab and charge the batteries to keep going.

Contents

Chapter 1

Introduction

1.1 Environmental framework

From 1972, when the United Nation Conference on Human Environment took place in Stockholm[1], to the signature of the Paris Agreement within the United Nations Framework Convention on Climate Change[2] where 195 countries agreed to reduce their emissions of greenhouse gases, many things have changed in our perception of environmental issues. Concerns about the impact of human activities on climate changes have grown exponentially together with the findings of scientific evidence in this direction (figure 1.1). Once the threat is identified, measures need to be taken to reduce emissions of greenhouse gases.

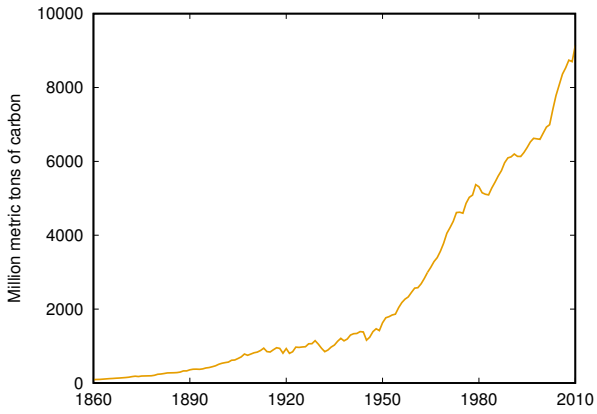

Figure 1.1: Evolution of carbon emissions worldwide from 1860 to 2010. Source. U.S. Department of Energy[3]

In figure 1.2, emissions are broken down by economic sector. This classification of the most pollutant economic activities elaborated by the International Panel On Climate Change (IPCC), provides also information about the sector with higher potential for reductions.

In this context, the development of clean technologies with the ability to substitute to some extent the processes with a high impact on carbon emissions becomes a priority for all the actors engaged in environmental issues. Thus, both the industrial budget and public resources to fund research related to green technologies have increased over the last years. One of the projects financed by the Spanish government is *Development of New Working Fluids, Components and Configurations for High Performance Absorption Heat Pumps-AHP2* in which this *PhD* thesis is included.

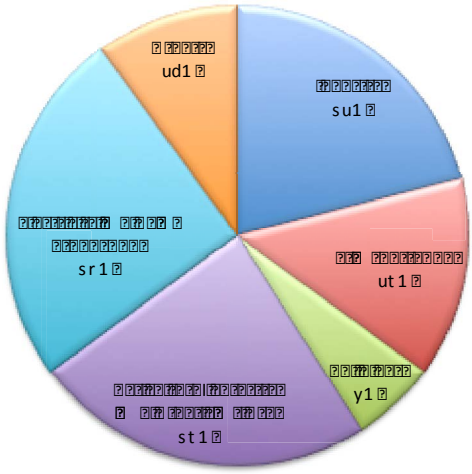

Figure 1.2: Evolution of carbon emissions. Source. IPCC[4]

1.2 Cooling/Heating technologies

Given that heat generation is responsible for an important part of the energy consumption and the cooling demands also largely contributes to energy consumption in industrial and domestic sectors[5], companies and public administrations[6] efforts are focused on the development of technologies leading to a reduction of their carbon print.

A scheme with the *Best Available Technologies* (BATs) for heat and cold production is shown in figure 1.3. Technologies are classified regarding their thermal output (heat or cold).

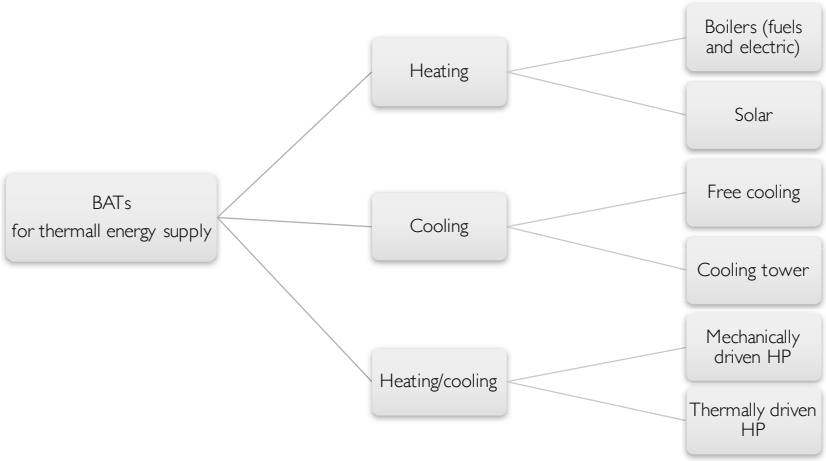

Figure 1.3: Scheme of technologies to produce thermal energy in industry and domestic sectors.

Among the systems to produce heat, we can distinguish between those using boilers and those using solar collectors where heat is transferred to a fluid which distributes it to the demanding point.

- Boilers. In electric boilers hot water is produced directly from electricity. Current passing

through an electrical resistance according to Joule's effect. Main advantage of electric boilers is that they allow producing heat when there is an excess on energy production, mainly due to production peaks due to favorable atmospheric conditions, such as windy days which give rise to large production in wind turbines. However, the use of electric boilers is not recommended when energy sources are fossil fuels since the efficiency of the global process would decay strongly. On the other hand, boilers using fuel vary depending on the source used, from the most pollutant such as coal to the most environmentally friendly such as biomass. However, all of them operate according to the same principle, conversion of the combustion enthalpy of the fuel to produce either hot water steam. Boilers are a mature technology largely use either in domestic or industrial sectors.

- Solar heating. Solar heating systems use solar collectors and a liquid handling unit to transfer heat to the load generally by using storage[5]. Depending on the energy final use, additional heat generation capacity may be needed. This additional heat can be obtained by boilers or by combined heat and power plants. Solar heating represents an environmentally attractive technology, however, systems should be properly dimensioned together with a suitable storage system to ensure heating demands are reached, no matter what the climate conditions are.

As indicated in scheme 1.3, cooling systems are mainly based on the use of natural sources of water and therefore, they are subjected to the availability of water close to the point of cooling demand.

- Ground water cooling. Ground water (or seawater) can be a source to supply cooling demands when the required temperature is above ambient temperatures. The capacity of this technology will depend on the ground water conditions. Energy inputs will be only the consume of the circulation pumps, so it can be considered CO_2-free.

- Cooling tower. Cooling towers uses the wet bulb principle to reduce the temperature of water letting air pass trough the water volume. The partial evaporation of the water volume leads to the reduction of the temperature of the liquid volume.

In a third group, we have heat pumps (HPs). Regardless of their energy source, HPs have the capability of providing heat and cold. HPs are more sophisticated than the technologies already described, and nowadays we can find them in an enormous number of applications.

- Mechanically driven HP. Heat pumps are thermodynamic devices with the capability of providing alternatively heat or cold. Their massive implementation for industrial or domestic uses is related to their versatility. HPs draw heat from a point and take it to a different one using a closed thermodynamic cycle. When they are mechanically driven, a key stage takes place in the compressor, where an electrically driven compressor rises the pressure of the heat transfer fluid. The main drawback of this technology is related with its intensive consumption of electric energy. Since its production demands a large amount of fossil fuels the net emissions of these devices are still important, mainly when we compare it with an alternative technology, such as absorption heat pumps (AHPs).

- Thermally driven HP. Heat pumps are, in general, less pollutant than systems based on the combustion of fuels. However, since mechanical heat pumps are driven by electric power, the resources and the emissions in production of the electric power should be included in the environmental impact of this technology.

1.3 Application: Absorption heat pumps

AHPs are today a mature technology[7, 8, 9] that may reduce the environmental impact of standard systems since they allow using thermal energy coming from residual heat currents or renewable sources to produce useful heat/cold. Main difference with traditional heat pumps is that AHPs are driven by thermal energy instead of using electric power, as it is shown in figure 1.4.

In AHP, the mechanical compression of the refrigerant, responsible of the large consumption of electric energy, is substituted by an absorption/desorption process, where the pressure of the absorbent is risen by *chemical compression*, since the large reduction in the specific volume makes the compression in liquid phase more affordable from the energetic point of view. However, this makes absorption systems more complex from the physico chemical point of view. Some of these issues will be addressed in the next section.

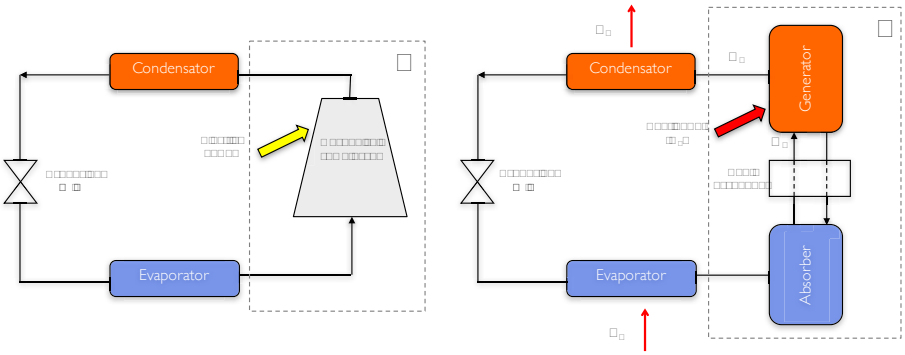

Figure 1.4: Scheme of a standard heat pump (a) and an absorption heat pump (b)

We can observe in figure 1.4 how both mechanical and absorption systems share three stages of the thermodynamic cycle. In the condenser, the refrigerant at high pressure is liquified releasing heat (Q_1) to the environment. Then the pressure decreases in the expansion valve, in the next stage the *useful cold* is produced by the evaporation of the refrigerant at low pressure where heat is *withdrawn* from the chilled room (Q_2). Until this step, both systems (see 1.4a and 1.4b) undergo the same stages. Then, in an standard HP the pressure of the refrigerant is risen by a mechanical compressor driven by electric power. On the other side, in an AHP, the refrigerant at low pressure and temperature changes to the liquid phase undergoing an absorption process (absorber). Then the mixture refrigerant/absorbent is pumped to increase its pressure. Normally a heat exchanger is used to pre-heat the rich mixture with the poor mixture coming from the generator, thus reducing the thermal energy demanded by the generator to separate the refrigerant from the absorbent and starting back the described cycle. Even though different configurations are possible[9], we refer to a simple cycle to introduce the main parameters to measure the performance of the heat pump.

First, the coefficient of performance (COP) provides the ratio between the useful heat (Q_2) exchanged in the evaporator and the heat used in the generator (Q_0) to separate absorbent and refrigerant. It is a measurement of the efficiency of the process, the higher COP is, the better will be its performance.

$$COP = \frac{Q_2}{Q_0} \tag{1.1}$$

Besides the COP, another key parameter to analyze the performance of the system is the circulation ratio, f. The circulation ratio is defined by the ratio between the mass of vapor

refrigerant produced in the generator and the mass of solution coming from the absorber [10], as indicated in equation 1.2.

$$f = \frac{m_w}{m_r} = \frac{w_r}{w_r - w_p} = \frac{w_r}{\Delta w}[10] \tag{1.2}$$

where m_r and m_p are the mass flows of rich (generator current out) and poor solutions (generator current in) and w_r and w_p are the respective mass fractions of those currents. High circulation ratios lead in general to low COP and so, they lead absorption systems towards poorer performances.

1.4 Target properties for the absorption process

To reach the requirements of the absorption-desorption potential working pairs (absorbent/refrigerant) should accomplish some properties to ensure that absorption and regeneration of the absorbent take place in such an extent that the whole process is reliable from the scientific and the economic points of view. These properties are listed below.

Absorption capacity. The absorption capacity of a given working pair is not a straightforward quantity. Since several factors influence that capacity, we will address here some of them. Absorption is an exothermic process, a heat sink (environment) is used to remove heat from the absorber, so large mixing enthalpies are not desirable. Besides that, liquefying the refrigerant requires that the absorbent is provided an at suitable vapor pressure depression[11]. A measurement of the suitability of the absorbent is given by the deviation from Raoult's law. A negative deviation indicate a decrease in the vapor pressure of the mixture and therefore an affinity of the refrigerant to be absorbed.

Transport properties. Heat and mass transfer of the refrigerant/absorbent mixtures are crucial for a good performance of the AHP. The absorption of the refrigerant requires a good molecular mobility of the components of the mixtures, thus low viscosities are required to ensure that. In an analogous way, diffusion coefficients provide very useful information about the mobility of each molecule in solution allowing to analyse the factors determining the dynamics of the whole system, also given by viscosity. Since viscosity undergoes an exponential decay with temperature and also decrease as the concentration of molecular solvents becomes higher, a critical issue is finding mixtures with low viscosity for high concentrations of the absorbent at low temperatures, the most unfavourable conditions for a suitable fluidity of the mixtures. In addition, low viscosities are also important to reduce the pumping costs.

Relative volatility. Once the absorption of the refrigerant has taken place and the solution has been pumped to a high pressure, both components need to be regenerated. This step is done in the generator by supplying thermal energy. So, a high relative volatility is needed in order to *distillate* the absorbant with minimal energetic and operational cost. When this is not achieved the installation of a rectification step may be necessary, as in the case of ammonia/water systems. This leads to an increase of the operational complexity and cost of the whole process.

Liquid range. The liquid range will determine the upper and lower limits of the operating temperatures. While in the absorber the problems are mainly related with the solidification of the mixtures, the maximum temperature that may be reached in the generator will be determined by the degradation temperature. To avoid crystallization or degradation, working pairs are expected to have a wide liquid range. This will also increase the versatility of the AHP, allowing the use of several steps[12] with the subsequent rise in the COP.

1.5 Commercially available working pairs

Given the requirements of the absorption process, the selection of refrigerant/absorbent working pairs becomes a problematic task. The current working pairs used in commercial equipment provide useful information on the properties sought for working pairs who may lead to more efficient systems.

Ammonia/water, NH_3/H_2O, is one of the working pairs implemented in commercial systems. One of its pros is the chemical stability of the mixture in a wide range of temperature and pressure conditions. Besides that, NH_3/H_2O is a cost efficient alternative[13]. On the other hand, due to the low relative volatility of the mixture a rectification stage is often required. It leads to an increase in thermal energy demands and thus, it reduces the efficiency of the process. Furthermore, the high operation pressure represent a drawback from the operational and economic points of view. Finally, the toxicity and the corrosive action on copper alloys is also a barrier for systems based on this working pair[13]. Physical and chemical properties of NH_3 and H_2O mixtures have been thoroughly studied and the reader is referred to those sources for further details[14, 15]

Water/lithium bromide, H_2O/LiBr, is also used in commercial absorption heat pumps. Among the advantages of this system are its chemical stability, low toxicity and environmental impact and economic feasibility. However, the low vapour pressure of water requires vacuum vessels[11] leading to an increase in the operating cost. Also, H_2O/LiBr mixtures present a significant corrosion capacity, specially at high LiBr concentrations and high temperatures. Since several characteristics of H_2O/LiBr are similar to potential H_2O/IL, a comparison between systems becomes pertinent. The lower temperature limit of application will be determined by the freezing temperature of water. However, crystalization problems in the absorber may take place if conditions of refrigerant/absorbent go below the freezing temperature. Vapour pressure of the absorbent is negligible and so, no rectification stage is needed. Viscosity should be kept as low as possible in order to reduce pumping costs and allow a suitable mass and heat transfer. This has been achieved by H_2O/LiBr systems but remains an open question for IL based working pairs. Regarding the absorption capacity, a measurement of its extent is the reduction in vapour pressure of the refrigerant during the absorption process. As it happens for H_2O/LiBr, large negative deviations from Raoult's law are sought for potential absorbents. Among the current commercial systems, the working pair water/LiBr is the one that gives rise to the highest energetic and economic efficiency using simple, well-engineered, and relatively compact systems[11]. Properties of H_2O/LiBr mixtures have been broadly studied[16, 17, 11].

A summary of the pros and cons of the commercial working pairs previously described is presented in table 1.1.

1.6 Role of ionic liquids in absorption heat pumps

Given the limitations of the current commercial systems, alternative working pairs with the capability of improving the performance of the available systems are searched. Among these alternatives, ionic liquids (ILs) are one of the most promising, namely using water as refrigerant.

ILs are often defined as salts melting under 100 $\circ$C [18, 19]. Over the last years they have atracted great interest from the scientific community due to their numerous potential applications[20, 21]. Their chemical structures, large and asymmetric ions, lead to very particular properties[18, 19]. Since there is a huge number of anions and cations, the massive number of possible combinations make the *tuning* of properties a remarkable characteristic of those fluids, as much as the complexity of the interactions governing their thermodynamic behaviour.

	+	−
	Wide range of T and P	Rectification stage (low relative volatility)
NH_3/H_2O	Economic feasibility	High working pressures required
		Toxicity and flammability
	Negative deviation from Raoult's law	Crystallization in the absorber
H_2O/LiBr	Good dynamics	Vacuum vessels required.
	Chemical stability of the mixture	Corrosion (mainly at high T)

Table 1.1: Pros and cons of commercially available working pairs for absorption heat pumps

Regarding their role as potential absorbents, there are mainly three issues to go through[22]. First, to ensure no crystalization[23, 24] in the absorber or degradation in the generator[25], a suitable potential absorbent must be selected. Second, ILs often present slow dynamics[26]. A detailed analysis of the factors influencing heat, mass and momentum transfer is required to reduce the effect of slow dynamics on the absorption process. Third, the absorption capacity will depend strongly on the chemical structure of the IL, so energetic quantities[27] of the refrigerant solvation into the absorbent and its solvation environment will play a key role in order to choose the chemical structures that better accomplish the process requirements.

Since a low vapor pressure [18] is a property shared by all ILs, the separation of refrigerant/absorbent in the generator will not represent a problem to overcome when using this sort of fluids.

1.7 State of the art

The role of ILs as absorbents in heat pumps has been addressed by different research groups over the last years from different points of view. Given that physical chemistry of ILs and their binary mixtures with water presents a significant complexity, experimental determination of key properties for water absorption needs to be complemented with theoretical studies. On one hand, the determination of physico chemical properties is required in order to investigate the systems that fit best with the process requirements, but on the other hand, studies at atomistic scale allow to understand the features in the chemical structure of ILs that lead to the target properties and also to understand and quantify how these features affect the systems behavior. Furthermore, on the side of the process simulation, important effort have been done to test the efficiency of different H_2O/IL working pairs. These simulations are based on the measured properties and also in correlation equations, so the results are strongly influenced by the quality of these data.

Wasserscheid and coworkers have published an extensive screening of ILs to be used as water absorbents[22]. According to this work, the suitability of the absorbent is based on its thermal stability, the vapor pressure of water in H_2O + IL solutions and their viscosities. Experimental procedures and target values are given for each one of three properties.

The thermal stability of ILs is addressed in a comprehensive way by Maton and coworkers[25]. Since there is no univocal definition for the thermal degradation temperature, a particular criterion should be established for each given process. Given that absorbents remain into the cycle for long periods of time, restrictive criterion is advised. Therefore, isothermal analysis are strongly recommended [28, 25, 29, 22] in order to provide a reasonable value for the upper limit of the liquid range. In any case, results should be taken with care since timescales and conditions of the actual absorption cycles are not fully represented during the experimental determination of the degradation temperature.

Dynamics of ILs and their mixtures with water have been studied during the last years. Experimental determination of viscosity[30, 26, 31] and diffusion coefficients[32, 33, 34, 35] have been used to generate a large amount of useful information. At the same time, knowledge about the role of impurities, the effect of temperature and water concentration has been improved. In addition, empirical[36, 37] and semi-empirical[38, 39, 40] models have been used to widen the temperature and pressure ranges and also to extrapolate out of the measurement conditions. Besides, atomistic models have provided interesting insights on the relationship between the chemical structure of the ILs and their slow dynamics, including the effect of the water concentration[41]. To achieve an accurate description of the dynamic behavior of ILs in molecular simulations two approaches have been followed, either ion charges are scaled[42, 43] by a factor between 0.7 and 0.9 or polarizable models are used[44, 45, 46]. Calculation of dynamic properties requires that trajectories have reached the diffusive regime[47].

The equilibrium properties of H_2O + IL solutions has also been studied. Some of these properties are critical to estimate the absorption capacity of ILs. Namely, activity coefficients[48] or vapor pressure of water in H_2O + IL mixtures[22] have been experimentally determined. Also, theoretical models provide very interesting information about the water affinity of the ILs. Kurnia et coworkers[49] have published an screening of the absorption capacity of a large number of ILs using COSMO-RS. Atomistic models also provide interesting results, often using free energy perturbation (FEP) as in Maginn et coworkers[27].

Data obtained from experimental measurements and correlation equations have been used to simulate the performance of the whole process. Commercial software and tools developed for this particular application have shown promising results[50, 51, 52, 53, 10]. However, further effort needs to be done to achieve better performances in H_2O/IL that of commercial H_2O/LiBr.

Very scarce publications regarding the performance of absorption heat pumps at industrial scale have been found. To the best of our knowledge only Wasserscheid and Seiler[54] have published an article describing the performance of a commercial system.

Chapter 2

Aims and scope

2.1 Framework of this PhD thesis

This PhD project was carried out within the project entitled *Development of New Working Fluids, Components and Configurations for High Performance Absorption Heat Pumps*. Its title provides a short description of the general objective. However, a better understanding is given by the following paragraph, part of the project summary, *development of new working fluids and components for absorption heat pumps and refrigeration systems to enlarge the operation range, improve the performance and increase the energy efficiency in new configurations. The new working fluids to be developed are mixtures of ionic liquids with natural refrigerants, like ammonia, CO_2 and water.*

The development of the project required the joint action of three research groups with different scientific backgrounds. The fields of expertise of these teams cover the areas of knowledge required for the design of working pairs for absorption heat pumps. In figure 2.1, an the knowledge areas of the groups are shown.

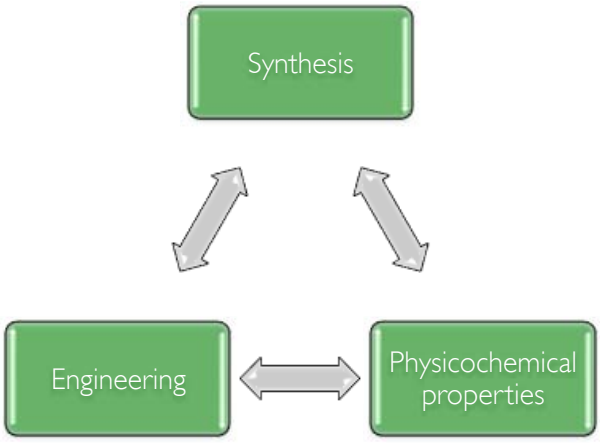

Figure 2.1: Research groups involved in the project

- The Organic Chemistry Group of the University of Vigo (Pontevedra, Spain) synthetized the ionic liquids and proposed new structures based on the physical properties and on engineering criteria for absorption systems. When the amount of ionic liquid required exceeded the synthesis capacity of the laboratory, the ionic liquids were supplied by a well-reputated company.

- The Mechanical engineering group, of University Rovira i Virgili (Tarragona, Spain) studied with the absorption of natural refrigerants into the ILs and carried out the engineering tests of the working pairs providing feedback based on these results to the other groups. Moreover, they were responsible of the project coordination.
- The Applied Physics group (FA2), in University of Vigo (Pontevedra, Spain), where I worked for my *PhD thesis*, was responsible for the identification and analysis of the key properties for the absorption of the refrigerants. Experimental and theoretical studies were performed in collaboration with other groups to find ILs meeting the application requirements.

In the sequence of successful collaborations between FA2 group and Thermodynamique et Interactions Moléculaires (TIM) group at Université Clermont-Auvergne (Clermont-Ferrand, France) that led to the joint supervision of a previous thesis, this PhD was also carried out under the cosupervision of Dr. Josefa García and Professor Agilio Pádua. Besides the funds from the aforementioned project, this work has also obtained financial support from the Ministère des Affaires Étrangères Française through a Bourse d'Excellence du Programme Eiffel. Regarding technical aspects, experimental tasks of the PhD were mainly carried out in the laboratories of the FA2 group while molecular simulation studies were performed in collaboration with the TIM group under the supervision of Prof. Pádua.

Other collaborations, which led to articles that are part of this PhD, took place with the Thermophysical Properties of the Fluids and Biomaterials Group in University of Santiago de Compostela (Santiago de Compostela, Spain) Group and with the Analitycal Chemistry Department of University of Vigo (Pontevedra, Spain).

This thesis is a co-supervision between Spanish and French Universities/Doctoral Schools, leading to the award of a doctoral degree from both institutions, under the auspices of a joint protocol.

2.2 Objectives

This PhD Thesis is focused on the thermophysical characterization of ILs and ILs/H_2O mixtures. With this aim, different structures have been studied and the results published in the articles that are part of this work. In table 2.1, we show the general information about the analysed ILs. Further information and the properties studied for each IL can be found in the articles.

The design of suitable absorbents is a critical step to develop efficient absorption heat pumps and it should be done based on the requirements of the application. The feasibility of the working pair H_2O/IL will be determined by the properties of the mixtures. Therefore, the general objectives of this work are:

1. Definition of the key properties for the absorption process and selection of the experimental and modelling methods to determine and study this properties.
2. Implementation of experimental and theoretical techniques to study potential candidates for absorbents in systems using water as refrigerant.
3. Analysis of the relationship between the structure of the ILs and the previously selected thermophysical properties.
4. Definition of the molecular structures of the absorbent anions leading to suitable properties for absorption heat pumps using water as refrigerant.

Ionic liquid	Abbreviature	CAS number
1-Ethylpyridinium bis (trifluoromethylsulfonyl) imide	$[C_2Py][NTf_2]$	712354-97-7
Choline bis (trifluoromethylsulfonyl) imide	$[Chol][NTf_2]$	827027-25-8
1-Ethyl-3-methylimidazolium triflate	$[C_1C_1Im][OTf]$	145022-44-2
1-Ethyl-3-methylimidazolium bis (perfluoromethylsulfonyl) imide	$[C_1C_1Im][BETI]$	216299-76-2
1-Ethylpyridinium methanesulfonate	$[C_2Py][MeSO_3]$	681481-41-4
1-Ethylpyridinium triflate	$[C_2Py][OTf]$	3878-80-6
Choline dihydrogen phosphate	$[Chol][H_2PO_4]$	83846-92-8
1-Ethylpyridinium dicyanamide	$[C_2Py][DCA]$	-
1-Ethylpyridinium acetate	$[C_2Py][Ac]$	-
Choline methanesulfonate	$[Chol][MeSO_3]$	-
Choline dicyanamide	[Chol][DCA]	-
Choline acetate	[Chol][Ac]	14586-35-7

Table 2.1: Ionic liquids studied in this PhD thesis

To achieve the general objectives, specific goals have been described in the research plan we have developed during the course of the PhD based on the initial research plan and the results obtained. These specific goals can be sumarized as follows:

(i) Application of different experimental techniques for a suitable characterisation of the samples. The main parameters to determine are water content and concentration of non-volatile compounds.

(ii) Experimental determination through different techniques of density, viscosity and electrical conductivity of pure ILs and binary systems IL/water.

(iii) Application of equations with empirical and theoretical basis to correlate and predict the measured experimental properties for the absorption process.

(iv) Exploring the potential of atomistic molecular dynamics to predict dynamic properties of binary systems IL/water systems minimizing the amount of experimental information required.

(v) Determination of the energetic quantities related to water solvation into the IL using atomistic molecular dynamics.

(vi) Exploring the influence of cations, anions and different alkyl chains and functional groups in the behaviour of the IL/H_2O mixtures through molecular dynamics, the role of hydrogen bonds being studied in detail.

2.3 Common background of the publications

This PhD thesis is written as a compilation of five articles already published in scientific journals indexed in the *Journal Citation Report (JCR)*.

All the articles deal with the study of physical properties of ILs with the aim of selecting potential absorbents using water as refrigerant. This is the common background of the five articles. However, they address this topic from different points of view that cover the general objectives

and the specific goals of this PhD. A short summary describing the aim of each publication is given in the following paragraphs.

- *Liquid range temperature of ionic liquids as potential working fluids for absorption heat pumps.* To determine the liquid range of six ionic liquids, DSC and TGA techniques have been used. Lower limits, given by liquid-solid state transitions, show a large dispersion depending on the ions involved and it is difficult to establish a pattern depending on ILs structure. For the upper limit, dynamic and isothermal modes were used, a conservative criterion was assumed to define the temperature of thermal degradation. Results do not consider chemical or mechanical effects. It was found that the choice of anion is the dominant effect compared to choice of cation in defining the liquid range.

- *Density and viscosity study of pyridinium based ionic liquids as potential absorbents for natural refrigerants: Experimental and modelling.* Two ionic liquids, $[C_2Py][NTf_2]$ and $[C_2Py][OTf]$, are studied. Density and viscosity are experimentally determined for pure systems, and also for $[C_2Py][OTf] + H_2O$ mixtures in the full range of concentrations. The data obtained were successfully correlated as a function of temperature. Furthermore, semitheoretical models were applied to predict density and viscosity outside of the measurement range. The models PC-SAFT and Hard-Sphere (HS) theory were used for density and viscosity respectively.

- *Studies of Volumetric and Transport Properties of Ionic Liquid-Water Mixtures and Its Viability To Be Used in Absorption Systems.* Density, viscosity and electrical conductivity of two ionic liquids, $[C_2Py][MeSO_3]$ and $[Chol][H_2PO_4]$, were measured. Given their melting points (both of them are solid at room temperature) only mixtures with water were studied. The effect of water concentration and temperature were investigated and correlation equations were applied. The non-volatile impurities were determined by HPLC.

- *Molecular Understanding of Pyridinium Ionic Liquids as Absorbents with Water as Refrigerant for Use in Heat Pumps.* The potential of atomistic molecular dynamics to describe dynamics and energetics quantities of two ILs, $[C_2Py][NTf_2]$ and $[C_2Py][OTf]$ and their mixtures with water was explored. Atomistic models were validated against experimental density data. Then, diffusion and viscosity were simulated, and these results qualitatively agree with experimental measurements. The Gibbs free energy of water solvation in the ILs was also simulated using free energy perturbation methods. Spatial distribution in solvation shells at molecular scale was studied and its relationship with the calculated properties was analysed.

- *Structural effects on dynamic and energetic properties of mixtures of ionic liquids and water.* Dynamic and energetic quantities of six ionic liquids and their mixtures with water were studied using molecular dynamics. Two cations, $[C_2Py]^+$ and $[Chol]^+$, and three anions $[MeSO_3]^-$, $[DCA]^-$ and $[Ac]^-$ were combined. Hydrogen bonding was quantified for all systems and its effect over the solvation of water into the ILs was shown. Also the interaction energies between ions and water were computed and the structural effects on the simulated properties were studied.

Chapter 3

Methodology

3.1 Experimental

3.1.1 Sample preparation

In every experimental procedure, a suitable sample preparation is a basic requirement to ensure that the sample are fully characterised and therefore, the indetermination related errors in the sample composition are minimised. All the chemicals studied in this thesis are commercially available and suppliers provide data information. This information is thoroughly provided in the experimental section of the chapters of this PhD thesis. However, we have considered neccessary giving a more detailed description of the sample preparation since the effect of impurities has shown to have a large impact on the determination of the properties of ionic liquids and it has also been a topic of discussion in the scientific community[55].

ILs are well known as fluids with a extremely low but measurable[56] vapor pressure. So far, distillation appears as a suitable technique to eliminate any volatile component contaminating the samples. Prior to each measurement series, ILs were place in vacuum conditions during at least 24 hours. An scheme of the vacuum system is shown in Figure 3.1.

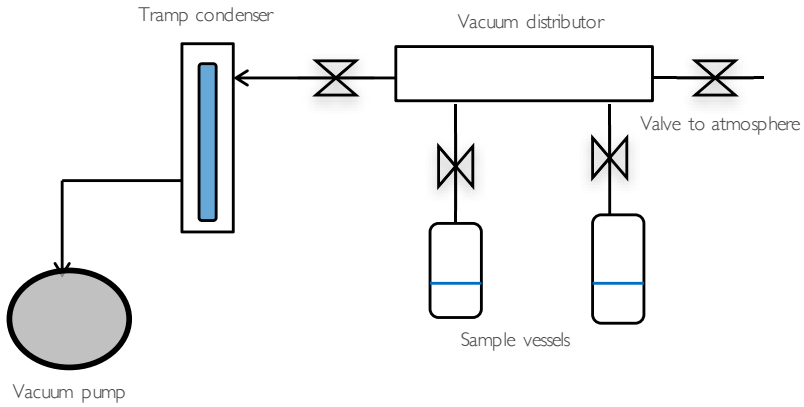

Figure 3.1: Scheme of a vacuum system used to remove volatile compounds from ILs.

During handling of the samples into the vacuum line an inert atmosphere of argon was set to ensure that the ILs did not absorb water from the atmosphere. To capture any volatile impurity and prevent the vacuum pump from damage, a trap condenser vessel with either liquid nitrogen

or solid carbon dioxide was used.

With the objective of determining the content of impurities two techniques were essayed. First, to determine the amount of water in the sample after the distillation in the vacuum line, Karl Fischer tritation (KF) was used. Its operation principle is based on the chemical reaction (equation 3.1) between water and the KF reagent (hydranal). The extent of this reaction produces an electric current between electrodes and its quantification provides the water content of the sample.

In this work, a KF titration DL32 METTLER TOLEDO was used. The determination of the water content was performed before and after the measurement to ensure that no water absorption took place during the measurement process.

$$H_2O + I_2 + SO_2 + CH_3OH + 3\,RN \longrightarrow [RNH]SO_4CH_3 + 2\,[RNH]I \tag{3.1}$$

No volatile impurities coming from the synthesis path are not removable with distillation techniques, however, its determination can be done through ionic chromatography (IC). IC, based on ion change separation, provides a detailed analysis of the ionic substances contained in a solution. An scheme of an ionic chromatographer is shown in figure 3.2. As indicated in figure 3.2, the solution (sample + eluent) is pumped through a column were ionic species have different retention times. An ionic detector placed after the separation column allows to compare the ionic conductivity with a blank reference, then the numerical treatment of these data provides an accurate quantification of the ionic impurities in the samples.

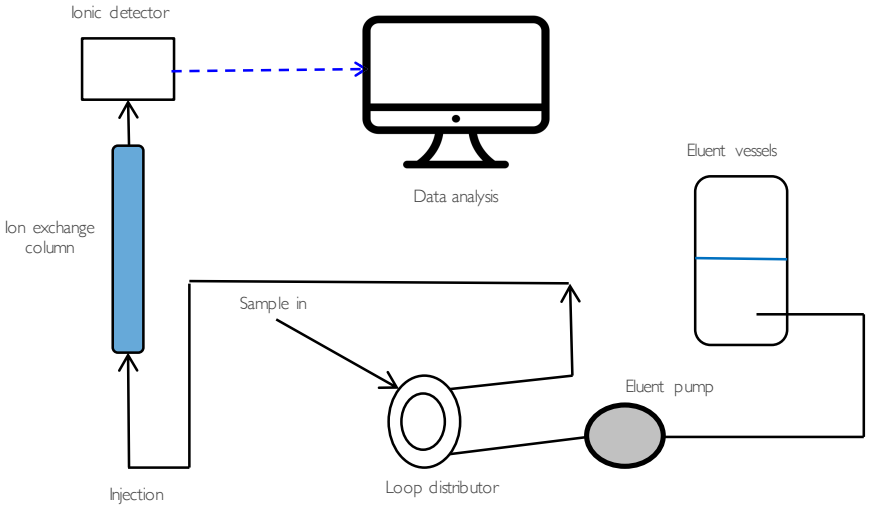

Figure 3.2: Scheme of an ionic chromatographer used to quantify ionic impurities.

IC was used in the article *Studies of Volumetric and Transport Properties of Ionic Liquid-Water Mixtures and Its Viability To Be Used in Absorption Systems* [57], part of this PhD thesis. The chromatographic system used (Metrohm) consists of a 792 Basic IC chromatograph equipped with a 20 μL loop Rheodyne injection valve, the column system, a 250 $\times$ 4 mm Metrosep A supp 4 (column packing of poly(vinyl alcohol) with quaternary ammonium groups and particle size of 9 μm), guard columns and filters. The program used to record the chromatographic data and Data Acquisition System was the 792 PC Software. System can be operated with chemical suppression mode with auto step when the loop sample is filled. As eluents, solutions of Na_2CO_3 and $NaHCO_3$ (standard flow 1 mL min^{-1} and pH 10), were used prepared, prior to its use, solutions were microfiltered and degassed.

3.1.2 Thermogravimetric analysis

Thermogravimetric analysis (TGA) is a technique allowing to study the effect of the temperature on the mass of a given substance. By measuring simultaneously mass and temperature, TGA provides information about the degradation temperature and also the time scale of the degradation process under the defined experimental conditions. Figure 3.3 shows an scheme of an standard thermogravimetric analyser. Its operation principle is well described by the simultaneous measuring systems, mass and temperature. Then collected data are analysed to obtain the degradation parameters of the sample.

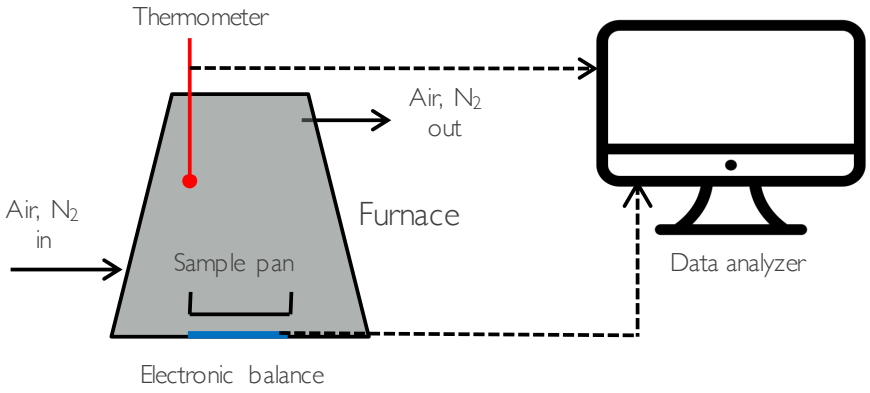

Figure 3.3: Scheme of an thermogravimetric analyser

A thermogravimetric analyser, TGA 7-Perkin Elmer[58] was used to determine the degradation temperatures of different ILs. It consists of an electrically driven ultramicrobalance whose precision is 0.1 μg. Since it undertakes high temperatures, building materials should be thermally stable. Mass measuring system is placed into an hermetically closed oven, reaching temperatures up to 900 °C. The highly resistive ceramic materials are coated with highly conductive metal in order to achieve an homogeneous temperature in short periods of time. Finally a thermocouple is also placed into the oven and, alike the mass detection system, connected to a data analyser provided with a software to collect the data. The thermogravimetric analyser allows to control the atmosphere during the measuring time. As purge gas, we used either N_2 or air, it is described in detail together with the flow rate and other experimental conditions in the article *Liquid range temperature of ionic liquids as potential working fluids for absorption heat pumps*[59].

TGA techniques have been widely applied to determine degradation temperature for different materials[60, 25]. In this PhD thesis, TGA techniques have used with the objective of establishing an upper limit for the liquid range, and thus for the operation temperature in the generator.

3.1.3 Differential Scanning Calorimeter

Differential scanning calorimetry (DSC) allows to study the response of a sample to a heat flow by comparing it with a well know pattern. Thus, thermal properties related to heat exchanges, such as heat capacity or state transition temperatures can be determined. Namely, DSC measures the differential effect that a certain amount of heat produces into the sample and a reference material[61]. Both systems, sample and reference are kept at the same temperature, thus, a control system (servo system) immediately increases the energy supplied to the sample or the reference material, depending on the process undertaken by the sample, either endothermic or

exothermic, scheme of a DSC device is given in figure 3.4. The record of the DSC curve is expressed in terms of heat flow versus temperature or time.

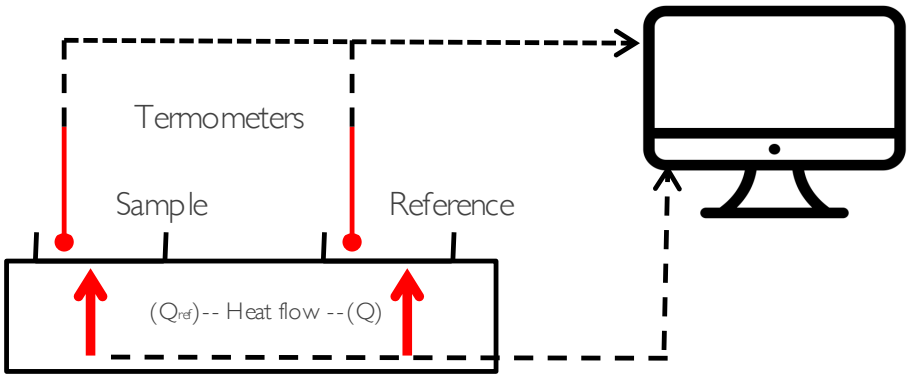

Figure 3.4: Scheme of a differential scanning calorimeter

Experiments were performed in a differential scanning calorimeter DSC Q100 TA-Instruments[62], with hermetically sealed aluminium pans and liquid nitrogen as coolant fluid. Temperature and heat calibration of this DSC was performed before to start the experiments. Indium was used to calibrate the DSC apparatus for all the subsequent parameters under the same experimental conditions than measurements.

So far, the main interest to use of DSC in this PhD in the determination of the low limit of the liquid range in IL that will be defined by the melting temperature (if the IL presents crystal structure) or glass transition (if only amorphous phase is presented).

3.1.4 Density

The ratio between mass and volume is a key property for process design and also for modelling other crucial properties for the water absorption, such as viscosity or free energy of solvation. Hereby, density determination of pure ionic liquids and their mixtures with water has been done using a vibrating tube densimeter. Its operation principle is based on the measurement of the resonant frequency of an oscillator filled with the testing fluid[63]. Oscillation is induced in the tube by two magnetic dynamic converters in connection with an electronic control and amplifier circuit which guarantees constant amplitude[64]. The relation between vibration period, τ, and density, ρ, is shown by equation 3.2.

$$\tau = 2\pi \left(\frac{m_0 + \rho V_0}{\kappa} \right)^{0.5} \tag{3.2}$$

where m_0 is the mass of the oscillator, V_0 is the volume of sample contained by the tube and κ is the elastic constant. Considering m_0 and V_0 are constant values for a given temperature, ρ would only be function of τ.

Figure 3.5 shows the main parts of an U-tube vibrating tube densimeter. According to the scheme, sample is introduced into the vibrating tube, assuring that no bubble air remains inside the tube. Thermostatic bath keeps the temperature in the setpoint, high conductivity materials should surround vibrating tube to quickly achieve an homogeneous temperature.

From equation 3.2, and isolating ρ we obtain equation 3.3 where the linear relationship between ρ and τ^2 allows to obtain the density once the calibration is done and constants A and B (equation 3.4) are calculated for the operation range.

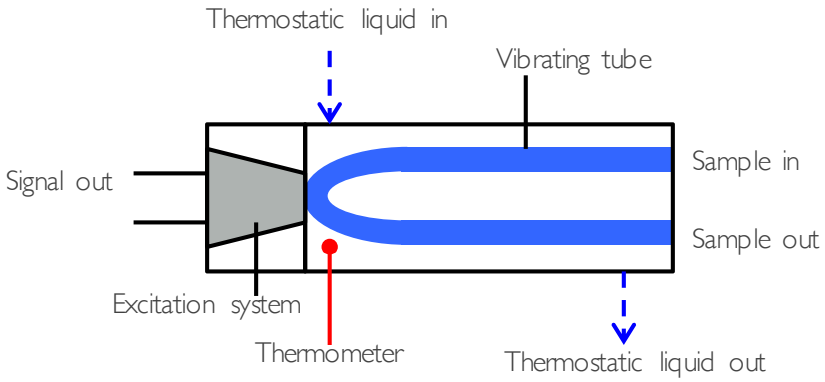

Figure 3.5: Scheme of a vibrating tube densimeter

$$\rho = \frac{\kappa}{4\pi^2 V_0}\tau^2 - \frac{m_0}{V_0} \tag{3.3}$$

$$A\,(T) = \frac{\kappa}{4\pi^2 V_0} \quad , \quad B\,(T) = \frac{m_0}{V_0} \tag{3.4}$$

In all cases calibration process was repeated before and after the measurement series to ensure that A and B remained constant.

Densities at atmospheric pressure were obtained with the DMA 4500 by Anton Paar and SVM 3000 Stabinger also by Anton Paar densimeters. Further details about experimental conditions can be found in the articles *Density and viscosity study of pyridinium based ionic liquids as potential absorbents for natural refrigerants: Experimental and modelling*[65] and *Studies of Volumetric and Transport Properties of Ionic Liquid-Water Mixtures and Its Viability To Be Used in Absorption Systems* [57].

3.1.5 Viscosity

Viscosity is a measurement of the internal friction of a fluid. As defined by Newton's law (equation 3.5) , the ratio between shear stress (τ_{xy}) and the shear rate (∂v_y / ∂x) allows to quantify this property. A caution must be taken, since this ratio only remains independent of the shear stress for the so-called Newtonian fluids. In this PhD thesis, two different techniques will be used to determine the viscosity of the studied systems: a rolling ball viscosimeter and a Stabinger.

$$\tau_{xy} = \eta\,\frac{\partial v_y}{\partial x} \tag{3.5}$$

Rolling ball viscosimeter is a sort of falling body device. In these apparatus viscosity is obtained from the free-fall time, in presence of gravity, of a solid body through the studied viscous fluid[64]. The working principle of these viscometers is based on Stoke's law. Thus, the motion of the solid body should be slow enough to ensure a laminar regime, and therefore neglect inertia effects. An analysis of the forces acting over the falling body, a ball in this particular case, allows to obtain the relation between the viscosity and the falling time in an straightforward way as indicated in eq. 3.6, where η is the viscosity, ρ_{ball} and ρ_{liq} the density of coating steal ball and the fluid respectively, t is the falling time and a and b are the calibrations constants.

$$\eta = a\left(\alpha, T\right) + \frac{b\left(\alpha, T\right)}{\rho_{ball} - \rho_{liq}} t \tag{3.6}$$

An scheme of an standard rolling bar viscosimeter is shown in figure 3.6. The glass capillary must be filled with the working fluid, for a suitable operation, we need to remove all bubbles air into the glass capillary. Once, this step is undertaken, the rolling ball is also placed into the capilar before socking it to the system. Then, we must let systems reach an homogeneous temperature, with that purpose a thermostatic bath is used. Once the set point is reached, the viscosimeter is ready to calculate the falling time between the light barriers that will be function of the inclination angle that has been previously selected.

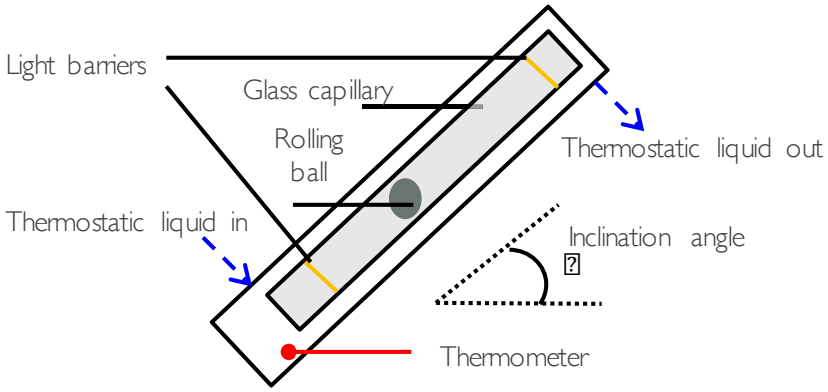

Figure 3.6: Scheme of a rolling ball viscosimeter

In work, an AMV 200 rolling ball viscosimeter (Anton Paar) was used. The calibration process is described in the experimental section of the article *Density and viscosity study of pyridinium based ionic liquids as potential absorbents for natural refrigerants: Experimental and modelling*[65]

Stabinger viscosimeter is based on a modification of the classic Couette type rotational viscosimeter. The idea behind its operation principle is the relation between the shear stress we need to apply to a body to make it rotate when it is sank into a fluid and its viscosity. As indicated by Newton's law, viscosity is the ratio between shear stress and shear rate. An scheme of the measurement cell can be found in figure 3.7. It consists of a rapidly rotating outer tube which contains the sample and an inner measuring bob rotating more slowly. The concentricity between outer tube and inner measurement rotor is ensured by the low density of the bob and the centrifugal forces created during rotation. Two different torques influence the speed of the measurement rotor: the driving torque, Td, and the retarding torque, Tr. A more detailed description can be found in the European Patent (EP 0 926 481 A2).

In work, a SVM 3000 Stabinger viscosimeter by Anton Paar was used. System also integrates a density measuring cell and a thermostatic bath working in a wide temperature range (268.15 to 378.15 K). Calibration need to be done using a well known fluid whose viscosity should be in the same order than the working fluid.

Viscosity measurements in the article *Studies of Volumetric and Transport Properties of Ionic Liquid-Water Mixtures and Its Viability To Be Used in Absorption Systems*[57] were done using a Stabinger.

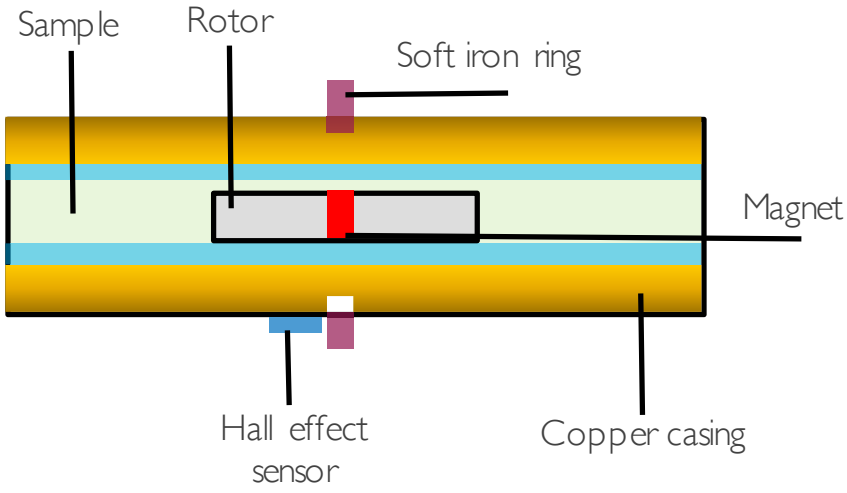

Figure 3.7: Scheme of a Stabinger cell

3.1.6 Diffusion coefficients

Self-diffusion (also referred as diffusion) of a given liquid is the random translation movement of the molecules in thermodynamic equilibria. The measurement of diffusion coefficients provides a comprehensive view of the factors influencing the dynamics of the systems studied in this PhD. The technique used to determine diffusion of ions and molecules was pulsed-field gradient spin-echo (PFGSE). Magnetic dipoles are oriented by magnetic pulses in time intervals of Δt. Displacement between pulses are correlated with the translational movement of each chemical entity. However, PFGSE technique registers molecular displacement without considering its causes, therefore it is very important to minimize the effect of the convection using directional gradients along each axis. Other undesirable factors such as heating by Joule's effect or the generation of Foucault's currents[66] during the measurement process should be kept under control. Further information about the experimental detail can be found somewhere else[67].

In this PhD diffusion some coefficients were determined using a Bruker Avance III HD 500 spectrometer operating at 500.13 MHz for 1H and 125.77 MHz for 13C, with a 5 mm pulsed-field z-gradient TXI probe. Experimental details can be found in *Molecular Understanding of Pyridinium Ionic Liquids as Absorbents with Water as Refrigerant for Use in Heat Pumps*[68].

3.1.7 Electrical conductivity

Electrical conductivity provides a measurement of the ability of a given material to let electric current pass through it. Conductivity of liquid solutions is mainly related with the concentration of ions and its mobility. In figure 3.8 a scheme of a conductivimeter is shown. According to the scheme, an external source produces a electrical potential between two electrodes, by measuring simultaneously this potential and the electric current induced the resistance of the solution can be easily obtained through Ohm's law. Since resistance is the reciprocal of conductance, it is only the geometry of the cell that allows to obtain the constant (G), obtained in the calibration process what will give the conductivity of the solution.3.7

$$\kappa = G \times K \tag{3.7}$$

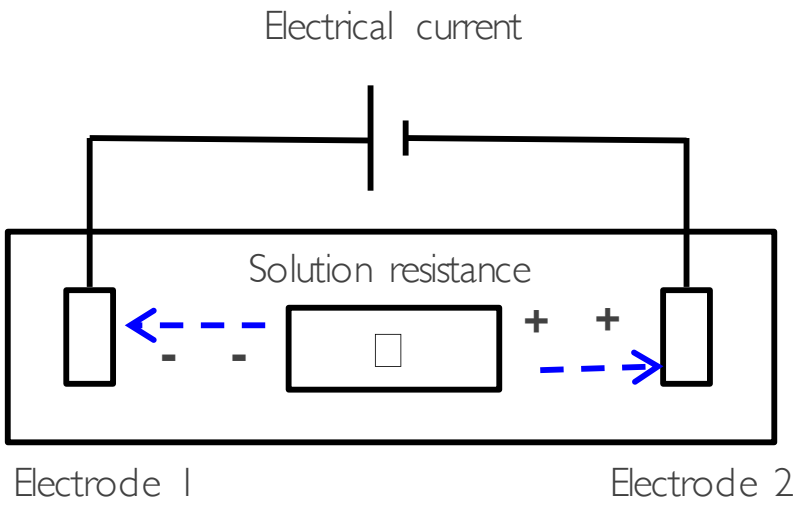

Figure 3.8: Scheme of a two electrodes conductivimeter

In this PhD thesis, the electrical conductivity was measured using a Crison CM35 conductivimeter. System is equipped with a thermometer, providing the two measurements simultaneously. Two platinum electrodes are placed into the samples. Crison Standard solutions were used for calibration proposes. Results and further details about the calibration process can be found in the article *Studies of Volumetric and Transport Properties of Ionic Liquid-Water Mixtures and Its Viability To Be Used in Absorption Systems*[57]

3.2 Modeling

3.2.1 PC-SAFT

Taking Wertheim's perturbation theory as starting point, Chapman and coworkers developed the Statistical Associated-Fluid Theory (SAFT). This equation of state (EoS) is the basis of different EoS which have been proven to be very successful describing the behavior of molecular fluids. Among SAFT based EoS, one of the most broadly used is the Perturbed Chain Statistical Associated-Fluid Theory (PC-SAFT). The main modification introduced by Gross and Sadowski[69] is the methodology used to calculate dispersive forces, since Helmholtz free energy is calculated using only the first and second terms of perturbation theory of Barker and Henderson.

According PC-SAFT model, molecules consist of a number of spheres joint together forming a chain. Potencial interaction function between spheres is described in equation 3.8[70].

$$u(r) = \begin{cases} \infty & r < (\sigma - s_1) \\ 3\epsilon & (\sigma - s_1) \leq r < \sigma \\ -\epsilon & \sigma \leq r < \lambda\sigma \\ 0 & r \geq \lambda\sigma \end{cases} \tag{3.8}$$

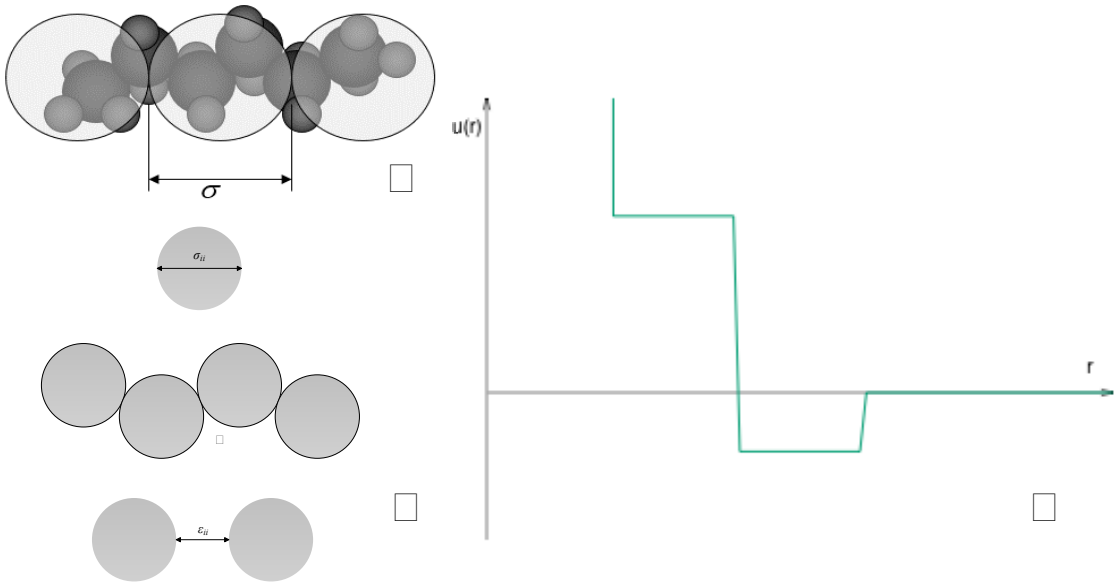

Figure 3.9: a) Scheme of a molecule modeled in PC-SAFT b) Spheres and interacting parameters od PC-SAFT c) Potential function between two spheres in PC-SAFT.

where r is the distance between two segments, σ is the temperature independent diameter, ϵ is depth of the potencial, λ is the reduced well width. A ratio of $S_1/\sigma = 0.12$ is asumed[70]. In figure 3.9, we can observe how the potencial function can be split into a repulsive and an attractive part.

According to Barker and Henderson perturbation theory soft repulsion terms can be modelled. Repulsive interactions are calculated using a reference fluid where no attractions are defined. The soft repulsion of molecules is described with a hard repulsion and a temperature dependent diameter defined in equation 3.9.

$$d\left(T\right) = \int_0^{\sigma} \left[1 - exp\left(-\frac{u\left(r\right)}{kT}\right)\right] dr \tag{3.9}$$

Integration of potencial function (eq. 3.8) leads to the hard segment diameter given by equation 3.10

$$d_i\left(T\right) = \sigma_i \left[1 - 0.12exp\left(-\frac{3\epsilon}{kT}\right)\right] \tag{3.10}$$

The complete EoS (eq. 3.12) is given by the ideal gas contribution, hard-chain contribution and the attractive interactions, given by the perturbation analysis.

$$Z = Z^{hc} + Z^{disp} + Z^{assoc} \tag{3.11}$$

Based on Wertheim's thermodynamic perturbation theory[71, 72, 73, 74], Chapman et coworkers [75, 76] developed an EoS (eq. 3.12 and 3.13) in which Z^{hc} can be obtained as a function of hard sphere properties and the number of segments comprised by each molecule.

$$Z^{hc} = \bar{m}Z^{hs} - \sum_i x_i \left(m_i - 1\right) \rho \frac{\partial ln\ g_{ii}^{hs}}{\partial \rho} \tag{3.12}$$

$$\bar{m} = \sum_i x_i m_i \tag{3.13}$$

where x_i is the mole fraction of chains of component i, m_i is the number of segments in a chain of component i, ρ is the density of the system and g_{ii}^{hs} is the radial pair distribution function for segments in the hard sphere system. Expressions used to calculate Z^{hs} and g^{hs} can be found in literature.[77, 78]

The attractive part of the chain interactions is calculated by the addittion of first and second term of the perturbation theory introduced into the reference state.Hereby, Helmholtz free energy is given by eq. 3.14

$$\frac{A^{disp}}{kTN} = \frac{A_1}{kTN} + \frac{A_2}{kTN} \tag{3.14}$$

Equations and procedure to calculate the terms A_1 and A_2 is presented by Gross and Sadowski[69].

3.2.2 Hard-Sphere Theory

Hard sphere (HS) theory attempts to model self-diffusion, viscosity and thermal conductivity. The method described by Assael[38, 79] has shown a very good capacity to correlate transport properties for different conditions of temperature and pressure and also to predict these properties out of the measuring range. For calculation convenience, HS theory uses reduced (adimensional) coefficients (eq. 3.15). The model accuracy is strongly dependent on the reduced volume, V/V_0, where V is the molar volume and V_0 the closed-packed molar volume, this extreme sensitivity is a key question for its application.

$$D^* = \left[\frac{\eta D_{SHS}}{\eta_0 D_0}\right]\left[\frac{V}{V_0}\right]^{2/3}, \quad \eta^* = \left[\frac{\eta_{SHS}}{\eta_0}\right]\left[\frac{V}{V_0}\right]^{2/3}, \quad \lambda^* = \left[\frac{\lambda_{SHS}}{\lambda_0}\right]\left[\frac{V}{V_0}\right]^{2/3} \tag{3.15}$$

The subscript SHS correspond to smooth hard-sphere coefficient (eq. 3.16), product of the value given by Enskog theory and the computed corrections calculated using molecular dynamics (MD).

$$D_{SHS} = D_E\,(D/D_E)_{MD}, \quad \eta_{SHS} = \eta_E\,(\eta/\eta_E)_{MD}, \quad \lambda_{SHS} = \lambda_E\,(\lambda/\lambda_E)_{MD} \tag{3.16}$$

Reduced coefficients for each transport property depend on the reduced volumes (see equation 3.15), that can be calculated by computational methods, however the uncertainty of this calculation suggests to use an alternative approach. According to equations 3.17-3.19 where M is the molar mass of the fluid, R is the universal constant of ideal gas, T is the absolute temperature and V the molar volume. Note also, that in each equation introduces a roughness factor (R_i) that accounts for the deviation from the sphericity and the translational coupling. R_i was set to 1, since ions were modelled as perfect spheres, avoiding to increase the complexity of the model.

$$D^* = \frac{D^*_{exp}}{R_D} = 5.030 \times 10^8 \left[\frac{M}{RT}\right]^{1/2} \frac{DV^{-1/3}}{R_D} \tag{3.17}$$

$$\eta^* = \frac{\eta^*_{exp}}{R_\eta} = 6.035 \times 10^8 \left[\frac{1}{MRT}\right]^{1/2} \frac{\eta V^{2/3}}{R_\eta} \tag{3.18}$$

$$\lambda^* = \frac{\lambda^*_{exp}}{R_\lambda} = 1.936 \times 10^7 \left[\frac{M}{RT}\right]^{1/2} \frac{\lambda V^{2/3}}{R_\lambda} \tag{3.19}$$

By plotting reduced transport properties versus V_r (equals to V/V_0) universal curves were obtained by using a large set of experimental data. Expressions 3.20-3.22 provide accurate overlaps when using coefficients given by Assael et coworkers[79]. However, a more recent work by Ciotta et coworkers [80] have widen the operation range of this theory with a new set of values, very convenient when dealing with the viscosity of dense fluids.

$$log_{10}\left[\frac{D^*_{exp}}{R_D}\right] = \sum_{i=0} 5a_{Di}\left(1/V_r\right)^i \tag{3.20}$$

$$log_{10}\left[\frac{\eta^*_{exp}}{R_\eta}\right] = \sum_{i=0}^{7} a_{\eta i}\left(1/V_r\right)^i \tag{3.21}$$

$$log_{10}\left[\frac{\lambda^*_{exp}}{R_\lambda}\right] = \sum_{i=0}^{4} a_{\lambda i}\left(1/V_r\right)^i \tag{3.22}$$

In table 3.1, values proposed by Ciotta et coworkers are presented, since it is the set of coefficients we have used hereby.

i	1	2	3	4	5	6	7
a_i	6.26871	−48.4793	243.447	−653.257	974.312	−763.616	251.193

Table 3.1: Coefficients of the universal curve proposed by Ciotta et coworkers[80].

The application of HS theory requires the fitting of the universal curves based on experimental data to the equations 3.17-3.19. Results will provide the reduced volume as a function of the temperature and thus, transport properties can be estimated out of the measuring range.

3.3 Atomistic theory

Different approaches can be chosen to study the physical chemistry of ionic liquids + water mixtures through molecular dynamics (MD). First, *ab initio MD* do not require the parametrization of chemical since it is based on the solution of Schrodinger equations, however the length of the trajectories and the dimension of the systems constrain its application to the analysis of dynamic and energetic quantities. Besides, the computational resources required are quite large even when for short trajectories and small systems. On the other side, *coarse grained MD* allows to study more complex chemicals such as polymers or proteins, larger systems and longer timescales are accesible. Nevertheless, instead of the representing the chemical structures as individual atoms joint by bonds, coarse grained models are based on the definition of atomic clusters giving a less realistic picture of the studied substances. Thus, atomistic MD was found to be the suitable technique since using a detailed representation of the chemical structures it provides accurate description of the target properties addressed in this PhD.

Atomistic MD solves Newton's equations of motion for a number of atoms taking part in the *experiment*. In MD *experiments*, samples will be the N number of particles place in the simulation box[81]. From their positions and momentum along the simulation time a large amount of physico-chemical properties can be calculated.

3.3.1 Atomistic model

In this PhD thesis, ionic liquids and water, were represented by a classical atomistic force field for organic compounds[82] containing intramolecular terms for covalent bond stretching, valence

angle bending and torsions, and intermolecular parameters for repulsion-dispersion Lennard-Jones (LJ) sites and for partial electrostatic charges on atomic sites. The functional form of the potential energy is given in eq. 3.23.

$$
\begin{aligned}
u = & \sum_{ij}^{\text{bonds}} \frac{k_b}{2}(r - r_0)^2 + \sum_{ijk}^{\text{angles}} \frac{k_\theta}{2}(\theta - \theta_0)^2 \\
& + \sum_{ijkl}^{\text{torsions}} \sum_{m=1}^{3} \frac{V_m}{2}[1 - (-1)^m \cos(m\phi)] \\
& + \sum_{ij}^{\text{nonbonded}} 4\epsilon_{ij} \left[\left(\frac{\sigma_{ij}}{r_{ij}} \right)^{12} - \left(\frac{\sigma_{ij}}{r_{ij}} \right)^{6} \right] + \frac{1}{4\pi\epsilon_0} \frac{q_i q_j}{r_{ij}}
\end{aligned}
\tag{3.23}
$$

The force field for ionic liquids was parameterized by Canongia Lopes and Padua[83, 84, 85, 86]. Water was represented by the SPC/E model[87].

To achieve a better description of ionic species, atomic partial charges are often reduced by a coefficient going from 0.7 to 0.9[45]. In this PhD thesis atomic charges given by the aforementioned references were scaled to 0.8 for all the ionic species after comparing the results of some macroscopic properties with full-charged model with more accurate results.

3.3.2 Simulation settings

A cutoff of 12 Å was applied to LJ interactions. Long-range electrostatic interactions were handled using the particle-particle particle-mesh[88] method, for a precision of 10^{-4} in electrostatic energy. Trajectories were generated at constant NpT using Nosé-Hoover thermostat and barostat. In all cases, a timestep of 1 fs was used.

Initial equilibrations of 1 ns were carried out starting from the configurations generated by Packmol. Then, production runs to calculate structural, thermodynamic and transport properties were performed over longer time scales, chosen according to the time needed for the systems to attain a diffusive regime[47].

All simulations were carried out in periodic cubic boxes. When pure ILs are simulated, the number of ions pairs was chosen to be 300. When ILs + water mixtures are studied, the number of water molecules to reach the desired concentration was added to 300 ion pairs.

3.3.3 Software tools

Different software tools were used in order to set the simulation environment and obtain information about the *samples*. As shown in figure 3.10, in a first step we need to build the files containing the topologies of the chemical we want to simulate and the parameters of the force field describing their interactions. Those files are the input for fftool[89] utility. Then, fftool creates auxiliar files used by Packmol[90] to build the initial configurations that are sent back to fftool to build the files used by LAMMPS[91, 92], the open source package developed in the Sandia National Laboratories.

3.3.4 Dynamics

The dynamic properties were studied attending to the self-diffusivity coefficients and the viscosity of the systems. However, to ensure these properties can be properly calculated we need to verify that the diffusive regime was reached. The criterion used all along the articles using

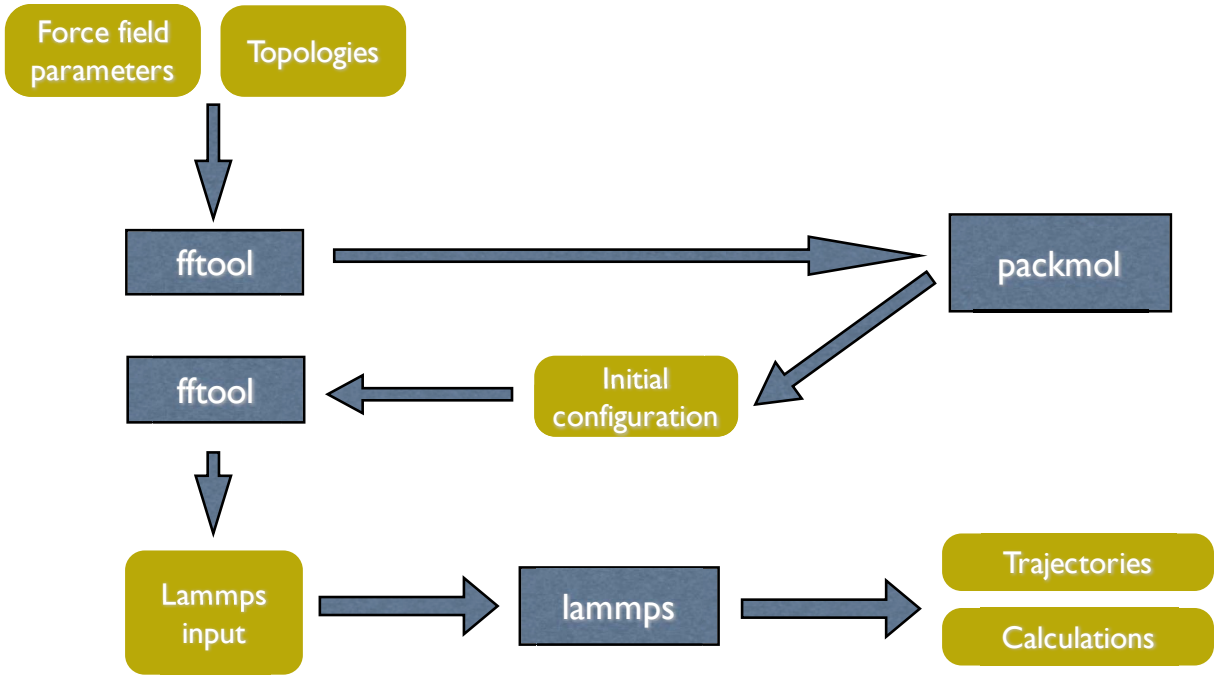

Figure 3.10: Flow diagram of the software used for the simulation experiments.

MD techniques was the calculation of β values (equation 3.24), explained in detail by Cadena et coworkers[47]. According to this criterion three different dynamic regimes are observed in liquids: ballistic ($\beta \approx 2$), subdiffusive ($\beta < 1$) and diffusive regimes ($\beta \approx 1$). The dynamics properties are calculated once the diffusive regime is reached and so β value is close to 1.

$$\beta(t) = \frac{d \log \left\langle \Delta r(t)^2 \right\rangle}{d \log t} \tag{3.24}$$

The microscopic dynamics is studied through calculations of diffusion coefficients. The self-diffusivity is obtained from the mean square displacement (eq. 3.25) calculated averaging over trajectories sufficiently long for the system to be in a diffusive regime.

$$D = \frac{1}{6} \lim_{t \to \infty} \frac{d}{dt} \left\langle \Delta r(t)^2 \right\rangle \tag{3.25}$$

Viscosity is a challenging quantity to calculate from MD simulations[93, 94, 95], especially for viscous fluids. In this work viscosity was calculated through the Green-Kubo relations using equilibrium trajectories[96]. The Green-Kubo method requires integration of the autocorrelations of the pressure tensor.

$$\eta = \frac{V}{kT} \int_0^\infty \left\langle p_{xy}(t) p_{xy}(0) \right\rangle dt \tag{3.26}$$

The autocorrelation were recorded using the multiple step correlator method of Ramirez et al.[97] implemented in LAMMPS. The result was averaged over three independent shear directions and the uncertainty was estimated from the standard deviation of these values.

3.3.5 Energetics of the water solvation

Energy exchanges during the phase-change of the refrigerant (water) in the absorbent (IL) are critical for the application of ionic liquids in refrigeration cycles. To accomplish these calculations, the algorithm so-called Free Energy Perturbation (FEP) was used.

The chemical potential of the solvation of water into different ILs was calculated. The idea behind this calculation is going from an initial state where a water molecule does not interact with the media (IL) to a final state where this water molecule is fully solvated. This transition is done through the modification of a coupling parameter, λ. For a correct sampling 20 intermediate states were set. Thus, the free energy of the solvation process is calculated according to eq. 3.27.

$$\Delta_0^1 A = \sum_{i=0}^{n-1} \Delta_{\lambda_i}^{\lambda_{i+1}} A = -kT \sum_{i=0}^{n-1} \ln \left\langle \exp\left(-\frac{U_{\lambda_{i+1}} - U_{\lambda_i}}{kT} \right) \right\rangle_{\lambda_i} \tag{3.27}$$

To avoid singularities due to overlap of sites at the moment when they are created or annihilated, soft-core LJ and electrostatic potentials were used[98]. For the systems we studied, a step of $\Delta\lambda = 0.05$ proved adequate, as was verified by the very low hysteresis when performing the FEP calculation both ways[99].

Chapter 4

Articles

4.1 Liquid range temperature of ionic liquids as potential working fluids for absorption heat pumps

- This article is the product of the collaboration between the Thermophysical Properties of Fluids and Biomaterials group (Universidad de Santiago de Compostela) and the Applied Physics Department (Universidad de Vigo).

- P.B.S. has designed and performed the thermogravimetric analysis (TGA) together with M.V. and J.J.P.

- P.B.S redacted a major part of the manuscript under the supervision of J.S. and J.G.

J. Chem. Thermodynamics 91 (2015) 127–135

Contents lists available at ScienceDirect

J. Chem. Thermodynamics

journal homepage: www.elsevier.com/locate/jct

Liquid range temperature of ionic liquids as potential working fluids for absorption heat pumps

M. Villanueva [a], J.J. Parajó [a], Pablo B. Sánchez [b], J. García [b], J. Salgado [a,*]

[a] Thermophysical Properties of Fluids and Biomaterials Group, Applied Physics Department, University of Santiago de Compostela, E-15782 Santiago de Compostela, Spain
[b] Applied Physics Department, Experimental Science Building, University of Vigo, E-36310 Vigo, Spain

ARTICLE INFO

Article history:
Received 9 April 2015
Received in revised form 20 July 2015
Accepted 26 July 2015
Available online 31 July 2015

Keywords:
Ionic liquids
Absorption heat pumps
Temperature operation range
Thermal stability
Phase transitions
TGA
DSC
Green chemistry
Energy
Sustainability

ABSTRACT

The liquid range temperature of six ionic liquids (ILs) was determined in this work with the aim to propose suitable absorbents for heat pump systems. The selected ILs have three different cations, imidazolium, pyridinium and choline and each was combined with four different anions $[NTf_2]^-$, $[OTf]^-$, $[MeSO_3]^-$ and $[BETI]^-$. The lower limit, given by solid – liquid transitions, was determined using differential scanning calorimetry (DSC). The upper limit is given by the degradation temperature. This temperature is determined using thermogravimetric technique (TGA). Dynamic and isothermal methods have been combined to estimate the maximum operation temperature. ILs ageing effect was also analysed in this work.

1. Introduction

Ionic liquids (ILs) are usually defined as salts melting under 100 °C. This definition is broadly accepted even though there is no chemical or physical significance in this temperature which has been chosen for historical reasons [1]. From the enormous number of ILs, the most common chemical structure is based on an organic cation together with an inorganic polyatomic anion [2]. The unique properties of the ILs [3] have brought great interest over the last years from industry and academia due to a large number of potential applications [4]. Since climate change stands out as one of the main challenges for the next decades, technologies leading to efficient energy production will play a crucial role. In this framework, absorption heat pumps are a great opportunity to reduce energy consumption of heating and refrigeration systems, since this technology allows either recovering residual heat or using renewable energies (as solar, bio-hydrogen...) to produce profitable thermal energy. Subsequently, the use of additional electric power is almost negligible. Therefore it is a technology of high added value in regions where the electrical network is not developed in addition to its high ecological benefits. Nevertheless conventional working pairs present several drawbacks which have limited the potential of absorption heat pumps [5]. Some of these problems are corrosion and crystallisation in the case of H_2O/LiBr, high working pressures, low relative volatility and NH_3 toxicity for NH_3/H_2O. Thus, improvements of absorption heat pumps by developing new working pairs (refrigerant/absorbent) have drawn the attention of companies and researchers. Seeking new working pairs involving ILs as absorbents occupy a principal role in these investigations [6,7]. This work is framed into the analysis of different ILs as candidates for absorption processes together with natural refrigerants such as water [8], ammonia or carbon dioxide.

To meet the requirements of absorption heat pumps, a first screening was performed paying special attention to the liquid range temperature. As it has been pointed out, crystallisation at low temperatures is one of the drawbacks for commercial LiBr/H_2O working pairs, therefore solid – liquid transitions should be analysed to prevent solid phase formations in the absorber [7], an important factor of any absorption refrigeration system [9]. On the other hand, since absorbents will remain within the system for long periods of time, thermal stability should be studied carefully not only as a function of temperature but also as a function of time.

* Corresponding author. Tel.: +34 881814110; fax: +34 881814085.
E-mail address: j.salgado.carballo@usc.es (J. Salgado).

http://dx.doi.org/10.1016/j.jct.2015.07.034
0021-9614/

Differential scanning calorimetry (DSC) was used to determine melting point (T_m) as much as the glass transition (T_g). These values may constrain the lower temperature operation range [10,11]. However it should be taken into account that real working fluids will be solutions of refrigerant/IL, where these temperatures are expected to be lower than those of pure IL, thereby partially easing the constraint [12].

In addition, the absorbents should be highly stable over a wide range of operating temperature in absorption devices [9]. Although, no unique criterion has been defined to determine thermal stability for a particular fluid, two operation modes are broadly known when thermogravimetric analysis is used. The so-called dynamic methods consist of performing a ramp of temperature with time by measuring simultaneously how mass sample changes. Results obtained are usually expressed in terms of degradation temperature or onset temperature [13]. This value provides qualitative information, as it has been broadly pointed out in the literature [13–15], but never a maximum operation temperature since it is observed that degradation starts below the onset temperature. In other words, the onset temperature overestimates the maximum operation temperature. For a deeper knowledge of this parameter, this analysis must be refined with isothermal scans. Additionally isothermal scans allow kinetic analysis of the degradation process by using the Arrhenius equation and an estimation of the degradation time for a given temperature.

Besides dynamic and isothermal scans, temperature conditions of the absorption process have been reproduced. Since during absorption cycles, the ILs undergo temperature changes (from absorber to generator and backwards) for extended periods of time. ILs thermal stability after several heating and cooling cycles has been studied. To our knowledge, this is the first time this sort of test has been reported for ILs.

At this point, and due to potential capabilities of ILs as absorbents, knowledge of physical and chemical properties becomes critical in order to select suitable candidates among a huge number of available ILs. The influence of the cation and anion, the length of the alkyl chain or different functional groups over ILs properties will allow "absorbent tunning" based on process requirements. Apart from the temperature operation range, other thermophysical properties such as solubility with the refrigerant, density, heat capacity, viscosity, surface tension or thermal conductivity; and also, factors as toxicity and environmental impact must be taken into account.

With the aim to acquire a deeper knowledge of cation and anion influence over the temperature operation range, six ionic liquids have been chosen for evaluation as potential absorbents for natural refrigerants (ammonia, water and carbon dioxide). The selected ILs are based on four different anions together with imidazolium, pyridinium and choline cations.

Four of the six ILs involve $[NTf_2]^-$ and $[OTf]^-$ anions and they were chosen because of their high thermal stability [16]. Other anions, $[BETI]^-$ and $[MeSO_3]^-$ [17] are not so extensively studied and they were chosen due to their structural similarity with $[NTf_2]^-$ and $[OTf]^-$. The influence of the cation over this property is minor compared to the anion, however it cannot be considered as a negligible factor. Thus, imidazolium, pyridinium and choline cation families have been selected to explore the cation effect over the decomposition temperature of the ILs.

TABLE 1
Structure and identification of selected ILs (all of them supplied by IoLiTec).

Name	Abbreviation CAS number	Chemical structure	Mass fraction purity
1-Ethylpyridinium bis (trifluoromethylsulfonyl) imide	$[C_2Py][NTf_2]$ 712354-97-7	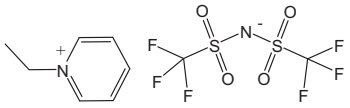	>0.99
Choline bis (trifluoromethylsulfonyl) imide	$[Chol][NTf_2]$ 827027-25-8	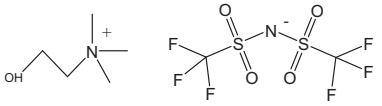	>0.99
1-Ethyl-3-methylimidazolium triflate	$[C_2C_1Im][OTf]$ 145022-44-2	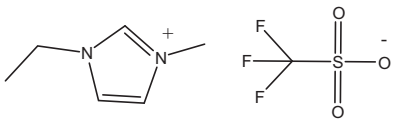	>0.99
1-Ethyl-3-methylimidazolium bis (perfluoroethylsulfonyl) imide	$[C_2C_1Im][BETI]$ 216299-76-2	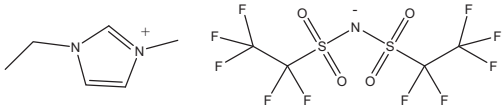	>0.98
1-Ethylpyridinium methanesulfonate	$[C_2Py][MeSO_3]$ 681481-41-4	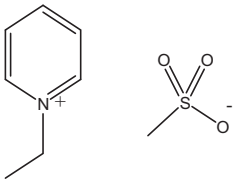	>0.95
1-Ethylpyridinium triflate	$[C_2Py][OTf]$ 3878-80-6	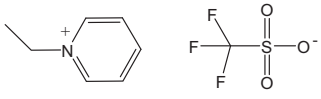	>0.99

2. Materials and methods

2.1. Chemicals

Six ionic liquids, provided by IoLiTec, were considered for this work, three contain the common cation, *viz.* 1-ethylpyridinium $[C_2Py]^+$, and the anions bis (trifluoromethylsulfonyl) imide $[NTf_2]^-$, triflate $[OTf]^-$, and methanesulfonate $[MeSO_3]^-$ The other two ILs have the common cation 1-ethyl-3-methylimidazolium $[C_2C_1Im]^+$, with the anions triflate and bis (perfluoroethylsulfonyl) imide $[BETI]^-$, and the sixth IL is choline bis (trifluoromethylsulfonyl) Imide [Chol] $[NTf_2]$. Identification names and numbers, purities and cations and anions chemical structures are presented in table 1.

2.2. Experimental

A differential scanning calorimeter DSC Q100 TA-Instruments with aluminium pans hermetically sealed was used to determine the different state transitions experienced by the IL during the heating and cooling cycles. Liquid nitrogen was used as the coolant fluid. Each sample (3 to 5 mg) was subjected to four ramps, two in cooling and two in the heating mode, with an isothermal step between them: (a) heating from (25 to 120) °C at 10 °C · min^{-1}, (b) isothermal step at 120 °C during 30 min to remove impurities [18] and to erase the thermal history of the sample, (c) cooling from (120 to −85) °C at 5 °C · min^{-1}, (d) isothermal step at −85 °C during 5 min and (d) heating from (−85 to 100) °C at 10 °C · min^{-1} and (e) cooling from 100 °C at −85 °C at 5 °C · min^{-1}. Temperatures transitions were determined from the DSC curves during the re-heating and re-cooling steps [19].

A thermogravimetric analyser (TGA 7-Perkin Elmer) operating in dynamic and isothermal modes under dry air atmosphere was used to perform thermogravimetric analysis [20]. Although the effect of the atmosphere becomes lower for long-term thermal stability studies [21], it was considered more appropriate to use air instead of an inert atmosphere in order to estimate the maximum operation temperature for different applications, where ILs can be in air contact.

Samples of (3 to 5) mg were placed in an open platinum pan. Dynamic experiments were performed at temperatures from (100 to 800) °C, with a heating rate of 10 °C · min^{-1} and a purge gas flow of 20 cm^3 · min^{-1}. Each analysis was repeated three times. Determination procedures of onset and ending temperatures were described in previous papers [20,21]. Furthermore, isothermal TG analysis at temperatures lower than t_{onset}, was used to determine the long-term thermal stability of ILs.

Besides the effects on the thermal stability owing to dynamic and isothermal regimes during absorption cycles, the ILs undergo temperature changes (from absorber to generator and backwards) for extended periods of time. For this reason, the thermal stability of the ILs after several heating and cooling cycles has been studied in order to reproduce roughly the effects of these temperature changes on this property. Each sample was subjected to two ramps, one in cooling and one in the heating mode, with an isothermal step between them: (a) heating from (50 to 175) °C at 5 °C · min^{-1}, (b) isothermal step at 175 °C during 15 min, (c) cooling from (175 to 50) °C at 5 °C · min^{-1}, (d) isothermal step at 50 °C during 15 min. The whole sequence was repeated eight times.

3. Results and discussion

3.1. DSC

Figure 1 shows the last ramp of heating and cooling of DSC analysis of the six ILs $[C_2Py][NTf_2]$, [Chol]$[NTf_2]$, $[C_2Py][OTf]$, $[C_2C_1Im][OTf]$, $[C_2Py][MeSO_3]$ and $[C_2C_1Im][BETI]$.

All the ILs show melting and freezing peaks, presenting these ILs as very good crystal-formers, although the DSC curve profiles show important differences associated with different thermal behaviour. Table 2 summarises state transition temperatures, such as melting, freezing, cold crystallisation and glass temperatures determined from these curves. As far as we are aware, information on the thermal behaviour of these ILs in heating and/or cooling ramps is scarce in the literature. Those values of transition temperatures found in the literature for these ILs are also presented in table 2.

Important agreement between our results and those of and other authors is, thus for $[C_2C_1Im][BETI]$, Ngo *et al.* [22] obtained freezing temperature (−12 °C) similar to our result, but values for the melting point (−1 °C) differ considerably from ours, probably due to different experimental conditions and different thermal history. However on the contrary, our results are in good concord with those of Shirota *et al.* [23] for the melting point. The $[C_2C_1Im][BETI]$ shows a glass transition (−52 °C) with enthalpic recovery. To distinguish it from a solid − solid transition, we have zoomed in the DSC scan and checked that it corresponds to a "stair step" which is the common appearance for a glass transition [24]. Afterwards, $[C_2C_1Im][BETI]$ shows a sub-cooling phenomenon, characterised by an incomplete crystallisation on the cooling ramp. Then a part of this IL passes from a glassy to a subcooled state, suffering a cold crystallisation followed by the melting transition. This cold crystallisation phenomenon is usually observed in the thermal behaviour of many ionic liquids. Agreeing with these results, Calvar *et al.* [18] and Fredlake *et al.* [10] found that some imidazolium based ILs show similar behaviour. Nevertheless this cannot be observed in pyridinium based ILs.

The [Chol]$[NTf_2]$ shows a very different profile on the heating ramp compared to the rest of the ILs. This profile is characterised by three endothermic peaks at (2, 27 and 33) °C. The first is attributed to a solid − solid transition and the last to the melting process. The origin of the peak at 27 °C, which is not completely resolved with the last peak, could be associated either to a solid − solid or to a melting transition. Taking into account that the temperatures of the second and third peaks (27 and 33 °C) do not change when the heating rate increases at 10 °C · min^{-1} (results are not shown), we think that the melting process of this IL takes place in two different phases at (27 and 33) °C. Similar behaviour and temperatures were also found by Yoshizawa-Fujita *et al.* [25] for this IL, with the usual shape found in the DSC of polymers with high molar mass [26,27]. Additionally, Nockeman *et al.* [28], indicated that the melting temperature for [Chol]$[NTf_2]$ is 30 °C although these authors do not show the DSC curves of this IL, this value is in relative good concordance with our results.

The $[C_2Py][OTf]$ shows two exothermic peaks in the cooling ramp and two endothermic peaks in the heating ramp. Other authors as Calvar *et al.* [18] have observed similar behaviour in some pyridinium and imidazolium based ILs with the same anion, $[OTf]^-$, which suggests a polymorphic-like behaviour that leads to the formation of crystals with different structures. Nevertheless, a deeper study is necessary to complement and confirm this result.

On the other hand, $[C_2Py][NTf_2]$ crystallises, at −21 °C, on cooling, but does not form a glass within the temperature range studied. A solid − solid transition at 21 °C and the melting point at 32 °C are detected during the heating ramp, agreeing in both cases with the results of Liu *et al.* [29]. This behaviour, not unusual in ILs, is also observed by Machanova *et al.* [30] and Stefan *et al.* [31] for ammonium and pyrrolidinium based IL, with the $[NTf_2]^-$ anion, observing in the last case, even two solid − solid transitions before the melting.

All melt at temperatures higher than 0 °C with the exception of $[C_2C_1Im][OTf]$ that melts at −14 °C. Wachter *et al.* [32] indicate that the solid − liquid transition of this IL is −10 °C, which is the maximum temperature of the melting peak, agreeing with the result of this work.

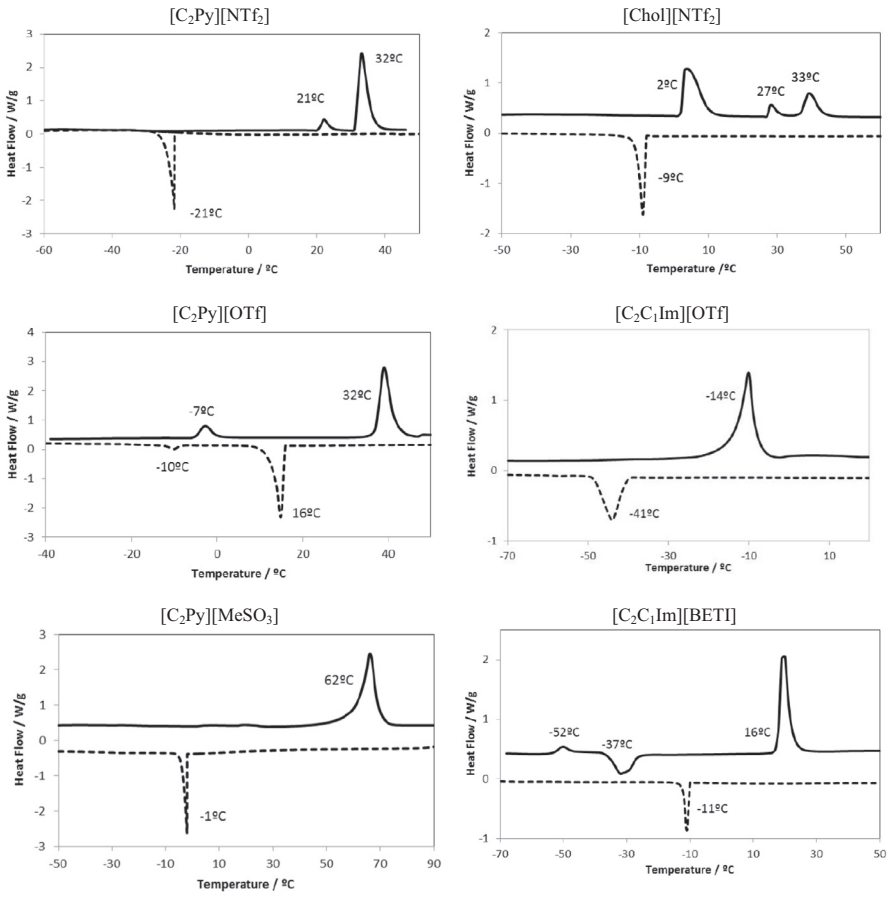

FIGURE 1. DSC curves (Exo down) on cooling (dashed line) and heating (solid line) scanning for the selected ILs.

TABLE 2
Freezing (t_f), melting (t_m), glass transition (t_g), cold crystallisation (t_{cc}) and solid – solid transition (t_{ss}) temperatures obtained from DSC curves under pressure of (990 ± 3) hPa and comparison with bibliographic results.

IL	Cooling step	Heating step		
	t_f/°C	t_m/°C	t_g/°C	Other/°C
$[C_2Py][OTf]$	16/−10			
$[C_2Py][MeSO_3]$	−1	62		
$[Chol][NTf_2]$	−9	27/33		2 (t_{ss})
		27 [25]		−1 (t_{ss}) [25]
		30 [28]		
$[C_2C_1Im][BETI]$	−11	16	−52	−37 (t_{cc})
	−12 [22]	−1 [22]		
		15 [23]		
$[C_2Py][NTf_2]$	−21	32		21 (t_{ss})
		31 [29]	−38 [29]	20 (t_{ss}) [29]
$[C_2C_1Im][OTf]$	−41	−14		
		−10 [32]		

Expanded uncertainties are $U(t) = \pm 2$ °C (0.95 level of confidence).

The sequence obtained for lowest limit for the liquid range of selected ILs is:

$$[C_2Py][MeSO_3] > [C_2Py][OTf] \approx [C_2Py][NTf_2] \approx [Chol][NTf_2] > [C_2C_1Im][BETI] > [C_2C_1Im][OTf].$$

Imidazolium based ILs show the lowest melting temperatures, whereas the highest corresponds to ILs containing pyridinium cations. Nevertheless a trend with the anion cannot be established in the same way.

With regard to freezing temperatures the sequence is a little bit different:

$$[C_2Py][OTf] > [C_2Py][MeSO_3] > [Chol][NTf_2] > [C_2C_1Im][BETI] > [C_2Py][NTf_2] > [C_2C_1Im][OTf].$$

A trend with anion or cation cannot be established for freezing temperatures. Although it is important to remark that, in both sequences, the two first ILs remain the same.

Substantial super cooling is observed for all the ILs, with the freezing point significantly lower than the melting point, with differences (T_m–T_f) occurring around (20 to 30) °C, except for $[C_2Py][NTf_2]$ and $[C_2Py][MeSO_3]$ which are higher than 50 °C, indicating a very slow crystallisation rate. This fact is very important and a positive observation for the application of ionic liquids as absorbents in absorption heat pumps to avoid the problem of crystallisation commonly observed in the current working pair, as previously pointed out.

3.2. Thermogravimetric analysis

3.2.1. Dynamic study

Figure 2 shows TG (a) and DTG (b) curves for the selected ILs. Reported curves have similar shapes for all ILs, characterised by a unique step with an intense loss weight, corresponding to a narrow DTG peak (50 °C approximately).

Table 3 shows onset and ending temperatures (t_{onset} and t_{endset}), weight at t_{onset} (W_{onset}), temperature corresponding to a 1% weight loss ($t_{1\%}$) and the temperature for DTG minimum (t_{peak}). These values were determined directly from TG and DTG curves using

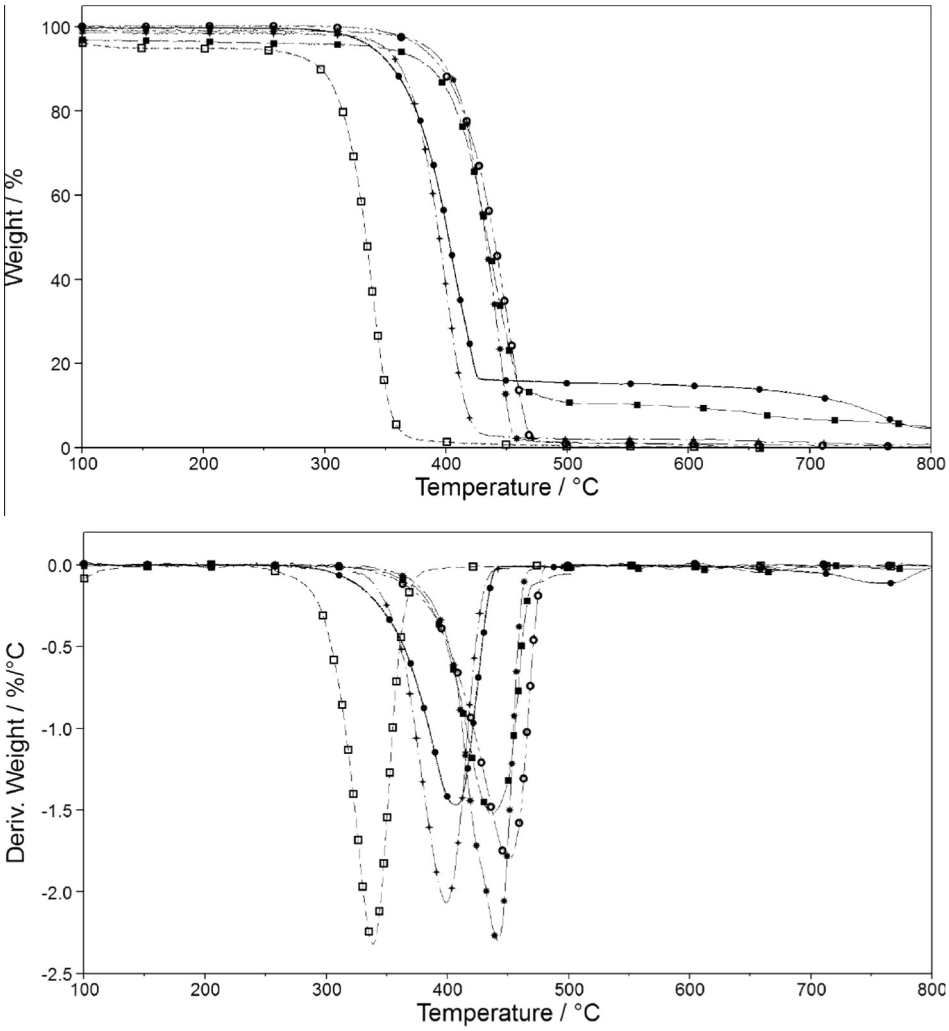

FIGURE 2. TG (a) and DTG (b) of ILs: (∗) [Chol][NTf_2], (■) [C_2C_1Im][OTf], (○) [C_2py][NTf_2], (○) [C_2py][OTf], (●) [C_2C_1Im][BETI], (□) [C_2py][$MeSO_3$].

TABLE 3
Thermal results from dynamic scans in air atmosphere under pressure of (990 ± 10) hPa. Onset and ending temperatures (t_{onset} and t_{endset}), weight at t_{onset} (W_{onset}), the temperature for DTG minimum (t_{peak}) and temperature corresponding to 1% loss weight ($t_{1\%}$).

IL	t_{onset}/°C	t_{endset}/°C	W_{onset}/%	t_{peak}/°C	$t_{1\%}$/°C
[Chol][NTf_2]	410	460	85	442	355
[C_2Py][NTf_2]	409	471	83	450	346
[C_2C_1Im][OTf]	404	458	87	436	338
[C_2Py][OTf]	371	416	86	399	328
[C_2C_1Im][BETI]	368	425	85	407	305
[C_2Py][$MeSO_3$]	315	353	85	339	265

Expanded uncertainties are $U(t)$ = ±4 °C and $U(W)$ = 1% (0.95 level of confidence).

methods widely described in previous papers published by our group [15,20,21]. Analysed ILs present a remarkable thermal stability, with onset temperatures higher than 350 °C, except for [C_2Py][$MeSO_3$] with t_{onset} of 315 °C. Although the onset temperature cannot be considered the upper limit of the liquid range as already noted, this parameter allows establishment of a sequence for the thermal stability of the ILs. Thus, the trend obtained is as follows:

$$[Chol][NTf_2] \approx [C_2Py][NTf_2] > [C_2C_1Im][OTf] > [C_2Py][OTf] > [C_2C_1Im][BETI] > [C_2Py][MeSO_3].$$

This sequence indicates that the anion has the strongest influence over the ILs thermal stability, with the $[NTf_2]^-$ conferring the highest resistance to thermal degradation, following closely by $[OTf]^-$. Thus, it is clear that the cation influence should also be taken into account with the imidazolium based ILs that provide the greatest thermal stability. These observations are in good agreement with previous works where ILs with similar cations or anions were studied [16,33–36].

Literature information regarding the degradation of these ILs is scarce and in most cases comparisons are difficult due to the influence of experimental conditions on results. Thus, Bittner *et al.* [36] use temperature of maximal decomposition rate (*i.e.* t_{peak} for us) and they found results similar to ours for [C_2Py][NTf_2].

Additionally, Heym *et al.* [17], with the scope of studying thermal stability, used temperature to reach a mass loss of 1% during TG experiments at different heating rates obtaining 348 °C for [C_2C_1Im][OTf]. This value is consistent with result obtained in this work (338 °C).

On the other hand, decomposition temperature (T_d) of [C_2C_1Im][BETI] was previously calculated by Ngo *et al.* [22], obtaining different values using either aluminium (423 °C) or alumina (462 °C) sample pan, both of them higher than the value obtained in this work. These authors used a nitrogen atmosphere and a heating rate of 20 °C · min^{-1}, whereas in this work

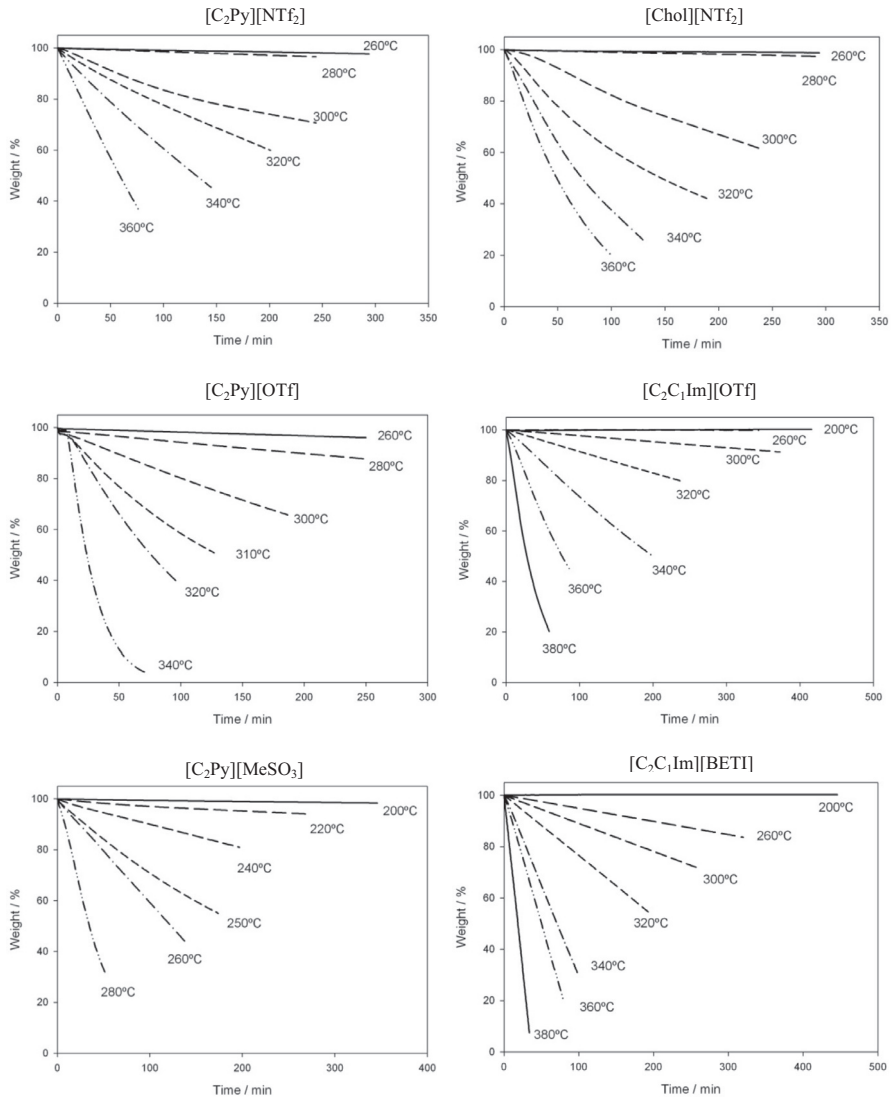

FIGURE 3. Isothermal scans at different temperatures of selected ILs.

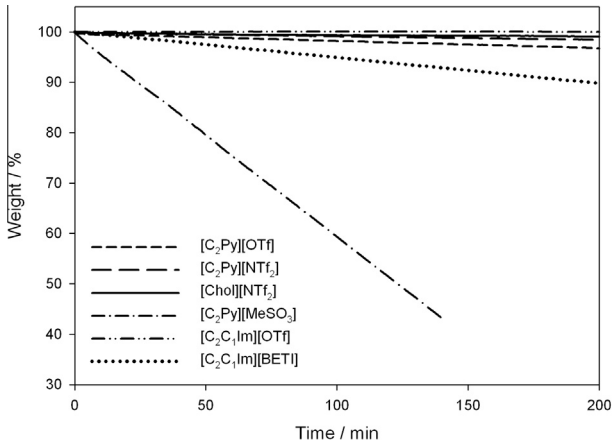

FIGURE 4. Comparison of isothermal scans of selected ILs at 260 °C.

air atmosphere and 10 °C · min^{-1} were chosen. As previous studies [21] have shown, the onset temperature can be up to 30 °C higher when the atmosphere changes from air to nitrogen. A similar effect takes place when the heating rate changes from (10 to 20) °C · min^{-1}.

TABLE 4
Activation energy, E_a, and pre-exponential factor of Arrhenius equation, A, of degradation process for the selected ILs.

IL	E_a/(kJ · mol^{-1})	$A' = \ln A$
[C_2Py][OTf]	185 ± 10	37.57 ± 1.69
[Chol][NTf_2]	170 ± 20	33.12 ± 5.33
[C_2C_1Im][OTf]	160 ± 5	30.39 ± 0.98
[C_2Py][NTf_2]	140 ± 20	27.57 ± 4.39
[C_2Py][$MeSO_3$]	140 ± 10	31.52 ± 1.57
[C_2C_1Im][BETI]	110 ± 5	21.61 ± 1.17

Leaving aside the dynamic nature of the experiments, the loss of weight at t_{onset} is around 15% in all the ILs, too high to claim that this temperature is the upper limit of the operation range, as mentioned above. So, to establish this upper limit, isothermal studies are necessary [21].

3.2.2. Isothermal study

With the aim to determine the maximum operating temperature of these ILs, isothermal scans at different temperatures lower

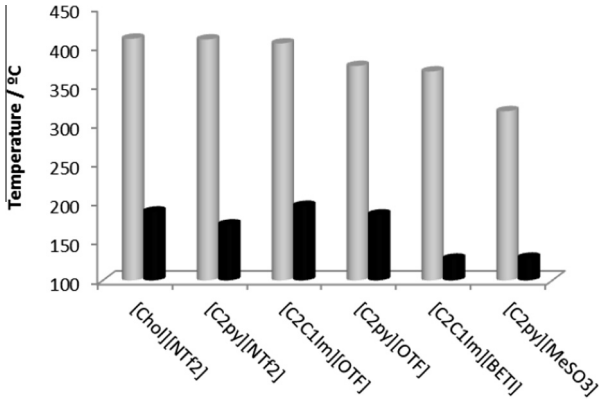

FIGURE 5. Comparison between t_{onset} (grey bar) and $t_{0.01/10h}$ (black bar).

TABLE 5
Maximum operating temperature (t, in °C) corresponding to three thermal degradation levels (1%, 5% and 10% in 10 h) calculated from Arrhenius parameter equation.

LI	t_{onset}/°C	$t_{0.01/10h}$/°C	$t_{0.05/10h}$/°C	$t_{0.1/10h}$/°C
[Chol][NTf_2]	410	190	205	215
[C_2Py][NTf_2]	409	170	190	200
[C_2C_1Im][OTf]	404	200	215	225
[C_2Py][OTf]	371	185	200	205
[C_2C_1Im][BETI]	368	130	150	160
[C_2Py][$MeSO_3$]	315	130	145	150

Uncertainties are $U(t_{onset}) = \pm 4$ °C (0.95 level of confidence) and $U(t_{0.01/10h}) = U(t_{0.05/10h}) = U(t_{0.1/10h}) = \pm 10$ °C (0.68 level of confidence).

than the corresponding t_{onset} were performed. Figure 3 shows these scans. As expected, weight loss corresponding to the highest selected temperature was very rapid, even for [C_2Py][NTf_2] at 360 °C (42 °C lower than the onset temperature), with one hour time enough to lose approximately the 60% of initial weight. Nevertheless scans at 260 °C for ILs with $[OTf]^-$ and $[NTf_2]^-$ anions and at 200 °C for other ILs during more than five hours do not imply detectable changes in mass samples.

Figure 4 shows a comparison between the isothermal scans at 260 °C. A similar trend than the one found with dynamic scans was obtained. The $[OTf]^-$ and $[NTf_2]^-$ based ILs are again the most stable, whereas [C_2Py][$MeSO_3$] weight loss at 260 °C is around 50% after 100 min.

The kinetics of decomposition was analysed from isothermal TGA results following the methodology reported in previous papers [18,19].

The temperature dependence on weight loss rate, k, is represented by the Arrhenius equation:

$$k = A \exp\left(\frac{-E_a}{RT}\right), \quad (1)$$

where E_a is the activation energy, R the gas constant and T the absolute temperature. The activation energy of the degradation process was obtained by fitting ln k and T^{-1}. The results are presented in table 4.

As far we are aware, activation energy values have not been published for these ILs, although these values are in agreement with those reported in the literature for other ILs with a similar cation and anion. From the results obtained and previous publications [14,18,19], it can be concluded that the activation energy follows the trend for a common anion ($[NTf_2]^-$ or $[OTf]^-$) choline > pyrrolidinium > pyridinium > imidazolium, whereas the anion sequence is:

$$[OTf]^- > [FAP]^- > [NTf_2]^- \approx [MeSO_3]^- > [BETI]^-.$$

3.3. Maximum operation temperature

As it was pointed out t_{onset} cannot be considered a maximum operating temperature. Thus, a long-term stability parameter, $t_{0.01/10h}$, that is the temperature necessary to reach a 1% weight loss after 10 h, is often used [16,27,29,37]. This parameter can be calculated from the Arrhenius equation, whose parameters are shown in table 4. A comparison between the values of t_{onset} and calculated $t_{0.01/10h}$ are presented in figure 5. Differences of 200 °C, approximately, between both temperatures are observed for all the selected ILs.

Depending on the application, the maximum operating temperature can vary, taking into account that the degradation level can be different. Thus, as expressed in previous papers [20], the criterion of $t_{0.01/10h}$ could be over strict, in which case the maximum operating temperature corresponding to three thermal degradation levels (1%, 5% and 10% in 10 h) is calculated using the above Arrhenius parameters that are shown in table 5.

In general, absorption systems will have operating temperatures lower than data shown in table 5. However, this issue must be analysed taking into account once the heat pump configuration is chosen. According to systems evaluated by Ayou *et al.* [38], these six ILs may accomplish the maximum operating temperature requirements with [C_2C_1Im][BETI] and [C_2Py][$MeSO_3$] which are close to this limit.

3.4. (Heating + cooling) cycles. ILs ageing

Regarding the application of absorption heat pumps, ILs behaviour after long periods of time remains as an open question, specifically the effects of ageing of the ILs after numerous absorption/desorption cycles. To the best of our knowledge, very few experiments have been done to study ageing effect on ILs [39].

His question is outlined using thermal techniques. (Heating + cooling) cycles were chosen to adapt the experimental procedure to absorption heat pump applications. The experimental procedure consists of 8 successive heating applications up to 175 °C and cooling up to 50 °C under air atmosphere.

Figure 6 shows the second (the first one was not considered because a low percentage of impurities, specially water, released to rise 100 °C) and the last heating TG curve for [C_2C_1Im][OTf] and [C_2Py][$MeSO_3$], which are the most and least thermally stable. No significant degradation related to successive (heating + cooling) cycles was found.

After the successive (heating + cooling) cycles, the same sample of these ILs was subjected to a heating from (50 to 800) °C at 10 °C · min^{-1} (figures not shown), *i.e.* the experimental conditions corresponded to dynamic studies, with the aim to determine the changes in characteristic temperatures after the cycles. Table 6 reports onset temperatures obtained from this dynamic study after the cycles (t'_{onset}). Results show there are no significant changes in dynamic curves as a consequence of the ageing.

Even though during this process ILs do not undergo other effects related with physical absorption, chemical interactions or mechanical factors, results seem to indicate that ageing does not affect to thermal stability.

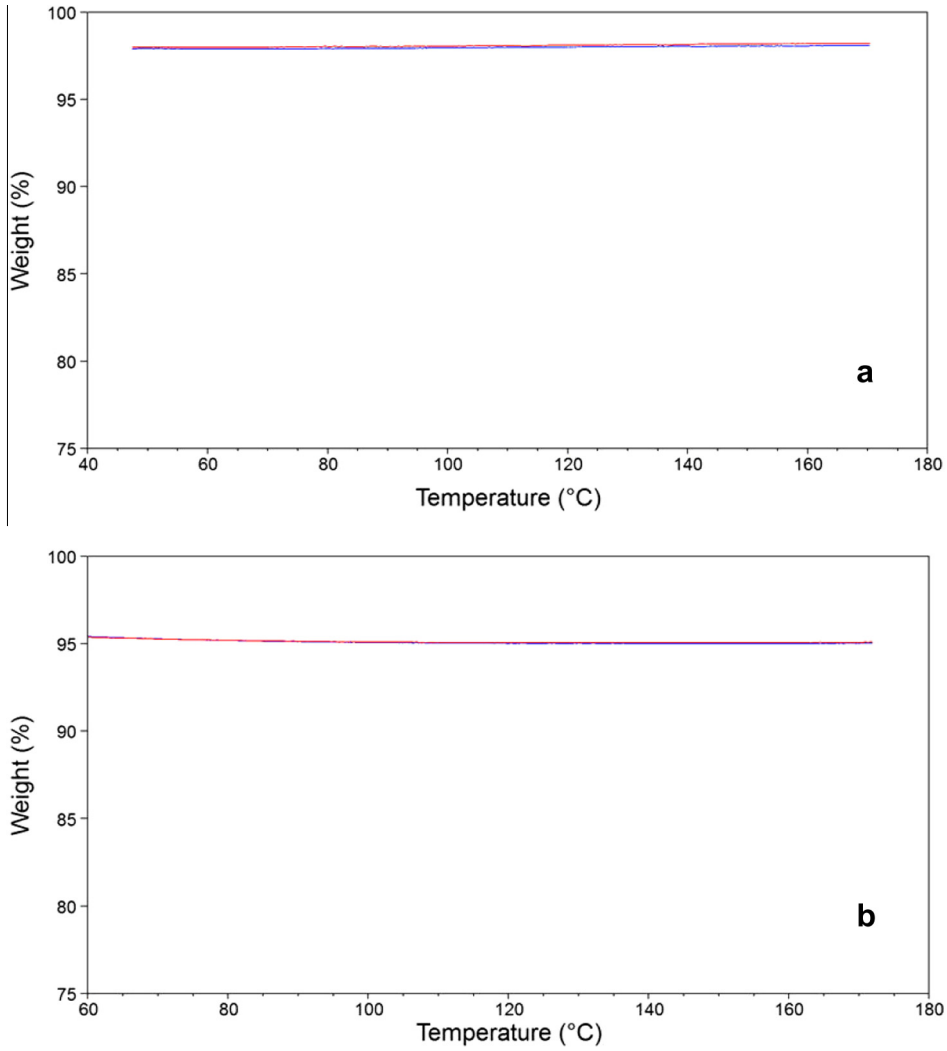

FIGURE 6. Comparison between the second and last curves of (heating + cooling) cycles of (a) $[C_2C_1Im][OTf]$ and (b) $[C_2Py][MeSO_3]$ ILs.

TABLE 6
Onset temperatures (t'_{onset}) of selected ILs obtained from dynamic studies after aging cycles.

IL	t'_{onset}/°C
$[Chol][NTf_2]$	410
$[C_2py][NTf_2]$	401
$[C_2C_1Im][OTf]$	405
$[C_2py][OTf]$	370
$[C_2C_1Im][BETI]$	362
$[C_2py][MeSO_3]$	321

Expanded uncertainties are $U(t) = \pm 4$ °C (0.95 level of confidence).

4. Conclusions

The liquid range of six different ILs has been determined in this work, using thermal analysis techniques. The main results are the following:

- All ILs show DSC curves peaks attributed to melting and freezing processes in heating and cooling scanning, respectively. The $[C_2Py][MeSO_3]$ and $[C_2Py][OTf]$ show the highest melting and freezing temperatures and $[C_2C_1Im][OTf]$ the lowest. Different ILs trends were obtained for melting and freezing processes.
- The six ILs studied show remarkable thermal stability with onset temperatures higher than 300 °C. The influence of the anion over this property is very strong with $[NTf_2]^-$ and $[OTf]^-$ anions the most resistant to thermal degradation. Nevertheless, temperatures provided by dynamic thermogravimetric studies cannot be considered to be the maximum operating temperature. Isothermal scans are necessary to determine this value.
- $[MeSO_3]^-$ and $[BETI]^-$ based ILs do not undergo significant thermal degradation up to 200 °C whereas for $[NTf_2]^-$ and $[OTf]^-$ based ILs significant degradation is not detected up to 250 °C under the same conditions.
- Activation energy of the degradation process has been determined using the Arrhenius equation and is compared with previous results for other ILs. Cation and anion influence on activation energy is defined by the following trends; for cation: choline > pyrrolidinium > pyridinium > imidazolium, and for anion: $[OTf]^- > [FAP]^- > [NTf_2]^- \approx [MeSO_3]^- > [BETI]^-$.
- The effect of successive heating to 175 °C and cooling to 50 °C cycles on the mass sample was analysed to estimate the effects on ageing of the ILs. Results indicate that this effect is negligible, since no detectable mass loss is associated with these cycles. Before and after the ageing, the TG curves show similar shapes and the same onset temperatures.

– According to the findings, the most adequate IL to operate in absorption devices is [C_2C_1Im][OTf] due to its lowest melting point and greatest thermal stability. Nevertheless, regarding their liquid range, none of the others should be discarded since they accomplish requirements for many heat pump configuration systems. To determine suitable ILs, other experimental and theoretical experimental studies will be made in the near future.

Acknowledgments

This study was financed by the projects DPI2012-38841-C02-02, CTQ2011-23925 (Ministerio de Economía y Competitividad of Spain and FEDER) and EM2013/031 (Xunta de Galicia, Spain) and the network REGALIS R2014/015 (Xunta de Galicia, Spain). Pablo B. Sánchez thanks to Ministerio de Economia y Competitividad of Spain for his PhD Grant framed in Plan Estatal de Investigación Científica y Técnica y de Innovación 2013-2016.

Authors thank to Dr. A. Domínguez from University of Vigo (Spain) for her advices in DSC curves interpretation.

References

[1] N.V. Plechkova, K.R. Seddon, Chem. Soc. Rev. 37 (2008) 123.
[2] J.S. Wilkes, P. Wasserscheid, T. Welton, Ionic Liquids in Synthesis, Wiley-VCH Verlag GmbH & Co. KGaA, Weinheim, Germany, 2007.
[3] P. Wasserscheid, T. Welton, Ionic Liquids in Synthesis, Wiley-VCH Verlag GmbH & Co. KGaA, Weinheim, Germany, 2007.
[4] J.F. Wishart, Energy Environ. Sci. 2 (2009) 956.
[5] M. Seiler, A. Kühn, F. Ziegler, X. Wang, Ind. Eng. Chem. Res. 52 (2013) 16519.
[6] D. Zheng, L. Dong, W. Huang, X. Wu, N. Nie, Renew. Sustainable Energy Rev. 37 (2014) 47.
[7] P. Wasserscheid, M. Seiler, ChemSusChem 4 (2011) 459.
[8] M. Khamooshi, K. Parham, U. Atikol, Adv. Mech. Eng. 2013 (2013) 1.
[9] P. Srikhirin, S. Aphornratana, S. Chungpaibulpatana, Renew. Sustainable Energy Rev. 5 (2000) 343.
[10] C.P. Fredlake, J.M. Crosthwaite, D.G. Hert, S.N.V.K. Aki, J.F. Brennecke, J. Chem. Eng. Data 49 (2004) 954.
[11] J.M. Crosthwaite, M.J. Muldoon, J.K. Dixon, J.L. Anderson, J.F. Brennecke, J. Chem. Thermodyn. 37 (2005) 559.
[12] D. Rengstl, V. Fischer, W. Kunz, Phys. Chem. Chem. Phys. 16 (2014) 22815.
[13] C. Maton, N. De Vos, C.V. Stevens, Chem. Soc. Rev. 42 (2013) 5963.
[14] M. Kosmulski, J. Gustafsson, J.B. Rosenholm, Thermochim. Acta 412 (2004) 47.
[15] J. Salgado, J.J. Parajó, J. Fernández, M. Villanueva, J. Chem. Thermodyn. 74 (2014) 51.
[16] Y. Cao, T. Mu, Ind. Eng. Chem. Res. 53 (2014) 8651.
[17] F. Heym, B.J.M. Etzold, C. Kern, A. Jess, Green Chem. 13 (2011) 1453.
[18] N. Calvar, E. Gómez, E.A. Macedo, Á. Domínguez, Thermochim. Acta 565 (2013) 178.
[19] H. Tokuda, K. Hayamizu, K. Ishii, M.A.B.H. Susan, M. Watanabe, J. Phys. Chem. B 108 (2004) 16593.
[20] J. Salgado, M. Villanueva, J.J. Parajó, J. Fernández, J. Chem. Thermodyn. 65 (2013) 184.
[21] M. Villanueva, A. Coronas, J. García, J. Salgado, Ind. Eng. Chem. Res. 52 (2013) 15718.
[22] H.L. Ngo, K. LeCompte, L. Hargens, A.B. McEwen, Thermochim. Acta 357–358 (2000) 97.
[23] H. Shirota, T. Mandai, H. Fukazawa, T. Kato, J. Chem. Eng. Data 56 (2011) 2453.
[24] L.C. Thomas, Modulated DSC: Measurement of Glass Transitions and Enthalpic Recovery. TA-Instruments Series, Paper 5, 2005.
[25] M. Yoshizawa-Fujita, Y. Kousa, K. Kidena, A. Ohira, Y. Takeoka, M. Rikukawa, Phys. Chem. Chem. Phys. 13 (2011) 13427.
[26] J.N. Hay, in: E.L. Charsley, S.B. Warrington (Eds.), Thermal Analysis Techniques and Applications, The Royal Society of Chemistry, Cambridge, 1992, pp. 156–179.
[27] M. Anouti, L. Timperman, Phys. Chem. Chem. Phys. 15 (2013) 6539.
[28] P. Nockemann, K. Binnemans, B. Thijs, T.N. Parac-Vogt, K. Merz, A.-V. Mudring, P.C. Menon, R.N. Rajesh, G. Cordoyiannis, J. Thoen, J. Leys, C. Glorieux, J. Phys. Chem. B 113 (2009) 1429.
[29] Q.-S. Liu, M. Yang, P.-F. Yan, X.-M. Liu, Z.-C. Tan, U. Welz-Biermann, J. Chem. Eng. Data 55 (2010) 4928.
[30] K. Machanová, Z. Wagner, A. Andresová, J. Rotrekl, A. Boisset, J. Jacquemin, M. Bendová, J. Solution Chem. 44 (2015) 790.
[31] S.C. Stefan, D. Lemordant, P. Biensan, C. Siret, B. Claude-Montigny, J. Therm. Anal. Calorim. 102 (2010) 685.
[32] P. Wachter, H.G. Schweiger, F. Wudy, H.J. Gores, J. Chem. Thermodyn. 40 (2008) 1542.
[33] N.M. Yunus, M.I. Abdul Mutalib, Z. Man, M.A. Bustam, T. Murugesan, J. Chem. Thermodyn. 42 (2010) 491.
[34] P. Verdía, M. Hernaiz, E.J. González, E.A. Macedo, J. Salgado, E. Tojo, J. Chem. Thermodyn. 69 (2014) 19.
[35] R. Tao, G. Tamas, L. Xue, S.L. Simon, E.L. Quitevis, J. Chem. Eng. Data 59 (2014) 2717.
[36] B. Bittner, R.J. Wrobel, E. Milchert, J. Chem. Thermodyn. 55 (2012) 159.
[37] T.J. Wooster, K.M. Johanson, K.J. Fraser, D.R. MacFarlane, J.L. Scott, Green Chem. 8 (2006) 691.
[38] D.S. Ayou, M.R. Currás, D. Salavera, J. García, J.C. Bruno, A. Coronas, Energy Convers. Manage. 84 (2014) 512.
[39] E.B. Fox, L.T. Smith, T.K. Williamson, S.E. Kendrick, Energy Fuels 27 (2013) 6355.

JCT 15-250

4.2 Density and viscosity study of pyridinium based ionic liquids as potential absorbents for natural refrigerants: Experimental and modelling

- This article is the product of the collaboration between the Thermophysical Properties of Fluids and Biomaterials group (Universidad de Santiago de Compostela) and the Applied Physics Department (Universidad de Vigo).
- P.B.S. has measured density and viscosity of the pure ionic liquids and applied the Hard Sphere model to pure ILs and mixtures to model viscosity.
- P.B.S redacted a major part of the manuscript under the supervision of J.G.

Fluid Phase Equilibria 405 (2015) 37–45

Contents lists available at ScienceDirect

Fluid Phase Equilibria

journal homepage: www.elsevier.com/locate/fluid

Density and viscosity study of pyridinium based ionic liquids as potential absorbents for natural refrigerants: Experimental and modelling

Pablo B. Sánchez[a], Moisés R. Currás[a], Marta M. Mato[a], Josefa Salgado[b,*], Josefa García[a,*]

[a] Department of Applied Physics, University of Vigo, 36310 Vigo, Spain
[b] Department of Applied Physics, University of Santiago de Compostela, 15782 Santiago de Compostela, Spain

ARTICLE INFO

Article history:
Received 31 March 2015
Received in revised form 16 June 2015
Accepted 25 June 2015
Available online 18 July 2015

Keywords:
Ionic liquids
Density
Viscosity
PC-SAFT
Hard-sphere

ABSTRACT

In this work, density and viscosity of two pyridinium based ionic liquids; 1-ethylpyridinium bis(trifluoromethylsulfonyl)imide, [C_2py][NTf_2], and 1-ethylpyridinium triflate, [C_2py][OTf] as well as [C_2py][OTf] + H_2O mixtures have been studied from experimental and theoretical point of view. Density and viscosity were measured, at several temperatures and atmospheric pressure. A linear equation and Vogel–Fulcher–Tammann equation correlated successfully density and viscosity behaviour. Coefficient of thermal expansion of pure ILs and their mixtures with water together with the excess molar volume and viscosity deviation of mixtures were also calculated. Excess molar volumes and viscosity deviations were described using a Redlich–Kister equation. Regarding to theoretical approach, PC-SAFT was used to model volumetric behaviour whereas Hard Sphere theory was used to study viscosity. The obtained results for pure ILs are satisfactory for both models, but for [C_2py][OTf] + H_2O mixtures the deviations are higher.

1. Introduction

Compression refrigeration systems have covered the predominant part of heating and cooling needs over the last decades. However these systems require an intensive use of electrical energy. Thus, energy saving solutions should be considered for the future. In this context, absorption technology could represent a suitable alternative to compression devices since absorption machines are mainly powered by external heat (waste heat, renewable energies as solar, etc.). So, electrical energy consumption is reduced drastically. Besides this advantage, absorption technology suffers from several problems as low efficiencies and also conventional working pairs present several drawbacks. For instance, NH_3/H_2O presents low system performance, necessity of using rectification towers or high driving heat source temperature as main problems. In case of H_2O/LiBr, the low operating pressure, crystallization and corrosion are the main difficulties. Thus, ionic liquids (ILs) have gained attention in both experimental and theoretical research as potential absorbents for heat pumps due to their possibilities of improving the performance of conventional working pairs.

Knowledge about thermophysical properties of refrigerant/absorbent systems is essential to design new absorption cycles, to scale up process equipment and to determine the heat pumps performance. In this work, two important properties, density and viscosity were studied to characterize new potential absorbents based on ILs. High densities would help to minimize the overall size of absorption equipment [1], and thus, the manufacture and the cost will be lower. In addition, density is also important to calculate other properties as dynamic viscosity or the performance of the absorption cycles. Regarding to viscosity, that influences heat and mass transfer, it should be as low as possible in order to reduce pumping power consumption and allow a high heat transfer.

After studying a bunch of ILs, most of them based on imidazolium cation, Khamooshi et al. [2] concluded that H_2O/ionic liquid working pairs have several advantages against the conventional working fluids (NH_3/H_2O and H_2O/LiBr). For example, these compounds could resolve the problems of crystallization, corrosion, toxicity, flammability, etc. Nevertheless, coefficient of

Abbreviations: IL, ionic liquid; [C_2py][NTf_2], 1-ethylpyridinium bis(trifluoromethylsulfonyl)imide; [C_2py][OTf], 1-ethylpyridinium triflate; DEHP, di(2-ethylhexyl) phthalate; DIDP, diisodecyl phthalate; C100, commercial standard; PC-SAFT, perturbed-chain statistical fluid theory; HS, hard-sphere; VFT, Vogel–Fulcher–Tammann; ARDs, average relative deviations; DMAX, maximum deviations; COP, coefficient of performance.

* Corresponding authors. Tel.: +34 986818753.
E-mail address: fafina@uvigo.es (J. García).

http://dx.doi.org/10.1016/j.fluid.2015.06.043
0378-3812/

List of symbols

M	molecular mass
m	number of segments of PC-SAFT
N	Avogadro constant
R	constant of ideal gas
R_η	roughness factor
s	standard error of estimate
T	absolute temperature
V	specific volume
V_r	reduced specific volume
V_0	close-packed volume
V^E	excess molar volumes
$\bar{V}_i^{E,\infty}$	partial molar volumes at infinite dilution of component i
x	mole fraction
Z	compressibility factor
α_p	isobaric coefficient of thermal expansion
$\Delta\eta$	viscosity deviation
ε	dispersive interaction energy of PC-SAFT
ε^{AiBi}	association energy of PC-SAFT
η	viscosity
$\eta^*_{\exp}$	reduced viscosity
κ^{AiBi}	effective association volume of PC-SAFT
ρ	density
σ	diameter of segment of PC-SAFT

performance (COP) is lower and the circulation ratio is higher than those obtained for conventional working pairs, due to the ILs high viscosity. Therefore, the cycle must operate with high circulation ratio, provoking the growth of energy requirements. In addition, ILs containing halides or tetrafluoroborate anions may give rise to corrosion problems or to generate HF in presence of water [3]. Thus, new ILs should be explored in order to find those with optimal thermophysical properties. Recently, Królikowska et al. [4,5] have proposed several ILs such as *N*-octylisoquinolinium thiocyanate, 1-butyl-1-methylpiperidinium dicyanamide or 1-butyl-1-methylpyrrolidinium dicyanamide for H_2O as alternative working pairs for the absorption heat pump cycle.

In this work, two pyridinium-based ionic liquids were considered, 1-ethylpyridinium bis(trifluoromethylsulfonyl)imide, $[C_2py][NTf_2]$, and 1-ethylpyridinium triflate, $[C_2py][OTf]$. Up to our knowledge, density and viscosity of these pyridinium-based ionic liquids cannot be found in literature. Density and viscosity of $[C_2py][OTf]$ and $[C_2py][NTf_2]$ (dry and hydrated) were measured at several temperatures and correlated with a linear and exponential equation respectively. Only $H_2O + [C_2py][OTf]$ mixtures were experimentally determined since $[C_2py][NTf_2]$ is not miscible in water. It is well known that, ILs containing $[NTf_2]^-$ anion provoke immiscibility in water mixtures [6].

From experimental density data, the isobaric coefficient of thermal expansion, α_p, of $[C_2py][NTf_2]$, $[C_2py][OTf]$ and $H_2O + [C_2py][OTf]$ system was obtained, since it is necessary to dimension the absorption system. Furthermore, excess molar volume and viscosity deviation were also calculated from density and viscosity experimental data and were correlated with Redlich–Kister type equation. From this data, mixture behaviour was studied, providing useful information for the application.

Previously, phase transitions and thermal stability of these ionic liquids had been analysed [7], concluding that no detectable change was observed at temperatures lower than 260 °C. Thus, from point of view of the application, both ILs present a suitable thermal stability.

Furthermore, models with strong physical background have used to study deeply ILs behaviour. Perturbed-chain statistical fluid theory, PC-SAFT, and hard-sphere, HS, were tested to analysed volumetric and viscometric behaviour, respectively, for $[C_2py][NTf_2]$ and $[C_2py][OTf]$ together with $H_2O + [C_2py][OTf]$ mixtures. Up to now, and up to our knowledge, PC-SAFT model was used to correlate and to predict thermophysical properties in H_2O + IL systems by Chen et al. [8], Passos et al. [9], Shahriari et al. [10], Domańska et al. [11] and Paduszyński et al. [12].

Hard Sphere (HS) theory, developed by Dymond and Assael [13,14] with the aim of modelling transport properties, was used to model viscosity. HS theoretical background should be placed on original Enskog hard sphere theory that had been able to predict transport properties of gases with high accuracy. However, even though many attempts were made to apply Enskog theory to dense fluids, it presented important limitations and results were not fully satisfactory. Hereby, Dymond and Assael introduced some modifications to original HS theory in order to extend its application to dense fluids. Recently Gaciño et al. [15] applied HS theory to 19 ionic liquids. However, as far as we are concerned, HS have not been used to model viscosity of H_2O + IL mixtures.

2. Experimental

ILs studied are commercially available and supplied by Iolitec, being their purity higher than 99% (Table 1). ILs were dried under vacuum of 0.1 Pa during at least 24 h prior to each measurement series. Water content was measured using a coulometric Karl-Fisher titration (Mettler Toledo DL32) before and after each measurements series, and it was found that there was no significant variation of the water quantity in the samples. Water content for dry $[C_2py][NTf_2]$ and $[C_2py][OTf]$ were 232 ppm and 90 ppm, respectively. The hydrophobic $[C_2py][NTf_2]$ was hydrated under atmospheric conditions until mass remained constant. Water content reached 4399 ppm. $[C_2py][OTf]$ was found to be miscible in the temperature range (283.15–353.15 K). To prepare $[C_2py][OTf] + H_2O$ mixtures, water was purified using a Milli-*Q* Plus system.

Solutions were prepared gravimetrically using a digital balance Sartorius CPA225D with an uncertainty of 0.00001 g. The error on the mole fraction composition of the mixtures induced due to balance uncertainty was estimated to be 5.10^{-5}.

Densities, ρ, of the pure compounds and the corresponding binary systems were measured using a vibrating tube densimeter Anton Paar DMA-4500, with automatic viscosity correction. Cell temperature was controlled by a thermostatic bath PolyScience with an uncertainty of ±0.01 K. The densimeter was calibrated using Milli-*Q* quality water and vacuum, according to the method of Lagourette et al. [16]. The uncertainty estimated in density through selected temperature range was of ±0.0001 g cm^{-3}.

Viscosity, η, of the pure substances and the corresponding binary mixtures were measured using an Anton Paar AMV 200 rolling ball viscometer according with the following equation:

$$\eta = a(\alpha, T) + \frac{b(\alpha, T)}{\rho_{\text{ball}} - \rho_{\text{liq}}} t \quad (1)$$

where a and b are calibration parameters, t, is the measured time using two magnetic sensors that a gold-coated steel ball needs to roll down in a glass capillary inclined an angle, α, filled with sample, a fixed distance, and ρ_{ball} and ρ_{liq} are the density of the ball and the sample, respectively. Temperature was controlled by a thermostatic bath Polyscience with an uncertainty of ±0.01 K.

To verify reproducibility of these measurements, calibration was performed for four inclination angles. Viscometer range goes from 15° to 90°, nevertheless due to the IL high viscosity selected angles

Table 1
Name, Abbreviation, CAS number and purity of the compounds studied in this work.

Name	Abbreviation	CAS number	Purity[a]
1-Ethylpyridinium bis(trifluoromethylsulfonyl)imide	$[C_2py][NTf_2]$	712354-97-7	>99%
1-Ethylpyridinium triflate	$[C_2py][OTf]$	3878-80-6	>99%

[a] Information supplied by Iolitec.

Table 2
Experimental density (ρ/g cm^{-3}) values for $[C_2py][NTf_2]$ and $[C_2py][OTf] + H_2O$ mixtures under pressure of (990 ± 10) hPa.

	$[C_2py][NTf_2]$ water ppm		$x\,[C_2py][OTf] + (1-x)\,H_2O$ molar fraction						
	239	4399	0	0.067	0.183	0.498	0.689	0.893	1
T (K)	ρ (g cm^{-3})								
283.15	1.5516	1.5468	0.9997	1.1764	1.2881	–	–	–	–
293.15	1.5414	1.5366	0.9982	1.1702	1.2802	1.3661	1.3872	1.4019	1.4090
298.15	1.5364	1.5316	0.9970	1.1670	1.2762	1.3619	1.3830	1.3977	1.4048
303.15	1.5314	1.5266	0.9956	1.1637	1.2721	1.3578	1.3788	1.3935	1.4006
313.15	1.5215	1.5166	0.9922	1.1569	1.2640	1.3494	1.3705	1.3852	1.3923
323.15	1.5116	1.5068	0.9880	1.1497	1.2557	1.3411	1.3623	1.3770	1.3841
333.15	1.5019	1.497	0.9832	1.1422	1.2473	1.3328	1.354	1.3688	1.3760
343.15	1.4922	1.4872	0.9778	1.1344	1.2387	1.3244	1.3459	1.3607	1.3678
353.15	1.4826	1.4775	0.9718	1.1263	1.2301	1.3161	1.3377	1.3527	1.3598

Standard uncertainty of ρ *is* $u = \pm 0.0001$ g cm^{-3}.

were 40°, 50°, 60°, 70°. Liquids used to carry out the calibration were Squalane, Di(2-ethylhexyl)phthalate (DEHP) [17], Diisodecyl phthalate (DIDP) [18] and commercial standard, C100, provided by Sigma Aldrich. DEHP and DIDP density and viscosity data were taken from literature. In case of C100, data were provided by Sigma Aldrich. Squalane and DEHP calibration process was made using a 1.8 mm capillary diameter (1.5 mm ball diameter) while DIDP and C100 calibration process required a 3 mm capillary diameter (2.5 mm ball diameter) due to their high viscosity. Calibration parameters (*a, b*) were fitting to a straight line. Five temperatures (25 °C, 37.5 °C, 40 °C, 50 °C, 60 °C) were used in order to build a calibration line for each inclination angle. At the end of calibration process, four calibration lines were obtained for each standard liquid, covering a viscosity range of 1–200 mPa s. Even though uncertainty provided by Anton Paar is 1%, after measurements it was considered that 3% would be a more realistic value.

3. Results and discussion

3.1. Experimental

Density data of dry and hydrated $[C_2py][NTf_2]$ as well as those of $[C_2py][OTf] + H_2O$ mixtures, in the interval 283.15–353.15 K, are reported in Table 2. Over this range, changes in the composition of the mixtures due to the vaporization of water are negligible [19]. Dry $[C_2py][NTf_2]$ density data vary from 1.55 to 1.48 g cm^{-3}, whereas dry $[C_2py][OTf]$ presents lower values ranged from 1.41 to 1.36 g cm^{-3}.

As expected, density grows as molar mass does. $[NTf_2]^-$ based IL presents higher densities than $[OTf]^-$ based IL. Although no references about density of these IL can be found, Yunus et al. [20] observed that this property decreases as the cation alkyl chain increases in $[C_npy][NTf_2]$ (n = 4, 8, 10, 12). Density data of $[C_2py][NTf_2]$, here presented, agree with this tendency. Additionally, a comparison between data of $[C_2py][OTf]$ (in this paper) and $[C_4py][OTf]$ [21] shows similar behaviour.

Fig. 1 shows densities for dry and hydrated $[C_2py][NTf_2]$. It can be observed that density decreases linearly with temperature. Densities of water saturated $[C_2py][NTf_2]$ are slightly lower than the densities of this dry IL (about 0.3%). Thus, from an industrial application point of view, water concentration effect over density is negligible, as it can be the case of the absorption cycles.

In Fig. 2, density trend with temperature for pure $[C_2py][OTf]$ and their mixtures with H_2O can be observed. In the mixtures, as it is expected from the pure compounds data, density decreases with increasing H_2O concentration.

Experimental densities were correlated with temperature using a linear equation:

$$\rho\left(\text{g cm}^{-3}\right) = a + bT \tag{2}$$

The characteristic parameters a and b are given in Table 3 together with the standard error of estimate, s.

$$s = \sqrt{\frac{\sum (Y - Y_i)^2}{N}} \tag{3}$$

being Y the measured value and Y_i the estimation of the adjustment and N the number of experimental data.

In all cases, adjustment lines described very accurately temperature dependence on density; nevertheless, linear fittings are slightly less precise as water concentration grows. Brennecke et al. have already pointed out this pattern [3] caused by the nonlinear behaviour of water density with temperature. Thus, pure water density was fitted to a polynomial equation of grade two.

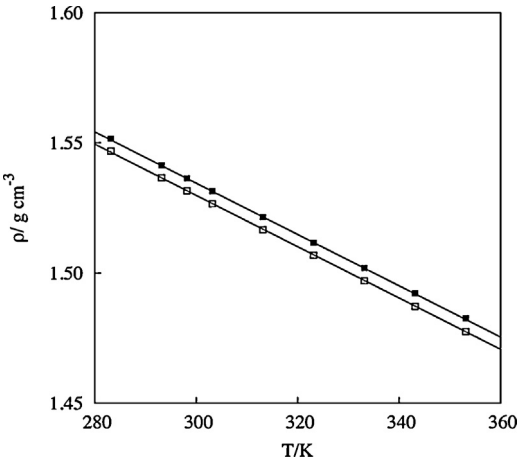

Fig. 1. Experimental density values for $[C_2py][NTf_2]$ dry (■) and hydrated (□). Linear correlations (—).

Table 3
Parameters of linear adjustment ($\rho = a + bT$) for density data.

	$[C_2py][NTf_2]$ water ppm		x $[C_2py][OTf] + (1-x)$ H_2O molar fraction						
	239	4399	0	0.067	0.183	0.498	0.689	0.893	1
	Linear fitting parameters of Eq. (2)								
a (g cm^{-3})	1.8301	1.8264	–	1.3805	1.5233	1.6104	1.6288	1.6423	1.6493
b (10^4/g cm^{-3} K^{-1})	−9.8471	−9.8867	–	−7.1676	−8.2920	−8.3330	−8.2460	−8.2056	−8.2020
s (10^4)	2.3	1.9	–	8.0	3.1	0.4	0.9	1.4	1.3

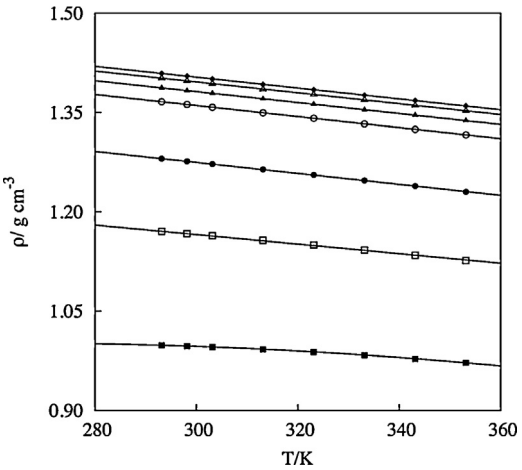

Fig. 2. Experimental density values for x $[C_2py][OTf] + (1-x)$ H_2O mixtures. $x = 0$ (■), $x = 0.067$ (□), $x = 0.183$ (●), $x = 0.498$ (○), $x = 0.689$ (▲), $x = 0.893$ (△), $x = 1$ (♦). Linear correlations (—) except $x = 0$ fitted to grade 2 polynomial equation.

Volumetric properties trends with temperature can be expressed by calculating the coefficient of thermal expansion, α_p, given by:

$$\alpha_p = -\frac{1}{\rho}\left(\frac{\partial \rho}{\partial T}\right)_p \tag{4}$$

Tendency of α_p with temperature for dry ILs and water are shown in Fig. 3. Given that density decreases linearly with temperature, α_p is positive and increases as temperature does for the ILs. Nevertheless, as it is usual, opposite tendency with temperature is found for molecular compounds, such as water. By comparing the ILs coefficient of thermal expansion data, it was found that IL based $[NTf_2]^-$ anion presents a slightly higher expansion than the IL with $[OTf]^-$ anion, 6.39 10^{-4} and 5.86 10^{-4} K^{-1}, respectively at 293.15 K.

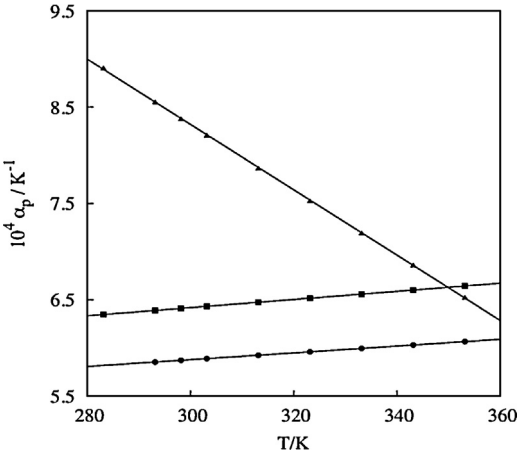

Fig. 3. Isobaric coefficient of thermal expansion for pure $[C_2py][NTf_2]$ (■), $[C_2py][OTf]$ (●) and H_2O (▲). Linear correlations (—).

The difference between α_p, for $[C_2py][NTf_2]$ and $[C_2py][OTf]$ is about 8%. Similar values of α_p were reported by Jacquemin et al. [22] for ammonium and imidazolium with $[NTf_2]^-$ anion. In the case of x $[C_2py][OTf] + (1-x)$ H_2O mixtures α_p increases with temperature in overall range of mole fraction, as it can be seen in Fig. 4. On the other hand, water presence leads to lower densities, and therefore to higher α_p values. This pattern is valid for the whole range of IL mole fractions (x) except for $x = 0.067$. It can be explained due to $\left(\partial\rho/\partial T\right)_p$ value, it remains nearly constant until water concentration reaches the highest value. At this point ($x = 0.067$), $\left(\partial\rho/\partial T\right)_p$ decreases significantly, and consequently α_p does so. Figs. 3 and 4 illustrate that behaviour.

The excess molar volumes, V^E, were calculated from the density values using the equation:

$$V^E = \sum_{i=1}^{n} x_i M_i \left[\left(\frac{1}{\rho}\right) - \left(\frac{1}{\rho_i}\right)\right] \tag{5}$$

where n is the number of components, x_i is the mole fraction of component i in the mixture, M_i its molecular mass, ρ and ρ_i are the experimental density of the mixture and of the pure component, i, respectively. The uncertainty of excess molar volume was estimated to be less than ±0.03 cm^3 mol^{-1}.

A Redlich–Kister-type equation was employed to correlate the V^E data:

$$V^E = x(1-x)\sum_{i=0}^{n} A_i (2x-1)^i \tag{6}$$

where x is the mole fraction of $[C_2py][OTf]$ and A_i, are adjustable coefficients given in Table 4 together with the standard error of estimate, s, previously defined (Eq. (3)).

In Fig. 5, the plot of V^E against mole fraction of $[C_2py][OTf]$ from 293.15 to 353.15 K is presented. As it is usual, for mixtures

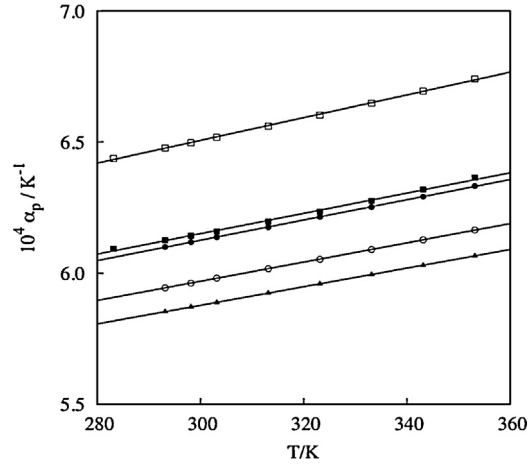

Fig. 4. Isobaric expansion coefficient for x $[C_2py][OTf] + (1-x)$ H_2O mixtures. $x = 0.067$ (■), $x = 0.183$ (□), $x = 0.498$ (●), $x = 0.689$ (○), $x = 0.893$ (▲). Linear correlations (—).

Table 4
Redlich–Kister adjustment coefficient of the excess molar volumes for x [C_2py][OTf] + (1 − x) H_2O mixtures.

T (K)	A_0	A_1	A_2	A_3	s
293.15	1.636	0.473	−0.131	1.744	0.006
298.15	1.741	0.395	0.002	1.619	0.009
303.15	1.815	0.346	0.197	1.446	0.007
313.15	2.012	0.163	0.384	1.316	0.013
323.15	2.186	−0.033	0.603	1.194	0.018
333.15	2.372	−0.092	0.892	0.988	0.019
343.15	2.534	−0.405	0.954	0.959	0.025
353.15	2.714	−0.450	1.112	0.601	0.025

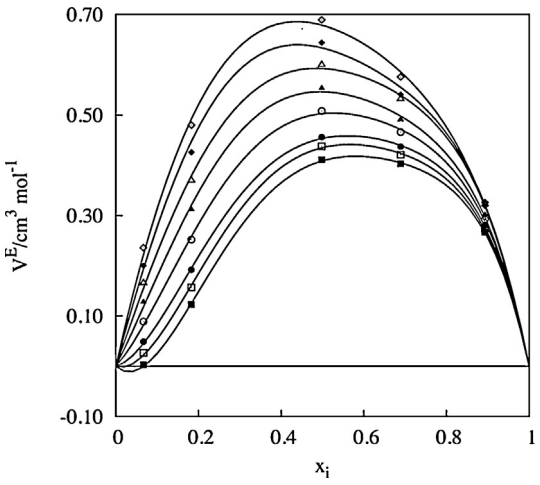

Fig. 5. Excess molar volume, V^E, for x [C_2py][OTf] + (1 − x) H_2O mixtures at different temperatures. 293.15 K (■), 298.15 (□), 303.15 (●), 313.15 (○), 323.15 (▲), 333.15 (△), 343.15 (♦) 353.15 (◊). Redlich–Kister correlations (—).

composed by an IL and a molecular component, the excess molar volumes are small. Positive excess molar volumes are found in overall range of mole fractions. This is in agreement with V^E data for other pyridinium-based ionic liquids with water, reported by Mokhtarani et al. [23] and by García-Miaja et al. [24] At mole fractions of 0.5 the values vary from 0.4 to 0.7 cm^3 mol^{-1} at 293.15 K and 353.15 K, respectively. Positive excess molar volume means that mixtures are less compact than the corresponding pure fluids. This fact is caused by the weakness of unlike-molecules (water-IL) interactions and the water accommodation into the IL network. Moreover, in Fig. 5 we can observe a positive increment of this magnitude with temperature, in special in the dilute region of IL. Thus, calculating the partial molar volumes at infinite dilution, Eqs. (7) and (8), it can be observed that the V^E growth with temperature is more pronounced in the dilute region of IL. Lehman et al. [25] explained this behaviour as a consequence of the hydrogen bond strength. This fact is in agreement with the high concentration of hydroxyl groups of water in this region.

$$\bar{V}_1^{E,\infty} = \sum_{i=0}^{3} A_i(-1)^i \quad (7)$$

$$\bar{V}_2^{E,\infty} = \sum_{i=0}^{3} A_i \quad (8)$$

Eqs. (7) and (8) are associated to infinite dilution of H_2O in [C_2py][OTf] IL, that is, x_{IL} = 0 and IL in H_2O (x_{IL} = 1), respectively. The partial molar volumes at infinite dilution are reported in Table 5.

Viscosity of dry and saturated [C_2py][NTf_2] as well as those of [C_2py][OTf] + H_2O mixtures at several temperatures are summarized in Table 6. As in case of density, influence of alkyl chain length over viscosity was studied by comparing our results with

Table 5
Partial molar volumes at infinite dilution for x [C_2py][OTf] + (1 − x) H_2O mixtures.

T (K)	[C_2py][OTf] + H_2O	
	$\bar{V}_1^{E,\infty}$	$\bar{V}_2^{E,\infty}$
293.15	−0.2713	3.7567
303.15	0.2198	3.8038
313.15	0.9172	3.8752
323.15	1.6278	3.9498
333.15	2.3675	4.1595
343.15	2.9343	4.0423
353.15	3.6749	3.9769

literature values. Viscosity of [C_2py][NTf_2] agrees with tendency found by Yunus et al. [20] for [$C_n$py][NTf_2] (n = 4,8,10,12). Longer cation alkyl chain leads to higher viscosity, which is the opposite trend than it was observed for density.

The three-parameter Vogel–Fulcher–Tammann (VFT) equation was used to correlate experimental viscosities of pure ILs as temperature function:

$$\eta = A \exp\left(\frac{B}{T - T_0}\right) \quad (9)$$

being η the dynamic viscosity, and A, B and T_0 the fitting parameters reported in Table 7 together with the standard error of estimate, s.

Fig. 6 illustrates that viscosity decreases drastically with temperature for dry and water saturated [C_2py][NTf_2]. Viscosity diminishes about 18% at 283.15 K and about 9% at 353.15 K when ILs are saturated. It shows that the influence of water concentration over viscosity is smaller at higher temperature (Table 6 and Fig. 6, Fig. 7). A similar behaviour was found previously by Machanová et al. [26] for other ILs.

The viscosity data of dry [C_2py][OTf] IL are 34% and 22% higher than those of dry [C_2py][NTf_2] at 293.15 K and 353.15 K, respectively. Thus, the nature of anion tends to have less significance when

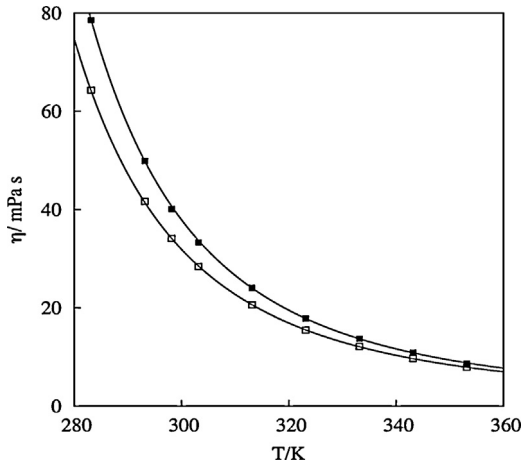

Fig. 6. Experimental viscosity values of [C_2py][NTf_2] dry (■) and hydrated (□). VFT correlations (—).

Table 6
Experimental viscosity (η, mPa s) values of $[C_2py][NTf_2]$ and $x[C_2py][OTf]+(1-x)$ $[H_2O]$ mixtures under pressure of (990 ± 10) hPa.

	$[C_2py][NTf_2]$ water ppm		x $[C_2py][OTf]+(1-x)$ H_2O molar fraction						
	239	4399	0	0.067	0.183	0.498	0.689	0.893	1
T (K)	η (mPa s)								
283.15	78.56	64.31	–	–	–	–	–	–	–
293.15	49.88	41.67	1.00	2.47	5.30	17.69	33.37	65.73	75.20
298.15	40.12	34.11	0.89	2.16	4.60	15.04	27.81	53.20	60.58
303.15	33.32	28.41	0.80	1.90	4.03	13.00	23.54	43.69	48.77
313.15	24.04	20.61	0.65	1.50	3.16	9.96	17.36	30.78	33.78
323.15	17.81	15.47	0.55	1.22	2.55	7.86	13.26	22.52	24.47
333.15	13.70	12.15	0.47	1.02	2.10	6.34	10.46	17.13	18.24
343.15	10.88	9.70	0.40	–	1.76	5.24	8.42	13.40	14.05
353.15	8.68	7.92	0.35	–	–	4.41	6.92	10.74	11.13

Relative uncertainty of η is estimated to be 3%.

Table 7
Parameters of exponential adjustment (VFT equation) for viscosity data.

	$[C_2py][NTf_2]$ water ppm		x $[C_2py][OTf]+(1-x)$ H_2O molar fraction						
	239	4399	0	0.067	0.183	0.498	0.689	0.893	1
	Parameters of Vogel–Fulcher–Tammann Eq. (9)								
T_0 (K)	161.8	163.0	170.2	175.1	165.6	149.1	151.5	157.4	162.5
A (mPa s)	0.1973	0.2181	0.0437	0.0747	0.1082	0.1571	0.1707	0.1790	0.1754
B (K)	726.7	683.0	385.6	413.9	497.0	680.5	747.2	801.6	792.0
s	0.224	0.089	0.003	0.007	0.016	0.023	0.021	0.049	0.184

temperature increases. In addition, the trend of viscosity with the anion is, also, opposite to that found for density. In other words, dry $[C_2py][OTf]$ is more viscous and less dense than dry $[C_2py][NTf_2]$ for the whole temperature range. This behaviour, for pyridinium based ionic liquids, could be explained considering ILs as microstructured fluids, in the same way that Jacquemin et al. [22] have done for imidazolium based ionic liquids.

The viscosity deviations, $\Delta\eta$, were calculated from the viscosity of the pure components, η_i, and viscosity of the mixture η_m:

$$\Delta\eta = \eta_m - \sum_{i=1}^{i=N} x_i\eta_i \tag{10}$$

To correlate viscosity deviation with the mole fraction, the following Redlich–Kister equation was used:

$$\Delta\eta = x(1-x)\sum_{i=0}^{n} A_i(2x-1)^i \tag{11}$$

where x is mole fraction of $[C_2py][OTf]$ and A_i, are adjustable coefficients given in Table 8 together with the standard error of estimate, s, at temperatures from 293.15 K to 353.15 K.

Negative viscosity deviations were found for nearly all data points presented in Fig. 8. Positive values can be attributed to experimental uncertainties, even though temperature might also have some influence on it. These results are consistent with excess molar volumes (Fig. 5). Weakening of interactions between

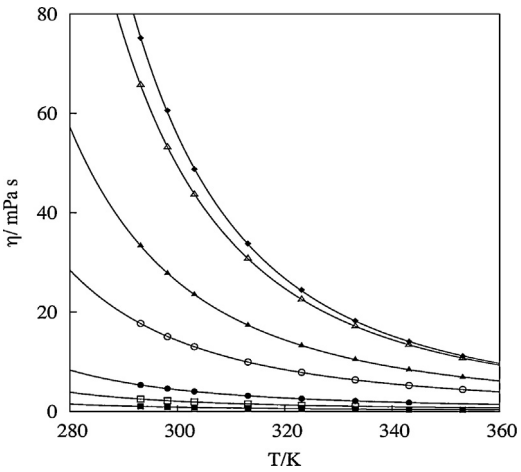

Fig. 7. Experimental viscosity values of x $[C_2py][OTf]+(1-x)$ H_2O mixtures. $x=0$ (■), $x=0.067$ (□), $x=0.183$ (●), $x=0.498$ (○), $x=0.689$ (▲), $x=0.893$ (△), $x=1$ (♦). VFT correlations (—).

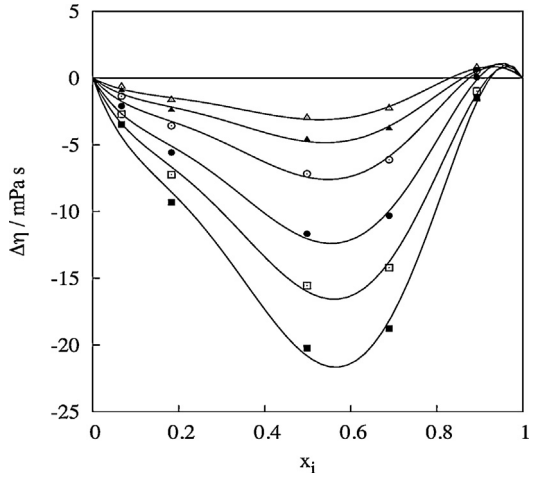

Fig. 8. Viscosity deviation, $\triangle\eta$, for x $[C_2py][OTf]+(1-x)$ H_2O mixtures at different temperatures. 293.15 K (■), 298.15 (□), 303.15 (●), 313.15 (○), 323.15 (▲), 333.15 (△). Redlich–Kister correlations (—).

Table 8
Coefficients of the Redlich–Kister adjustment of the viscosity deviations for x [C_2py][OTf] + (1 − x) H_2O mixtures.

T (K)	A_0	A_1	A_2	A_3	s
293.15	−83.47	−47.17	68.54	122.18	1.48
298.15	−64.11	−34.21	53.82	93.22	1.11
303.15	−48.24	−23.83	46.19	76.65	0.91
313.15	−29.76	−13.30	31.75	51.67	0.62
323.15	−19.07	−7.36	21.83	34.84	0.42
333.15	−12.37	−3.72	16.85	25.79	0.31

unlike-molecules and packing effects leading less compact mixtures implies negative viscosity deviations. $\Delta\eta$ becomes less negative as temperature rises, it can be explained regarding to exponential decay of viscosity with temperature that becomes more pronounced for pure IL.

3.2. Modelling

To model volumetric behaviour PC-SAFT equation of state (EoS) developed by Gross and Sadowski [27,28] was used. In terms of the compressibility factor, Z, PC-SAFT EoS is given as:

$$Z = Z^{id} + Z^{hc} + Z^{disp} + Z^{assoc} \quad (12)$$

where (id) is the ideal gas contribution, (hc) is the hard-chain term, (disp) is the dispersive part and (assoc) is the contribution due to association. The first three terms depend on three pure molecular parameters (m, σ_i and ε_i) that represent the chain length, the segment diameter and the dispersive energy per segment, respectively. Regarding to the association contribution, two pure-component parameters determine the associating: the association energy (ε^{AiBi}) and the effective association volume (κ^{AiBi}). A_i and B_i are the association sites of pure components i. So, five parameters are necessary when association is taken into account. In general, to obtain cross-association parameters between two different associating substances i and j, simple combining rules for cross-association were suggested by Wolbach and Sandler [29], which were used in this work.

The parameters for water were taken from literature [28], whereas for [C_2py][NTf_2] and [C_2py][OTf], were optimized using densities measured in this work at atmospheric pressure and several temperatures using the software developed by Pfohl et al. [30]. A 2B scheme was used (one associating site) because quite good results were obtained to represent the volumetric behaviour. This scheme was used by authors such as Passos et al. [9], Rahmati-Rostami et al. [31]. Other authors [8,12,32] have used more than one associating site. Table 9 shows fitted parameters together with the average relative deviations (ARDs %) for the correlations:

$$\text{ARD\%} = 100 \cdot \left(\frac{Y_{exp} - Y_{cal}}{Y_{exp}} \right) \quad (13)$$

where Y is the corresponding property.

Fig. 9 shows density correlations at atmospheric pressure of selected ILs using PC-SAFT with the parameters from Table 9. The ARDs% obtained are lower than 0.5% in the temperature range 283.15–353.15 K. With the same parameters densities of mixtures were predicted. In Fig. 10, it can be seen that the model predicts fairly well the volumetric behaviour at high mole fractions of IL (the relative deviations are lower than 2%) in the temperature range 283.15–353.15 K, whereas at low IL mole fractions deviations increase up to 7%. To explain this pattern, it is necessary to clarify that ILs parameters have been optimised using density data shown in Table 2 whereas water parameters have been optimised using saturated densities and vapour pressures, that are out of pressure and temperature ranges where predictions have been made (Fig. 10). Thus, for the higher water concentration, the higher deviations are found.

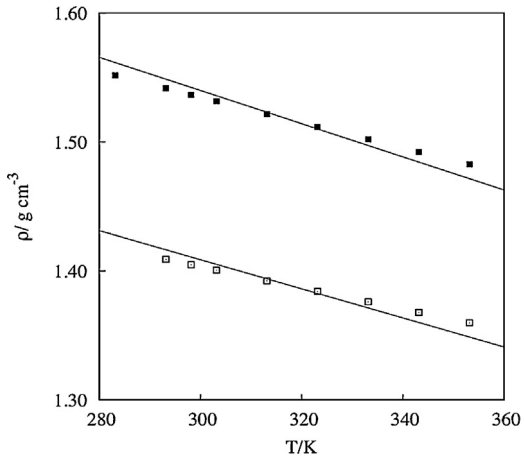

Fig. 9. Experimental density values for [C_2py][NTf_2] (■) and [C_2py][OTf] (□). PC-SAFT correlations (—).

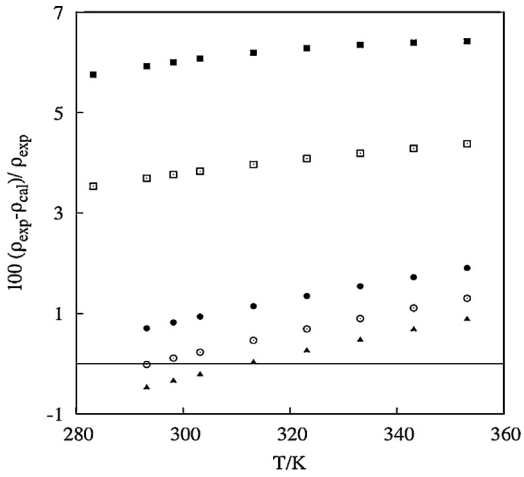

Fig. 10. Deviations between experimental and predicted densities using PC-SAFT for x [C_2Py][OTf] + (1 − x) H_2O system. x = 0.067 (■), x = 0.183 (□), x = 0.498 (●), x = 0.689 (○), x = 0.893 (▲).

HS formulated by Dymond and Assael (DA) uses reduced coefficients instead of calculating transport properties directly. Similar scheme can be used to model thermal conductivity or diffusivity. Regarding to viscosity, Eq. (14) is used to obtain the relation between this transport property and its adimensional equivalent as a function of the specific volume, where η^*_{exp} is reduced viscosity, N is Avogadro constant, M is the molecular mass, R constant of ideal gas, T is the absolute temperature, η is calculated viscosity, V is the specific volume and R_η is the roughness factor; parameter that shows the sphericity deviation of the molecule.

$$\eta^*_{exp} = \frac{16\pi^{1/2}}{5}(2N)^{1/3}\left[\frac{1}{MRT}\right]^{1/2}\frac{\eta V^{2/3}}{R_\eta} \quad (14)$$

Table 9
PC-SAFT characteristic parameters and average relative deviation for IL and H_2O.

	PC-SAFT parameters					Average relative devition (%)		
	σ (Å)	m	ε/k_B (K)	ε^{AB}/k_B (K)	κ^{AB}	p_{sat}	ρ_{liqsat}	ρ_{patm}
$[C_2py][NTf_2]$	3.2876	9.5723	272.52	130.67	0.02793			0.4
$[C_2py][OTf]$	3.0877	9.0344	292.89	126.54	0.02989			0.5
H_2O [8]	3.0007	1.0656	366.51	2500.7	0.03487	1.9	6.8	

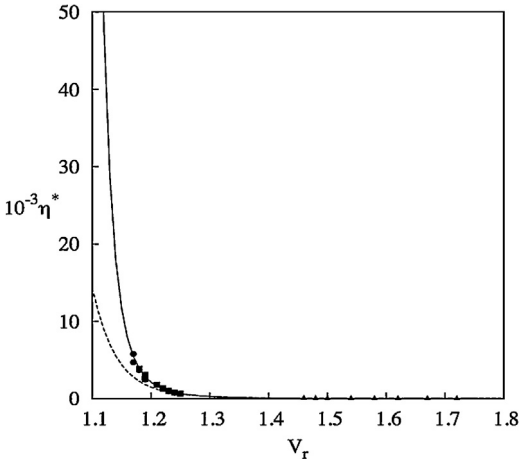

Fig. 11. Universal curves obtained using Ciotta (—) and Assael parameters (- -). Datapoints for $[C_2py][NTf_2]$ (■), $[C_2py][OTf]$ (●) and H_2O (▲).

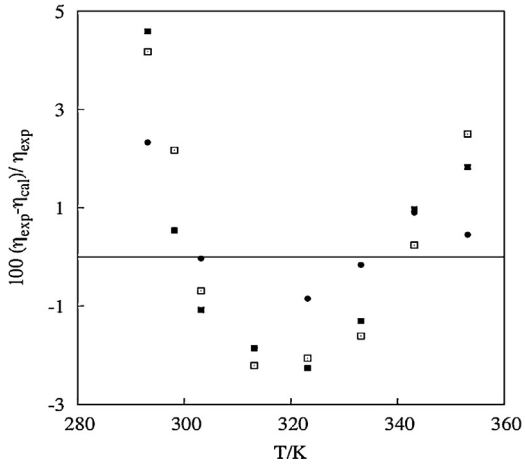

Fig. 12. Deviations between experimental viscosity values and HS calculated values for $[C_2py][NTf_2]$ (■), $[C_2py][OTf]$ (□) and H_2O (●).

On the other hand, universal curves were extrapolated for V_0/V values higher than 0.66, upper limit for original Enskog theory. These universal curves relate reduced coefficients with reduced specific volume (V_r), coefficient between specific volume (V) and close-packed volume (V_0) by using some experimentally determined parameters. Recently, Ciotta et al. have published an extent to Assael works with new parameters [33] improving the model capacity for high dense fluids (Eq. (15)),

$$\log_{10}\left(\eta^*_{exp}\right) = \sum_{i=0}^{i=N} a_i \left(\frac{1}{V_r}\right)^i \tag{15}$$

Universal curves are shown in Fig. 11 to illustrate differences between DA and Ciotta paremeters. Both parameters lead to same curves if V_r is higher than 1.2, otherwise Ciotta parameters will provide better results than initial DA values. Therefore, Ciotta parameters have been used in this work.

Over the last decades HS has been applied to model different families of molecular compounds [13–15,34,35]. Recently Gaciño et al. applied successfully HS theory to 19 ionic liquids obtaining an ARD of 2,3% [15]. In this work, H_2O, $[C_2py][OTf]$, $[C_2py][NTf_2]$ viscosity have been modelled with HS. Results (Fig. 12) confirm HS as a powerful tool to model ionic liquids transport properties. Average deviations were 0.89%, 1.96%, 1.80% while maximum deviations (DMAX) were 2.33%, 4.17%, 4.59% for H_2O, $[C_2py][OTf]$, $[C_2py][NTf_2]$, respectively.

By assuming that mixtures behave in the same way than pure compounds, Assael proposed mixing rules (Eqs. (16) and (17)). This procedure has been tested for alkane mixtures [34] and alkane alkylbenzene mixtures [35].

$$V_{0,m} = \sum_i x_i V_{0,i} \tag{16}$$

$$R_{\eta,m} = \sum_i x_i R_{\eta,i} \tag{17}$$

While it has worked well for alkane mixtures, it was unable to model mixtures of alkylbenzenes and alkanes. Hereby, HS have been applied to x $[C_2py][OTf] + (1-x)$ H_2O mixtures, using input data from pure components. Deviations obtained were out of the expected range with DMAX values up to 100%. Therefore an interaction parameter (d) was introduced to calculated $V_{0,m}$. According with this modification, Eq. (16) becomes:

$$V_{0,m} = x_1 V_{0,1} + x_2 V_{0,2} + x_1 x_2 d \tag{18}$$

However, deviations are still considerably high, DMAX values up to 21% and ARD values up to 6%. Due to lack of physical significance of the introduced parameter and deviations obtained, to our concern, this modification does not increase the versatility of HS theory as a modelling tool for IL-water mixtures.

4. Summary and conclusions

Density and viscosity of $[C_2py][NTf_2]$ and x $[C_2py][OTf] + (1-x)$ H_2O mixtures have been studied from an experimental and theoretical point of view. Main results can be summarized as follows:

- Measurements have been taken in a temperature range of 283.15–353.15 K and atmospheric pressure. Density decreases linearly with temperature whereas viscosity decreases exponentially. Linear and VFT equations were used to correlate density and viscosity data, respectively.
- Experimental results have shown different trends for density and viscosity: $\rho_{[C2py][NTf2]} > \rho_{[C2py][OTf]}$ and $\eta_{[C2py][OTf]} > \eta_{[C2py][NTf2]}$.
- Density and viscosity of $[C_2py][NTf_2]$ (dry and hydrated) together with those of x $[C_2py][OTf] + (1-x)$ H_2O mixtures were measured at different IL mole fractions. The effect of water concentration over density and viscosity has been clarified. Viscosity decreases sharply as water concentration grows up while density dependence on water concentration is much smoother.
- Mixture properties, such as excess molar volume and viscosity deviation have been calculated. Positive excess molar volumes

and negative viscosity deviations were found all over IL concentration range. These results are consistent, and they are caused by weaker interactions of IL-IL and H_2O–H_2O and packing effects of water into IL network.

- PC-SAFT was used to model *pVT* behaviour. ILs characteristic parameters were optimised using measured density data. Density of pure ILs was modelled satisfactorily, however x $[C_2py][OTf] + (1-x)$ H_2O densities are well predicted for high IL concentration (2% deviation) while deviation increases until 7% for high water concentrations.
- HS theory was used to model viscosity. Reasonably good results were obtained for pure IL (deviations under 2%), nevertheless when applying this model to x $[C_2py][OTf] + (1-x)$ H_2O mixtures, it was not possible to predict viscosities with acceptable deviations. Same scheme could be reproduced using diffusivity and thermal conductivity to validate obtained results.
- From the application point of view, ILs should present high density and mainly, low viscosity. Since viscosity represents one the main barriers for ILs applications, factors such as dependency on temperature and water presence should be considered in order to reduce viscosity. Other properties should be analysed to find a suitable IL for absorption heat pumps: liquid range, heat capacity, mixing enthalpy or factors such as toxicity. These studies will be treated in a near future.

Acknowledgments

This study was financed by the projects DPI2012-38841-C02-02 (Ministerio de Economía y Competitividad of Spain and FEDER) and EM2013/031 (Xunta de Galicia, Spain) and the network REGALIS R2014/015 (Xunta de Galicia, Spain). Pablo B. Sánchez thanks to Ministerio de Economia y Competitividad of Spain for his PhD Grant framed in Plan Estatal de Investigación Científica y Técnica y de Innovación 2013–2016.

References

[1] M.R. Currás, M.F. Costa Gomes, P. Husson, A.A.H. Padua, J. Garcia, J. Chem. Eng. Data 55 (2010) 5504.
[2] M. Khamooshi, K. Parham, U. Atikol, Adv. Mech. Eng. 2013 (2013) 1.
[3] J.F. Brennecke, H. Rodríguez, J. Chem. Eng. Data 51 (2006) 2145.
[4] M. Królikowska, M. Zawadzki, M. Królikowski, J. Chem. Thermodyn. 70 (2014) 127.
[5] M. Królikowska, K. Paduszyński, M. Zawadzki, J. Chem. Eng. Data 58 (2013) 285.
[6] E.J. González, E.A. Macedo, Fluid Phase Equilib. 383 (2014) 72.
[7] P.B. Sánchez, J.J. Parajó, J. Garcia, M. Villanueva, J. Salgado, Thermal analysis of pyridinium and choline based ionic liquids, in: International workshop on Ionic Liquids WILS 2014, March 24–25, 2014, Concepción (Chile), Elsevier, 2014.
[8] Y. Chen, F. Mutelet, J.-N. Jaubert, J. Phys. Chem. B 116 (2012) 14375.
[9] H. Passos, I. Khan, F. Mutelet, M.B. Oliveira, P.J. Carvalho, L.M.N.B.F. Santos, C. Held, G. Sadowski, M.G. Freire, J.A.P. Coutinho, Ind. Eng. Chem. Res. 53 (2014) 3737.
[10] R. Shahriari, M.R. Dehghani, B. Behzadi, Ind. Eng. Chem. Res. 51 (2012) 10274.
[11] U. Domańska, M. Zawadzki, K. Paduszyński, M. Królikowski, J. Phys. Chem. B 116 (2012) 8191.
[12] K. Paduszyniski, U. Domaníska, J. Phys. Chem. B 116 (2012) 5002.
[13] M.J. Assael, J.H. Dymond, M. Papadaki, P.M. Patterson, Int. J. Thermophys. 13 (1992) 269.
[14] M.J. Assael, M. Papadaki, P.M. Patterson, J.H. Dymond, Fluid Phase Equilib. 75 (1992) 245.
[15] F.M. Gaciño, M.J.P. Comuñas, J. Fernández, S.K. Mylona, M.J. Assael, Int. J. Thermophys. 35 (2014) 812.
[16] B. Lagourette, C. Boned, H. Saint-Guirons, P. Xans, H. Zhou, Meas. Sci. Technol. 3 (1992) 699.
[17] K.R. Harris, J. Chem. Eng. Data 54 (2009) 2729.
[18] K.R. Harris, S. Bair, J. Chem. Eng. Data 52 (2007) 272.
[19] M. Zaoui-Djelloul-Daouadji, A. Negadi, I. Mokbel, L. Negadi, J. Chem. Thermodyn. 69 (2014) 165.
[20] N.M. Yunus, M.I. Abdul Mutalib, Z. Man, M.A. Bustam, T. Murugesan, J. Chem. Thermodyn. 42 (2010) 491.
[21] H. Guerrero, S. Martín, V. Pérez-Gregorio, C. Lafuente, I. Bandrés, Fluid Phase Equilib. 317 (2012) 102.
[22] J. Jacquemin, P. Husson, A.A.H. Padua, V. Majer, Green Chem. 8 (2006) 172.
[23] B. Mokhtarani, A. Sharifi, H.R. Mortaheb, M. Mirzaei, M. Mafi, F. Sadeghian, J. Chem. Thermodyn. 41 (2009) 323.
[24] G. García-Miaja, J. Troncoso, L. Romaní, J. Chem. Eng. Data 52 (2007) 2261.
[25] J. Lehmann, M.H. Rausch, A. Leipertz, A.P. Fröba, J. Chem. Eng. Data 55 (2010) 4068.
[26] K. Machanová, A. Boisset, Z. Sedláková, M. Anouti, M. Bendová, J. Jacquemin, J. Chem. Eng. Data 57 (2012) 2227.
[27] J. Gross, G. Sadowski, Ind. Eng. Chem. Res. 40 (2001) 1244.
[28] J. Gross, G. Sadowski, Ind. Eng. Chem. Res. 22 (2002) 5510.
[29] J.P. Wolbach, S.I. Sandler, Ind. Eng. Chem. Res. 37 (1998) 2917.
[30] O. Pfohl, S. Petkov, G. Brunner, Usage of PE. A Program to Calculate Phase Equilibria, Herbert Utz Verlag, München, 1998, ISBN: 3-89675-410-6.
[31] M. Rahmati-Rostami, B. Behzadi, C. Ghotbi, Fluid Phase Equilib. 309 (2011) 179.
[32] M.B. Oliveira, F. Llovell, J.A.P. Coutinho, L.F. Vega, J. Phys. Chem. B 116 (2012) 9089.
[33] F. Ciotta, J.P.M. Trusler, V. Vesovic, Fluid Phase Equilib. 363 (2014) 239.
[34] M.J. Assael, J.H. Dymond, M. Papadaki, P.M. Patterson, Int. J. Thermophys. 13 (1992) 659.
[35] M.J. Assael, A.E. Kalyva, K.E. Kakosimos, K.D. Antoniadis, Int. J. Thermophys. 30 (2009) 1733.

4.3 Studies of Volumetric and Transport Properties of Ionic Liquid-Water Mixtures and Its Viability To Be Used in Absorption Systems

- This article is the product of the collaboration between the Thermophysical Properties of Fluids and Biomaterials group (Universidad de Santiago de Compostela), the Analytical Chemistry Department (Universidad de Vigo) and the Applied Physics Department (Universidad de Vigo).
- P.B.S. has carried out the all the experimental measurements and applied the correlation equations to describe physical properties.
- P.B.S redacted a major part of the manuscript under the supervision of J.G. and E.G-R.

ACS Sustainable Chemistry & Engineering

Research Article

pubs.acs.org/journal/ascecg

Studies of Volumetric and Transport Properties of Ionic Liquid–Water Mixtures and Its Viability To Be Used in Absorption Systems

Pablo B. Sánchez,[†] Josefa García,[*,†] Josefa Salgado,[‡] and Elisa González-Romero[*,§]

[†]Departamento de Física Aplicada, Universidad de Vigo–Campus Vigo, Lagoas-Marcosende s/n, 36310 Vigo, Spain

[‡]Departamento de Física Aplicada, Universidad de Santiago de Compostela–Campus Vida, 15782 Santiago de Compostela, Spain

[§]Departamento de Química Analítica y Alimentaria, Universidad de Vigo–Campus Vigo, Lagoas-Marcosende s/n, 36310 Vigo, Spain

Supporting Information

ABSTRACT: Binary systems of two ionic liquids (ILs), 1-ethylpyridinium methanesulfonate $[C_2Py][MeSO_3]$ and choline dihydrogen phosphate $[Chol][H_2PO_4]$, and water have been experimentally studied. Density, viscosity, electrical conductivity and proton activity have been measured at several temperatures covering all the miscibility range. From density data, isobaric coefficient of thermal expansion was calculated to study the volumetric behavior of the mixtures. All volumetric data were fit using polynomial equations. The Vogel–Fulcher–Tamman (VFT) equation accurately describes the temperature dependence of viscosity for all systems. Systems based on $[C_2Py][MeSO_3]$ are less dense and viscous than those involving $[Chol][H_2PO_4]$, making $[C_2Py][MeSO_3]$ more suitable for absorption systems where pumping cost has a significant importance. Electrical conductivity data were adjusted using the Casteel–Amis equation. Similar trends were found for both systems, although ionic conductivity is higher for $[C_2Py][MeSO_3]$ + H_2O mixtures. The relation between viscosity and electrical conductivity was also explored. According to Walden plots, ILs present low ionicity; however, internal friction and ionic concentration does not seem to be enough to explain the behavior of ionic conductivity and IL concentration. Proton activity measurements show different tendencies with molar fraction of each IL, $[C_2Py][MeSO_3]$ leads to lower pa_{H+} values than $[Chol][H_2PO_4]$ in the binary mixtures. Results of ionic conductivity and proton activity suggest a higher corrosive potential of $[C_2Py][MeSO_3]$ + H_2O; however, a further analysis needs to be done to evaluate this risk in absorption systems. Finally, a composition analysis based on ionic chromatography (IC) was carried out to obtain insight about its effect on their physicochemical properties.

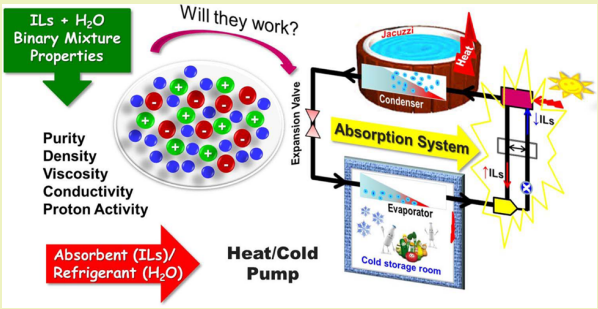

KEYWORDS: *Ionic liquid, Density, Viscosity, Electrical conductivity, Proton activity, Absorbent*

INTRODUCTION

Reducing the footprint of energy production systems is one of the main challenges for scientific and industrial communities. As a consequence, environmentally friendly technologies that may help reduce the use of natural resources are gaining presence and visibility over recent years. Among the consumption sectors, the heating and cooling industry occupies a considerable part of the overall numbers. In this field, one alternative to traditional heat pumps based on compression devices is absorption heat pumps.[1] In absorption systems, thermal energy works as a driving force instead of electric power used for mechanical compressors, thus it brings the opportunity of recovering heat disposal or using solar energy to satisfy heating and cooling demands. Nevertheless, commercial absorption systems based mainly on two working pairs (refrigerant/absorbent), H_2O/LiBr and NH_3/H_2O, present several drawbacks;[2] corrosion and crystallization problems in the case of water and lithium bromide and low relative volatility and toxicity in the case of ammonia and water. Therefore, the use of working pairs based on water and ionic liquid (H_2O/IL) appears as a suitable option[3−5] because their properties are expected to allow an efficient absorption/desorption process and to overcome the disadvantages of the commercial systems. It is important to define the target properties for a fluid to fit the requirements of the absorption process. (i) Wide liquid range renders flexibility for temperatures in the absorber and the generator, liquid–solid transitions and decomposition temperature provide the lower and upper limit of the liquid range.[2] (ii) Heat and mass transfer are crucial for absorption systems to work efficiently, thus low viscosities and high thermal conductivities will improve the performance of the absorption system.[6] (iii) Thermodynamics of the absorption process is also a critical issue for refrigeration systems, negative enthalpies of the mixture (H_2O/IL), negative deviation of

Received: July 6, 2016
Revised: August 11, 2016
Published: August 16, 2016

DOI: 10.1021/acssuschemeng.6b01541
ACS Sustainable Chem. Eng. 2016, 4, 5068–5077

Table 1. Name, Abbreviation, CAS Number, Purity, Molecular Weight and Melting Temperature of the Compounds Studied in This Work

name	abbreviation	CAS Number	purity[a]	MW (g mol^{-1})	T_m (°C)
1-ethylpyridinium methanesulfonate	$[C_2Py][MeSO_3]$	681481-41-4	>95%	203.26	62[25]
choline dihydrogen phosphate	$[Chol][H_2PO_4]$	83846-92-8	>99%	201.16	126[26]

[a]Mass fraction. Information supplied by Iolitec.

Raoult's law and low water vapor pressure are target properties for absorption working pairs.[7] In addition, a low corrosive potential is also important to avoid the problem caused by H_2O/LiBr.

Ionic liquids (ILs) are salts melting under 100 °C.[8] Despite there being no physical significance at that temperature,[9] it has become a commonly used definition. It is also very frequent to talk about room temperature ionic liquids (RTILs), when IL melting temperature is about 20−30 °C. It is again a diffuse definition as there is no unique room temperature and melting points cannot be predicted with accuracy.[10] Because the ILs studied in this work, $[C_2Py][MeSO_3]$ (1-ethylpyridinium methanesulfonate) and $[Chol][H_2PO_4]$ (choline dihydrogen phosphate), are solid at room temperature, a definition based on the chemical structure and the physical and chemical properties was found to be more appropriate.

ILs are usually based on an organic cation and an inorganic polyatomic anion.[11] It leads to unique properties, among them, their very low (but measurable) vapor pressure,[12] wide liquid range (caused by low melting points),[13,14] high thermal stabilities[15] and wide electrochemical windows,[16] make ILs environmental friendly candidates for different applications.[17−19]

Ionic liquids melting above room temperature present some drawbacks when physical characterization needs to be done. Difficulties during the drying process or possible damages in the experimental equipment caused by solidification are issues to deal with. Nevertheless, because industrial applications very often involve mixtures of ILs with different solvents instead of pure components, we have chosen to study the behavior of water + IL mixtures. By doing so, we avoid the problem of manipulating solid ILs and we obtain useful information to evaluate whether studied systems may work satisfactorily as working pairs for absorption heat pumps.

Although the properties of water + IL mixtures have been broadly studied,[20−24] there is still a lack of data of water mixtures for many ILs. Hereby, mixtures of water with two ILs with a relatively high melting point have been studied in the concentration range that solubility allows. Thus, protic and aprotic ILs and water mixtures will be assessed, analyzing their volumetric and dynamic properties, as well as the proton activity of these solutions.

In this work, density and viscosity of two water + IL mixtures, $[C_2Py][MeSO_3]$ and $[Chol][H_2PO_4]$, were measured. These properties provide very useful information for the development of industrial applications. While high densities are usually an advantage that ILs accomplish very often, viscosity values are one the main barriers for the implementation of ILs at industrial scale, mainly for low temperature applications. Nevertheless, it does not seem reliable to reach organic solvent viscosities due to ILs structures and interactions, alternatives such as high temperature applications or mixtures base on ILs together with different solvents may help to reduce the viscosity problem. For that reason, effects of temperature and water concentrations over the aforementioned properties will be discussed. Electrical conductivity, somehow related with other transport properties, is also a remarkable property for ILs, since electrochemical applications usually demand a good ionic mobility. A quantitative analysis of the electrical conductivity and pH (proton activity, a_{H+}) have been carried out to explore the corrosive potential of the studied systems in absorption heat pumps. Moreover, the relationship between all transport properties has been analyzed. Finally, a detailed study of the ILs impurities by ion chromatography has been also included.

EXPERIMENTAL SECTION

Materials and Solutions. Reagents of maximum purity available were purchased from IoLiTec Ionic Liquids Technologies GmbH (Heilbronn, Germany). Some details of the compounds selected for this study are given in Table 1 and its structures in Scheme S1. Solutions were prepared gravimetrically using a digital balance Sartorius CPA225D with an uncertainty of 0.00001 g. The error on the mole fraction composition of the mixtures induced due to balance uncertainty was estimated to be 5.10^{-5}. All reagents used in the chromatographic assays (H_2SO_4 as regenerating agent, $NaHCO_3$ and Na_2CO_3 as mobile phase) and electrolytes as KH_2PO_4 were provided by Sigma-Aldrich. The reagents used as standard solution for the anion quantification by ionic chromatography (analytical grade sodium salts of F^-, Cl^-, Br^-, NO_3^-, PO_4^{3-} with 12 H_2O and SO_4^{2-}) were obtained from Panreac and used as received. All diluted solutions were prepared by using Milli-Q grade water. The molar fraction range studied for each ILs and the correlation to other concentration units (molar, M, and mass percentage, %) are given in Table 2. Notice that the wide concentration range under study is for $[C_2Py][MeSO_3]$ due to both higher solubility and hydroscopic properties observed in comparison with $[Chol][H_2PO_4]$.

Table 2. Equivalence of the Molar Fraction, Mass Percentage and Molar Concentration for the Systems Studied

x_{IL}	%mass	M/mol L^{-1}
	$[C_2Py][MeSO_3]$	
0.0039	4.25	0.21
0.0168	16.15	0.77
0.0317	26.96	1.26
0.0650	43.96	1.97
0.1842	71.81	3.00
0.3830	87.40	3.52
	$[Chol][H_2PO_4]$	
0.0400	4.27	0.21
0.0163	15.58	0.74
0.0316	26.71	1.22
0.0620	42.48	1.85
0.1651	68.82	2.73

APPARATUS AND PROCEDURES

Density and Viscosity Measurements. Density and dynamic viscosity measurements of the pure liquids and mixtures were performed with a rotational viscometer Anton Paar Stabinger SVM3000. The basic operating principles and schematic set up of the Stabinger Viscometer are described and

DOI: 10.1021/acssuschemeng.6b01541
ACS Sustainable Chem. Eng. 2016, 4, 5068−5077

laid down in a European Patent (EP 0 926 481 A2). The density cell is a glass u-tube, which is excited to produce mechanical resonant vibrations according to DIN 51757. The viscosity cell is based on a tube filled with the sample in which a hollow measuring rotor floats. The SVM 3000 uses Peltier elements for fast and efficient thermostatting. The temperature uncertainty (k = 2) is 0.02 K from T = (288.15 to 378.15) K. Over the temperature range studied, the expanded viscosity uncertainty (k = 2, 95% confidence level) is estimated to be 2%.[27] Following the methodology exposed in previous works,[28,29] these uncertainties were checked by means of the viscosity standard oil Cannon N350, with maximum deviations of 0.05% and 1.1%, for density and viscosity, respectively. This apparatus automatically corrects the influence of viscosity on the measured density.

Electrical Conductivity Measurements. The electrical conductivity was measured with a Crison CM35 conductivimeter at different temperatures. The electrodes (two platinum) were placed into the samples at a prefixed temperature. Crison Standard solutions of 0.147, 1.413 and 12.88 mS·cm^{-1} were used for calibration proposes. Further details of the calibration procedure can be found somewhere else.[30] Electrical conductivity uncertainties are estimated to be 1.10^{-2} mS·cm^{-1}.

Proton Activity Measurements. The pH-meter 744 Metrohm was used to obtain the pH measurements. A thermopar is included into the electrode body. When it is not in use, the electrode is kept in KCl 3.5 M. The calibration with standard buffer solutions of pH 4 and 7 (Metrohm) was done prior to measurements, using the Nernst equation:[31]

$$E = E^0 - 0.059\ \mathrm{pH} \quad (1)$$

The 59.0 mV slope change in the electrode potential results from a 10-fold change in the proton concentration of the monovalent ion, H^+ (n = 1), and 2.303RT/nF where R is the universal gas constant, 8.134 JK^{-1} mol^{-1}; F is the Faraday constant, 9.648 × 10^4 C mol^{-1}; T is the absolute temperature in Kelvin and n is the ionic charge of the proton ion.

Notice that the Nernst ions of opposite charge tend to associate into loosely bound ion pairs in more concentrated solutions, thus reducing the number of ions that are free to donate or accept electrons at an electrode. This is because ions in solution interact with each other and with H_2O molecules. In this way, ions behave chemically like they are less concentrated than they really are (or measured). For this reason, the Nernst equation cannot accurately predict half-cell potentials for solutions in which the total ionic concentration exceeds about 10^{-3} M, such as is the case here (Table 2). Then, if the Nernst equation is applied to more concentrated solutions, the term in the equation pH must be expressed in "effective concentrations" or activities of the electroactive ionic species as proton activity, being the Nernst equation[31] expressed as follows:

$$E = E^0 + 0.059/n \log a_{H+} \quad (2)$$

where n is the ionic charge. The activity coefficient γ (gamma) relates the concentration of a proton ion to its activity in a a given solution through the relation $a_{H+} = \gamma\ C_{H+}$

In these experiments, the "effective" proton concentration (proton activity, a_{H+}) is given by the IL and its interactions with water.

Measurements by Ion Chromatography (IC). The ion chromatographic (IC) method is based on ion-exchange separation mechanisms and provides detailed anionic profiles including anionic counterions and impurities. This approach can be used for quality assurance, impurity analysis, and trace-level residue analysis. Therefore, IC system with conductometric detection was used to analyze both ionic liquid (IL) anions, $[MeSO_3]^-$ and $[H_2PO_4]^-$, which better suited the purpose of low-level quantification of anionic profiles and gave us a better knowledge of the impurities content. The chromatographic system (Metrohm, Germany) can be operated with chemical suppression mode (regenerating agents are 50 mM of H_2SO_4 and ultrapure water) with auto step when the loop sample is filled. The following components are included: 792 Basic IC chromatograph equipped with a 20 μL loop Rheodyne injection valve. The column system was a 250 × 4 mm Metrosep A supp 4 (column packing of poly(vinyl alcohol) with quaternary ammonium groups and particle size of 9 μm), guard columns and filters. The program used to record the chromatographic data and Data Acquisition System was the 792 PC Software Version 1.0 (Metrohm Ltd., Switzerland). The eluent was 1.8 mM Na_2CO_3 and 1.7 mM $NaHCO_3$ (standard flow 1 mL. min^{-1} and pH ≈ 10), freshly prepared, which was microfiltered (0.45 μm filter) and degassed (30 min in ultrasonic bath) before use. This mobile phase determined that the system peak appeared at a retention time of 9.97 min under the experimental conditions and column used. The ionic liquids were analyzed at a concentration of around 10 ppm and its solubility in the mobile phase was previously checked to the injection of 20 μL of sample into the chromatographic system.

RESULTS AND DISCUSSION

Volumetric Properties: Density. *Density Measurements.* Densities of $[C_2Py][MeSO_3]$ + H_2O and $[Chol][H_2PO_4]$ + H_2O mixtures at different temperatures are shown in Table S1. Range of concentrations is determined by the miscibility range of the solution, for $[C_2Py][MeSO_3]$ it goes up to 0.3830 whereas for $[Chol][H_2PO_4]$ it increases 0.1651, both referred to the molar fraction of IL. Vaporization of water has limited the upper limit of the temperature range. In all cases, density decreases as temperature goes up, as expected (Figure 1). Data were fit to either linear or to polynomial equations. Linear fittings describe the relation between density and temperature very accurately when the mixture is concentrated in IL, nevertheless, the accuracy of linear fittings decreases as water concentration grows, and thus, polynomial equations of second order were used. Brennecke et al. have already pointed out this pattern[20] caused by the nonlinear behavior of water density with temperature. Fitting parameters together with the R^2 of the fitting are listed in Table S2 (Supporting Information).

Despite the concentrations of IL not being identical for both systems, from Figure 1 it is possible to state that $[Chol][H_2PO_4]$ mixtures are denser than mixtures based on $[C_2Py][MeSO_3]$. Although, higher densities are desirable for working pairs,[32] refrigerant/absorbent, it is not, in general, the key criteria to select working fluids for absorption heat pumps.

Volumetric behavior can also be analyzed by calculating the isobaric coefficient of thermal expansion, α_p, given by

$$\alpha_p = -\frac{1}{\rho}\left(\frac{\partial \rho}{\partial T}\right)_p \quad (3)$$

Trends of α_p with temperature are shown in Figure 2. It can be observed that α_p increases with temperature for all IL concentrations. Note also that the effect of temperature over α_p becomes smaller as IL concentration grows. It leads to a

DOI: 10.1021/acssuschemeng.6b01541
ACS Sustainable Chem. Eng. 2016, 4, 5068−5077

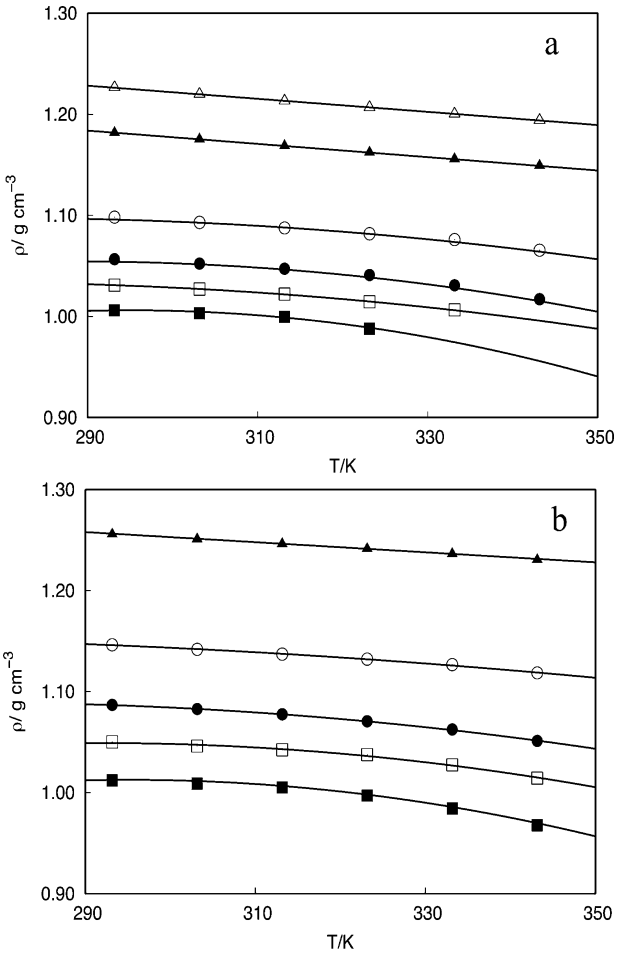

Figure 1. Experimental density values: (a) x $[C_2Py][MeSO_3]$ + (1 − x) H_2O mixtures. x = 0.0039 (■), x = 0.0168 (□), x = 0.0317 (●), x = 0.0650 (○), x = 0.1842 (▲), x = 0.3830 (△). (b) x $[Chol][H_2PO_4]$ + (1 − x) H_2O mixtures. x = 0.0040 (■), x = 0.0163 (□), x = 0.0316 (●), x = 0.0620 (○), x = 0.1651 (▲), fitting lines (—).

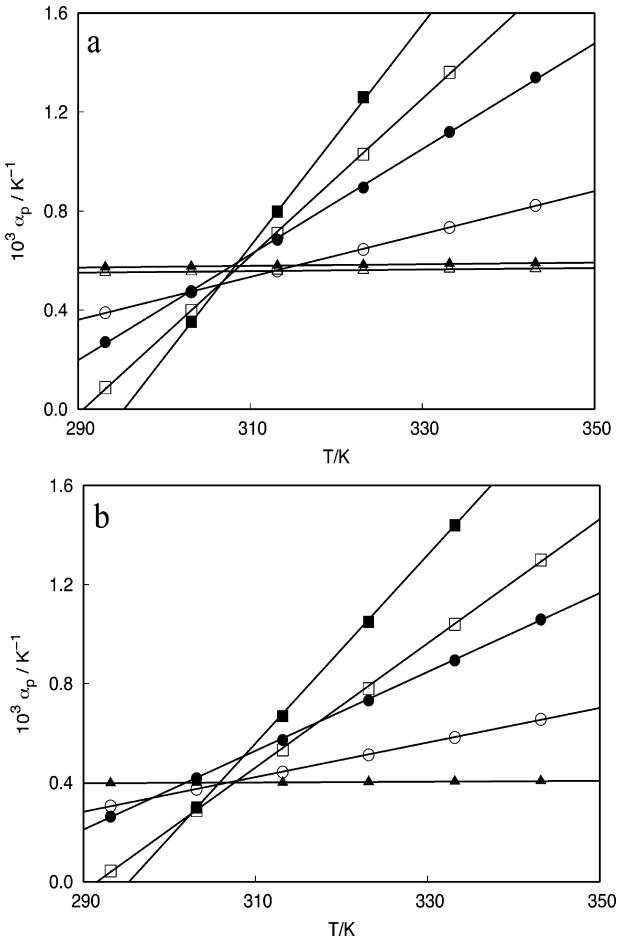

Figure 2. Isobaric expansion coefficients: (a) x $[C_2Py][MeSO_3]$ + (1 − x) H_2O mixtures at several temperatures. x = 0.0039 (■), x = 0.0168 (□), x = 0.0317 (●), x = 0.0650 (○), x = 0.1842 (▲), x = 0.3830 (△). (b) x $[Chol][H_2PO_4]$ + (1− x) H_2O mixtures. x = 0.0040 (■), x = 0.0163 (□), x = 0.0316 (●), x = 0.0620 (○), x = 0.1651 (▲). Fitting lines (—).

crossover at about 310 K, the explanation yields on the density dependence on temperature for different IL concentrations. Mixtures with higher concentrations in IL show linear dependence with temperature while those with higher water concentrations show a quadratic dependence. According to eq 3, the slope of trendlines shown in Figure 2 is expected to be higher as water concentration of the mixture rises. Even though this analysis is qualitatively consistent, to our view, further work needs to be done in order to establish a relationship between the crossover temperature and the components of the mixture.

Thermal expansion coefficient (α_p) shows values lower than 1.6×10^{-3} K^{-1} for both ILs. In the temperature range studied (from 293.15 to 343.15 K), these ILs aqueous systems lead to nearly identical coefficients of thermal expansion. Thus, α_p should not be a criterion to choose one IL over the other for some particular application, in this case, as absorbent for water refrigerant in an absorption cycle.

Transport Properties: Viscosity, Electrical Conductivity and Proton Activity. *Viscosity Measurements.* Viscosities of $[C_2Py][MeSO_3]$ + H_2O and $[Chol][H_2PO_4]$ + H_2O mixtures at different temperatures are shown in Table S1 (Supporting Information). The three-parameter Vogel−Fulcher−Tammann (VFT) eq 4 was used to correlate experimental viscosities as a function of temperature:

$$\eta = A \cdot \exp\left(\frac{B}{T - T_0}\right) \quad (4)$$

being η the dynamic viscosity, and A, B and T_0 the fitting parameters reported in Table S3 (Supporting Information) together with the R^2 of the fitting. Figure 3 illustrates that viscosity decreases drastically as temperature rises. Most ionic liquids have undesirable high viscosity; to deal with this problem one possible approach is lowering the viscosity by adding a molecular solvent. Thus, experimental measurements of both IL + H_2O systems show how viscosity decreases as the content of water increases for all temperatures.

However, the effect of water over viscosity is more important at lower temperatures (Figure 3). This pattern was already found for $[C_2Py][OTf]$ + H_2O systems.[29] Dynamic studies at molecular scales have pointed out the lubricating action of molecular solvents over the dynamics of ionic liquids[33,34] for different concentrations of water. A reliable explanation yield on the weakening of the Coulombic interactions between ions

DOI: 10.1021/acssuschemeng.6b01541
ACS Sustainable Chem. Eng. 2016, 4, 5068−5077

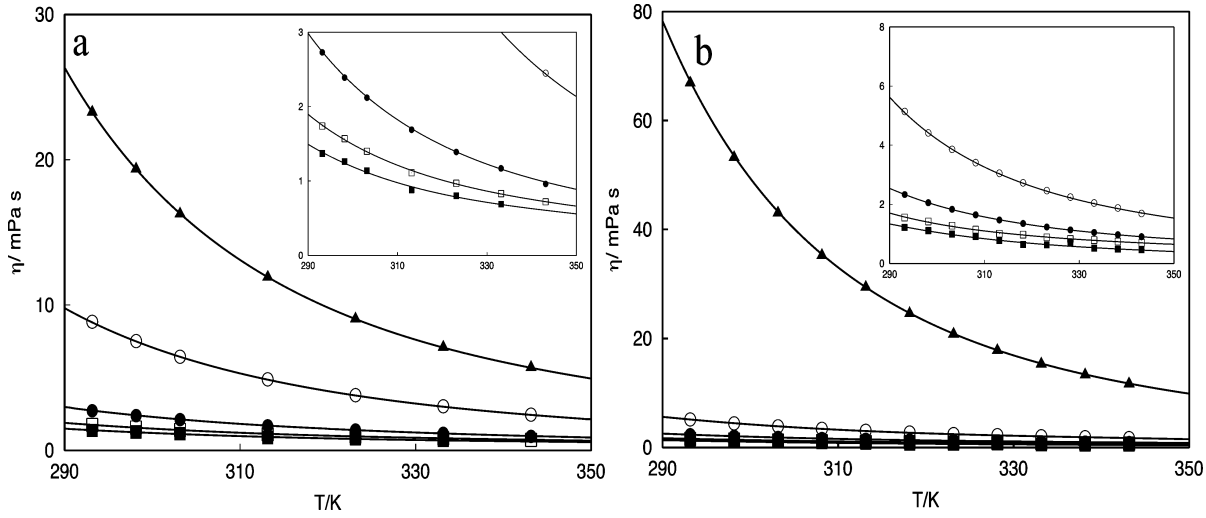

Figure 3. Experimental viscosity values: (a) x $[C_2Py][MeSO_3]$ + (1 − x) H_2O mixtures. x = 0.0168 (■), x = 0.0317 (□), x = 0.0650 (●), x = 0.1842 (○), x = 0.3830 (▲). (b) x $[Chol][H_2PO_4]$ + (1 − x) H_2O mixtures. x = 0.0040 (■), x = 0.0163 (□), x = 0.0316 (●), x = 0.0620 (○), x = 0.1651 (▲). Fitting lines (—).

would lead to a higher ionic mobility, and therefore to decrease the viscosity of systems.

Both systems, IL + H_2O, present very different solubility. Whereas the most concentrated $[C_2Py][MeSO_3]$ + H_2O solution has a molar fraction $x_{[C2Py][MeSO3]}$ = 0.3830, for $[Chol][H_2PO_4]$ the highest molar fraction is $x_{[Chol][H2PO4]}$ = 0.1651 (see Table 2 for concentration equivalences). However, by comparing all experimental data, it is possible to establish the viscosity sequence as follows, $\eta_{[C2py][MeSO3]} < \eta_{[Chol][H2PO4]}$. Thus, attending to viscosity, systems $[C_2Py][MeSO_3]$ + H_2O are found to be more suitable than $[Chol][H_2PO_4]$ + H_2O for absorption systems using water as refrigerant.

Previously, the system $[C_2Py][OTf]$ was studied by us as a potential absorbent for absorption heat pumps using water as refrigerant.[29] Given that, $[C_2Py][OTf]$ and $[C_2Py][MeSO_3]$ share the same cationic structure, $[C_2Py]^+$, a detailed comparison of both systems could provide interesting information about the effect of the anionic structure apart from their suitability to work as absorbents for absorption heat pumps. Trends of density and viscosity for IL + H_2O systems are $\rho_{[C2py][OTf]} > \rho_{[C2Py][MeSO3]}$ and $\eta_{[C2py][OTf]} < \eta_{[C2py][MeSO3]}$. Inverse trends are found for both properties, in terms of atomic interactions, the larger charge delocalization caused by the trifluoromethyl group (CF_3) group compared to methyl group (CH_3) could explain this effect, since it would smooth the electrostatic interactions and therefore improve ionic mobility, giving place to lower viscosities. It would also lead to the formation of more compacted ionic networks and therefore higher densities. This statement also agrees with their solid−liquid transition temperatures, 16 and 62 °C for $[C_2Py][OTf]$ and $[C_2Py][MeSO_3]$, respectively.[25]

Viscosity measurements show how different ionic structures lead to drastic differences in this property when the mixtures are highly concentrated in IL, especially at low temperatures. These differences become much smaller for diluted solutions where water concentration prevailed over the IL or when temperature rises. Therefore, the addition of an organic solvent or the rising of the working temperature represent two interesting strategies to overcome problems related to the high viscosity of ILs.

Electrical Conductivity Measurements. Figure 4 shows dependence on electrical conductivity (κ) with IL molar fraction (x_{IL}) at several temperatures. Casteel−Amis[35] eq 5 was used to fit experimental data. Fitting parameters are given in Table S4 (Supporting Information).

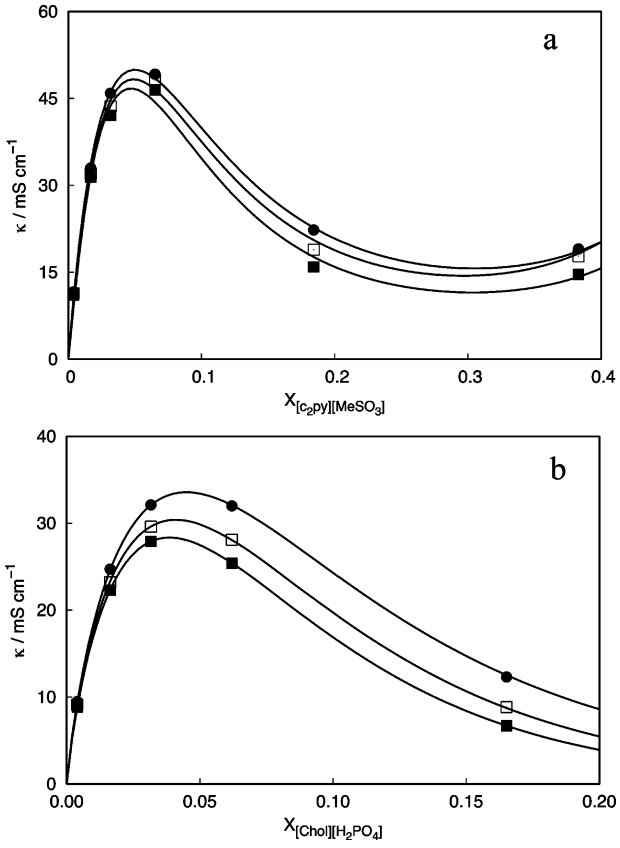

Figure 4. Electrical conductivity versus x_{LI} at several temperatures. T = 298.15 K (■), T = 313.15 K (□), T = 333.15 K (●), fitting lines (—). (a) $[C_2Py][MeSO_3]$ + H_2O. (b) $[Chol][H_2PO_4]$ + H_2O.

DOI: 10.1021/acssuschemeng.6b01541
ACS Sustainable Chem. Eng. 2016, 4, 5068−5077

$$\kappa = \kappa_{max}\left(\frac{x_{IL}}{x_{IL,max}}\right)^{n} \exp\left[m(x_{IL} - x_{IL,max})^2 - n\left(\frac{x_{IL} - x_{IL,max}}{x_{IL,max}}\right)\right] \quad (5)$$

being κ the electrical conductivity, and κ_{max}, m and n the fitting parameters reported in Table S4 (Supporting Information) together with the R^2 of the fitting.

A qualitative analysis of Figure 4a,b indicates that ionic mobility is higher for $[C_2Py][MeSO_3]$ than for $[Chol][H_2PO_4]$ mixtures. Therefore, it is in agreement with the viscosity values, $\eta_{[C2Py][MeSO3]} < \eta_{[Chol][H2PO4]}$, because a lower internal friction is expected to improve IL dynamics and therefore it would favor charge transport. The comparison of the electrical conductivity between the ILs with same cation, $[C_2Py]^+$, and different anion, $[MeSO_3]^-$ and $[OTf]^-$, indicates that the trend in conductivity is $\kappa_{[C2py][OTf]} < \kappa_{[C2py][MeSO3]}$, being around 5% lower for the $[OTf]^-$ counterion.

By comparing Figure 4a,b again, we observe similar tendencies of ionic conductivity with IL molar fraction. For dilute solutions, κ grows drastically with x_{IL}. Then, all curves reach a maximum at molar fraction about 0.05 and 0.04 for $[C_2Py][MeSO_3]$ and $[Chol][H_2PO_4]$ respectively, values for each temperature are provided in Table S1 (Supporting Information). After that point, ionic conductivity decreases as concentration of IL grows. This pattern was already found for other binary systems involving IL + H_2O systems.[36−40] Two mechanisms are often mentioned as responsible for this behavior. On one hand the increase in the ionic concentration should lead to higher ionic conductivities since more charge is available to be transported. On the other, the descent in ionic mobility, since interactions (electrostatic and dispersive) between cation−anion and cation−cation become stronger, will have the opposite effect. Therefore, a balance between mechanisms will bring maximum conductivity. To assess this hypothesis, measurements were taken at three different temperatures, from 298 to 333 K. Linear tendencies with positive slope were found in all cases. The effect of temperature over conductivity is more important as IL concentration grows, for $[C_2Py][MeSO_3]$ goes from 0.013 to 0.16 mS cm^{-1} K^{-1} and for $[Chol][H_2PO_4]$ from 0.018 to 0.17 mS cm^{-1} K^{-1}, which is roughly an increase of 10 times in the slope when x_{IL} moves from the most diluted solution to the most concentrated (Figure S1 in the Supporting Information).

Because temperature has critical impact over ionic mobility, we will expect that κ_{max} happens at higher IL concentrations. Although this trend was found, its extent, smaller than expected, suggests that other factors may also contribute to κ dependence with x_{IL}.[33,41]

Viscosity and Electrical Conductivity Relationship. The relation between these two properties is often enlightened by Walden's rule. From eq 6, where Λ is the molar conductivity, η the viscosity, and C is a constant; we have obtained the so-called Walden's plot. Further details can be found elsewhere.[42]

$$\Lambda = \frac{C}{\eta} \quad (6)$$

In Figure 5, IL + H_2O mixtures with similar IL concentrations are represented. Deviation from the ideal line[21] (slope equals to 1) would provide, according to Ueno et al.,[43] a measurement of the ionicity of the IL. Both systems

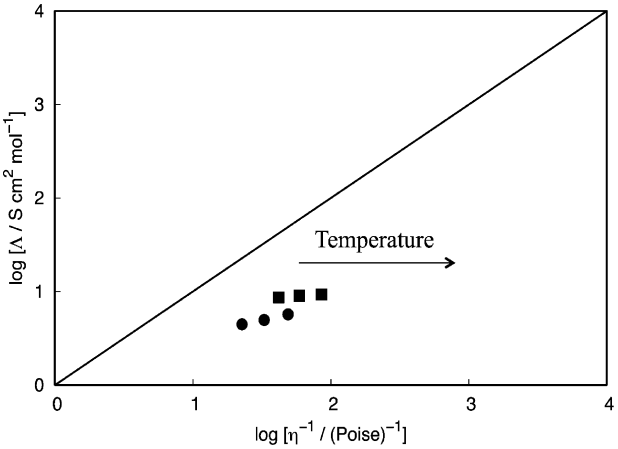

Figure 5. Walden plot of the $[C_2Py][MeSO_3]$ ($x_{[C2Py][MeSO3]}$ = 0.065) + H_2O (■) and $[Chol][H_2PO_4]$ ($x_{[Chol][H2PO4]}$ = 0.062) + H_2O mixtures (●) at 298.15, 313.15, 333.15 K. The straight solid line through the origin with a slope of 1 represents the so-called ideal KCl line.[42]

fall into the area of poor ILs, in terms of ionicity, no significant differences between these systems were found since they show similar ratios between Λ and $1/\eta$. Temperature effect is also shown in Figure 5. As temperature rises, points are displaced to the right. It is consistent with the fact that temperature effect over viscosity is stronger that its effect over electric conductivity. Previously, several authors have analyzed the behavior of several IL + H_2O systems,[44,45] results indicate that aqueous solutions of ILs do not follow Walden's rule qualitatively, even though trends found suggest a physical background for the value of C.[45]

Proton Activity Measurements. Because the solvent is pure water, the experimental proton activity, a_{H+} or "effective" proton concentration (see the Experimental Section) of these mixtures was also determined, these measurements are representative rather than exhaustive, and its effect is shown in Figure 6, together with the electrical conductivity data. The proton activity (expressed as pa_{H+}) depends strongly on x_{IL}. Systems show different trends, depending mainly on the anion structure, since the pK_a values of both conjugated acid of aliphatic amines or unsatured pyridines increase with the increasing alkylsubtitution and render the corresponding cations a basic character (see structures in Scheme S1), although the charge and structure of these cations will influence the polarity and the solvent properties of the ionic liquids.

For the [C_2Py][MeSO3] (Figure 6a), pa_{H+} is 3.42 at $x_{[C2Py][MeSO3]}$ = 0.0039, this value decreases drastically with the increase of $x_{[C2Py][MeSO3]}$ up to 0.0371, thus [C_2Py][MeSO3] plays the role of an acidic species, where the minimum pa_{H+} is close to the x_{IL} where the conductivity presents its highest value (46.72 mS cm^{-1} at x_{IL} = 0.047). Afterward, the pa_{H+} values increase slightly with x_{IL}, reaching the value of 2.74 at x_{IL} = 0.3830. Keeping in mind the structure for $[C_2Py][MeSO_3]$, which is a six-membered unsaturated ring that is more basic than the pyridinium and imidazolium cations with a methanesulfonate (conjugated-base of a very strong methanesulfonic acid, $MeSO_3H$, with a pK_a = −1.8) as counteranion,[46,47] it should be expected to yield a "neutral" (in the acidic/base sense) ionic liquid product.[48] This is the case of $[C_2Py][OTf]$ (note structures are similar), with proton activities of pa_{H+} 6.42 and 5.91 at x_{IL} = 0.067 and x_{IL} =

DOI: 10.1021/acssuschemeng.6b01541
ACS Sustainable Chem. Eng. 2016, 4, 5068−5077

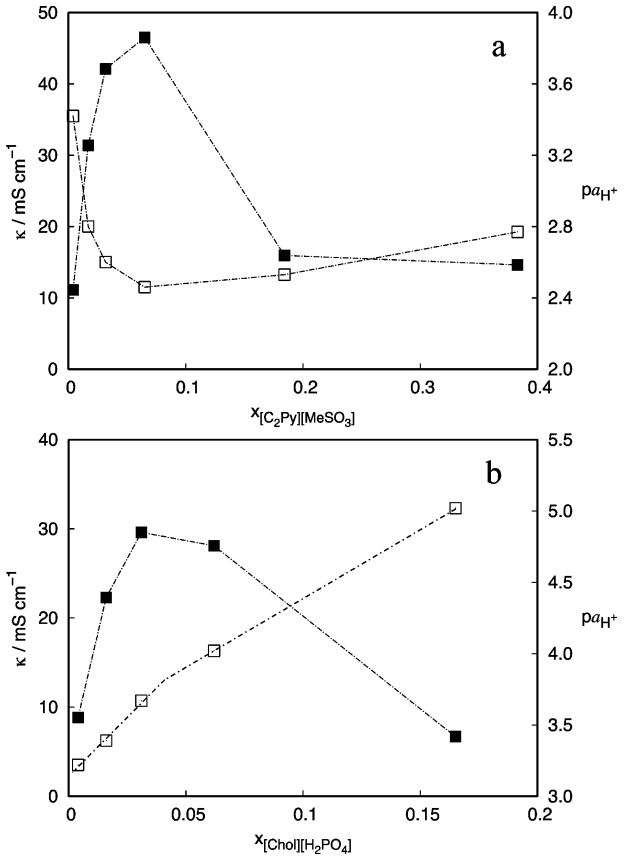

Figure 6. Electrical conductivity (■) and pa_{H+} (□) versus x_{IL} at 298.15 K. (a) $[C_2Py][MeSO_3]$ + H_2O; (b) $[Chol][H_2PO_4]$ + H_2O. Notice that the points are joined for better following the trends in electrical conductivity (Casteel–Amis fitting in Figure 4) and pa_{H+}.

0.689, respectively, where the weak acidity at high x_{IL} can be attributed to the presence of free fluoride ion (conjugated-base of a weak fluorhydric, HF, with a pK_a = 3.2). However, these $[C_2Py][MeSO_3]$ mixtures exhibit a stronger acidity than expected, and this behavior, although we cannot yet offer an conclusive explanation, seems to be caused by some impurities from the acid used as precursor in the synthesis. This hypothesis will be discussed later (next section and Figure 7a).

For $[Chol][H_2PO_4]$ (Figure 6b), the most diluted solution, x_{IL} = 0.0040, has a proton activity of 3.22, increasing with x_{IL} during the whole concentration range, at x_{IL} = 0.1651 the pa_{H+} is 4.99 (see Table 2 for concentration equivalences). Furthermore, the pa_{H+} trend shows two straight lines with the increasing of x_{IL}, whose equations are as follows: pa_{H+} = (3.168 ± 0.004) + (13.4 ± 0.2) $x_{[Chol][H2PO4]}$ for the first linear trend ($x_{[Chol][H2PO4]} \leq 0.0316$) and pa_{H+} = (3.29 ± 0.05) + (10.4 ± 0.5) $x_{[Chol][H2PO4]}$ for the second linear trend ($x_{[Chol][H2PO4]} \geq 0.0316$), both with a good linear correlation (R^2 = 0.9999 and R^2 = 0.999, respectively), Figure 6b(□)), and the crossing point roughly coincides with the maximum of the conductivity value (28.34 mS cm^{-1} at x_{IL} = 0.0386). According to its structure (Scheme S1), formed by an acyclic and saturated with a hydroxylfuntionalized side chain also on the cation-dependent degree of hydrogen bonding and an "amphoteric" counteranion, with the potential to both accept and donate protons depending on the other substances present in the media,[47] these experimental results show that the dihydrogen phosphate acts as Brønsted acid counteranion at diluted binary mixtures, being amphoteric at high IL concentration, where the pa_{H+} tends to reach the theoretical value of 4.7 (semisum of pK_{a1} = 2.2 and pK_{a2} = 7.2 of phosphoric acid system) or experimental value of 4.36 for 1.845 M potassium dihydrogen phosphate solution at the same concentration (Table 2) and it acts as a second order buffered solution.

Moreover, it should be noted that $[Chol][H_2PO_4]$ gives a lower Brønsted acidity (higher pa_{H+} values) than the observed for the $[C_2Py][MeSO_3]$ at high molar fraction and probably, this is due to the strong Brønsted acidity of the hydrogen sulfate counteranion or methanesulfonic acid that can be present as impurities, in good agreement with what is found in the literature.[49]

Trends of electrical conductivity and proton activity for ILs + H_2O systems are $\kappa_{[Chol][H2PO4]} < \kappa_{[C2Py][OTf]} < \kappa_{[C2Py][MeSO3]}$ and $a_{H+[C2Py][OTf]} < a_{H+[Chol][H2PO4]} < a_{H+[C2Py][MeSO3]}$. The above discussion means that commercial $[C_2Py][MeSO_3]$, such as that which is supplied (without further purification), provides a major acidity to its binary mixtures, giving very high proton activities (down to pa_{H+} 2.8). Thus, besides being more hygroscopic and with a high electrical conductivity value (Figure 6 and Table S1) to act as an electrolyte makes $[C_2Py][MeSO_3]$ more corrosive than $[Chol][H_2PO_4]$ or $[C_2Py][OTf]$, therefore being more available to participate in the redox process onto the metallic or alloy materials junctions of absorption systems.

ILs Quantification by Ionic Chromatography. As previously mentioned, the IC method is focused on the quantitative determination of anionic impurity profiles in ionic liquids, including not only halogen anions such as fluoride (F^-) or chloride (Cl^-) or bromide (Br^-), but also additional commonly encountered anions: hydrogen sulfate and sulfate system (both detected as SO_4^{2-}), acetate (CH_3COO^-), nitrate (NO_3^-), triflate ($CF_3SO_3^-$), methanesulfonate ($MeSO_3^-$), dihydrogen- and hydrogen- and phosphate system (all detected as HPO_4^{2-}) and tetrafluorborate (BF_4^-). Therefore, IC with conductometric detection (details described in the Experimental Section) was applied to chromatographically separate all these potential ions that can also be present as impurities or counterions, useful to study the possible interferences between each other. The chromatographic parameters of all anions essayed are shown in Table S5 (Supporting Information).

Representative IC chromatograms are shown in Figure 7 for both counterions $[MeSO_3]^-$ and $[H_2PO_4]^-$. The tables inset in the same figure summarize the elution and quantification results for the detected anions. As is illustrated in Figure 7, the presence of small amounts of some ionic impurities in the ILs was found. For $[MeSO_3]^-$, halides ions as fluoride and chloride, together with sulfate ions were detected at 0.040, 0.129, and 0.210 ppm, respectively, giving a purity of IL up to 97.1%. The presence of fluoride and hydrogen sulfate ions (detected as sulfate but used as precursor in the form of sulfuric acid in the synthesis) or the methanesulfonic acid may explain the low pa_{H+} for this IL. This behavior is very far from expected for a neutral anion, as discussed before (Figure 6a). A comparative ion chromatographic study for $[C_2Py][OTf]$ that presents the same cation but different anion, where the hydrogens of the methyl group of methanesulfonate ions are substituted by fluorides, was done (chromatogram not shown). In this case, only fluoride ion at 0.058 ppm was found as impurity and its hydrolysis can justify the light acidity at higher x_{IL} as described

DOI: 10.1021/acssuschemeng.6b01541
ACS Sustainable Chem. Eng. 2016, 4, 5068–5077

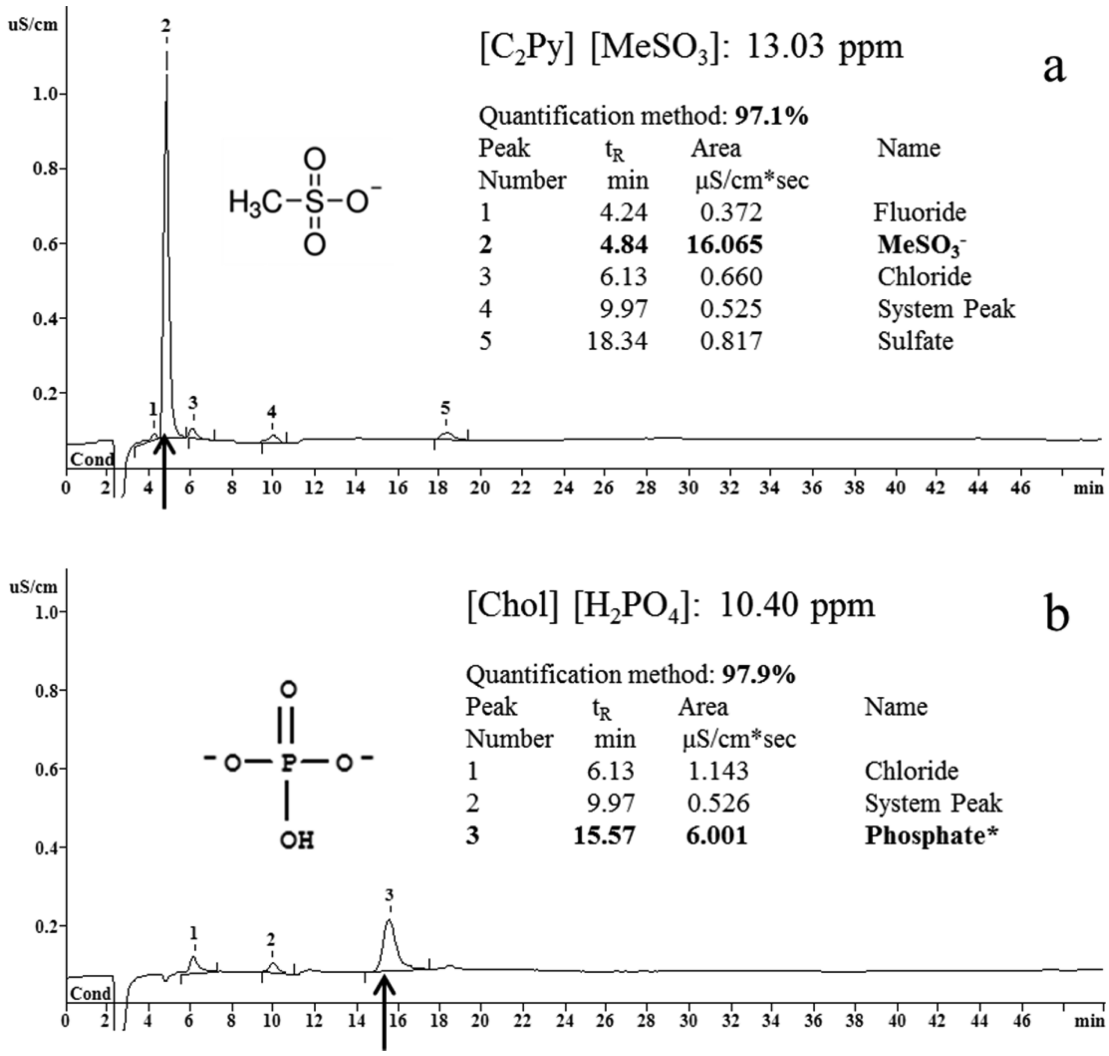

Figure 7. Ion chromatograms of (a) $[C_2Py][MeSO_3]$ and (b) $[Chol][H_2PO_4]$ using an eluent containing 1.8 mM Na_2CO_3 + 1.7 mM $NaHCO_3$ (pH ≈ 10) and a flow rate of 1 mL min^{-1} during 50 min of elution time. The peaks highlighted by the arrow are due to the counterions of ILs. The inset shows the quantification table of the trace highlighted ions found in the chromatogram for each ILs. *Notice that the mobile phase is pH around 10, and then all detected species will be at the predominant form according to its pK_a values.

in the previous section (Proton Activity). For $[H_2PO_4]^-$, only chloride ion was found as impurity at the concentration level of 0.224 ppm, giving a purity of IL up to 97.9%.

The chromatographic peaks at 9.97 min in Figure 7 were ascribed to carbonate (system peak, SP) after checking that this peak did not increase with the injection of higher ILs concentrations. However, if bromide ion were present as impurity, the chromatographic elution conditions should be changed to avoid the interference of the SP in the quantification of bromide ion (t_R at 9.79 min) (Figure S1 and Table S5 in the Supporting Information).

It is well-known that ILs containing halide contaminants are problematic because it can produce the modification of some physicochemical properties such as viscosity (increase) or density (decrease) that can seriously affect the usefulness of the IL as a solvent for a given application.[50] Moreover, the combination of halide presence with high acidity and conductivity makes them more corrosive, making an evaluation of the materials compatibility necessary to prevent any damages that may affect the durability of the equipment. Because this is not conclusive, additional studies need to be done (some experiments are in course).

CONCLUSIONS

In this work binary mixtures of $[C_2Py][MeSO_3]$ + H_2O and $[Chol][H_2PO_4]$ + H_2O covering all the miscibility range have been prepared. Several physical and chemical properties have been determined at temperatures from 293 to 343 K and at atmospheric pressure. Density measurements have been taken for all systems and isobaric coefficients of thermal expansion were calculated. Viscosity was determined, and all data were fit satisfactorily using Vogel−Fulcher−Tammann equation. Electrical conductivity was also measured, and data were adjusted to the Casteel−Amis equation. Besides that, proton activity of all systems was analyzed taking the impurities quantified through ionic chromatography into account. Trends found are summarized in the following bullet points:

- ρ ($[C_2Py][MeSO_3]$ + H_2O) < ρ ($[Chol][H_2PO_4]$ + H_2O)

DOI: 10.1021/acssuschemeng.6b01541
ACS Sustainable Chem. Eng. 2016, 4, 5068−5077

- η ([C_2Py][$MeSO_3$] + H_2O) < η ([Chol][H_2PO_4] + H_2O)
- κ ([C_2Py][$MeSO_3$] + H_2O) > κ ([Chol][H_2PO_4] + H_2O)
- pa_{H+}([C_2Py][$MeSO_3$] + H_2O) < pa_{H+} ([Chol][H_2PO_4] + H_2O)

According to these statements, [C_2Py][$MeSO_3$] appears as a more appropriate candidate for absorption systems. Miscibility range and viscosity are key factors enforcing this option. However, high proton activities together with high electrical conductivities may lead to corrosion problems. Further measurements need to be done to study this possibility in detail.

■ ASSOCIATED CONTENT

Supporting Information

The Supporting Information is available free of charge on the ACS Publications website at DOI: 10.1021/acssuschemeng.6b01541.

Density (ρ/g·cm^{-3}), viscosity (η/mPa·s) and electrical conductivity (κ/mS·cm^{-1}) data for [C_2Py][$MeSO_3$] + H_2O and [Chol][H_2PO_4] + H_2O mixtures with temperature modification and its fitting parameters to corresponding equations (Tables S1 to S4 and Figure S1), ionic chromatogram of anion standard solution and table with quantification parameters (Table S5 and Figure S2) (PDF).

■ AUTHOR INFORMATION

Corresponding Authors

*Josefa García. E-mail: fafina@uvigo.es; Fax: +34 986 812 322; Tel.: +34 986 818 753.

*Elisa González-Romero. E-mail: eromero@uvigo.es; Fax: +34 986 812 322; Tel: +34 986 812240.

Author Contributions

The paper was written through contributions of all authors. All authors have given approval to the final version of the paper.

Funding

Spanish Ministry of Economy and Competitiveness, MINECO (CTM2014-52471-R, DPI2012-38841-C02-02, CTQ2011-23925, EM2013/031) Xunta de Galicia/FEDER Networks Projects (REGALIS-R2014/015 and BIOAUGA-R2014/030)

Notes

The authors declare no competing financial interest.

■ ACKNOWLEDGMENTS

Authors kindly acknowledge the support of the following institutions: Spanish Ministry of Economy and Competitiveness, MINECO, (CTM2014-52471-R, DPI2012-38841-C02-02, CTQ2011-23925, EM2013/031), Xunta de Galicia (XUGA/FEDER) the networks: REGALIS-R2014/015 and BIOAUGA-R2014/030. Pablo B. Sánchez thanks Ministerio de Economia y Competitividad of Spain for his Ph.D. Grant framed in Plan Estatal de Investigación Científica y Técnica y de Innovación 2013−2016.

■ ABBREVIATIONS

ILs, ionic liquids; C_2Py, 1-ethylpyridinium cation; Chol, choline cation; OTf, trifluoromethanesulfonate or Triflate anion; NTf_2, bis(trifluoromethylsulfonyl)imide anion; x_{IL}, molar fraction of IL

■ REFERENCES

(1) Wasserscheid, P.; Seiler, M. Leveraging gigawatt potentials by smart heat-pump technologies using ionic liquids. *ChemSusChem* **2011**, *4* (4), 459−463.

(2) Seiler, M.; Kühn, A.; Ziegler, F.; Wang, X. Sustainable Cooling Strategies Using New Chemical System Solutions. *Ind. Eng. Chem. Res.* **2013**, *52*, 16519−16546.

(3) Popp, S.; Bösmann, A.; Wölfel, R.; Wasserscheid, P. Screening of ionic liquid/H2O working pairs for application in low temperature driven sorption heat pump systems. *ACS Sustainable Chem. Eng.* **2015**, *3* (4), 750−757.

(4) Khamooshi, M.; Parham, K.; Atikol, U. Overview of Ionic Liquids Used as Working Fluids in Absorption Cycles. *Adv. Mech. Eng.* **2013**, *2013*, 1−7.

(5) Zheng, D.; Dong, L.; Huang, W.; Wu, X.; Nie, N. A review of imidazolium ionic liquids research and development towards working pair of absorption cycle. *Renewable Sustainable Energy Rev.* **2014**, *37*, 47−68.

(6) Srikhirin, P.; Aphornratana, S.; Chungpaibulpatana, S. A review of absorption refrigeration technologies. *Renewable Sustainable Energy Rev.* **2001**, *5*, 343−372.

(7) Kurnia, K. A.; Pinho, S. P.; Coutinho, J. a. P. Designing ionic liquids for absorptive cooling. *Green Chem.* **2014**, *16* (8), 3741.

(8) Brennecke, J. F.; Maginn, E. J. Ionic liquids: Innovative fluids for chemical processing. *AIChE J.* **2001**, *47* (11), 2384−2389.

(9) Plechkova, N. V.; Seddon, K. R. Applications of ionic liquids in the chemical industry. *Chem. Soc. Rev.* **2008**, *37* (1), 123−150.

(10) Welton, T. Room-temperature ionic liquids. Solvent for synthesis and catalysis. *Chem. Rev.* **1999**, *99* (8), 2071−2083.

(11) Wasserscheid, P.; Welton, T. *Ionic Liquids in Synthesis*; Wasserscheid, P., Welton, T., Eds.; Wiley-VCH Verlag GmbH & Co. KGaA: Weinheim, Germany, 2007; Vol. *1*.

(12) Earle, M. J.; Esperança, J. M. S. S.; Gilea, M. A.; Lopes, J. N. C.; Rebelo, L. P. N.; Magee, J. W.; Seddon, K. R.; Widegren, J. A. The distillation and volatility of ionic liquids. *Nature* **2006**, *439* (7078), 831−834.

(13) Fredlake, C. P.; Crosthwaite, J. M.; Hert, D. G.; Aki, S. N. V. K.; Brennecke, J. F. Thermophysical Properties of Imidazolium-Based Ionic Liquids. *J. Chem. Eng. Data* **2004**, *49* (4), 954−964.

(14) Crosthwaite, J. M.; Muldoon, M. J.; Dixon, J. K.; Anderson, J. L.; Brennecke, J. F. Phase transition and decomposition temperatures, heat capacities and viscosities of pyridinium ionic liquids. *J. Chem. Thermodyn.* **2005**, *37* (6), 559−568.

(15) Maton, C.; De Vos, N.; Stevens, C. V. Ionic liquid thermal stabilities: decomposition mechanisms and analysis tools. *Chem. Soc. Rev.* **2013**, *42* (13), 5963−5977.

(16) Quinn, B. M.; Ding, Z.; Moulton, R.; Bard, A. J. Novel Electrochemical Studies of Ionic Liquids. *Langmuir* **2002**, *18* (25), 1734−1742.

(17) Shiddiky, M. J. a; Torriero, A. a J. Application of ionic liquids in electrochemical sensing systems. *Biosens. Bioelectron.* **2011**, *26* (5), 1775−1787.

(18) Olivier-Bourbigou, H.; Magna, L.; Morvan, D. Ionic liquids and catalysis: Recent progress from knowledge to applications. *Appl. Catal., A* **2010**, *373* (1−2), 1−56.

(19) Wishart, J. F. Energy applications of ionic liquids. *Energy Environ. Sci.* **2009**, *2* (9), 956−961.

(20) Brennecke, J. F.; Rodríguez, H. Temperature and Composition Dependence of the Density and Viscosity of Binary Mixtures of Water + Ionic Liquid. *J. Chem. Eng. Data* **2006**, *51*, 2145−2155.

(21) Pires, J.; Timperman, L.; Jacquemin, J.; Balducci, A.; Anouti, M. Density, conductivity, viscosity, and excess properties of (pyrrolidinium nitrate-based Protic Ionic Liquid+propylene carbonate) binary mixture. *J. Chem. Thermodyn.* **2013**, *59*, 10−19.

(22) Carvalho, P. J.; Regueira, T.; Santos, L. M. N. B. F.; Fernandez, J.; Coutinho, J. a P. Effect of water on the viscosities and densities of 1-butyl-3- methylimidazolium dicyanamide and 1-butyl-3-methylimidazolium tricyanomethane at atmospheric pressure. *J. Chem. Eng. Data* **2010**, *55* (2), 645−652.

DOI: 10.1021/acssuschemeng.6b01541
ACS Sustainable Chem. Eng. 2016, 4, 5068−5077

4.4 Molecular Understanding of Pyridinium Ionic Liquids as Absorbents with Water as Refrigerant for Use in Heat Pumps

- This article is the product of the collaboration between the Thermodinamique et Intéractions Moléculaires group (Université Blaise Pascal) and the Applied Physics Department (Universidad de Vigo).
- P.B.S. has performed the MD simulations and the data analysis to calculate the physical properties.
- P.B.S redacted a major part of the manuscript under the supervision of A.A.H.P.

Molecular Understanding of Pyridinium Ionic Liquids as Absorbents with Water as Refrigerant for Use in Heat Pumps

Pablo B. Sánchez
Institut de Chimie de Clermont Ferrand, Université Clermont Auvergne, CNRS, Clermont-Ferrand 63000, France

Departamento de Física Aplicada, Universidad de Vigo, Vigo, Spain

Mounir Traikia, Alain Dequid, and Agílio A. H. Pádua
Institut de Chimie de Clermont Ferrand, Université Clermont Auvergne, CNRS, Clermont-Ferrand 63000, France

Josefa García
Departamento de Física Aplicada, Universidad de Vigo, Vigo, Spain

DOI 10.1002/aic.15690
Published online in Wiley Online Library (wileyonlinelibrary.com)

Aiming at developing new absorbent/refrigerant working pairs for heat pumps, thermodynamic and transport properties of two pyridinium ionic liquids (ILs), N-ethylpyridinium bis(trifluoromethanesulfonyl)amide and N-ethylpyridinium trifluoromethanesulfonate were studied using molecular simulation and nuclear magnetic resonance techniques. The microscopic structure of the ILs and the solvation environment of water, including hydrogen bonding, were studied. Free-energies of solvation of water were obtained using perturbation methods, and the values agree with experimental observations. Self-diffusion coefficients and viscosity were computed and compared with nuclear magnetic resonance measurements and literature. Simulations predict slower dynamics when compared with experiment: diffusion coefficients are underpredicted, whereas viscosity is overpredicted. As such, simulation is consistent in a Stokes-Einstein sense. The trends in transport properties due to changing anion, to the presence of water and the effect of temperature are well predicted. © 2017 American Institute of Chemical Engineers *AIChE J*, 00: 000–000, 2017
Keywords: absorption, ionic liquids, thermodynamics/classical, simulation, molecular

Introduction

Cooling and heating demands cover a considerable part of the energy consumption worldwide, with a significant percentage of this energy being supplied by mechanical heat pumps based on compression systems. Even though the implementation of these systems has been massive over the last decades, their intensive use of electric energy has stimulated growing interest in the development of alternative technologies to cover heating and cooling demands. In that context, absorption heat pumps appear to be a suitable technology to supply heating and cooling for either industrial or domestic uses. Instead of using electric energy as main input, absorption systems use mostly thermal energy.[1,2] This allows recovering residual heat currents from industrial process to generate useful thermal energy; in domestic applications renewable sources, such as solar energy, could reduce the consumption of fossil resources. Absorption systems based on traditional working pairs, such as H_2O/LiBr and NH_3/H_2O, are a mature technology nowadays and detailed information can be found in the literature.[3] However, the aforementioned absorption systems present several drawbacks[4] related to the properties of the working pairs. While the implementation of systems based on the H_2O/LiBr pair is limited by crystallization and corrosion problems, with NH_3/H_2O the drawbacks are the high working pressures, low relative volatility and the toxicity of ammonia. In that context, working pairs based in ionic liquids (ILs) as absorbents together with natural refrigerants such as water or carbon dioxide (and other molecules such as methanol, propane, etc.) have attracted the attention of the scientific and industrial communities.[5]

ILs are usually defined as salts melting under 100°C.[6,7] Their chemical structures contain large, asymmetric organic ions, leading to unique properties that have been intensively studied[7–9] over the last decade. The enormous amount of possible combinations of cations and anions makes it possible to tune ILs properties. In spite of being an advantage for their application in many industrial processes, this variety also brings the need for efforts to understand how different chemical structures affect the physical and chemical properties.

Regarding their role as potential absorbents, the chemical and physical properties that an IL should accomplish can be divided in three groups. First, a large absorption capacity. Interactions between absorbent (IL) and refrigerant (H_2O) determine the absorption capacity, even if other factors such as transport properties are also very important to achieve a suitable absorption rate. A large negative deviation from

Additional Supporting Information may be found in the online version of this article.

Correspondence concerning this article should be addressed to A. A. H. Pádua at agilio.padua@uca.fr.

Raoult's law is often stated as a thermodynamic quantity that illustrates the suitability of an IL to be used in absorption heat pumps.[4] Another assessment of non-ideality is the refrigerant activity coefficient, often determined at infinite dilution. Second, a wide liquid range is also a desirable property of the IL as absorbent. To avoid crystallization problems in the absorber a low temperature of liquid–solid transition is desirable. The upper limit of the liquid range, given by the IL decomposition temperature, will allow to operate at higher temperatures, thus increasing the efficiency of the system.[10] Thirdly, a low vapor pressure,[6] property shared by all ILs, will allow an easy separation refrigerant/absorbent in the generator.

The complexity of the interactions governing the behaviour of ILs renders the task of reaching a detailed knowledge very challenging. Progress can be made by combining experimental and theoretical work to improve out fundamental understanding of the interactions, structure and dynamics of ILs and their mixtures at a molecular level. Among the methods to describe ILs at the atomistic level, molecular dynamics (MD) is the tool of choice since it allows description of the length and time scales necessary to represent these heterogeneous and complex liquid phases.[11–13] ILs are characterized by a balance between electrostatic and van der Waals interactions, as well as an asymmetric shape, conformational flexibility and charge delocalization, all of which have to be described in detail, otherwise the results from molecular modeling may not accurately reproduce the properties of real systems or phenomena.

Therefore, with the aim of improving our knowledge on physical chemistry of pure ILs and IL + water mixtures, we have carried out an analysis of the microscopic structure, dynamic and thermodynamic quantities of *N*-ethylpyridinium bis(trifluoromethanesulfonyl)imide, $[C_2Py][NTf_2]$, and *N*-ethylpyridinium trifulorosulfonate (or triflate), $[C_2Py][OTf]$, and their mixtures with water. We intend to explore ILs that may comply to the requirements for use in absorption systems, namely, in combination with water as refrigerant. In particular, the two ILs selected allow analysis of the effect of the anion. Furthermore, a pyridinium cation with a short alkyl chain $[C_2Py]^+$ was chosen based on the smaller amount of information available compared to imidazolium-based ILs. Even though pyridinum cations lead in general to higher viscosities than imidazolium cations,[14] they are also expected to present a larger water absorption capacities. From the point of view of simulation methods, the first question we want to address here is the pertinence of scaling the charges of the ions to improve representation of dynamics at different temperatures. Second, as was already pointed out, several questions regarding the microscopic structure will be addressed, such as comparison of the local ordering of ions in pure ILs and in mixtures with water, or statistics of hydrogen bonds. Third, free energy quantities related to the solvation of water in the two ILs will be reported. And finally, dynamic quantities such as diffusion coefficients and viscosity will be calculated to provide a microscopic view, namely, on the role of cations and anions on the transport properties of the mixture. The hydrophobicity of $[C_2Py][NTf_2]$ gives rise to a limited miscibility with water, therefore our analysis of microscopic structure and transport properties is performed only for mixtures of water with $[C_2Py][OTf]$. The mole fraction of water was chosen to be $x_{H_2O}=0.104$, representative of the lower concentration of refrigerant at the generator level in refrigeration cycles.[15] The present work will complement experimental studies available in the literature for the ILs and mixtures described here. While density and viscosity of $[C_2Py][NTf_2]$ and $[C_2Py][OTf]$ have been previously measured,[16–18] no data about energetics of water solvation were found.

Methods

Force field molecular simulation

All chemical components studied in this work, ILs and water, were represented by a classical atomistic force field for organic compounds[19] containing intramolecular terms for covalent bond stretching, valence angle bending and torsions, and intermolecular parameters for repulsion-dispersion Lennard-Jones (LJ) sites and for partial electrostatic charges on atomic sites. Atoms of the same molecule or ion separated by more than four bonds interact also through the non-bonded terms, while those separated by exactly three bonds interact through Lennard-Jones and Coulomb terms scaled by 0.5. The functional form of the potential energy is given in Eq. 1.

$$u=\sum_{ij}^{\text{bonds}}\frac{k_b}{2}(r-r_0)^2+\sum_{ijk}^{\text{angles}}\frac{k_\theta}{2}(\theta-\theta_0)^2 + \sum_{ijkl}^{\text{torsions}}\sum_{m=1}^{3}\frac{V_m}{2}[1-(-1)^m\cos(m\phi)] + \sum_{ij}^{\text{nonbonded}}4\epsilon_{ij}\left[\left(\frac{\sigma_{ij}}{r_{ij}}\right)^{12}-\left(\frac{\sigma_{ij}}{r_{ij}}\right)^{6}\right]+\frac{1}{4\pi\epsilon_0}\frac{q_iq_j}{r_{ij}} \quad (1)$$

The force field for ILs was parameterized by Canongia Lopes and Padua.[20–22] Water was represented by the SPC/E model.[23] MD simulations were performed using the LAMMPS[24,25] open source package. Initial configurations were created using the Packmol[26] and fftool[27] utilities. All simulations were carried out in periodic cubic boxes containing 300 ion pairs. In mixtures the number of water molecules to reach the desired concentration was added to 300 ion pairs. A cutoff of 12 Å was applied to LJ interactions. Long-range electrostatic interactions were handled using the particle-particle particle-mesh[28] method, for a precision of 10^{-4} in electrostatic energy. A timestep of 1 fs was used in all simulations. Trajectories were generated at constant NpT using Nosé-Hoover thermostat and barostat. Initial equilibrations of 1 ns were carried out starting from the configurations generated by Packmol. Most simulations were performed at 343 K, which is a realistic temperature considering the application in absorption heat pumps, namely, it is an upper bound to the operation temperature. Running MD simulations of IL systems at high temperatures has advantages in sampling configurations of these viscous fluids. At temperatures different from 343 K additional 0.2 ns runs were performed to equilibrate at the target temperature. Production runs to calculate structural, thermodynamic, and transport properties were performed over longer time scales, chosen according to the time needed for the systems to attain a diffusive regime.[12] Atomistic force fields with fixed electrostatic partial charges may not reproduce dynamic properties well[29,30] leading in general to fluids that are too viscous and to diffusion coefficients that are too low, even if density and structure may be predicted correctly. There are several methods to improve the molecular force fields in order to attain better agreement with experimental transport properties. The simplest option is to reduce the weight of columbic interactions by scaling down the charges of ions. Typically, atomic partial charges are reduced by a coefficient going from 0.7 to

0.9.[30] A more complex and realistic method is to include polarization explicitly.[30,31] However, due to the higher computational cost of polarizable models, charge-scaling is frequently used as a reliable shortcut. In this work, the full charge model and a 0.8 charge-scaled version are tested and the influence on some key macroscopic properties is evaluated.

Quantities related to the phase-change of the refrigerant are very important for application in absorption-refrigeration. Structural and energetic quantities related to the solvation process of water in the two ILs were studied. Free energy perturbation (FEP) was used to determine the chemical potential of water from simulation. A parameter λ was introduced to couple the water-IL interactions such that with $\lambda = 0$ water does not interact with the IL solvents, and with $\lambda = 1$ the interactions are fully coupled. By sampling this free energy route along 20 steps, the residual chemical potential of water is calculated. To avoid singularities due to overlap of sites at the moment when they are created or annihilated, soft-core LJ and electrostatic potentials were used.[32] For the systems we studied, a step of $\Delta\lambda = 0.05$ proved adequate, as was verified by the very low hysteresis when performing the FEP calculation both ways[33] (see Figure S3). Thus, the free energy of the solvation process is calculated according to Eq. 2.

$$\Delta_0^1 A = \sum_{i=0}^{n-1} \Delta_{\lambda_i}^{\lambda_{i+1}} A = -kT \sum_{i=0}^{n-1} \ln \left\langle \exp\left(-\frac{U_{\lambda_{i+1}} - U_{\lambda_i}}{kT} \right) \right\rangle_{\lambda_i} \quad (2)$$

At each value of the coupling parameter, the system was equilibrated during 0.05 ns and FEP data accumulated for 0.15 ns (4 ns overall simulation time).

The microscopic dynamics of the ILs is studied through calculations of diffusion coefficients and viscosity. The self-diffusivity is obtained from the mean square displacement (Eq. 3) calculated averaging over trajectories sufficiently long for the system to be in a diffusive regime. Among the ways of ensuring the diffusive regime is reached, we chose to evaluate the parameter β (Eq. 4)

$$D = \frac{1}{6} \lim_{t \to \infty} \frac{d}{dt} \langle \Delta r(t)^2 \rangle \quad (3)$$

$$\beta(t) = \frac{d \log \langle \Delta r(t)^2 \rangle}{d \log t} \quad (4)$$

Three different dynamic regimes are observed in liquids: ballistic ($\beta \approx 2$), subdiffusive ($\beta < 1$), and diffusive regimes ($\beta \approx 1$). Cadena et al.[12] explained in detail the physical basis and application for ILs. The β values for our simulations are shown in supplementary information (Figure S4).

Viscosity is a challenging quantity to calculate from MD simulations,[34–37] especially for viscous fluids. Two different approaches may be chosen to calculate viscosity: the Green-Kubo relations using equilibrium trajectories,[38] or non-equilibrium techniques.[38,39] Non-equilibrium methods impose very large velocity gradients and this may lead to non-linear behaviour or large temperature gradients in the simulation box. The Green-Kubo method requires integration of the autocorrelations of the pressure tensor.

$$\eta = \frac{V}{kT} \int_0^\infty \langle p_{xy}(t) p_{xy}(0) \rangle dt \quad (5)$$

The autocorrelation were recorded using the multiple step correlator method of Ramirez et al.[40] with $m = 2$ and $p = 16$ implemented in LAMMPS. The result was averaged over three independent shear directions. The uncertainty was estimated from the standard deviation of these values.

Diffusion coefficients by NMR

The pulsed-field gradient spin-echo NMR technique (PFGSE, also named DOSY) was used to measure the self-diffusion coefficients of both cation and anion species by observing the ^{13}C nucleus. The IL samples were inserted into 5 mm NMR tubes and coaxial capillary tubes loaded with DMSO-d_6 (lock and shim solvent) were put inside, thus avoiding any contact between DMSO-d_6 with the samples. The carbon chemical shift of DMSO-d_6 was used as external reference at 39.5 ppm.

A Bruker Avance III HD 500 spectrometer operating at 500.13 MHz for ^1H and 125.77 MHz for ^{13}C, with a 5 mm pulsed-field *z*-gradient TXI probe, was used. The sample temperature was fixed at 303, 323, and 343 K and controlled within ± 0.01 K by a variable-temperature control unit using air gas flow and calibrated with a glycol sample. We used a modified Bruker PGSE sequence for measuring the ^{13}C decay under gradient pulsing and ^1H decoupling. For each sample, the probe was carefully tuned and 90 pulses evaluated. For each DOSY experiment we optimized the pulse gradients and diffusion time to get an attenuation of about 20 for the signal with the two contradictory constrains: set minimum diffusion time ($D20 = 0.2$–0.6 s) to minimize convection and minimum gradient pulses length ($P30 = 1.6$–5 ms) to obtain sufficient attenuation but to avoid heating effect of the gradients coil and keep below maximum rating. The signals ($AQ = 0.8$ s) were accumulated 512 times for a linear set of 16 different values of gradients distributed from 1 to 45 G/cm. The relaxation delay was set to 5 s and 8 dummy scans where programmed prior to acquisition. The determination of self-diffusion coefficients used the Bruker T1/T2 module of TopSpin v3.5 for each peak. For the cation, we took the average of the different available peaks.

Results

Analysis of charge scaling: density

Electrostatic interactions play a crucial role in ILs. As several authors pointed out[29,30,41] full charge models lead to slow dynamics, causing difficulties to perform simulations at low temperatures. We opted to scale charges of ions (full partial charge values shown in Figure 1) by a factor of 0.8 and use the density to test if the force field model reproduces experiment. Results of density calculations with full and scaled charges are shown in Figures 2 and 3, indicating that scaled charges provide density values closer to experiment, both for pure ILs and also for $[C_2py][OTf] + H_2O$ mixtures. Reduction of charges lowers the density slightly, and in this case the full charge model overestimated the experimental densities by about 3%. Namely, scaled charges model reduces the average density deviation of pure $[C_2Py][OTf]$ from 3.1 to 0.42% and from 3.9 to 1.1% for $[C_2Py][NTf_2]$. A similar pattern was found for $[C_2Py][OTf]+H_2O$ mixtures, with average deviation going from 3.9 to 0.38% when partial charges are scaled. Given these results, all subsequent simulations in this work were done with ion partial charges scaled by 0.8.

Microscopic structure

The spatial arrangement at the molecular scale constitutes structural information that can be linked to the dynamic and

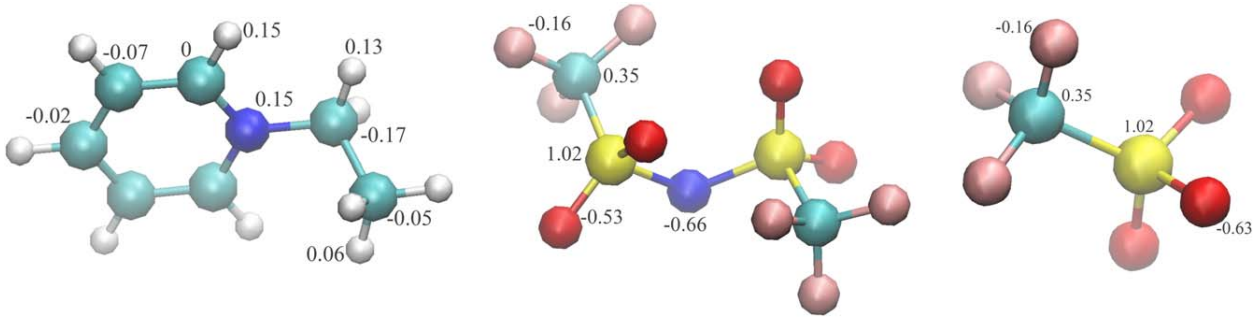

Figure 1. Partial charges of atoms in the $[C_2Py]^+$ cation and the OTf^- and NTf_2^- anions (full charges of the original force field, not scaled).

[Color figure can be viewed at wileyonlinelibrary.com]

the thermodynamic properties. Thus, radial and spatial distribution functions were computed to examine the ordering of the ions in the pure ILs and in the mixtures with water, which is important to characterize local solvation environments.

Three representative atoms in pyridinium cation were chosen: nitrogen (N_{Py}), carbon in para position (C_P) and the terminal carbon in the ethyl group (C_E). These atoms were chosen to elucidate structural features on different parts of the cation. The radial distribution functions of these cation atoms and the O and F atoms of the anions were calculated and are plotted in Figure 4. The main feature is that the first peaks due to the O atoms of the anions are more intense than the peaks of the F atoms (comparing panels a and c). This was expected for the N_{Py} because of electrostatic arguments, given that the negative partial charge of O is nearly four times that of F. Similar behaviour is found in the radial distributions of O and F with respect to C_P and C_E, which are nearly non-charged atoms. Another difference appears between the C_P–H $\cdots$ O and C_P–H $\cdots$ F, the first being significantly more intense because of the polarity of the C–H bond. These structural features comparing the O and F atoms of the anions are similar for NTf_2^- (panels b and d).

The differences between radial distributions of OTf^- and NTf_2^- are small, although the structure of the first and second-neighbour shells in the former IL appears more marked, as seen by the drop of the RDF curves below 1.0 at distances between 6 and 8 Å, which is more pronounced for OTf^-, a smaller, more rigid ion than NTf_2^-.

The differences between the structure of both ILs become more apparent when no orientational averaging is done and 3D spatial distribution functions are plotted (Figure 5). The O atoms are found with high probability in regions close to the C_P, specially so in the OTf^- based IL. The F atoms are found predominantly above and below the plane of the pyridinium ring, also more intensely in the OTf^- based IL. Therefore, a highly ordered ionic network appears more tangible in $[C_2Py][OTf]$ and as a consequence $[C_2Py][NTf_2]$ is expected to remain liquid at lower temperatures, as was experimentally found by differential scanning calorimetry.[42]

Despite their similar structures, $[C_2Py][NTf_2]$ and $[C_2Py][OTf]$ present very different solvation features, with the NTf_2^- based IL being strongly hydrophobic, while the OTf^- IL is miscible with water over the entire composition range. This difference is expected to be linked to structural differences in the solvation shells around water. Therefore, exploring the relative positions between different sites will allow us to identify the groups governing the interactions between water and the IL,[43] and this knowledge will contribute to choose or tailor the IL for efficient water absorption. A simulation box with 35 water molecules and 300 $[C_2Py][OTf]$ ion pairs (0.104 mole fraction of water) was setup to study the structure of the mixture. Radial distributions of water atoms around the SO_3^- and

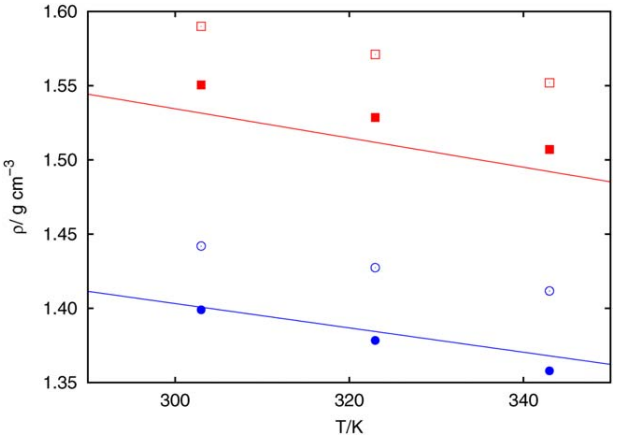

Figure 2. Density of $[C_2Py][OTf]$ (blue) and $[C_2Py][NTf_2]$ (red).

Experimental data[18] (line) and simulation results with full charges (open symbols) and ion charges scaled by 0.8 (filled symbols). [Color figure can be viewed at wileyonlinelibrary.com]

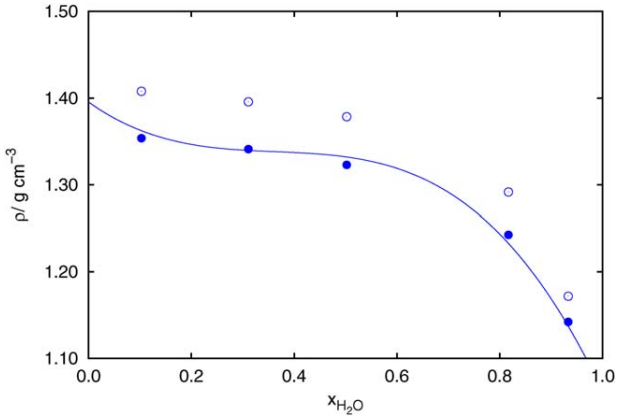

Figure 3. Density of $[C_2Py][OTf]$ + water mixtures.

Experimental data[18] (line) and simulation results with full charges (open symbols) and ion charges scaled by 0.8 (filled symbols). [Color figure can be viewed at wileyonlinelibrary.com]

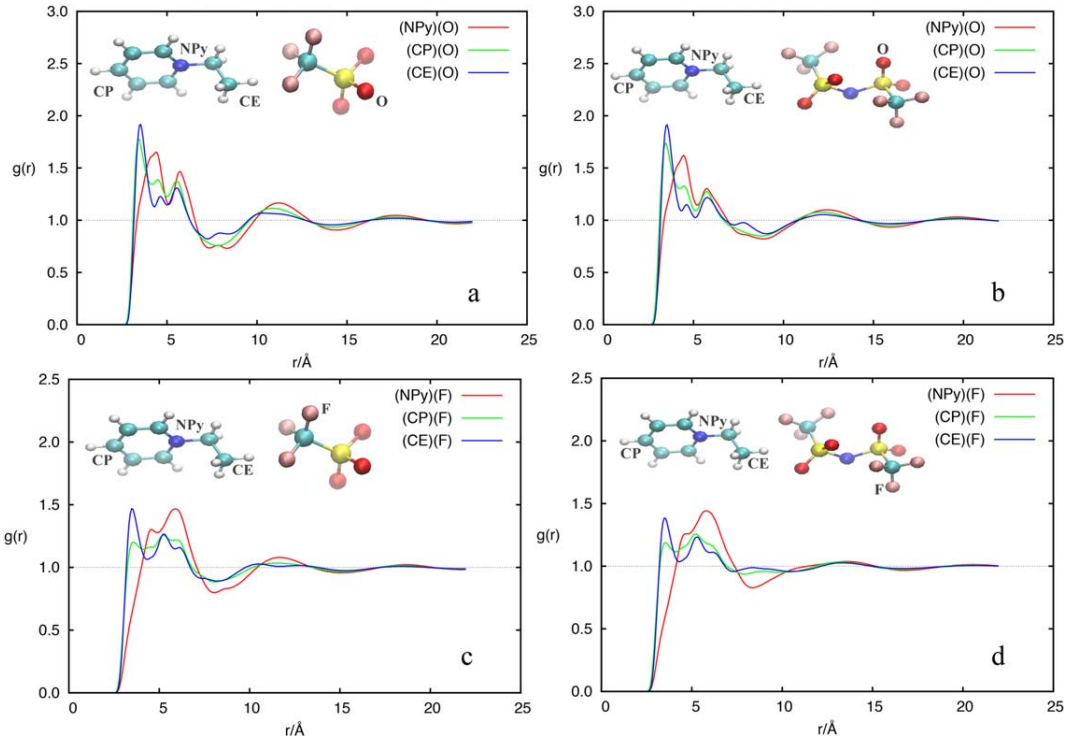

Figure 4. Radial distribution functions (RDFs) of several key sites for [C_2Py][OTf] and [C_2Py][NTf_2] at 343 K.

[Color figure can be viewed at wileyonlinelibrary.com]

CF_3 groups of the anions suggest that hydrogen bonds between H_2O and SO_3^- play an important role in the solvation. The CF_3 group appears as a hydrophobic group, without increased local density of water molecules in its surroundings. The presence of the second trifluoromethyl group in NTf_2^- will increase the hydrophobicity of this anion, as will be shown below by the free energy quantities of solvation. Apart from this visual approach, we quantified the number of hydrogen bonds, by defining length and the angle criteria[44] so that an hydrogen bond is considered when the donor H atom and the acceptor electronegative atom are separated by less than 2.5 Å, and the angle at the H atom is $180^\circ \pm 30^\circ$. According to these criteria, 65% of Hw establish H-bonds with the sulfonate groups. When water arrangement around the pyridinium cation is plotted less directional interactions are found, as can be consulted in Supplementary Information, Figure S1. This analysis shows the strong role of the anion in the absorption of water. Among the functional groups in OTf^-, the SO_3^- group favors water absorption although hydrogen bonds, while the CF_3 group appears hydrophobic (see Figure 6 and 7). The analysis of hydrogen bonding is useful to determine the suitability of ILs as absorbent.[45]

Free energy of solvation

The suitability of an absorbent is related to deviation from the ideal behavior in Raoult's law,[2,4] with more negative deviations resulting from a higher affinity between absorbent and refrigerant. Some authors have characterized this affinity by measuring or simulating the partial pressure of refrigerant.[46,47] In this work, we calculate the infinity dilution activity coefficient of water in the ILs, in order to establish a criterion independent of concentration.[2,15] The chemical potential of water allows calculation of Henry's law constant.[48]

Free energy quantities were calculated to complement the structural view of the ILs and the solvation of water presented above. The FEP algorithm was used to calculate the residual

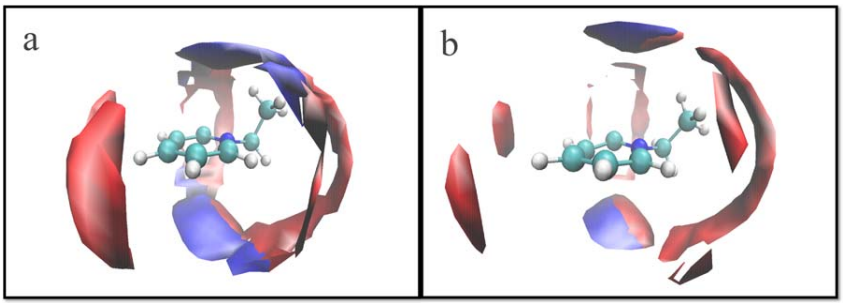

Figure 5. Spatial distribution functions (SDFs) of O and F atoms of the anions around the pyridinium cation in [C_2Py][OTf] (a) and [C_2Py][NTf_2] (b).

The blue isosurface is drawn at 2.5 times the average density of F atoms; the red isosurface is drawn at four times the average density of O atoms. [Color figure can be viewed at wileyonlinelibrary.com]

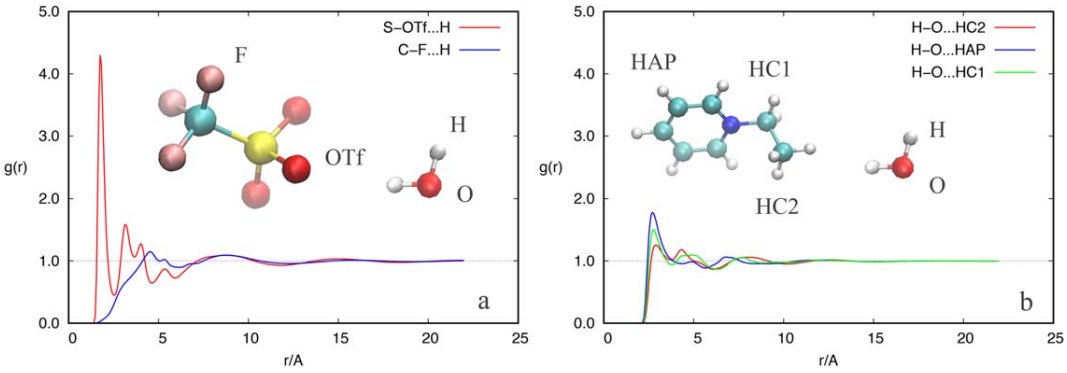

Figure 6. RDF for $[C_2Py][OTf] + H_2O$ water solution ($x_{H_2O}=0.104$).

Assessment of hydrogen bonding between water and both ions. (a) OTf^- and (b) C_2Py^+. [Color figure can be viewed at wileyonlinelibrary.com]

chemical potential μ^{res} of water in the ILs, from which the free energy of solvation and Henry's law constant can be obtained. The FEP procedure was applied on the two thermodynamic routes corresponding to activation and deactivation of a solute molecule, in order to check for hysteresis issues. As can be seen in Figure S3 the two routes coincide closely, meaning that sampling was sufficient for a reliable evaluation of the free energy difference between the initial and final states.

The residual chemical potential calculated from the present free energy methods corresponds to transfer of the solute from an ideal gas state to the solution (with infinite dilution behaviour) at constant density. It is related to the free energy of solvation $\Delta_{solv}G^\circ$ through an ideal gas contribution (the free energy of solvation is the difference between the solute in an ideal gas state at 1 bar and the solute at infinite dilution):

$$\Delta_{solv}G^\circ = \mu_i^{res} + RT \ln\left(\frac{\rho^\infty RT}{p^\circ}\right) \quad (6)$$

and the Henry's law constant follows:

$$H_i = \rho^\infty RT \exp\left(\frac{\mu_i^{res}}{RT}\right) \quad (7)$$

The results are collected in Table 1, where it can be seen that the Henry's law constant is much smaller in $[C_2Py][OTf]$ than in $[C_2Py][NTf_2]$, and the free energy of solvation negative in the former IL, compatible with the hydrophilic nature of $[C_2Py][OTf]$ and hydrophobic nature of $[C_2Py][NTf_2]$ known from experiment. Calculations using molecular simulation of Henry's constants of water in phosphonium ILs are available in the literature[49] and are of similar order as those obtained here.

An estimation of the solubility of water in the two ILs leads to $x_{H_2O}=0.1$ in $[C_2Py][NTf_2]$ and to a value higher than 1 (total miscibility) in $[C_2Py][OTf]$, which agree well with experiment, although quantitative estimations of water solubility from our simulations are not simple because it is not possible to ignore the activity coefficient of water in the IL solutions above a certain point in concentration (and our calculations refer to solutions behaving as in the state of infinite dilution, with no solute-solute interactions).

The agreement with experiment allows to consider the FEP method as able to predict the suitability of potential absorbents. It also demonstrates the hydrophobicity of the anion NTf_2^-, which must be discarded as an absorbent for water-based refrigerated systems. According to the same results, $[C_2Py][OTf]$ appears as a potential candidate regarding its thermodynamic quantities, since its liquid range[42] and relative volatility fit within the application requirements. However, the calculated thermodynamic quantities and the comparison with

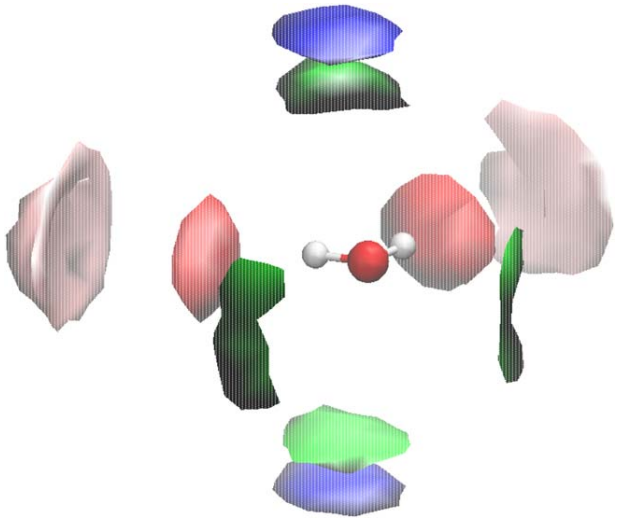

Figure 7. Water solvation environment for $[C_2Py][OTf] + H_2O$ water solution ($x_{H_2O}=0.104$).

The isosurfaces are drawn at 10 times the average density for O (OTf^-) (red) and and 3.5 times the average density for other atoms, F (OTf^-) (pink), N (C_2Py^+) (blue), and para-C (green) (C_2Py^+). [Color figure can be viewed at wileyonlinelibrary.com]

Table 1. Residual Chemical Potential and Henry's Constant of Water in the ILs at 343 K

	$[C_2Py][NTf_2]$	$[C_2Py][OTf]$
μ^{res}/kJ mol^{-1}	−11.2±0.3	−18.5±0.9
$\Delta_{solv}G^\circ$/kJ mol^{-1}	5.8 ± 0.3	−0.9±0.8
H/bar	2.35±0.22	0.23±0.07

The uncertainties are evaluated from the discrepancy between the coupling and decoupling routes.

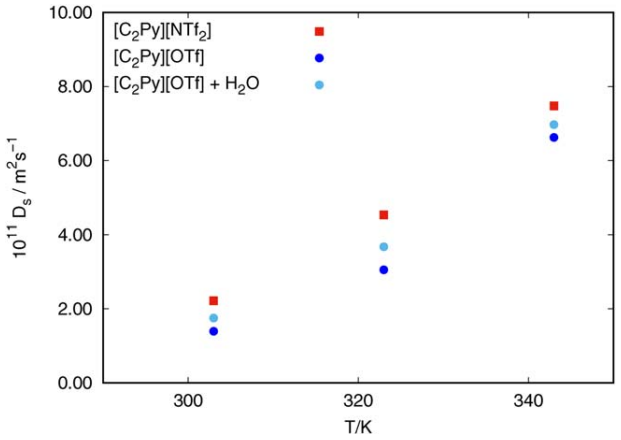

Figure 8. Average self-diffusivity of [C_2Py][NTf_2], [C_2Py][OTf], and [C_2Py][OTf] + H_2O water solution (x_{H_2O}=0.104) at different temperatures.

[Color figure can be viewed at wileyonlinelibrary.com]

some literature values[49] suggest that other ILs may present a higher water affinity. We will study other ILs in the future, in order to assess their suitability as water absorbents.

Dynamic properties

The need of pumping solutions with high concentrations of IL, which are viscous, may represent a barrier for the implementation of ILs in absorption heat pumps. Besides that, the microscopic dynamics influence heat and mass transfer, both of them critical either during the absorption or desorption process.[4] Therefore, the influence of different ions, of temperature and water content are explored here to better understand their impact on transport properties.

In Figure 8 simulation results for the self-diffusion coefficient of the two ILs and of the mixture with water are plotted. Even though a relatively narrow temperature range is covered, the diffusion coefficient increases by a factor of 4 when temperature rises from 303 to 343 K, in agreement with the known large effect of temperature on the dynamics of ILs. The different series show that the NTf_2^- anion leads to higher diffusivities than OTf^-, an issue that will be analysed in more detail below. It is also shown that water (x_{H_2O}=0.104) has a significant effect increasing the diffusivity of [C_2Py][OTf].

Diffusivity of [C_2Py][NTf_2] is higher than that of [C_2Py][OTf], consistent with experimental viscosities,[18] experimental diffusivity (Table 2). NTf_2^- is a less coordinating anion, as seen by the less marked microscopic structure shown in Figures 4 and 5, leading in general to low viscosity ILs, in spite of the large anion volume when compared to OTf^-. Calculation of the individual ion diffusion coefficients provides a more detailed view of the dynamics of ILs, giving a measurement of the relative contribution of each component to the dynamics of the whole system. According to Figure 9 cations diffuse faster than anions in all cases. The lower cation and anion mobilities in [C_2Py][OTf] compared to [C_2Py][NTf_2] are registered in cations and anions alike, and the same is observed in the presence of water, indicating the strongly correlated motion of cations and anions in molten salts and electrolytes. The mobility of water molecules is considerably higher than that of ions, and water also fluidifies the system leading to increased diffusion of all species.[50]

Results of viscosity calculations are presented in Table 3, and compared with experimental values published previously. As expected from the analysis of the diffusion coefficients, viscosity values from simulation using the present force field are almost exactly twice as large as experimental values. Therefore, in spite of a systematic deviation, the relative viscosities of the two ILs and of the mixture with water are very well predicted from simulation. Furthermore, the diffusion coefficients from simulation are predicted to be half of the experimentally observed values, where viscosity is predicted to be twice the experimental values, meaning that MD gives a coherent view of the two transport coefficients, in the sense of Stokes-Einstein equation. As such, we would expect that, if interactions models were adjusted to one of the transport properties, the other would be predicted quantitatively.

As mentioned before, high viscosities may represent a drawback for the implementation of ILs in absorption heat pumps, for this reason it is pertinent to establish a comparison between the viscosity of traditional systems based on lithium salts[51,52] and different IL + water mixtures[18,53,54] where ILs are potential absorbers for heat pumps. Although a detailed comparison is difficult due to the different experimental conditions, for most of the potential working pairs based on ILs (H_2O/IL) viscosities are in the same order than that of traditional (H_2O/LiBr) systems. For instance, while a mixture of [C_2Py][OTf] + H_2O with 0.758 mass fraction of IL has a viscosity of 4.6 mPa s,[18] the viscosity of a mixture LiBr + H_2O with 0.585 mass fraction of salt has a viscosity of 6.8 mPa s,[51] both at 298 K. It is also important to take into consideration the strong dependence of viscosity on temperature and water concentration. Regarding temperature, viscosity follows an Arrhenius-type behavior with exponential decay,[55] experimental data are very often fitted to Vogel-Fulcher-Tammann equation.[56] The increase of water concentration reduces largely the viscosity of the mixtures. Besides that, the viscosity of mixtures with a high water content becomes less dependent on temperature and even on the nature of the IL solution.[57] The critical step in the absorption process will be the absorber.[1,4] However, the viscosity of working pairs based on ILs can lie within the required limits for use in absorption heat pumps.

Table 2. Experimental and Simulated (exp/sim) Self-Diffusion Coefficients of the Individual Ions Forming [C_2Py][NTf_2], [C_2Py][OTf], and [C_2Py][OTf] + H_2O (x_{H_2O}=0.104)

D(exp/sim)/10^{-11} m^2s^{-1}						
	[C_2Py][NTf_2]		[C_2Py][OTf]		[C_2Py][OTf] + H_2O	
T/K	[C_2Py]	[NTf_2]	[C_2Py]	[OTf]	[C_2Py]	[OTf]
303	6.2/2.5	4.2/1.9	3.5/1.6	2.5/0.94	4.4/2.0	3.3/1.2
323	10.8/5.5	7.2/3.4	7.1/3.5	5.1/2.0	7.8/4.1	6.0/2.7
343	19.9/8.6	13.5/6.1	12.3/7.5	9.2/4.7	13.4/7.7	10.1/5.3

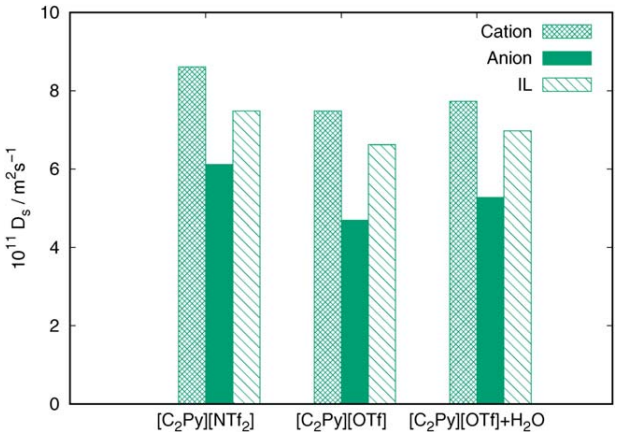

Figure 9. Self-diffusion coefficients of individual ions at 343 K.

In the IL + water mixture the diffusion coefficient of water is $D(H_2O) = 36.2\times10^{-11}\ m^2s^{-1}$. [Color figure can be viewed at wileyonlinelibrary.com]

Conclusions

In the present work we aimed to use MD simulation to explore the microscopic structural, energetic, and transport properties of two ILs and a mixture with water, in the scope of absorption/refrigeration pairs of working fluids. Pulsed-field gradient spin-echo NMR experiments provided diffusion coefficients for comparison with the calculations from simulation. The interaction models used have not been adjusted to any properties of ionic-liquid/water mixtures, therefore the simulation results are true (attempted) predictions.

One IL, $[C_2Py][NTf_2]$, is more hydrophobic whereas the other, $[C_2Py][OTf]$, is more hydrophilic, actually miscible with water across the entire composition range at ambient temperature. The first set of simulation results concerns microscopic structure. The radial distribution functions of both ILs are very similar, although those for the smaller OTf^- reveal a more marked ordering in the bulk liquid phase when compared to the larger an more flexible NTf_2^-. Hydrogen bonding patterns of water with the $[C_2Py][OTf]$ were analyzed and they show that the dominant H-bond occurs between water and the negatively charged O atoms of the anion.

Next, the free energy of solvation of water in the two ILs was calculated from free-energy perturbation. From these free energies we estimated the solubility of water and the simulations agree extremely well with experiment: we estimate a solubility of $x_{H_2O}=0.1$ in $[C_2Py][NTf_2]$ and total miscibility with $[C_2Py][OTf]$, which matches experiment.

Finally, diffusion coefficients and viscosities were calculated from equilibrium MD trajectories, using the Einstein and Green-Kube expressions, respectively. The results for the two ILs and for the mixture containing water are all consistent: diffusion coefficients are in all cases underestimated by a factor 2, and viscosities are overestimated by a factor 2 as well. Therefore, our results for the transport coefficients are mutually consistent in a Stokes-Einstein sense, although they show systematic deviations.

Table 3. Simulated and Experimental Viscosity of $[C_2Py][NTf_2]$, $[C_2Py][OTf]$, and $[C_2Py][OTf] + H_2O$ ($x_{H_2O} = 0.104$) at 343 K

	$[C_2Py][NTf_2]$	$[C_2Py][OTf]$	$[C_2Py][OTf] + H_2O$
η_{sim}/mPa s	20.5 ± 2.0	30.2 ± 4.3	25.9 ± 4.2
η_{exp}/mPa s[18]	10.9 ± 0.2	14.1 ± 0.3	13.4 ± 0.3

Overall we conclude that molecular simulation provides valuable insights at the microscopic level concerning the structural, thermodynamic, and transport properties of ILs and mixtures with interest for applications, namely, in refrigeration systems. The ability of simulation to restore trends correctly, either in terms of molecular structure as in thermodynamic conditions (such as temperature or composition), is valuable for the design of technological fluids. In particular, here we studied the effects of the choice of anion of the IL and of mixing with water on solvation and transport properties, which are key for the choice of working pairs. One perspective for future work concerns the influence of different functional groups in the ILs.

Acknowledgments

P.B.S. acknowledges support under the Plan Estatal de Investigación Científica y Técnica financed by Ministerio de Economía y Competitividad (DPI2012-38841-CO2-O2) and under the network REGALIS 2014/015 financed by Xunta de Galicia.

Literature Cited

1. Khamooshi M, Parham K, Atikol U. Overview of ionic liquids used as working fluids in absorption cycles. *Adv Mech Eng*. 2013;2013:1–7.
2. Zheng D, Dong L, Huang W, Wu X, Nie N. A review of imidazolium ionic liquids research and development towards working pair of absorption cycle. *Renew Sustain Energy Rev*. 2014;37:47–68.
3. Rodríguez-Muñoz JL, Belman-Flores JM. Review of diffusion-absorption refrigeration technologies. *Renew Sustain Energy Rev*. 2014;30:145–153.
4. Seiler M, Kühn A, Ziegler F, Wang X. Sustainable cooling strategies using new chemical system solutions. *Int Eng Chem Res*. 2013;52:16519–16546.
5. Wasserscheid P, Seiler M. Leveraging gigawatt potentials by smart heat-pump technologies using ionic liquids. *ChemSusChem*. 2011;4(4):459–463.
6. Welton T. Room-temperature ionic liquids. Solvent for synthesis and catalysis. *Chem Rev*. 1999;99(8):2071–2083.
7. Wasserscheid P, Welton T. *Ionic Liquids in Synthesis*, 2nd ed. Weinheim, Germany: Wiley-VCH, 2007.
8. Plechkova NV, Seddon KR. Applications of ionic liquids in the chemical industry. *Chem Soc Rev*. 2008;37(1):123–150.
9. Brennecke JF, Maginn EJ. Ionic liquids: innovative fluids for chemical process. *AIChE J*. 2001;47(11):2384–2389.
10. Ayou DS, Currás MR, Salavera D, García J, Bruno JC, Coronas A. Performance analysis of absorption heat transformer cycles using ionic liquids based on imidazolium cation as absorbents with 2,2,2-trifluoroethanol as refrigerant. *Energy Convers Manage*. 2014;84:512–523.
11. Lopes JNACL, Padua AAH. Nanostructural organization in ionic liquids. *J Phys Chem B*. 2006;110(7):3330–3335.
12. Cadena C, Zhao Q, Snurr RQ, Maginn EJ. Molecular modeling and experimental studies of the thermodynamic and transport properties of pyridinium-based ionic liquids. *J Phys Chem B*. 2006;110(6):2821–2832.
13. Kashyap HK, Annapureddy HVR, Raineri FO, Margulis CJ. How is charge transport different in ionic liquids and electrolyte solutions?. *J Phys Chem B*. 2011;115(45):13212–13221.
14. Crosthwaite JM, Muldoon MJ, Dixon JK, Anderson JL, Brennecke JF. Phase transition and decomposition temperatures, heat capacities and viscosities of pyridinium ionic liquids. *J Chem Thermodyn*. 2005;37(6):559–568.
15. Yokozeki A, Shiflett MB. Water solubility in ionic liquids and application to absorption cycles. *Ind Eng Chem Res*. 2010;49(19):9496–9503.

16. Liu QS, Yang M, Yan PF, Liu XM, Tan ZC, Welz-Biermann U. Density and surface tension of ionic liquids [Cnpy][NTf2] (n = 2, 4, 5). *J Chem Eng Data*. 2010;55(11):4928–4930.
17. Bittner B, Wrobel RJ, Milchert E. Physical properties of pyridinium ionic liquids. *J Chem Thermodyn*. 2012;55:159–165.
18. Sánchez PB, Currás MR, Mato MM, Salgado J, García J. Density and viscosity study of pyridinium based ionic liquids as potential absorbents for natural refrigerants: Experimental and modelling. *Fluid Phase Equilib*. 2015;405:37–45.
19. Jorgensen WL, Maxwell DS, Tirado-Rives J. Development and testing of the Opls all-atom force-field on conformational energetics and properties of organic liquids. *J Am Chem Soc*. 1996;118(45):11225–11236.
20. Canongia Lopes JN, Pádua AAH. Molecular force field for ionic liquids composed of triflate or bistriflylimide anions. *J Phys Chem B*. 2004;108(43):16893–16898.
21. Canongia Lopes JN, Pádua AAH. Molecular force field for ionic liquids III: imidazolium, pyridinium, and phosphonium cations; chloride, bromide, and dicyanamide anions. *J Phys Chem B*. 2006; 110(39):19586–19592.
22. Pádua AA. Force field for ionic liquids. 2016. Available at https://github.com/agiliopadua/ilff
23. Berendsen HJC, Grigera JR, Straatsma TP. The missing term in effective pair potentials. *J Phys Chem*. 1987;91(24):6269–6271.
24. Plimpton S. Fast parallel algorithms for short-range molecular dynamics. *J Comput Phys*. 1995;117:1–19.
25. Plimpton S. LAMMPS. Molecular dynamics simulator. 2015. Available at http://lammps.sandia.gov
26. Martínez L, Andrade R, Birgin E, Martínez J. PACKMOL: a package for building initial configurations for molecular dynamics simulations. *J Comput Chem*. 2009;30(13):2157–2164.
27. Pádua AA. Force field tool. 2016. Available at https://github.com/agiliopadua/fftool
28. Hockney RW, Eastwood JW. *Computer Simulation Using Particles*, 1st ed. New York, NY: CRC Press, 1989.
29. Bhargava BL, Balasubramanian S. Refined potential model for atomistic simulations of ionic liquid [bmim][PF6]. *J Chem Phys*. 2007; 127(11):1–6.
30. Schröder C. Comparing reduced partial charge models with polarizable simulations of ionic liquids. *Phys Chem Chem Phys*. 2012; 14(9):3089.
31. Borodin O. Polarizable force field development and molecular dynamics simulations of ionic liquids. *J Phys Chem B*. 2009; 113(33):11463–11478.
32. Beutler TC, Mark AE, van Schaik RC, Gerber PR, van Gunsteren WF. Avoiding singularities and numerical instabilities in free energy calculations based on Mol. Simul.s. *Chem Phys Lett*. 1994;222(6):529–539.
33. Chipot C. Free-energy calculations. Measuring free-energy differences using computer simulations. 2010:1–112.
34. Mondello M, Grest GS. Viscosity calculations of n-alkanes by equilibrium molecular dynamics. *J Chem Phys*. 1997;106(22):9327
35. Köddermann T, Paschek D, Ludwig R. Molecular dynamic simulations of ionic liquids: a reliable description of structure, thermodynamics and dynamics. *ChemPhysChem*. 2007;8(17):2464–2470.
36. Tenney CM, Maginn EJ. Limitations and recommendations for the calculation of shear viscosity using reverse nonequilibrium molecular dynamics. *J Chem Phys*. 2010;132(1):1–8.
37. Zhang Y, Maginn EJ. Direct correlation between ionic liquid transport properties and ion pair lifetimes: a molecular dynamics study. *J Phys Chem Lett*. 2015;705(3):700–705.
38. Evans PT, Cummings DJ. Nonequilibrium molecular dynamics properties and non newtonian fluid approaches to transport rheology. *Ind Eng Chem Res*. 1992;31:1237–1252.
39. Müller-Plathe F, Reith D. Cause and effect reversed in non-equilibrium molecular dynamics: an easy route to transport coefficients. *Comput Theor Polym Sci*. 1999;9:203–209.
40. Ramírez J, Sukumaran SK, Vorselaars B, Likhtman AE. Efficient on the fly calculation of time correlation functions in computer simulations. *J Chem Phys*. 2010;133(15):1–12.
41. Marin-Rimoldi E, Shah JK, Maginn EJ. Monte Carlo simulations of water solubility in ionic liquids: a force field assessment. *Fluid Phase Equilib*. 2015;407:117–125.
42. Villanueva M, Parajó J, Sánchez PB, García J, Salgado J. Liquid range temperature of ionic liquids as potential working fluids for absorption heat pumps. *J Chem Thermodyn*. 2015;91:127–135.
43. Zhu X, Wang Y, Li H. The structural organization in aqueous solutions of ionic liquids. *AIChE J*. 2009;55(1):198–205.
44. Zielkiewicz J. Structural properties of water: comparison of the SPC, SPCE, TIP4P, and TIP5P models of water. *J Chem Phys*. 2005; 123(10):1–6.
45. Liu X, Zhou G, Zhang X, Zhang S. Molecular dynamics simulation of desulfurization by ionic liquids. *AIChE J*. 2010;56(11):405–410.
46. Popp S, Bösmann A, Wölfel R, Wasserscheid P. Screening of ionic liquid/H_2O working pairs for application in low temperature driven sorption heat pump systems. *ACS Sustain Chem Eng*. 2015;3(4): 750–757.
47. Daiguji H, Hihara E. Molecular dynamics study of the liquid–vapor interface of lithium bromide aqueous solutions. *Heat Mass Transfer*. 1999;35:213–219.
48. Shah JK, Maginn EJ. Monte Carlo simulations of gas solubility in the ionic liquid 1-n-butyl-3-methylimidazolium hexafluorophosphate. *J Phys Chem B*. 2005;109(20):10395–10405.
49. Wu H, Maginn EJ. Water solubility and dynamics of CO_2 capture ionic liquids having aprotic heterocyclic anions. *Fluid Phase Equilib*. 2014;368:72–79.
50. Kelkar M, Maginn E. Effect of temperature and water content on the shear viscosity of the ionic liquid 1-ethyl-3-methylimidazolium bis (trifluoromethanesulfonyl) imide as studied by atomistic simulations. *J Phys Chem B*. 2007;111(18):4867–4876.
51. Wimby JM, Berntsson TS. Viscosity and density of aqueous solutions of LiBr, LiCl, ZnBr2, CaCl2, and LiN03, 1, single salt solutions. *J Chem Eng Data*. 1994;39:68–72.
52. Wimby JM, Berntsson TS. Viscosity and density of aqueous solutions of LiBr, LiCl,ZnBr2, CaCl2, and LiN03, 2, two-salt solutions. *J Chem Eng Data*. 1994;39:73–78.
53. Brennecke JF, Rodríguez H. Temperature and composition dependence of the density and viscosity of binary mixtures of water + ionic liquid. *J Chem Eng Data* 2006;51:2145–2155.
54. Constantinescu D, Schaber K, Agel F, Klingele MH, Schubert TJS. Viscosities, vapor pressures, and excess enthalpies of choline lactate + water, choline glycolate + water, and choline methanesulfonate + water systems. *J Chem Eng Data* 2007;52:1280–1285.
55. Sánchez PB, García J, Salgado J, González-Romero E. Studies of volumetric and transport properties of ionic liquid–water mixtures and its viability to be used in absorption systems. *ACS Sus Chem Eng*. 2016;4(9):5068–5077.
56. Fulcher GS. Analysis of recent measurements of the viscosity glasses. *J Am Ceram Soc*. 1925;8(6):339–355.
57. Fendt S, Padmanabhan S, Blanch HW, Prausnitz JM. Viscosities of acetate or chloride-based ionic liquids and some of their mixtures with water or other common solvents. *J Chem Eng Data*. 2011; 56(1):31–34.

Manuscript received Sep. 5, 2016, and revision received Jan. 12, 2017.

4.5 Structural effects on dynamic and energetic properties of mixtures of ionic liquids and water

- This article is the product of the collaboration between the Thermodinamique et Intéractions Moléculaires group (Université Blaise Pascal) and the Applied Physics Department (Universidad de Vigo).
- P.B.S. has performed the MD simulations and the data analysis to calculate the physical properties.
- P.B.S redacted a major part of the manuscript under the supervision of A.A.H.P.

Journal of Molecular Liquids 242 (2017) 204–212

Contents lists available at ScienceDirect

Journal of Molecular Liquids

journal homepage: www.elsevier.com/locate/molliq

Structural effects on dynamic and energetic properties of mixtures of ionic liquids and water

Pablo B. Sánchez[a,b], Josefa García[b], Agílio A.H. Pádua[a,*]

[a] Institut de Chimie de Clermont Ferrand, Université Clermont Auvergne & CNRS, Clermont-Ferrand 63000, France
[b] Departamento de Física Aplicada, Universidad de Vigo, Spain

ARTICLE INFO

Article history:
Received 26 April 2017
Received in revised form 21 June 2017
Accepted 23 June 2017
Available online 5 July 2017

Keywords:
Ionic liquids
Water
Molecular simulation
Solvation
Hydrogen bonding
Transport properties

ABSTRACT

The aim of this study is to improve our understanding of the microscopic and macroscopic properties of mixtures of ionic liquids with water, in the context of working pairs for absorption heat cycles. We report a molecular dynamics study of dynamic properties (viscosity and diffusion coefficients), water solvation (free energy and local solvation environments) and hydrogen bonding in mixtures of six ionic liquids with water, at two concentrations $x_{H_2O} = 0.104$ and $x_{H_2O} = 0.900$. Three anions, methanesulfonate, dicyanamide and acetate; and two cations, N-ethylpyridinium and cholinium, were chosen due to their potential for water absorption and halogen-free structures. Simulation results capture the trends of experimental data, and were interpreted in terms of the molecular structures and interactions. The strength of hydrogen bonding is a major criterion determining the affinity of an ionic liquid towards water. In particular, the cholinium cations compete with water establishing hydrogen bonds with the acetate anions and this is not favourable in terms of water affinity. Dicyanamide anions lead to the systems with lower viscosity.

1. Introduction

Ionic liquids (ILs) are among the most promising classes of solvents, reaction or separation media or technological fluids of the XXI century [1,2]. Due to their tuneable physical and chemical properties, and recyclability, ionic liquids appear as alternatives for many applications [3–5], within the trend of sustainable chemistry, reduce the environmental footprint of chemical and processes. Concerns of sustainability are central when choosing alternatives to traditional industrial processes.

Among the potential uses of ionic liquids, absorption heat pumps present an opportunity to reduce the emissions of greenhouse gases in heating/cooling systems. The advantages and challenges of this technology were already treated in detail [6,7]. The scientific community is seeking alternatives to improve the performance of traditional working pairs of refrigerant/absorbent and amidst the most promising working pairs are those based on ILs together with water as refrigerant [8,9].

Most research in this field is focused on identifying which ILs fit with the requirements of the application. Due to their particular chemical structure, large and asymmetrical ions with a highly delocalized charge, all ILs share certain properties such as extremely low vapor pressures and flammability; many have low melting points and wide electrochemical windows [10,11]. However, many chemical structures are possible through choice of ions or chemical functional groups, leading to an enormous amount of possible combinations with a large variety in some of the key properties for water absorption. As such, it is essential to improve our present fundamental understanding of the physical chemistry of mixtures of ionic liquids with molecular compounds. Thus, a study of the cation and anion effects on the relevant properties for absorption processes is necessary, in order to tailor the structure of the ILs, attaining the technical requirements. Two of those key properties are the absorption capacity and the transport properties of IL + water mixtures.

An adequate water absorption capacity is a limiting factor, since the change in pressure of the refrigerant is done by an absorption/desorption process. In other words, the suitable IL should have a significant ratio between the water absorbed and the volume of IL [12] meaning that absorbents with large water affinity are required. This is often quantified by measuring the deviation from Raoult's law [13] or the refrigerant's activity coefficient at infinite dilution [14]. Besides the thermodynamic quantities related to water absorption, the transport properties of the IL + water systems have an enormous importance, because high viscosities are frequently a barrier for their industrial implementation. Besides increasing the

* Corresponding author.
E-mail address: agilio.padua@uca.fr (A.A. Pádua).

http://dx.doi.org/10.1016/j.molliq.2017.06.109
0167-7322/

pumping cost of the process, slow dynamics have a negative impact in the heat and mass transfer, and therefore in the water absorption mechanism [9].

The complexity of the interactions that govern the behaviour of ionic liquids makes it very difficult to achieve a detailed understanding of all the factors determining their properties. Together with experimental work, done mainly over the last decade, the use of theoretical tools proved very powerful in explaining the structure-property relations in IL systems. Some of main advances concern the nanostructural segregation [15] of the IL phases, the main factors influencing their dynamics [16] or the nature of charge transport [17] in IL media, in all of these cases using molecular dynamics simulation (MD) techniques.

In this work, MD was used to study the thermodynamics of water solvation in ILs and the dynamics of six IL + water mixtures. In all cases, two water concentrations, $x_{H_2O} = 0.104$ and $x_{H_2O} = 0.900$, have been investigated. These concentrations were chosen because we intend to study the effect of water on the properties of IL + H_2O mixtures, being interesting to have two very different concentrations. Also, these concentrations reproduce the conditions in the generator and the absorber of an absorption refrigeration cycle . The chemical structures of the ILs consist of two cations and three anions, allowing to see how each ion affects the final properties of the mixtures. Factors related to the microscopic structure and local ordering, or to the interaction energies between different functional groups, including a quantification of hydrogen bonding, were also analysed. Some of the methods used in the present study were used in a recent work on a related topic [18].

2. Methods

The compounds studied here were represented by a molecular force field compatible with the Optimised Potential for Liquid Simulations All Atom (OPLS-AA) [19], with specific parameter sets for ionic liquids (CL&P) [20–22]. This is a model with harmonic bonds and angles, torsion energy terms given by cosine series, and non-bonded interactions described by fixed electrostatic partial charges and Lennard-Jones atomic sites.

Integer, fixed-charge models lead to slower dynamics in ionic liquids, with diffusion coefficients that are too low and viscosities that are too high [18]. Therefore, we scaled atomic charges of all ions have by factor of 0.8, following previous studies [23,24] that pointed out that the transport properties of ILs are better described by charge-scaled than full-charged models. Water was represented by the SPC/E model [25].

Molecular dynamics (MD) simulations were performed using the LAMMPS [26,27] open source package. Initial configurations were created using the Packmol [28] and fftool [29] utilities. All simulations were carried out in periodic cubic boxes containing 300 ion pairs and 35 water molecules, for systems with high IL content and water mole fraction $x_{H_2O} = 0.104$, whereas systems with a low IL concentration $x_{H_2O} = 0.900$ contained 100 ion pairs and 900 water molecules. A cutoff of 12 *Å* was applied to LJ interactions and electrostatics were handled using the particle-particle particle-mesh [30] method with a precision of 10^{-4} in electrostatic energy. The timestep was set to 1 fs. All simulations were run at constant *NpT* by means of Nosé-Hoover thermostat and barostat at 343 K and 1 bar. These conditions above room temperature were chosen to ensure the systems reach the diffusive regime within a reasonable time, thus shortening the length of the simulations. Furthermore, this temperature corresponds to the conditions of in the generator [9] of an absorption refrigeration process.

Initial equilibrations of 1 ns were carried out starting from the configurations generated by Packmol. Longer trajectories were needed to calculate thermodynamic and dynamic properties, so we ensured that systems had effectively reached the diffusive regime by computing the β parameter [16] (Eq. (1)) and checking that its value was close to unity.

$$\beta(t) = \frac{d\log\langle\Delta r(t)^2\rangle}{d\log t} \tag{1}$$

Viscosity is a key property for any technological application. Here we calculate viscosity of six different ILs and their aqueous mixtures, at low and high water concentrations. Viscosity was calculated from the equilibrium trajectories using the Green-Kubo method, i.e. integration of the autocorrelations of components of the pressure tensor (Eq. (2)).

$$\eta = \frac{V}{kT}\int_0^\infty \langle p_{xy}(t)p_{xy}(0)\rangle dt \tag{2}$$

The autocorrelations were recorded using the multiple step correlator method [31] with $m = 2$ and $p = 16$ implemented in LAMMPS. The result was averaged over three independent shear components and the uncertainty was estimated from the standard deviation of these values.

Diffusion coefficients of the different species were calculated from the mean square displacement (Eq. (3)) once the systems reached the diffusive regime [16].

$$D = \frac{1}{6}\lim_{t\to\infty}\frac{d}{dt}\langle\Delta r(t)^2\rangle \tag{3}$$

Thermodynamic quantities related to the absorption process are crucial in the intended application of the IL mixtures in absorption cycles, so we calculated the solvation free energies of water, the refrigerant. The free energy perturbation [32] (FEP) method was used to calculate chemical potentials. We used 20 intermediate states to attain an accurate sampling of the free energy difference corresponding to the creation (or annihilation) of one solute (water) molecule. The total trajectory time for the full free energy routes was 4 ns, and at each activation stage an equilibration period was allowed before acquisition. Details on the creation and annihilation transformations can be found in supplementary formation (Figure S1). A good superposition of creation and annihilation routes was the criterion to choose the conditions of the free-energy calculation. Since SPC/E water has no intramolecular energy terms, no corrections are required in order to calculate the solvation free energy.

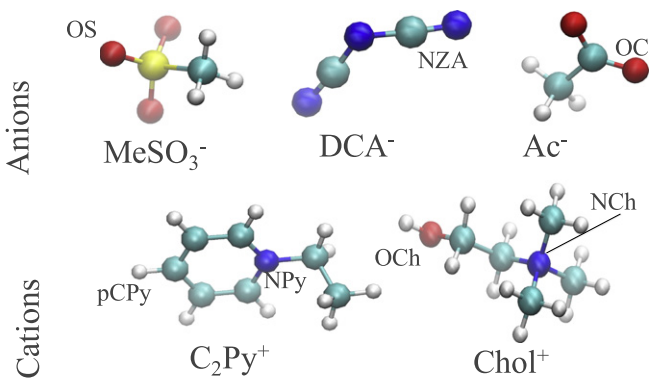

Fig. 1. Chemical structures contained of chemical species of this work and selected interaction sites for radial and spatial distribution functions.

Table 1
Simulated viscosity of IL + H_2O binary systems at two water compositions and 343 K.

	η/ mPa s	
	$x_{H_2O} = 0.104$	$x_{H_2O} = 0.900$
$[C_2Py][MeSO_3]$	20.4 ± 2.7	1.53 ± 0.02
$[C_2Py][DCA]$	9.1 ± 1.1	1.34 ± 0.03
$[C_2Py][Ac]$	15.2 ± 1.4	2.40 ± 0.02
$[Chol][MeSO_3]$	106.9 ± 31.4	1.69 ± 0.08
[Chol][DCA]	12.7 ± 1.6	1.28 ± 0.03
[Chol][Ac]	114.1 ± 26.6	2.60 ± 0.29

3. Results

The chemical structures of the ions studied here are shown in Fig. 1. Simulated densities at 343 K are also shown in Table S1.

3.1. Dynamic properties

Dynamic properties were calculated for mixtures of ILs with water at two compositions, $x_{H_2O} = 0.104$ and $x_{H_2O} = 0.900$. In Table 1 viscosities at 343 K are shown. These results give a picture of the dynamics of each system where the first thing we note is how an increase in water content reduces drastically the magnitudes and differences in viscosities, and thus a high water content diminishes the influence of the IL on the transport properties.

Experimental values are not available in the literature for all our mixtures, therefore direct comparison is not always possible. Regardless of water content, systems containing the DCA^- anion are the least viscous, especially at $x_{H_2O} = 0.104$. This is in agreement with experimental information from the literature, with DCA^- based ILs remarked as being low-viscosity salts [33,34]. The viscosity of IL + water mixtures containing Ac^- and DCA^- with a common cation was determined [35] showing that DCA^- ILs have a much lower viscosity. Further explanations of the dynamic behaviour of ILs containing cyano anions can be found in Weber and Kirchner [36].

Experimental viscosities of $[C_2Py][MeSO_3] + H_2O$ were reported at different temperatures and concentrations [37] and the present simulations are in qualitative agreement with the data. In order to uncover the trends between $MeSO_3^-$ and Ac^- ILs, experimental data of systems containing those anions together with 1-ethyl-3-methylimidazolium cation, ($C_2C_1Im^+$), were analysed. At 353 K, the experimental viscosity of $[C_2C_1Im][MeSO_3] + H_2O$ is 1.3 and 12.3 mPa s, for water mole fraction of 0.12 and 0.90, respectively [38]. For $[C_2C_1Im][Ac] + H_2O$ at $x_{H_2O} = 0.10$ the viscosity is 13.0 mPa s [39], thus following the same trend we observed in the simulations with the pyridinium cation. Imidazolium ILs normally have lower viscosities than the pyridinium counterparts (with comparable side chains [40].

Another pattern we notice from Table 1 is how the presence of $Chol^+$ leads to an increase in viscosity. This trend is also observed experimentally [41,42].

Individual diffusion coefficients of ions and water were obtained from Eq. (3) after ensuring that the diffusive regime had been reached according to the β criterion [16]. Results are plotted in Fig. 2 and values given in the Supplementary Information Table S2. As expected, water diffuses faster than the ions in all of the mixtures, with D values that are dependent strongly on the ions, mainly at low water concentrations ($x_{H_2O} = 0.104$): the ratio of diffusion coefficient of water with respect to the ions goes from 1.5 for $[C_2Py][Ac]$) to 15 for $[Chol][MeSO_3]$. In water-rich mixtures, $x_{H_2O} = 0.900$, water diffuses between 2.5 and 3.5 times faster than the ions. An explanation for this behaviour may be the strength of the H_2O-anion binding, which we will address in detail in the following sections. Concerning ion mobility, the results indicate that dynamics are a result of an interplay of both ions, without a unique trend. Nonetheless, DCA^- leads in all cases to faster dynamics, whereas $Chol^+$ cation slows down sharply the dynamic of the mixtures. Again, scarce experimental data on these properties were found. But diffusivities of $MeSO_3^-$ and Ac^- with a common cation [38,43] show that simulations predict the relations between structure and transport properties reliably.

3.2. Energetics of water solvation

The Gibbs energy of solvation of water in the six ILs, and also the Henry's law constant (defined as $p_{H_2O} = Hx_{H_2O}$) of water, were calculated from the residual chemical potential of water in the ILs obtained using the free energy perturbation (FEP) method, and are

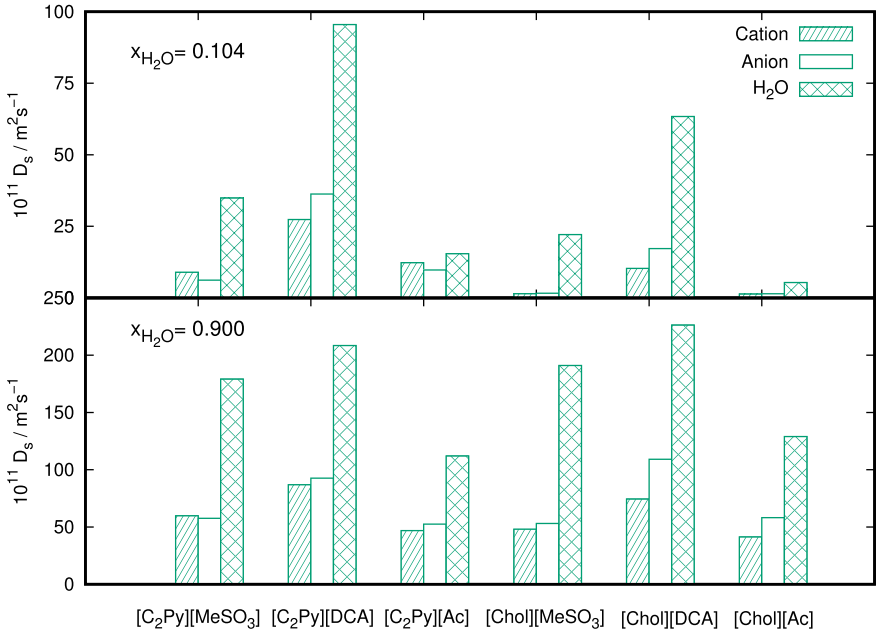

Fig. 2. Individual diffusion coefficients for ILs + H_2O mixtures at 343 K, each bar chart representing the water mole fraction indicated.

Table 2
Henry's constant of water in the ILs at 343 K.

IL	$\Delta_{solv}G^{\circ}$ / $kJmol^{-1}$	H/ bar
$[C_2Py][MeSO_3]$	−1.48	0.19
$[C_2Py][DCA]$	−3.8	0.082
$[C_2Py][Ac]$	−16.6	0.0011
$[Chol][MeSO_3]$	0.71	0.40
[Chol][DCA]	−3.0	0.11
[Chol][Ac]	−12.5	0.0040

listed in Table 2. Details of the calculation procedure are given in our previous publication [18] and residual chemical potentials are listed in Table S3 of the supplementary information.

The ordering of IL regarding their affinity for water is as follows: $[C_2Py][Ac] > [Chol][Ac] > [C_2Py][DCA] > [Chol][DCA] > [C_2Py][MeSO_3] > [Chol][MeSO_3]$

This trend is in agreement with the anion playing the key role during the solvation process [44,45]. Among the three different anions, acetate is by far the one presenting a larger water affinity, followed by dicyanamide and methanesulfonate. Studies of these systems are scarce in literature, but nonetheless they allow to infer that simulation results are correct, at least qualitatively. Vapor pressure measurements [46] showed that carboxylate anion leads to larger water affinity than methanesulfonate, with cholinium cation. Another study [47] indicates that among carboxylate anions, addition of either an alkyl chain or an HO^- group reduces the interactions with water, which will increase Henry's law constants. The vapor pressure of water in dicyanamide ILs has been determined for two different cations [48] and, even tough experimental conditions are not the same, the results allow to infer that DCA^- ILs present larger water affinity than those based on $MeSO_3^-$.

When analysing the influence of the cation on water affinity, we realise that despite this being a minor effect compared to the role of the anion, it cannot be considered negligible. Namely, C_2Py^+ ILs show a stronger water affinity than those based on $Chol^+$, with a lower Gibbs energy of solvation by about 10%. Considering the chemical structures of pyridinium and cholinium this could be surprising since $Chol^+$ with its asymmetry and OH^- group could seem to be "friendlier" towards polar solutes than the aromatic ring in C_2Py^+. In the next sections we will address this issue by analysing the liquid-phase structure at the atomistic scale, the structure of solvation shells and the interaction energies between components.

3.3. Insights from microscopic structure

The ordering of ions around water provides relevant information and insights that can be related to the thermodynamic and transport properties of the systems.

In Fig. 3 the radial distribution functions (RDFs) of six mixtures with a low water concentration, $x_{H_2O} = 0.104$, are plotted. As indicated by the thermodynamic quantities of solvation in the ILs (Table 2), differences in the ILs-water interactions are mainly determined by the anion. The height of the peak corresponding to water-anion distributions in the RDFs (red line) backs the idea that stronger binding between water and anion groups will lead to larger

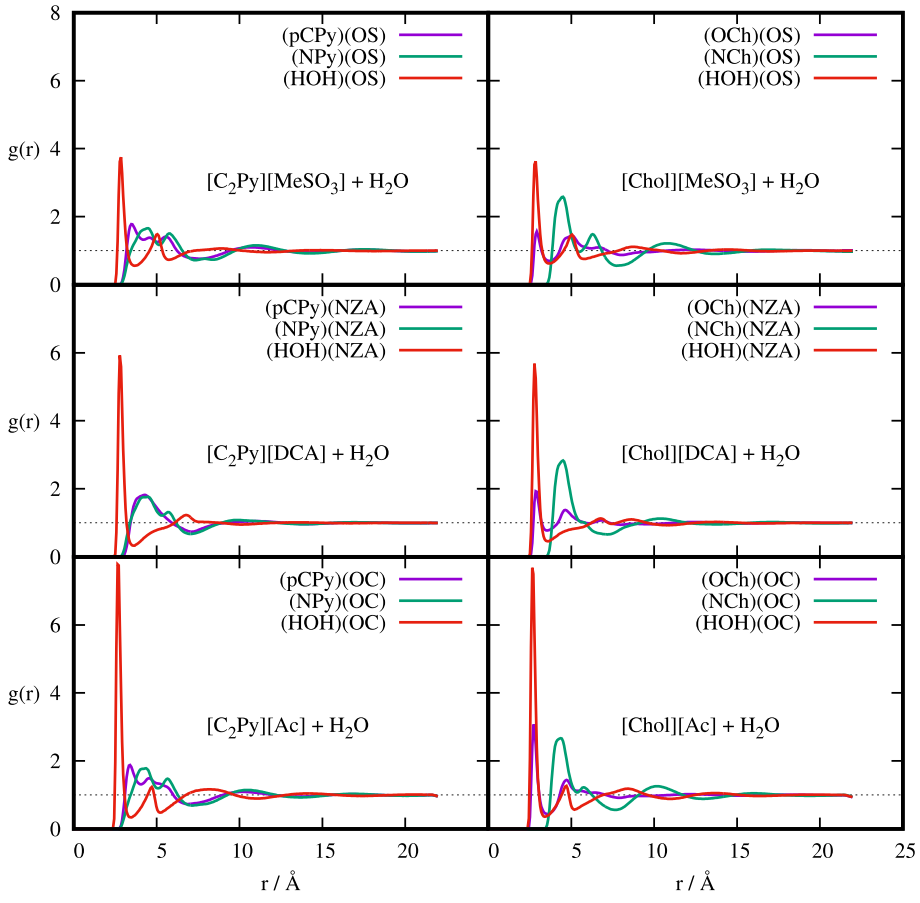

Fig. 3. Radial distribution functions of ILs + H_2O mixtures with $x_{H_2O} = 0.104$ (300 ions pairs and 35 water molecules). Nomenclature of sites is indicated in Fig. 1. HOH represents the oxygen of the water molecules.

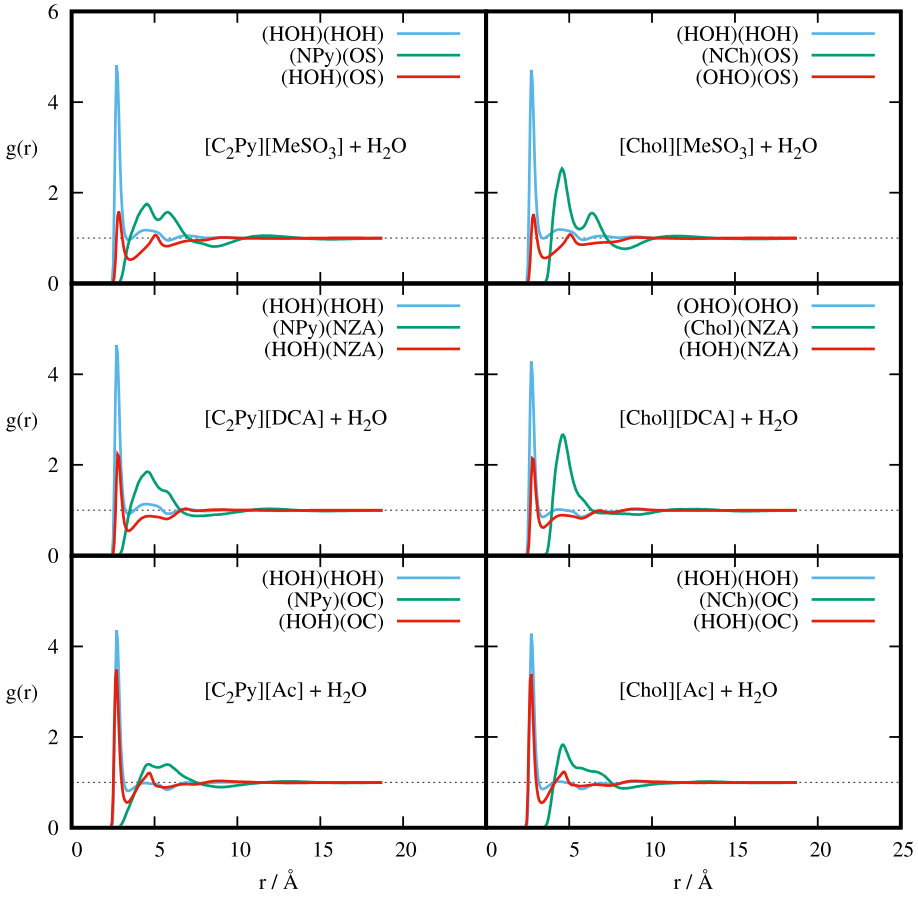

Fig. 4. Radial distribution functions of ILs + H_2O systems with $x_{H_2O} = 0.900$ (100 ion pairs and 900 water molecules). Nomenclature of sites is indicated in Fig. 1. HOH represents the oxygen of the water molecules.

absorption capacities of the ionic liquid. RDFs suggest bonding of water with H-bond acceptor groups of the anion. In the SI we include water-water RDFs, which have very intense first peaks, typically of some water self-association in systems where this species is diluted (therefore the local density of pairs found becomes much larger than the average). The intensity of water-water first peaks is strongly dependent on the anion, being lower in acetate ILs because water binds strongly to the anion and less to other water molecules.

The increase in water concentration leads to important changes in the microscopic ordering of the mixtures. In Fig. 4, for $x_{H_2O} = 0.900$, we observe that the water-water peak is higher than the water-anion peak suggesting formation of water clusters, which is normal at this composition corresponding to ca. 50% in volume fraction. Water-anion interactions in Fig. 4 keep the same trend observed in Fig. 3 and in the simulated Henry's law constant.

Another pattern in water affinity was found analysing the cation effect (see Table 2). The presence of $Chol^+$ leads to a decrease in solubility (increase in Henry's law constant). When we observe the effect of the cation on the atomistic ordering, we notice that for cholinium ILs a peak appears between the OH group of the cation and negatively-charged O or N atoms of the anions (see Figs. 3 and 4). This peak, corresponding to a cholinium-anion H-bond is at the same distance as the water-anion H-bonds. Although the intensity of the cation-anion peak is lesser, it suggests a competition between cholinium and water for the H-bond acceptor positions of the anion, explaining the reduction in water affinity when C_2Py^+ is replaced by $Chol^+$. Spatial distribution functions (SDFs) of [C_2Py][Ac] and [Chol][Ac] in Fig. 5 support that idea, showing how the cholinium OH group and H_2O compete in the anion solvation shell for the H-bond positions. This competition will hinder water solvation: steric impediments for water to form hydrogen bonding with the anion and an energetic barrier related to the anion-cation binding. This effect has been observed for different acetate ionic liquids where the presence of additional OH groups led to decrease in water affinity [47]. An extended analysis of hydrogen bonding will be performed in the next section in order to quantify this effect.

As happens with water affinity, structural insights help us understand certain patterns in the dynamics of IL + water mixtures. Regarding the cation effect, all cholinium systems have a well-defined peak at approximately 5 Å between NCh and the anion. This suggests a more marked ordering that cat lead to slower dynamics and also higher melting points of cholinium ILs [37,42]. Fig. 4 indicates how first peaks denoting interaction between water molecules (blue lines) are quantitatively the most important. Thus, water clustering clearly facilitates the fluidicy of the systems [49,50].

3.4. Hydrogen bonding

In Table 3 the likelihood of different hydrogen bonds in the studied mixtures is reported. A distance of 2.5 Å and an angle of 30° were used as criteria [51] for counting a hydrogen bond. Note that the presence of $Chol^+$ increases largely the number of potential hydrogen donors and acceptors because of the OH of this cation. However, this group is a very weak acceptor and essentially only acts as H-bond

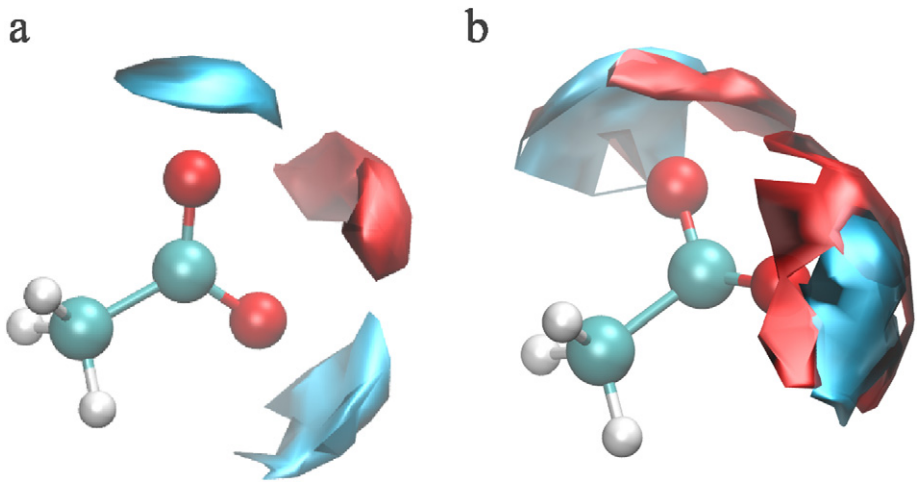

Fig. 5. Solvation environment of [cat][Ac], in (a) cat = C_2Py^+ and (b) $Chol^+$. Blue isosurfaces represent water hydrogen and red isosurfaces the hydrogen of either C_2Py^+ ring or the $Chol^+$ hidroxi group in a and b, respectively.

donor, mainly towards the nucleophilic groups of the anions and, to a minor extent, towards water.

Among the anions studied, acetate is the stronger H-bond acceptor. The carboxilate group forms in all cases more H-bonds than either the sulfonate or the cyano groups, roughly 1.5 times more. This supports that water absorption in the IL is favoured by H-bonding with the anion, thus anions with strong nucleophilic centres should be selected when large water affinity is sought.

On the side of H-bond donors, results in Table 3 demonstrate that water is a better H-bond donor than cholinium, since the relative frequency of hydrogen bonds (number of occurrences divided by the number of interaction sites, donor or acceptor) is larger for the solvent than for the cation.

In systems with a high water concentration, the presence of H-bonds between water molecules suggests the presence of clustering, since the frequency of bonds is slightly above one per molecule. No significant differences were found between systems, this clustering formation being of similar extent irrespective of the IL. This could be linked to the reduction of viscosity in mixtures when water concentration reaches a certain value, independently of the IL.

An analysis of the intensities of H-bonds is illustrated in Fig. 6. In Fig. 6a, the distribution of H-bonds as a function of the length

Table 3
Frequency of different hydrogen bonds for all the studied systems. Values shown in the table are the number of hydrogen bonds per interaction site, either donors or acceptors, taking the minimum value among both of them.

	$x_{H_2O} = 0.104$	$x_{H_2O} = 0.900$
$[C_2Py][MeSO_3] + H_2O$		
SO...HO	0.66	0.83
HO...HO	0.14	1.13
$[C_2Py][DCA] + H_2O$		
CN...HO	0.69	1.18
HO...HO	0.11	1.14
$[C_2Py][Ac] + H_2O$		
CO...HO	0.90	1.81
HO...HO	0.14	1.12
$[C_2Py][Ac] + H_2O$		
CO...HO	0.90	1.81
HO...HO	0.14	1.12
$[Chol][MeSO_3] + H_2O$		
SO...HOCh	0.52	0.18
SO...HO	0.63	0.78
HO...HO	0.14	1.12
$[Chol][DCA] + H_2O$		
CN...HOCh	0.46	0.12
CN...HO	0.64	1.13
HO...HO	0.11	1.11
$[Chol][Ac] + H_2O$		
CO...HOCh	0.96	0.15
CO...HO	0.89	1.77
HO...HO	0.03	1.10

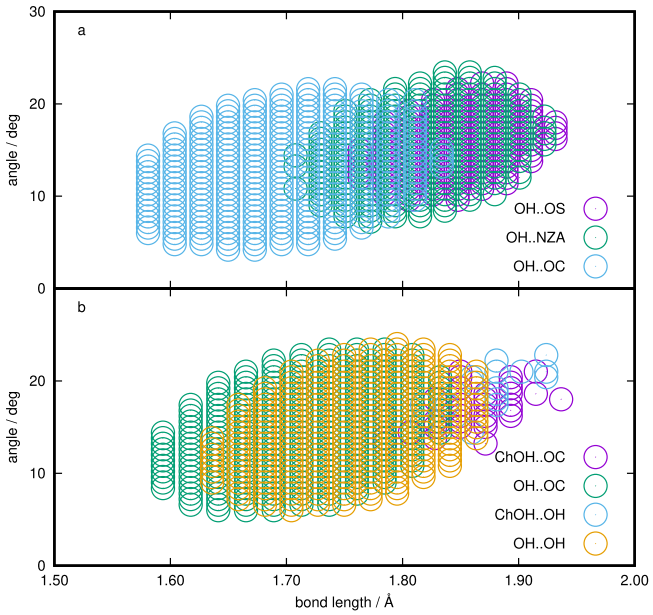

Fig. 6. Hydrogen bond distribution as a function of the length and angle depending on a) the anion b) all posibilities in a [Chol][Ac] + H_2O system with $x_{H_2O} = 0.900$. Nomenclature of sites of anions are indicated in Fig. 1. OH represent water atoms unless prefix Ch is set, in these cases it represents $Chol^+$ hidroxi group.

and the angle between water and the anion is shown. No significance difference between $MeSO_3^-$ and DCA^- is observed (the areas of higher H-bond frequency overlap). However, acetate appears to be a stronger nucleophilic group, with binding between water and the carboxilate group not only more likely to happen but also stronger. A detailed study of hydrogen bonding in aqueous mixtures using *ab initio* molecular dynamics (AIMD) by Kirchner and coworkers [52] confirms the strength of this H-bond. According to this work, in some configurations proton transfer would occur from water forming acetic acid. In Fig. 6b, the [Chol][Ac] + H_2O mixture was chosen as a representative system because it contains several kinds of H-bond. Cholinium is shown to be a weaker H-bond donor than water, no matter the H-bond acceptor to which it is associating. In spite of the lower frequency and relative weakness of H-bonds, cholinium influences the dynamic and energetic properties of the mixtures.

3.5. Interaction energies

To asses the interaction energies between the constituent species of the mixtures we defined a neighbouring criterion: two molecules or ions are considered neighbours when the distance between two atoms, one from each, is shorter than $2\sigma_{LJ}$. Only those entities were considered in the calculation of interaction energies shown in Fig. 7.

Cation-anion interaction energies are shown in Fig. 7. Although systems based on DCA^- have smaller interaction energies (in absolute terms), which is consistent with faster dynamics, these differences seem too small by themselves to explain the disparity in viscosity values. The same can be said for the effect of larger interaction energies $Chol^+$ that do not appear sufficiently larger to explain the drastic increase in viscosity of cholinium systems.

Regarding the interactions of the ions with water, the energies in Fig. 7 capture well the affinity trend of the anions and also the higher affinity of $Chol^+$ when compared to C_2Py^+, discussed before in terms of solvation free energies.

The effect of a higher water concentration can be observed in Fig. 8. Here the interaction energies between neighbouring water molecules were also calculated and their values are larger than interactions with the ions. Again, there is a consistency between the interaction energies and the frequency of association between water and the different ions given by H-bond statistics in Table 3.

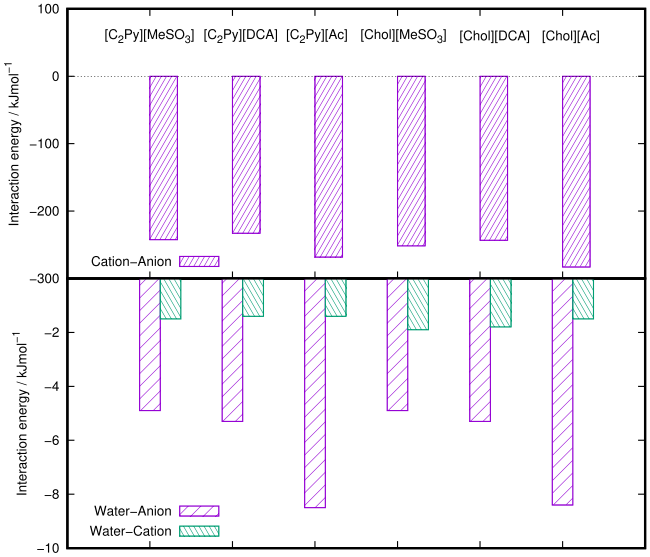

Fig. 7. Interaction energies (Coulomb + van der Waals) between the components of mixtures IL + H_2O with $x_{H_2O} = 0.104$.

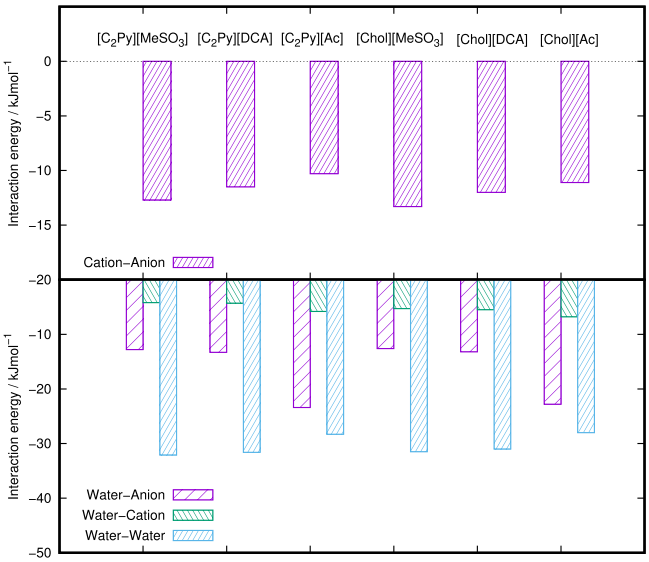

Fig. 8. Interaction energies (Coulomb + van der Waals) between the components of mixtures IL + H_2O with $x_{H_2O} = 0.900$.

4. Conclusions

The molecular dynamics results presented in this work capture the experimental trends of dynamic properties for the mixtures of ionic liquids with water, in terms of the nature of the ions composing the ionic liquids (pyridynium and cholinium cations, and methanesulfonate, dicyanamide and acetate anions). Two compositions were studied, one rich in IL (x_{H_2}) = 0.104) and one rich in water (x_{H_2}) = 0.900). Cholinium ionic liquids have the slower dynamics among those studied, whereas dicyanamide is the anion giving rise to lower viscosities.

We calculated thermodynamic properties of solvation, namely chemical potentials at infinite dilution, and also examined the microscopic structure of solvation layers through radial and spatial distribution functions. Results are compared with literature in terms of water affinity of the ILs. Contrary to expectations, cholinium ILs present lesser water affinity than those based on pyridinium, because cholinium competes with water for hydrogen-bonding with the anions. Regarding the anions, acetate leads to higher water affinity than the other anions studied.

The microscopic structure explains in a large extent the properties of the mixtures studied. Namely, $Chol^+$ leads to more organised systems and thus to slower dynamics. This is also supported by slight increase in the interaction energies between ions. The frequency of H-bonds (consistent with RDFs) and the energetics of interactions in the liquid phases back the higher water affinity of acetate ILs.

According to the results obtained, water affinity is mainly related with the ability of the anion to establish hydrogen bonds with water, thus the carboxylate anion shows a larger absorption capacity than the other anions. The presence of cholinium cation, which carries a H-bond donor site, reduces the absorption capacity and also leads to higher viscosities. This suggests that cations with no H-bond donor sites and giving rise to weaker anion-cation interactions are more suitable for use in ionic liquid absorbents in heat pumps.

Acknowledgements

P.B.S. acknowledges support under the Plan Estatal de Investigación Científica y Técnica (DPI2012-38841-CO2-O2) financed

by Ministerio de Economía y Competitividad (Spain) and under Bourse d'Excellence Eiffel by the Ministère des Affaires Étrangères (France).

Appendix A. Supplementary data

Supplementary data to this article can be found online at http://dx.doi.org/10.1016/j.molliq.2017.06.109.

References

[1] J.F. Brennecke, E.J. Maginn, Ionic liquids: innovative fluids for chemical processing, AIChE J. 47 (11) (2001) 2384–2389. http://dx.doi.org/10.1002/aic.690471102.

[2] N.V. Plechkova, K.R. Seddon, Applications of ionic liquids in the chemical industry, Chem. Soc. Rev. 37 (1) (2008) 123–150. http://dx.doi.org/10.1039/B006677J.

[3] J.F. Wishart, Energy applications of ionic liquids, Energy Environ. Sci. 2 (9) (2009) 956–961. http://dx.doi.org/10.1039/b906273d.

[4] D.R. MacFarlane, N. Tachikawa, M. Forsyth, J.M. Pringle, P.C. Howlett, G.D. Elliott, J.H. Davis, M. Watanabe, P. Simon, C.A. Angell, Energy applications of ionic liquids, Energy Environ. Sci. 7 (1) (2014) 232–250. http://dx.doi.org/10.1039/c3ee42099j.

[5] D.Z. Troter, Z.B. Todorovic, D.R. Dokic-Stojanovic, O.S. Stamenkovic, V.B. Veljkovic, Application of ionic liquids and deep eutectic solvents in biodiesel production: a review, Renew. Sust. Energ. Rev. 61 (2016) 473–500. http://dx.doi.org/10.1016/j.rser.2016.04.011.

[6] P. Srikhirin, S. Aphornratana, S. Chungpaibulpatana, A review of absorption refrigeration technologies, Renew. Sust. Energ. Rev. 5 (2001) 343–372. http://dx.doi.org/10.1016/S1364-0321(01)00003-X.

[7] W. Wu, B. Wang, W. Shi, X. Li, Absorption heating technologies: a review and perspective, Appl. Energy 130 (2014) 51–71. http://dx.doi.org/10.1016/j.apenergy.2014.05.027.

[8] M. Khamooshi, K. Parham, U. Atikol, Overview of ionic liquids used as working fluids in absorption cycles, Adv. Mech. Eng. 2013 (2013) 1–7. http://dx.doi.org/10.1155/2013/620592.

[9] M. Seiler, A. Kühn, F. Ziegler, X. Wang, Sustainable cooling strategies using new chemical system solutions, Ind. Eng. Chem. Res. 52 (2013) 16519–16546. http://dx.doi.org/10.1021/ie401297u.

[10] T. Welton, Room-temperature ionic liquids. Solvent for synthesis and catalysis, Chem. Rev. 99 (8) (1999) 2071–2083. http://dx.doi.org/10.1021/cr980032t.

[11] P. Wasserscheid, T. Welton, Ionic Liquids in Synthesis, vol. 1. Wiley-VCH Verlag GmbH & Co. KGaA, Weinheim, Germany, 2007, 1–721. http://dx.doi.org/10.1002/9783527621194.

[12] A. Yokozeki, M.B. Shiflett, Water solubility in ionic liquids and application to absorption cycles, Ind. Eng. Chem. Res. 49 (19) (2010) 9496–9503. http://dx.doi.org/10.1021/ie1011432.

[13] D. Zheng, L. Dong, W. Huang, X. Wu, N. Nie, A review of imidazolium ionic liquids research and development towards working pair of absorption cycle, Renew. Sust. Energ. Rev. 37 (2014) 47–68. http://dx.doi.org/10.1016/j.rser.2014.04.046.

[14] H. Wu, E.J. Maginn, Water solubility and dynamics of CO2 capture ionic liquids having aprotic heterocyclic anions, Fluid Phase Equilib. 368 (2014) 72–79. http://dx.doi.org/10.1016/j.fluid.2014.02.003.

[15] J.N.A.C.L. Lopes, A.A.H. Padua, Nanostructural organization in ionic liquids, J. Phys. Chem. B 110 (7) (2006) 3330–3335. http://dx.doi.org/10.1021/jp056006y.

[16] C. Cadena, Q. Zhao, R.Q. Snurr, E.J. Maginn, Molecular modeling and experimental studies of the thermodynamic and transport properties of pyridinium-based ionic liquids, J. Phys. Chem. B 110 (6) (2006) 2821–2832. http://dx.doi.org/10.1021/jp056235k.

[17] H.K. Kashyap, H.V.R. Annapureddy, F.O. Raineri, C.J. Margulis, How is charge transport different in ionic liquids and electrolyte solutions? J. Phys. Chem. B 115 (45) (2011) 13212–13221. http://dx.doi.org/10.1021/jp204182c.

[18] P.B. Sánchez, M. Traikia, A. Dequidt, A.A. Pádua, J. García, Molecular understanding of pyridinium ionic liquids as absorbents with water as refrigerant for use in heat pumps, AIChE J. 00 (2017) (00–00). http://dx.doi.org/10.1002/aic.15690.

[19] W.L. Jorgensen, D.S. Maxwell, J. Tirado-Rives, Development and testing of the Opls all-atom force-field on conformational energetics and properties of organic liquids, J. Am. Chem. Soc. 118 (45) (1996) 11225–11236. http://dx.doi.org/10.1021/ja9621760.

[20] J.N. Canongia Lopes, A.A.H. Pádua, Molecular force field for ionic liquids composed of triflate or bistriflylimide anions, J. Phys. Chem. B 108 (43) (2004) 16893–16898. http://dx.doi.org/10.1021/jp0476545.

[21] J.N. Canongia Lopes, A.A.H. Pádua, Molecular force field for ionic liquids III: imidazolium, pyridinium, and phosphonium cations; chloride, bromide, and dicyanamide anions, J. Phys. Chem. B 110 (39) (2006) 19586–19592. http://dx.doi.org/10.1021/jp063901o.

[22] A.A. Pádua, Force field for ionic liquids, 2016, https://github.com/agiliopadua/ilff. http://dx.doi.org/10.5281/zenodo.18619.

[23] B.L. Bhargava, S. Balasubramanian, Refined potential model for atomistic simulations of ionic liquid [bmim][PF6], J. Chem. Phys. 127 (11) (2007) 1–6. http://dx.doi.org/10.1063/1.2772268.

[24] C. Schröder, Comparing reduced partial charge models with polarizable simulations of ionic liquids, Phys. Chem. Chem. Phys. 14 (9) (2012) 3089. http://dx.doi.org/10.1039/c2cp23329k.

[25] H.J.C. Berendsen, J.R. Grigera, T.P. Straatsma, The missing term in effective pair potentials, J. Phys. Chem. 91 (24) (1987) 6269–6271. http://dx.doi.org/10.1021/j100308a038.

[26] S. Plimpton, Fast parallel algorithms for short-range molecular dynamics, J. Comput. Phys. 117 (1995) 1–19.

[27] S. Plimpton, LAMMPS. Molecular dynamics simulator, 2015, http://lammps.sandia.gov.

[28] L. Martínez, R. Andrade, E. Birgin, J. Martínez, PACKMOL: a package for building initial configurations for molecular dynamics simulations, J. Comput. Chem. 30 (13) (2009) 2157–2164. http://dx.doi.org/10.1002/jcc.

[29] A.A. Pádua, Force field tool, 2016, https://github.com/agiliopadua/fftool.

[30] R.W. Hockney, J.W. Eastwood, Computer simulation using particles, 1st edition ed., CRC Press, NY, 1989.

[31] J. Ramírez, S.K. Sukumaran, B. Vorselaars, A.E. Likhtman, Efficient on the fly calculation of time correlation functions in computer simulations, J. Chem. Phys. 133 (15). (2010) http://dx.doi.org/10.1063/1.3491098.

[32] C. Chipot, Free-energy calculations. Measuring free-energy differences using computer simulations, 2010.

[33] D.R. MacFarlane, J. Golding, S. Forsyth, M. Forsyth, G.B. Deacon, Low viscosity ionic liquids based on organic salts of the dicyanamide anion, Chem. Commun. 68 (16) (2001) 1430–1431. http://dx.doi.org/10.1039/b103064g.

[34] I. Bandres, R. Alcalde, C. Lafuente, M. Atilhan, S. Aparicio, On the viscosity of pyridinium based ionic liquids: an experimental and computational study, J. Phys. Chem. B 115 (43) (2011) 12499–12513. http://dx.doi.org/10.1021/jp203433u.

[35] E. Quijada-Maldonado, S. Van Der Boogaart, J.H. Lijbers, G.W. Meindersma, A.B. De Haan, Experimental densities, dynamic viscosities and surface tensions of the ionic liquids series 1-ethyl-3-methylimidazolium acetate and dicyanamide and their binary and ternary mixtures with water and ethanol at T = (298.15 to 343.15 K), J. Chem. Thermodyn. 51 (2012) 51–58. http://dx.doi.org/10.1016/j.jct.2012.02.027.

[36] H. Weber, B. Kirchner, Complex structural and dynamical interplay of cyano-based ionic liquids, J. Phys. Chem. B 120 (9) (2016) 2471–2483. http://dx.doi.org/10.1021/acs.jpcb.6b00098.

[37] P.B. Sánchez, J. García, J. Salgado, E. González-Romero, Studies of volumetric and transport properties of ionic liquid-water mixtures and its viability to be used in absorption systems, ACS Sustain. Chem. Eng. 4 (9) (2016) 5068–5077. http://dx.doi.org/10.1021/acssuschemeng.6b01541.

[38] A. Stark, A.W. Zidell, M.M. Hoffmann, Is the ionic liquid 1-ethyl-3-methylimidazolium methanesulfonate [emim][MeSO3] capable of rigidly binding water? J. Mol. Liq. 160 (3) (2011) 166–179. http://dx.doi.org/10.1016/j.molliq.2011.03.014.

[39] C. Jiménez de la Parra, J.R. Zambrano, M.D. Bermejo, Á. Martín, J.J. Segovia, M.J. Cocero, Influence of water concentration in the viscosities and densities of cellulose dissolving ionic liquids. Correlation of viscosity data, J. Chem. Thermodyn. 91 (2015) (2015) 8–16. http://dx.doi.org/10.1016/j.jct.2015.07.015.

[40] R.L. Gardas, J.A.P. Coutinho, Group contribution methods for the prediction of thermophysical and transport properties of ionic liquids, AIChE J. 55 (5) (2009) 1274–1290. http://dx.doi.org/10.1002/aic.11737.

[41] P.B. Sánchez, M.R. Currás, M.M. Mato, J. Salgado, J. García, Density and viscosity study of pyridinium based ionic liquids as potential absorbents for natural refrigerants: experimental and modelling, Fluid Phase Equilib. 405 (2015) 37–45. http://dx.doi.org/10.1016/j.fluid.2015.06.043.

[42] A.J.L. Costa, M.R.C. Soromenho, K. Shimizu, I.M. Marrucho, J.M.S.S. Esperança, J.N.C. Lopes, L.P.N. Rebelo, Density, thermal expansion and viscosity of cholinium-derived ionic liquids, ChemPhysChem 13 (7) (2012) 1902–1909. http://dx.doi.org/10.1002/cphc.201100852.

[43] W. Shi, K. Damodaran, H.B. Nulwala, D.R. Luebke, Theoretical and experimental studies of water interaction in acetate based ionic liquids, Phys. Chem. Chem. Phys. 14 (45) (2012) 15897–15908. http://dx.doi.org/10.1039/c2cp42975f.

[44] J.L. Anthony, E.J. Maginn, J.F. Brennecke, Solution thermodynamics of imidazolium-based ionic liquids and water, J. Phys. Chem. B 105 (October 2001) 10942–10949. http://dx.doi.org/10.1021/jp0112368.

[45] N. Merkel, C. Weber, M. Faust, K. Schaber, Influence of anion and cation on the vapor pressure of binary mixtures of water+ionic liquid and on the thermal stability of the ionic liquid, Fluid Phase Equilib. 394 (2015) 29–37. http://dx.doi.org/10.1016/j.fluid.2015.03.001.

[46] D. Constantinescu, K. Schaber, F. Agel, M.H. Klingele, T.J.S. Schubert, Viscosities, vapor pressures, and excess enthalpies of choline lactate + water, choline glycolate + water, and choline methanesulfonate + water systems, J. Chem. Eng. Data 52 (2007) 1280–1285. http://dx.doi.org/10.1021/je7000232.

[47] I. Khan, K.A. Kurnia, T.E. Sintra, J.A. Saraiva, S.P. Pinho, J.A.P. Coutinho, Assessing the activity coefficients of water in cholinium-based ionic liquids: experimental measurements and COSMO-RS modeling, Fluid Phase Equilib. 361 (2014) 16–22. http://dx.doi.org/10.1016/j.fluid.2013.10.032.

[48] M. Królikowska, M. Zawadzki, M. Królikowski, Physicochemical and thermodynamic study on aqueous solutions of dicyanamide – based ionic liquids, J. Chem. Thermodyn. 70 (2014) 127–137. http://dx.doi.org/10.1016/j.jct.2013.10.034.
[49] M. Moreno, F. Castiglione, A. Mele, C. Pasqui, G. Raos, Interaction of water with the model ionic liquid [bmim][BF4]: molecular dynamics simulations and comparison with NMR data, J. Phys. Chem. B 112 (26) (2008) 7826–7836. http://dx.doi.org/10.1021/jp800383g.
[50] B.L. Bhargava, Y. Yasaka, M.L. Klein, Computational studies of room temperature ionic liquid-water mixtures, Chemical Communications 47 (22) (2011) 6228–6241. http://dx.doi.org/10.1039/c1cc10575b.
[51] J. Zielkiewicz, Structural properties of water: Comparison of the SPC, SPCE, TIP4P, and TIP5P models of water, J. Chem. Phys. 123 (10) (2005) 1–6. http://dx.doi.org/10.1063/1.2018637.
[52] M. Brehm, H. Weber, A.S. Pensado, A. Stark, B. Kirchner, Proton transfer and polarity changes in ionic liquid–water mixtures: a perspective on hydrogen bonds from ab initio molecular dynamics at the example of 1-ethyl-3-methylimidazolium acetate–water mixtures—Part 1, Phys. Chem. Chem. Phys. 14 (15) (2012) 5030. http://dx.doi.org/10.1039/c2cp23983c.

Chapter 5

Conclusions

The aim of this project was the development of new working pairs for absorption heat pumps based on natural refrigerants. The main conclusions of this work can be summarized as follows:

- Key properties of potential candidates to be used as absorbents in absorption heat pumps were studied in this work. The following ILs were considered: $[C_2Py][NTf_2]$, $[Chol][NTf_2]$, $[C_1C_1Im][OTf]$, $[C_1C_1Im][BETI]$, $[C_2Py][MeSO_3]$, $[C_2Py][OTf]$, $[Chol][H_2PO_4]$, $[C_2Py][DCA]$, $[C_2Py][Ac]$, $[Chol][MeSO_3]$, $[Chol][DCA]$ and $[Chol][Ac]$.

- The liquid range of potential working pairs was determined by the phase transitions of ILs (lower limit) and their thermal degradation (upper limit). Solidification temperature, measured using DSC techniques, is mainly determined by the internal organisation of the ionic structure, with well-structured ILs leading to higher melting points. The effect of the refrigerant (water) is expected to rise the melting point and reduce this operational problem. The degradation temperature, measured by TGA techniques, requires an isothermal analysis that complements dynamic studies. Results show that the upper limit of the liquid range is mainly determined by the anion while cations play a minor role.

- Experimental measurements of density and viscosity provide useful information to choose potential for heat pumps. These properties are also required for the design of the absorption cycle. Both temperature and water concentration have a large effect on viscosity, whose temperature dependence is well-described by the Vogel-Fulcher-Tamman equation. Besides, PC-SAFT and HS models show a good predictive capacity outside of the measuring range although both of them require the use of experimental data to obtain the parameters of the theoretical models.

- In an absorption cycle the working pair water/IL will always be a binary system, therefore, the applicability of ILs with melting points above room temperature can be explored. The analysis of the effect of water and temperature on ionic conductivity, combined with the viscosity measurements, show that ionic concentration and ionic mobility will cause opposite effects on the electrical conductivity of the solutions. Even tough electrical conductivity is not among the key properties for the absorption process, low values will avoid corrosion problems, such as those present in the commercial working pair H_2O/LiBr.

- Atomistic molecular dynamics is a powerful tool to study IL properties at molecular level. Scaling the charges of the ionic species to 0.8e provides a better description of the ILs/H_2O mixtures, specially of their dynamic properties. Qualitative agreement with experimental data has been obtained and factors influencing the dynamic properties of the systems and

water affinity have been identified. According to our results, a better ionic organisation leads to more viscous fluids, so large charge delocalization will favour faster dynamics. The water affinity is governed by the capacity of the anion to form hydrogen bonds with water. Results of Henry's constant at infinite solution calculated by free energy perturbation back this statement.

- The role of the anion and the cation in the dynamic properties of ILs/H_2O mixtures as well as thermodynamics of water solvation in the ILs were interpreted by MD simulations. Radial and spatial distribution functions showing the solvation environment of water in the ILs explain how interactions between ions and water affect to the dynamic properties of the system. The interaction energies between ions also support this analysis. Regarding to the thermodynamics of the solvation process, the insights provided by simulation point out the relationship between the ability of the anion to establish hydrogen bonds with water as the main issue favouring water absorption. On the other hand, competition between water and cation for the acceptor positions of the anion reduces significantly the absorption capacity of the IL.

- After combining the experimental and theoretical techniques implemented and used throughout the articles that are part of this work, we have concluded that [C_2Py][Ac] is the candidate showing a higher potential as absorbant for heat pumps using water as refrigerant. Even though a deeper analysis should be done in order to determine all the aspects of the absorption/desorption process, [C_2Py][Ac] accomplishes three of the main requirements for an efficient water absorption.

  (i) Good absorption capacity. Among the studied ILs [C_2Py][Ac] has the largest (negative) Gibbs free energy of solution of water, the reason rest on the affinity between the carboxilate group and water, as indicated by hydrogen bond quantification. A weak interaction between anion and cation also favours this behaviour.

  (ii) The dynamic properties studied by atomistic MD and supported by experimental data from different literature sources present reasonable values compared with other potential candidates. Even tough [C_2Py][DCA]/H_2O mixtures have lower viscosities, the difference in their water affinity is enough to justify the selection of carboxilate based ILs.

  (iii) Thermal stability is a weaker point of acetate based ILs. Since this property is mainly related with the anion, it will be a limitation of working pairs containing acetate ILs. However, according to several studies generators in single stage configurations reach temperatures of 80 °C. Up to this temperature, the thermal stability of [C_2Py][Ac] seems to be assured. However, special care should be taken in more complex configurations where higher temperatures might be reached in the generator.

As previously described, the design of water/IL working pairs for heat pumps was accomplished from different perspectives, from experimental determination of key properties for the absorption process to molecular simulations to improve the knowledge at atomistic level of different levels. This strategy has proven to be positive since results enhance the comprehension of the relation between chemical structures and the target properties for this application.

Further works should lead to the establishment a systematic procedure to quantify the acceptable ranges for the properties of the water + ILs mixtures. As a starting point,

$[C_2Py][Ac]/H_2O$ could be chosen to simulate the absorption/desorption process and eventually, try this system at pilot scale to measure the performance of the system through the calculation of the COP and circulation ratio.

Bibliography

[1] United Nations Conference on the Human Environment, Declaration of the United Nations Conference on the Human Environment (1972).

[2] United Nations Framework Convention on Climate Change, Paris Agreement (2015). doi:FCCC/CP/2015/L.9.

[3] T. Boden, G. Marland, R. Andres, Global, Regional, and National Fossil-Fuel CO2 Emissions, Carbon Dioxide Information Analysis Center, Oak Ridge National Laboratory, U.S. Department of Energy, Oak Ridge, Tenn., U.S.A., 2015. doi:10.3334/CDIAC/00001_V2015.

[4] K. Edenhofer, O., R. Pichs-Madruga, Y. Sokona, E. Farahani, S. Kadner, T. Z. Seyboth, A. Adler, I. Baum, S. Brunner, P. Eickemeier, B. Kriemann, J. Savolainen, S. Schlömer, C. von Stechow, J. Minx, IPCC, 2014: Climate Change 2014: Mitigation of Climate Change. Contribution of Working Group III to the Fifth Assessment Report of the Intergovernmental Panel on Climate Change, Cambridge Uiversity Press, Cambrigde, United Kingdom and New York, NY, USA, 2014.

[5] N. P. Garcia, K. Vatopoulos, A. P. Lopez, C. Thiel, Best available technologies for the heat and cooling market in the European Union. JRC Scientif and Policy Reports., Tech. rep., Institute for Energy and Transport, Luxembourg (2012). doi:10.2790/5813.

[6] European Comission, Directive 2009/28/EC on the Promotion of the use of energy from renewable sources, Tech. rep., European Parliament (2009).

[7] H. Daiguji, E. Hihara, Molecular dynamics study of the liquid-vapor interface of lithium bromide aqueous solutions, Heat and mass transfer 35 (1999) 213–219.

[8] P. Srikhirin, S. Aphornratana, S. Chungpaibulpatana, A review of absorption refrigeration technologies, Renewable and Sustainable Energy Reviews 5 (2001) 343–372. doi:10.1016/S1364-0321(01)00003-X.

[9] W. Wu, B. Wang, W. Shi, X. Li, Absorption heating technologies: A review and perspective, Applied Energy 130 (2014) 51–71. doi:10.1016/j.apenergy.2014.05.027.

[10] D. Zheng, L. Dong, W. Huang, X. Wu, N. Nie, A review of imidazolium ionic liquids research and development towards working pair of absorption cycle, Renewable and Sustainable Energy Reviews 37 (2014) 47–68. doi:10.1016/j.rser.2014.04.046.

[11] M. Seiler, A. Kühn, F. Ziegler, X. Wang, Sustainable Cooling Strategies Using New Chemical System Solutions, Industrial & Engineering Chemistry Research 52 (2013) 16519–16546. doi:dx.doi.org/10.1021/ie401297u.

[12] D. S. Ayou, M. R. Currás, D. Salavera, J. García, J. C. Bruno, A. Coronas, Performance analysis of absorption heat transformer cycles using ionic liquids based on imidazolium cation as absorbents with 2,2,2-trifluoroethanol as refrigerant, Energy Conversion and Management 84 (2014) 512–523. doi:10.1016/j.enconman.2014.04.077.

[13] J. L. Rodríguez-Muñoz, J. M. Belman-Flores, Review of diffusion-absorption refrigeration technologies, Renewable and Sustainable Energy Reviews 30 (2014) 145–153. doi:10.1016/j.rser.2013.09.019.

[14] B. Ziegler, C. Trepp, Equation of state for ammonia-water mixtures, International Journal of Refrigeration 7 (2) (1984) 101–106. doi:10.1016/0140-7007(84)90022-7.

[15] Y. M. El-Sayed, M. Tribus, Winter Annual Meeting of the American Society of Mechanical Engineers, in: THERMODYNAMIC PROPERTIES OF WATER-AMMONIA MIXTURES THEORETICAL IMPLEMENTATION FOR USE IN POWER CYCLES ANALYSIS, 1985, pp. 89–95.

[16] J. M. Wimby, T. S. Berntsson, Viscosity and Density of Aqueous Solutions of LiBr, LiCl, ZnBr2, CaCl2, and LiN03, 1, Single Salt Solutions, Journal of Chemical & Engineering Data 39 (1994) 68–72. doi:10.1021/je00013a019.

[17] J. M. Wimby, T. S. Berntsson, Viscosity and Density of Aqueous Solutions of LiBr, LiCl,ZnBr2, CaCl2, and LiN03, 2, Two-Salt Solutions, Journal of Chemical & Engineering Data 39 (1994) 73–78. doi:10.1021/je00013a019.

[18] T. Welton, Room-temperature ionic liquids. Solvent for synthesis and catalysis, Chem.Rev 99 (8) (1999) 2071–2083. doi:10.1021/cr980032t.

[19] P. Wasserscheid, T. Welton, Ionic Liquids in Synthesis, Vol. 1, Wiley-VCH Verlag GmbH & Co. KGaA, Weinheim, Germany, 2007. doi:10.1002/9783527621194.

[20] J. F. Brennecke, E. J. Maginn, Ionic liquids: Innovative fluids for chemical processing, AIChE Journal 47 (11) (2001) 2384–2389. doi:10.1002/aic.690471102.

[21] N. V. Plechkova, K. R. Seddon, Applications of ionic liquids in the chemical industry, Chemical Society Reviews 37 (1) (2008) 123–150. doi:10.1039/B006677J.

[22] S. Popp, A. Bösmann, R. Wölfel, P. Wasserscheid, Screening of ionic liquid/H2O working pairs for application in low temperature driven sorption heat pump systems, ACS Sustainable Chemistry and Engineering 3 (4) (2015) 750–757. doi:10.1021/acssuschemeng.5b00062.

[23] C. P. Fredlake, J. M. Crosthwaite, D. G. Hert, S. N. V. K. Aki, J. F. Brennecke, Thermophysical Properties of Imidazolium-Based Ionic Liquids, Journal of Chemical & Engineering Data 49 (4) (2004) 954–964. doi:10.1021/je034261a.

[24] D. Rengstl, V. Fischer, W. Kunz, Low-melting mixtures based on choline ionic liquids., Physical chemistry chemical physics : PCCP 16 (41) (2014) 22815–22. doi:10.1039/c4cp02860k.

[25] C. Maton, N. De Vos, C. V. Stevens, Ionic liquid thermal stabilities: decomposition mechanisms and analysis tools., Chemical Society reviews 42 (13) (2013) 5963–77. doi:10.1039/c3cs60071h.

[26] I. Bandres, R. Alcalde, C. Lafuente, M. Atilhan, S. Aparicio, On the viscosity of pyridinium based ionic liquids: an experimental and computational study, Journal of Physical Chemistry B 115 (43) (2011) 12499–12513. doi:10.1021/jp203433u.

[27] H. Wu, E. J. Maginn, Water solubility and dynamics of CO2 capture ionic liquids having aprotic heterocyclic anions, Fluid Phase Equilibria 368 (2014) 72–79. doi:10.1016/j.fluid.2014.02.003.

[28] M. Villanueva, A. Coronas, J. García, J. Salgado, Thermal Stability of Ionic Liquids for Their Application as New Absorbents, Industrial & Engineering Chemistry Research 52 (2013) 15718–15727. doi:10.1021/ie401656e.

[29] J. Salgado, J. J. Parajó, J. Fernández, M. Villanueva, Long-term thermal stability of some 1-butyl-1-methylpyrrolidinium ionic liquids, Journal of Chemical Thermodynamics 74 (2014) 51–57. doi:10.1016/j.jct.2014.03.030.

[30] J. F. Brennecke, H. Rodríguez, Temperature and Composition Dependence of the Density and Viscosity of Binary Mixtures of Water + Ionic Liquid, J. Chem. Eng. Data 51 (2006) 2145–2155. doi:10.1021/je0602824.

[31] M. Atilhan, J. Jacquemin, D. Rooney, M. Khraisheh, S. Aparicio, Viscous Behavior of Imidazolium-Based Ionic Liquids, Industrial & Engineering Chemistry Research 52 (47) (2013) 16774–16785. doi:10.1021/ie403065u.

[32] A. Noda, K. Hayamizu, M. Watanabe, Pulsed-Gradient Spin - Echo 1 H and 19 F NMR Ionic Diffusion Coefficient , Viscosity , and Ionic Conductivity of Non-Chloroaluminate Room-Temperature Ionic Liquids, J. Phys. Chem. B 105 (2001) 4603–4610. doi:10.1021/jp004132q.

[33] H. Tokuda, K. Ishii, A. Bin, H. Susan, S. Tsuzuki, K. Hayamizu, M. Watanabe, Physicochemical Properties and Structures of Room-Temperature Ionic Liquids . 3 . Variation of Cationic Structures Physicochemical Properties and Structures of Room-Temperature Ionic Liquids . 3 . Variation of Cationic Structures, J. Phys. Chem. B 110 (2006) 2833–2839. doi:10.1021/jp053396f.

[34] H. Tokuda, K. Hayamizu, K. Ishii, A. Bin, H. Susan, M. Watanabe, Physicochemical Properties and Structures of Room Temperature Ionic Liquids . 2 . Variation of Alkyl Chain Length in Imidazolium Cation Physicochemical Properties and Structures of Room Temperature Ionic Liquids . 2 . Variation of Alkyl Chain Length in Im, J. Phys. Chem. B 109 (2005) 6103–6110. doi:10.1021/jp044626d.

[35] H. Tokuda, K. Hayamizu, K. Ishii, M. A. B. H. Susan, M. Watanabe, Physicochemical Properties and Structures of Room Temperature Ionic Liquids. 1. Variation of Anionic Species, The Journal of Physical Chemistry B 108 (42) (2004) 16593–16600. doi:10.1021/jp047480r.

[36] G. S. Fulcher, Analysis of recent measurements of the viscosity glasses, Journal of the American Ceramic Society 8 (6) (1925) 339–355.

[37] E. J. González, B. González, E. A. Macedo, Effect of the relative humidity and isomeric structure on the physical properties of pyridinium based-ionic liquids, Journal of Chemical Thermodynamics 86 (2015) 96–105. doi:10.1016/j.jct.2015.02.020.

[38] M. J. Assael, J. H. Dymond, M. Papadaki, P. M. Patterson, Correlation and prediction of dense fluid transport coefficients. I. n-alkanes, International Journal of Thermophysics 13 (2) (1992) 269–281. doi:10.1007/BF00504436.

[39] S. E. Quiñones-Cisneros, J. Fernández, C. K. Zéberg-Mikkelsen, J. García, General Friction Theory Viscosity Model for the PC-SAFT Equation of State, AIChEdoi:10.1002/aic.10755.

[40] F. M. Gaciño, M. J. P. Comuñas, J. Fernández, S. K. Mylona, M. J. Assael, Correlation and Prediction of Dense Fluid Transport Coefficients. IX. Ionic Liquids, International Journal of Thermophysics 35 (5) (2014) 812–829. doi:10.1007/s10765-014-1626-0.

[41] B. L. Bhargava, Y. Yasaka, M. L. Klein, Computational studies of room temperature ionic liquid-water mixtures., Chemical Communications 47 (22) (2011) 6228–6241. doi:10.1039/c1cc10575b.

[42] O. Borodin, G. D. Smith, Structure and dynamics of N-methyl-N-propylpyrrolidinium bis(trifluoromethanesulfonyl)imide ionic liquid from molecular dynamics simulations, Journal of Physical Chemistry B 110 (2006) 11481–11490. doi:10.1021/jp061593o.

[43] E. Marin-Rimoldi, J. K. Shah, E. J. Maginn, Monte Carlo simulations of water solubility in ionic liquids: A force field assessment, Fluid Phase Equilibria 407 (2015) 117–125. doi:10.1016/j.fluid.2015.07.007.

[44] O. Borodin, Polarizable force field development and molecular dynamics simulations of ionic liquids., The Journal of Physical Chemistry B 113 (33) (2009) 11463–78. doi:10.1021/jp905220k.

[45] C. Schröder, Comparing reduced partial charge models with polarizable simulations of ionic liquids, Physical Chemistry Chemical Physics 14 (9) (2012) 3089. doi:10.1039/c2cp23329k.

[46] C. E. S. Bernardes, K. Shimizu, J. N. C. Lopes, P. Marquetand, E. Heid, O. Steinhauser, C. Schröder, Additive polarizabilities in ionic liquids, Phys. Chem. Chem. Phys. 18 (3) (2016) 1665–1670. doi:10.1039/C5CP06595J.

[47] C. Cadena, Q. Zhao, R. Q. Snurr, E. J. Maginn, Molecular modeling and experimental studies of the thermodynamic and transport properties of pyridinium-based ionic liquids., The journal of physical chemistry. B 110 (6) (2006) 2821–2832. doi:10.1021/jp056235k.

[48] H. Passos, I. Khan, F. Mutelet, M. B. Oliveira, P. J. Carvalho, L. M. N. B. F. Santos, C. Held, G. Sadowski, M. G. Freire, J. A. P. Coutinho, Vapor–Liquid Equilibria of Water + Alkylimidazolium-Based Ionic Liquids: Measurements and Perturbed-Chain Statistical Associating Fluid Theory Modeling, Industrial & Engineering Chemistry Research 53 (9) (2014) 3737–3748. doi:10.1021/ie4041093.

[49] K. A. Kurnia, S. P. Pinho, J. a. P. Coutinho, Designing ionic liquids for absorptive cooling, Green Chemistry 16 (8) (2014) 3741. doi:10.1039/C4GC00954A.

[50] A. Yokozeki, M. B. Shiflett, Water solubility in ionic liquids and application to absorption cycles, Industrial and Engineering Chemistry Research 49 (19) (2010) 9496–9503. doi:10.1021/ie1011432.

[51] Y. J. Kim, S. Kim, Y. K. Joshi, A. G. Fedorov, P. A. Kohl, Thermodynamic analysis of an absorption refrigeration system with ionic-liquid/refrigerant mixture as a working fluid, Energy 44 (1) (2012) 1005–1016. doi:10.1016/j.energy.2012.04.048.

[52] X. Zhang, D. Hu, Performance analysis of the single-stage absorption heat transformer using a new working pair composed of ionic liquid and water, Applied Thermal Engineering 37 (2012) 129–135. doi:10.1016/j.applthermaleng.2011.11.006.

[53] M. Khamooshi, K. Parham, U. Atikol, Overview of Ionic Liquids Used as Working Fluids in Absorption Cycles, Advances in Mechanical Engineering 2013 (2013) 1–7. doi:10.1155/2013/620592.

[54] P. Wasserscheid, M. Seiler, Leveraging gigawatt potentials by smart heat-pump technologies using ionic liquids., ChemSusChem 4 (4) (2011) 459–63. doi:10.1002/cssc.201000191.

[55] K. R. Seddon, A. Stark, M. J. Torres, Influence of chloride, water, and organic solvents on the physical properties of ionic liquids, Pure and Applied Chemistry 72 (12) (2000) 2275–2287. doi:10.1351/pac200072122275.

[56] M. J. Earle, J. M. S. S. Esperança, M. A. Gilea, J. N. C. Lopes, L. P. N. Rebelo, J. W. Magee, K. R. Seddon, J. A. Widegren, The distillation and volatility of ionic liquids., Nature 439 (7078) (2006) 831–834. doi:10.1038/nature04451.

[57] P. B. Sánchez, J. García, J. Salgado, E. González-Romero, Studies of Volumetric and Transport Properties of Ionic Liquid–Water Mixtures and Its Viability To Be Used in Absorption Systems, ACS Sustainable Chemistry & Engineering 4 (9) (2016) 5068–5077. doi:10.1021/acssuschemeng.6b01541.

[58] Elmer, P.: Users Manual. Series TGA7 Thermal Analysis System (1993).

[59] M. Villanueva, J. Parajó, P. B. Sánchez, J. García, J. Salgado, Liquid range temperature of ionic liquids as potential working fluids for absorption heat pumps, The Journal of Chemical Thermodynamics 91 (2015) 127–135. doi:10.1016/j.jct.2015.07.034.

[60] C. L. Chiang, R. C. Chang, Y. C. Chiu, Thermal stability and degradation kinetics of novel organic/inorganic epoxy hybrid containing nitrogen/silicon/phosphorus by sol-gel method, Thermochimica Acta 453 (2) (2007) 97–104. doi:10.1016/j.tca.2006.11.013.

[61] J. J. Parajó Vieito, Application of calorimetry and thermal analysis to determine the liquid range and the environmental toxicity of ionic liquids, Ph.D. thesis, Universidad de Santiago de Compostela (2016).

[62] T. Instruments, TA Instruments : DSC Differential Scanning Calorimeter Calorimeter. Q Series (2007).

[63] C. Tropea, A. Yarin, J. Foss, Springer Handbook of Experimental Fluid Mechanics, Volumen I, Springer, 2007.

[64] D. Cabaleiro, Development of new heat transfer media for improving efficiency in energy systems . Conventional fluids and nanofluids, Ph.D. thesis, University of Vigo (2016).

[65] P. B. Sánchez, M. R. Currás, M. M. Mato, J. Salgado, J. García, Density and viscosity study of pyridinium based ionic liquids as potential absorbents for natural refrigerants: Experimental and modelling, Fluid Phase Equilibria 405 (2015) 37–45. doi:10.1016/j.fluid.2015.06.043.

[66] Guilhem PAGES, La R.M.N. Chromatographique, Ph.D. thesis, Université Paul Cezanne Aix-Marseille III (2006).

[67] C. S. Johnson Jr., Diffusion ordered nuclear magnetic resonance spectroscopy: principles and applications., Progress in Nuclear Magnetic Resonance Spectroscopy 34 (1999) 203–256. doi:10.1016/S0079-6565(99)00003-5.

[68] P. B. Sánchez, M. Traikia, A. Dequidt, A. A. Pádua, J. García, Molecular Understanding of Pyridinium Ionic Liquids as Absorbents with Water as Refrigerant for Use in Heat Pumps, AIChE Journal 00 (2017) 00–00. doi:10.1002/aic.15690.

[69] J. Gross, G. Sadowski, Perturbed-Chain SAFT: An Equation of State Based on a Perturbation Theory for Chain Molecules, Industrial & Engineering Chemistry Research 40 (4) (2001) 1244–1260. doi:10.1021/ie0003887.

[70] S. S. Chen, A. Kreglewski, Applications of the Augmented van der Waals Theory of Fluids. I., Pure Fluids 81 (10) (1977) 1048.

[71] M. S. Wertheim, Fluids with highly directional attractive forces. I. Statistical thermodynamics, J. Stat. Phys. 35 (1984) 19.

[72] M. S. Wertheim, Fluids with highly directional attractive forces. II. Thermodynamic perturbation theory and integral equations, J. Stat. Phys. 35 (1984) 35.

[73] M. S. Wertheim, Fluids with highly directional attractive forces. III. Multiple attraction sites, J. Stat. Phys. 42 (1986) 459.

[74] M. S. Wertheim, Fluids with highly directional attractive forces. IV. Equilibrium polymerization, J. Stat. Phys. 42 (1986) 477.

[75] W. G. Chapman, G. Jackson, K. E. Gubbins, Phase equilibria of associating fluids. Chain molecules with multiple bonding sites., Mol. Phys. 65 (1988) 1057.

[76] W. G. Chapman, K. E. Gubbins, G. Jackson, M. Radosz, New Reference Equation of State for Associating Liquids, Ind. Eng. Chem. Res 29 (1990) 1709.

[77] T. Boublik, Hard-Sphere Equation of State, J. Chem. Phys. 53 (1970) 471.

[78] G. A. Mansoori, N. F. Carnahan, K. E. Starling, W. T. Leland, Equilibrium Thermodynamic Properties of the Mixture of Hard Spheres, J. Chem. Phys. 54 (1971) 1523.

[79] M. Assael, M. Papadaki, P. Patterson, J. H. Dymond, Correlation and Prediction of Dense Fluid Transport Coefficients. II. Simple Molecular Fluids, Fluid Phase Equilibria 75 (1992) 245–255.

[80] F. Ciotta, J. P. M. Trusler, V. Vesovic, Extended hard-sphere model for the viscosity of dense fluids, Fluid Phase Equilibria 363 (2014) 239–247. doi:10.1016/j.fluid.2013.11.032.

[81] D. Frenkel, B. Smith, Understanding Molecular Simulations. From Algorithms to Applications, 2nd Edition, Academic Press, Cornwall, 2002.

[82] W. L. Jorgensen, D. S. Maxwell, J. Tirado-Rives, Development and Testing of the Opls All-Atom Force-Field on Conformational Energetics and Properties of Organic Liquids, Journal of the American Chemical Society 118 (45) (1996) 11225–11236. doi:10.1021/ja9621760.

[83] J. N. Canongia Lopes, A. A. H. Pádua, Molecular force field for ionic liquids composed of triflate or bistriflylimide anions, Journal of Physical Chemistry B 108 (43) (2004) 16893–16898. doi:10.1021/jp0476545.

[84] J. N. Canongia Lopes, A. A. H. Pádua, Molecular force field for ionic liquids III: Imidazolium, pyridinium, and phosphonium cations; chloride, bromide, and dicyanamide anions, Journal of Physical Chemistry B 110 (39) (2006) 19586–19592. doi:10.1021/jp063901o.

[85] J. N. Canongia Lopes, A. A. H. Pádua, K. Shimizu, Molecular force field for ionic liquids IV: Trialkylimidazolium and alkoxycarbonyl-imidazolium cations; alkylsulfonate and alkylsulfate anions, Journal of Physical Chemistry B 112 (16) (2008) 5039–5046. doi:10.1021/jp800281e.

[86] A. A. Pádua, Force field for ionic liquids (2016). doi:10.5281/zenodo.18619.
URL https://github.com/agiliopadua/ilff

[87] H. J. C. Berendsen, J. R. Grigera, T. P. Straatsma, The Missing Term in Effective Pair Potentials, Journal of Physical Chemistry 91 (24) (1987) 6269–6271. doi:10.1021/j100308a038.

[88] R. W. Hockney, J. W. Eastwood, Computer simulation using particles, 1st Edition, CRC Press, NY, 1989.

[89] A. A. H. Pádua, Force field tool (2016).
URL https://github.com/agiliopadua/fftool

[90] L. Martínez, R. Andrade, E. Birgin, J. Martínez, PACKMOL: A Package for Building Initial Configurations for Molecular Dynamics Simulations, Journal of computational chemistry 30 (13) (2009) 2157–2164. doi:10.1002/jcc.

[91] S. Plimpton, Fast Parallel Algorithms for Short-Range Molecular Dynamics, Journal of Computational Physics 117 (1995) 1–19.

[92] S. Plimpton, LAMMPS. Molecular dynamics simulator (2015).
URL http://lammps.sandia.gov

[93] M. Mondello, G. S. Grest, Viscosity calculations of n-alkanes by equilibrium molecular dynamics, The Journal of Chemical Physics 106 (22) (1997) 9327. doi:10.1063/1.474002.

[94] T. Köddermann, D. Paschek, R. Ludwig, Molecular Dynamic Simulations of Ionic Liquids: A Reliable Description of Structure, Thermodynamics and Dynamics, ChemPhysChem 8 (17) (2007) 2464–2470. doi:10.1002/cphc.200700552.

[95] C. M. Tenney, E. J. Maginn, Limitations and recommendations for the calculation of shear viscosity using reverse nonequilibrium molecular dynamics, Journal of Chemical Physics 132 (014103) (2010) 1–8. doi:10.1063/1.3276454.

[96] D. J. Evans, Peter T. Cummings, Nonequilibrium Molecular Dynamics Properties and Non Newtonian Fluid Approaches to Transport Rheology, Ind. Eng. Chem. Res 31 (1992) 1237–1252. doi:10.1021/ie00005a001.

[97] J. Ramírez, S. K. Sukumaran, B. Vorselaars, A. E. Likhtman, Efficient on the fly calculation of time correlation functions in computer simulations, Journal of Chemical Physics 133 (15). doi:10.1063/1.3491098.

[98] T. C. Beutler, A. E. Mark, R. C. van Schaik, P. R. Gerber, W. F. van Gunsteren, Avoiding singularities and numerical instabilities in free energy calculations based on molecular simulations, Chemical Physics Letters 222 (6) (1994) 529–539. doi:10.1016/0009-2614(94)00397-1.

[99] C. Chipot, Free-energy calculations. Measuring free-energy differences using computer simulations (2010).

Appendix A

Resumen de la tesis doctoral

A.1 Contexto de la tesis doctoral

La tesis doctoral *"Caracterización termofísica de nuevos absorbentes basados en líquidos iónicos para el refrigerante natural, agua"* dirigida por la Dra. Josefa García Sánchez y el Dr. Agílio A. H. Pádua se enmarca dentro del proyecto *"Desarrollo de Nuevos Fluidos de Trabajo, Componentes y Configuraciones para Bombas de Calor de Absorción de Altas Prestaciones-AHP2"* financiado por el Ministerio de Economía y Competitividad y versa sobre el estudio de propiedades físico químicas de líquidos iónicos.

Para la consecución del objetivo global del proyecto, el desarrollo de nuevos pares de trabajo agua + líquido iónico (LI) para su aplicación en sistemas de bomba de calor por absorción, es necesario definir las propiedades clave que debe tener un absorbente para asegurar un rendimiento adecuado en la producción de frío/calor. A partir de estas propiedades deberá realizarse el diseño de LIs como potenciales absorbentes para bombas de calor por absorción utilizando agua como refrigerante.

Antes de definir las propiedades que consideraremos críticas para el desarrollo del proceso, se hace necesario describir brevemente el funcionamiento de una bomba de calor por absorción (ver figura B.1).

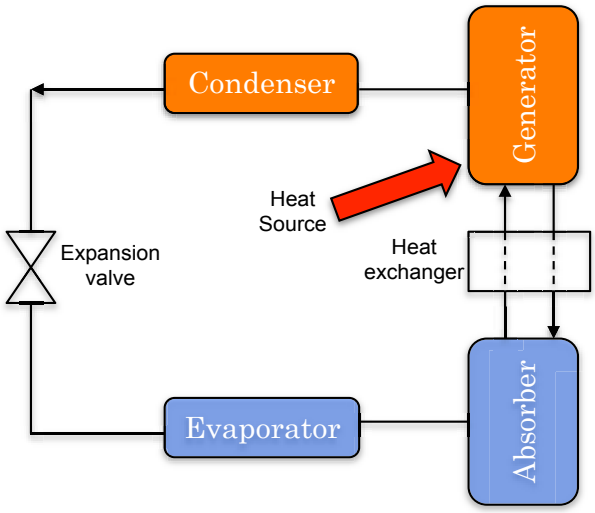

Figure A.1: Esquema del funcionamiento de una bomba de calor por absorción

Una bomba de calor por absorción es un dispositivo termodinámico capaz de proporcionar frío y calor consumiendo, en su mayor parte, energía térmica en contraste con los sistemas de bomba de calor tradicionales también llamados bombas de compresión mecánica, que requieren un consumo extensivo de energía eléctrica. En los sistemas de absorción o sistemas de compresión química, un proceso de absorción/desabsorción se utiliza para incrementar la presión del refrigerante, aprovechando la reducción drástica en el volumen específico que se produce en el cambio de fase vapor-líquido. Una vez absorbido el refrigerante (en estado líquido), el aumento en la presión se hace mediante el bombeo de la mezcla refrigerante/absorbente, siendo su consumo energético muy inferior al del compresor utilizado en los sistemas tradicionales. Una vez elevada la presión, el absorbente se regenera mediante la aplicación de energía térmica antes de su entrada al condensador. Con el objetivo de llevar a cabo el proceso de absorción de una manera eficiente se hace necesario garantizar que el par de trabajo cumpla los siguientes requisitos:

1. Capacidad de absorción. El cambio de fase del refrigerante se realiza mediante un proceso de absorción. Es difícil determinar una única propiedad que proporcione una medida de la capacidad de absorción puesto que son varios los factores que influyen en la marcha de este proceso. Con frecuencia se identifican las desviaciones negativas de la ley de Raoult como el factor determinante para una adecuada absorción de refrigerante, sin embargo, las propiedades de transporte o las entalpías de mezcla son factores que en menor medida afectarán también al proceso de absorción que, en general, está asociado a disoluciones exotérmicas, en consecuencia, es necesario utilizar un sumidero de calor para mantener para evitar el aumento de temperatura durante la absorción de refrigerante.

2. Elevada volatilidad relativa. La regeneración del refrigerante se realiza mediante destilación. En el generador, una fuente térmica se aplica a la mezcla refrigerante/absorbente, una elevada volatilidad relativa favorece la separación de ambos fluidos en una sola etapa mejorando la eficiencia del proceso. En el caso de pares de trabajo H_2O/LI este aspecto no representa un problema puesto que una de las características fundamentales de los LIs es su baja presión de vapor, facilitando así su separación de otros solventes con mayores volatilidades como es el caso del agua.

3. Rango líquido. Aunque dependerá de la configuración elegida para el ciclo termodinámico, la diferencia entre las temperaturas de absorción (temperatura inferior) y la regeneración (temperatura superior) del refrigerante puede ser elevada. En cualquier caso, es necesario que la mezcla refrigerante/absorbente se encuentren en estado líquido en este rango de temperatura y sean estables tanto térmica como químicamente en todo el rango de temperaturas durante largos periodos de tiempo.

4. Viscosidad. En este apartado se ha seleccionado la viscosidad como la más relevante de las propiedades de transporte para esta aplicación, si bien tanto la transferencia de calor como la de materia también juegan un papel importante en este proceso. Absorbentes con baja viscosidad facilitarán la absorción del refrigerante, además, dado que el incremento de la presión del refrigerante se hace en estado líquido mediante el bombeo de la mezcla refrigerante/absorbente, una menor viscosidad disminuirá el coste del proceso de bombeo.

Otros aspectos, como la capacidad de corrosión, relacionada con la conductividad eléctrica y el pH de la disolución, o la toxicidad de los compuestos utilizados, así como la viabilidad económica del proceso deben ser tenidos en cuenta a la hora de diseñar nuevos pares de trabajo para bombas de calor por absorción.

El conjunto de estos factores determinará la eficiencia del proceso, que se define de una manera global a partir de dos parámetros fundamentales, el COP (ec. B.1) y el ratio de recirculación (ec. B.2).

$$COP = \frac{calor\ útil\ (evap.)}{calor\ consumido\ (gen.)} \tag{A.1}$$

$$Ratio\ recirculación = \frac{flujo\ vapor}{flujo\ disolución} \tag{A.2}$$

El COP es un indicador de la eficiencia global de la bomba de calor, definido como la energía útil que el sistema es capaz de proporcionar entre la energía térmica consumida en el generador (ec. B.1, por tanto, un COP más alto implicará una mayor eficiencia energética. Por otra parte, el ratio de recirculación es un indicador del desempeño del ciclo de absorción, dado que cuanto menor sea la cantidad de absorbente para producir una cantidad determinada de vapor, menor será la demanda térmica del generador, un ratio de recirculación más alto (ec.) será también ventajoso para la eficiencia del sistema además de permitir un dimensionamiento adecuado de los equipos.

A.2 Enfoque de la tesis doctoral y técnicas utilizadas

El estudio de las citadas propiedades se ha abordado tanto desde el punto de vista experimental como teórico. A lo largo de esta tesis doctoral, se han utilizado diversas técnicas experimentales, modelos semiteóricos para la predicción y correlación de las propiedades medidas y análisis atomísticos utilizando simulación molecular para una comprensión más profunda de los diferentes factores que influyen en las propiedades estudiadas.

1. Pretratamiento de las muestras. Con el objetivo de eliminar las impurezas y caracterizar las muestras, los líquidos iónicos se han depositado durante al menos 24 horas en una línea de vacío. En el caso de líquidos iónicos puros el contenido en agua se ha determinado con un Karl Fischer (KF) antes de cada medida. Asimismo, en uno de los artículos de esta tesis, el contenido en sales procedentes de la síntesis del líquido iónico, se ha determinado mediante técnicas cromatográficas.

2. Determinación del rango líquido. En la determinación del rango líquido se han utilizado el análisis termogravimétrico (TGA) para la estimación del límite superior y el análisis calorimétrico diferencial (DSC) para el límite inferior. En el primer caso, se han llevado a cabo estudios dinámicos e isotermos, utilizando un criterio conservador a la hora de establecer la temperatura máxima de operación, debido a largo periodo de tiempo que el absorbente permanecerá en el circuito. En el caso del DSC, las transiciones de fase de estado se han estudiado con el objetivo de determinar la temperatura de solidificación que definirá el límite inferior del rango líquido.

3. Determinación experimental y modelización propiedades físcas. La determinación de la densidad de los líquidos iónicos y sus mezclas con agua se ha realizado utilizando un densímetro de tubo vibrante. Los datos obtenidos se han modelizado en función de la temperatura mediante modelos lineales y a utilizando la ecuación de estado PC-SAFT. La viscosidad se ha medido utilizando un viscosímetro tipo “rolling ball” y un viscosímetro rotacional (Stabinger) mientras que los modelos utilizados para su correlación y predicción han sido la ecuación Vogel-Fulcher-Tamman (VFT) y el modelo Hard-Sphere (HS). Además,

la conductividad eléctrica de mezclas de agua + líquido iónico se ha medido para dos sistemas concretos, analizando el efecto de la concentración de agua sobre esta propiedad, los datos obtenidos se han ajustado a la ecuación Casteel-Amis.

4. Estudio atomístico de sistemas agua/LI. Junto con el trabajo experimental y la modelización de los resultados, el estudio a nivel atomístico de mezclas agua + líquido iónico aporta información sobre la dinámica y la energía de solvatación del agua en líquido iónico. Los estudios de dinámica molecular incluyen varios líquidos iónicos puros y mezclas con agua. El software LAMMPS y los parámetros publicados por Pádua y Canongia Lopes para líquidos iónicos han sido utilizados para este análisis. Las propiedades calculadas mediante simulación molecular son la densidad, utilizada para la validación del modelo, propiedades dinámicas como la viscosidad y los coeficientes de difusión de las sustancias presentes en cada mezcla. Los efectos de la temperatura y la concentración de agua se han analizado. Además, la energía libre de Gibbs a dilución infinita para la absorción de agua en el líquido iónico se ha calculado utilizando el algoritmo FEP implementado en LAMMPS. La dependencia de las propiedades citadas se ha analizado en base a las funciones de distribución espacial de los iones y la formación de enlaces de hidrógeno entre estos y el agua.

A.3 Resumen de los resultados

Dado que esta tesis doctoral se presenta como un compendio de artículos, el resumen de los resultados obtenidos se presenta siguiendo este mismo esquema.

En el artículo *Liquid range temperature of ionic liquids as potential working fluids for absorption heat pumps*, el análisis termogravimétrico (TGA, siglas en inglés) y el barrido calorimétrico diferencial (DSC, siglas en inglés) se han empleado para determinar el rango líquido de seis líquidos iónicos. Mientras que el DSC permite obtener las transiciones de fase, y de este modo, la temperatura de solidificación y posibles transiciones vítreas, los resultados proporcionados durante el análisis TGA permite establecer un límite máximo, a partir del cual es LI se degrada por acción de la temperatura, si bien, ha de tenerse en cuenta que factores como la estabilidad química o mecánica del líquido iónico no son consideradas durante estas medidas.

Los ILs estudiados no muestran un patrón claro en sus transiciones de fase en función de los iones que lo conforman. La complejidad de sus interacciones provoca que se produzcan diferentes cambios de fase tanto exotérmicos como endotérmicos, si bien, como es frecuente en fluidos complejos, las transiciones de fase se producen a distintas temperaturas en función de la pendiente de la rampa de temperatura. En algunos casos, se ha encontrado que energía no se corresponde como una transición sólido-líquido, lo que sugiere un intercambio energético debido a una reorganización en la estructura interna de los LIs. Los seis LIs líquidos estudiados tienen temperaturas de solidificación que van desde los -14 ºC del $[C_2C_1Im][OTf]$ hasta los 62 ºC del $[C_2Py][MeSO_3]$.

En cuanto a la determinación del límite superior del rango líquido, es fundamental diferenciar entre dos tipos de análisis complementarios, el dinámico y el isotermo. En el primero, la temperatura se incrementa a velocidad constante hasta provocar la degradación térmica de la muestra, a partir de la curva de masa frente a tiempo se calculará la temperatura onset. En el análisis isotermo, las muestras son mantenidas a temperatura constante durante un tiempo determinado, en función de la velocidad de degradación de la muestra. En este segundo análisis, se partirá de la temperatura onset, reduciéndola hasta que la pérdida de masa se considere despreciable. Este criterio implica una dosis de arbitrariedad, en nuestro caso se ha optado por

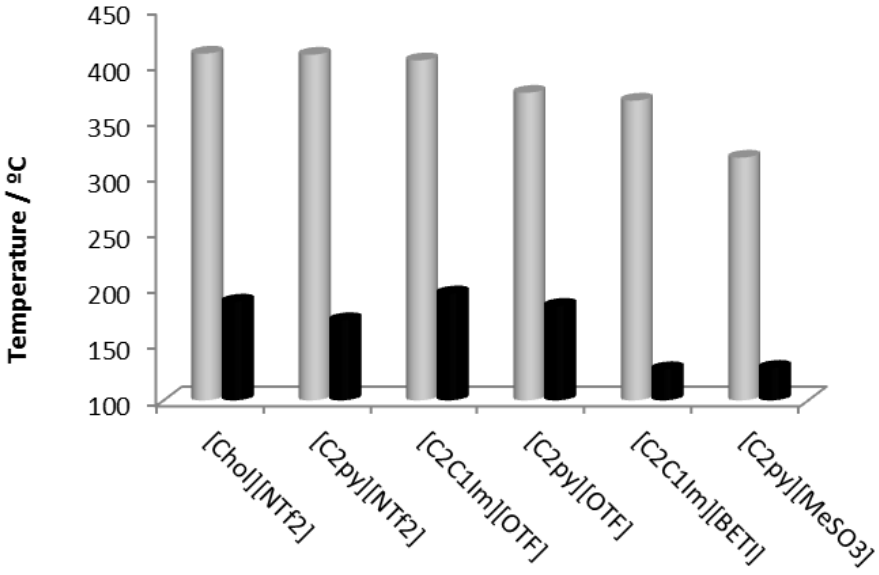

Figure A.2: Temperaturas onset (gris) y temperatura de acuerdo con el criterio $t_{0.01/10h}$ (negro) para los seis LIs estudiados

un criterio restrictivo, al tratarse de una aplicación en la que el líquido iónico pasará un periodo de tiempo largo sometido a altas temperaturas. En la figura B.2 puede observarse la diferencia entre la temperatura onset y la temperatura de degradación, siendo habiéndose seleccionado una pérdida de masa del 1% después de 10 horas.

En el artículo *Density and viscosity study of pyridinium based ionic liquids as potential absorbents for natural refrigerants: Experimental and modelling* se ha estudiado la densidad y la viscosidad de dos líquidos iónicos: 1-ethylpyridinium bis(trifluoromethylsulfonyl)imide, $[C_2Py][NTf_2]$ y 1-ethylpyridinium triflate, $[C_2Py][OTf]$. Junto con la determinación experimental de estas propiedades, la versión Perturbed Chain de la ecuación de estado Statistical Fluid Theory (PC-SAFT) y el modelo Hard Sphere (HS) se han aplicado para la predicción de la densidad y la viscosidad, respectivamente. Es importante salientar que para el modelo HS, los parámetros actualizados por Ciotta y colaboradores mejoran la capacidad predictiva del modelo para fluidos densos tal y como se indica en la figura B.3b. En ambos casos, los modelos, PC-SAFT y HS, han producido resultados satisfactorios cuando al aplicarse a líquidos iónicos puros.

También se ha comprobado experimentalmente la diferencia de solubilidad del agua en ambos líquidos iónicos. De este resultado puede concluirse la hidrofobicidad del grupo trifluorometil, puesto que mientras el LI formado por el anión $[OTf]-$ y el agua son miscibles en todo el rango de concentraciones, el anión $[NTf_2]^-$ da lugar a compuestos de mayor hidrofobicidad. En consecuencia, su utilización como absorbente en bombas de calor debe descartarse. Por el contrario, en este mismo artículo, densidad y viscosidad para las mezclas $[C_2Py][OTf]$ + H_2O se ha determinado y los modelos utilizados para los componentes puros se han aplicado, en este caso, su capacidad predictiva disminuye notablemente con respecto a los líquidos iónicos puros.

En el artículo *Studies of Volumetric and Transport Properties of Ionic Liquid-Water Mixtures and Its Viability To Be Used in Absorption Systems*, también desde el punto de vista experimental, se han explorado distintas propiedades en sistemas agua / líquido iónico. Una de las particularidades de los sistemas estudiados es que, ambos LIs son sólidos a temperatura ambiente. En consecuencia, se ha descartado el estudio de los LIs puros y se han analizado los sistemas binarios ($LI + H_2O$), dado que en un sistema de bomba de calor por absorción el fluido de trabajo

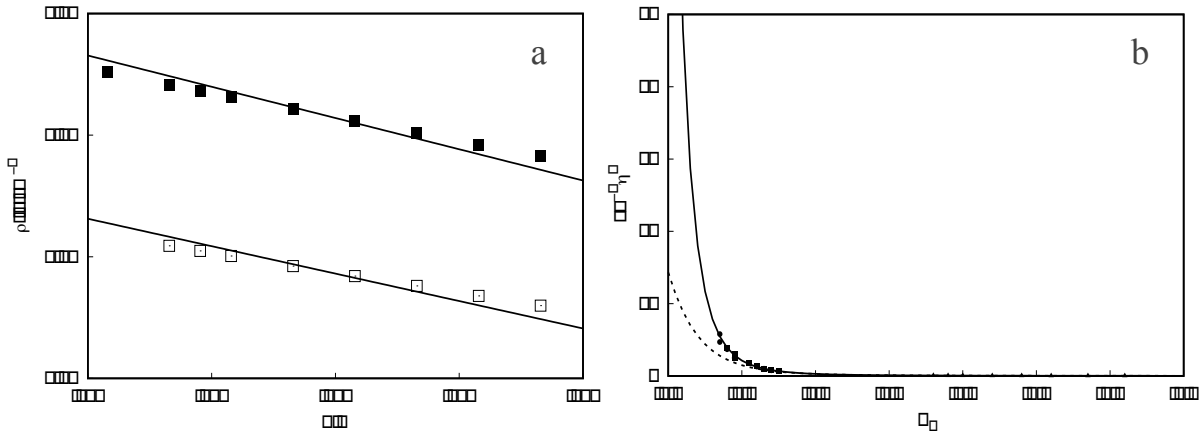

Figure A.3: (a). Predicciones de PC-SAFT para la densidad de los líquidos iónicos puros $[C_2Py][NTf_2]$ (cuadrados negros) y $[C_2Py][OTf]$ (cuadrados blancos) (b) Ajuste de los sistemas estudiados a la curva curva universal (viscosidad reducida frente a volumen reducido) propuesta por Ciotta y colaboradores (línea continua) frente a los valores propuestos por Assael y colaboradores (línea discontinua)

siempre será un sistema binario, el punto de fusión del absorbente puro no supone un problema para su aplicación en ciclos de absorción.

Las mezclas estudiadas son etilpiridinio metanosulfonato $[C_2Py][MeSO_3]$ y colina dihidrógenofosfato $[Chol][H_2PO_4]$, en ambos casos con agua. Además de la densidad y la viscosidad, con sus respectivos ajustes polinómicos en el caso de la densidad y exponencial decreciente (VFT) para la viscosidad; en el mencionado artículo se han publicado datos del pH y la conductividad eléctrica en función de la temperatura y la concentración de agua. Tal y como se indica en la figura B.3, el efecto de la concentración de LI provoca un incremento de la conductividad eléctrica en la disolución. Sin embargo, a partir de un determinado valor (en torno a $X_{LI} = 0.06$) la conductividad desciende de manera acusada, debido en parte al descenso en la movilidad de los iones provocada por el aumento en la viscosidad de la mezcla.

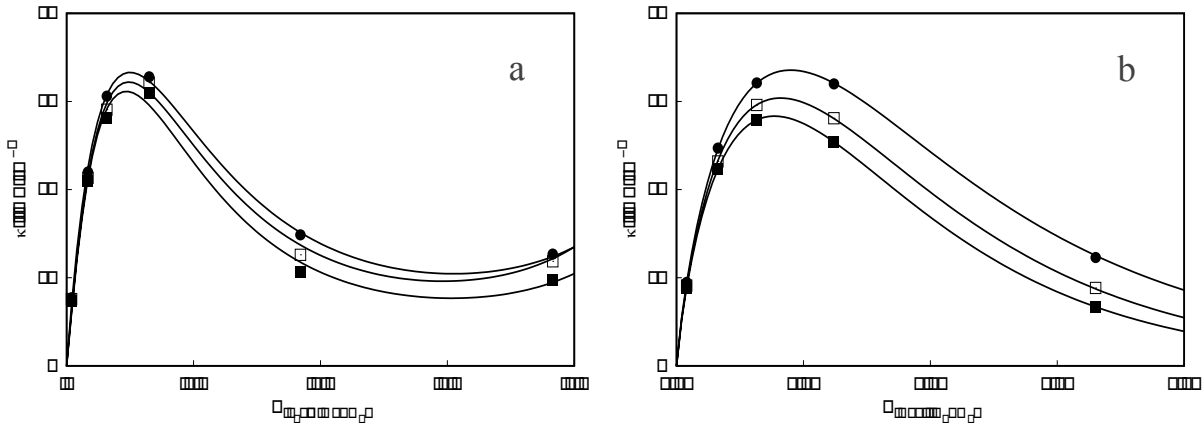

Figure A.4: Conductividad eléctrica en función de la temperatura, 298.15 K (cuadrado negro), 315.15 (cuadrado blanco), 333.15 (círculo negro) y la fracción molar de LI para los sistemas (a) $[C_2Py][MeSO_3]$ + H_2O y (b) $[Chol][H_2PO_4]$ + H_2O.

En el artículo *Molecular Understanding of Pyridinium Ionic Liquids as Absorbents with Water as Refrigerant for Use in Heat Pumps* el comportamiento de los LIs $[C_2Py][NTf_2]$ y $[C_2Py][OTf]$ se ha estudiado a partir técnicas de dinámica molecular. Este enfoque permite un análisis a escala atómica de los factores que influyen en las propiedades físico químicas de cada fluido. Se ha aplicado un campo de fuerzas tipo OPLS, utilizando valores parametrizados de manera específica para estos compuestos. Basándose en los datos experimentales de densidad publicados previamente, el modelo ha sido validado. De este modo y de acuerdo con otras referencias bibliográficas se ha optado por escalar las cargar parciales de las sustancias iónicas en un factor de 0,8.

A partir del modelo descrito, se han explorado las posibilidades que la dinámica molecular ofrece para la selección de líquidos iónicos como potenciales absorbentes. Por una parte, los factores que inciden en la dinámica del sistema se han estudiado a partir de los coeficientes de difusión de los diferentes iones y del agua. También se ha explorado el efecto de la temperatura en la difusión de cada ión y del sistema global. Junto con los coeficientes de difusión, se ha calculado la viscosidad de cada uno de los sistemas, obteniéndose resultados consistentes con los datos experimentales.

Otra de las propiedades críticas para esta aplicación, la capacidad de absorción del agua en el líquido iónico se ha abordado calculando la energía libre de Gibbs de la solvatación del agua en el líquido iónico. Con este objetivo, se ha aplicado el algoritmo *free energy perturbation* (FEP), cuyos resultados se avanzan en la figura B.5, y cuya descripción detallada puede encontrarse en los trabajos de Chipot y colaboradores. Al igual que en el caso de las propiedades dinámicas, los resultados son consistentes con los datos experimentales. Asimismo, en la organización a escala atómica de los iones y el agua se observan las causas que provocan una mayor o menor afinidad entre el líquido iónico y el agua. El factor determinante es la afinidad entre las posiciones aceptoras de protones del anión y el agua.

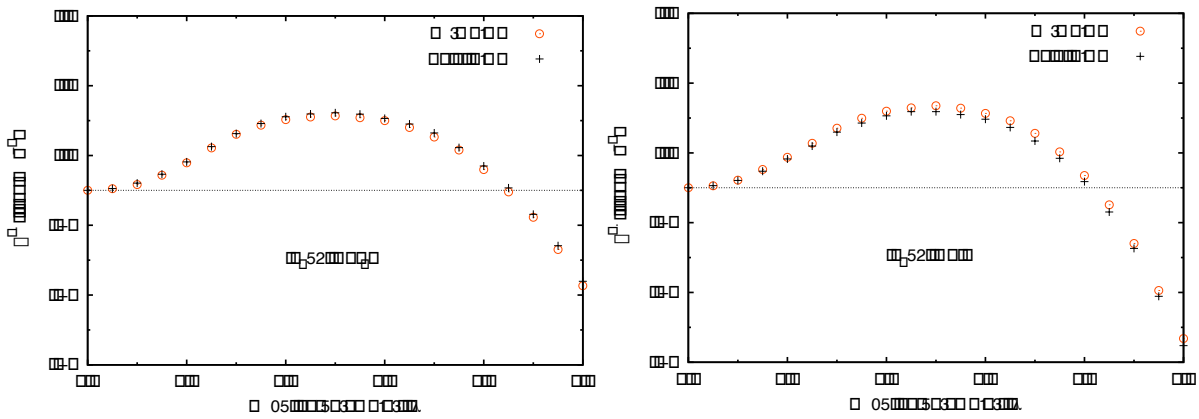

Figure A.5: Rutas de formación y aniquilación de una molécula de agua en dos líquidos iónicos puros, $[C_2Py][NTf_2]$ y $[C_2Py][OTf]$. La diferencia entre $\lambda = 0$ (el agua no interacciona con el medio) $\lambda = 1$ (la interacción entre agua y medio es completa) determina el potencial químico puesto en juego durante la solvatación del agua.

En el artículo *Structural effects on dynamic and energetic properties of mixtures of ionic liquids and water* se desarrollan con más extensión y se amplían a un mayor número de sistemas las técnicas empleadas en el artículo anterior. Concretamente, se han seleccionado dos cationes $[C_2Py]^+$ y $[Chol]^+$ y tres aniones $[MeSO_3]^-$, $[DCA]^-$ y $[Ac]^-$ y se han estudiado las seis combinaciones posibles. En todos los casos, se han seleccionado dos mezclas con agua, con fracciones molares

de x_{H_2O} = 0.104 y x_{H_2O} = 0.900, con el objetivo de simular las condiciones que pueden darse en la aplicación objeto de estudio.

Las propiedades dinámicas de las mezclas se han analizado siguiendo un procedimiento análogo al del artículo anterior. A mayores, se ha incluido el análisis del efecto que sobre las mezclas tiene incrementar la concentración de agua. Una vez más, los resultados son consistentes con los datos experimentales y proporcionan información relevante sobre los principales factores que influyen en la dinámica de las mezclas agua + líquido iónico. De la misma forma, la afinidad entre el agua y los diferentes LIs se ha simulado mediante FEP. Los resultados permiten hacer una selección previa en función de su capacidad de absorción.

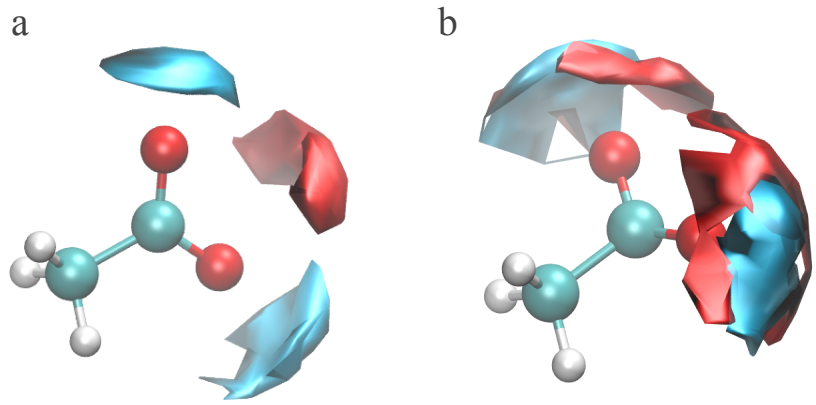

Figure A.6: Competencia por las posiciones aceptoras de protones en sistemas con un ión común, el acetato $[Ac]^-$ y dos cationes, el $[C_2Py]^+$ (a) y $[Chol]^+$ (b). En azul, se muestra el hidrógeno del agua mientras que en rojo están el hidrógeno más ácido de cada catión.

Junto con la simulación de las propiedades críticas para las bombas de calor por absorción, se han estudiado con detalle los factores a escala atómica que afectan a estas propiedades. En concreto, se han cuantificado los enlaces de hidrógeno entre los diferentes grupos funcionales de este sistema, tanto su frecuencia como su intensidad han sido tenidas en cuenta y en ambos casos, los resultados muestran la gran influencia que los puentes de hidrógeno tienen en la solvatación del agua en el líquido iónico. Asimismo, cuando los enlaces de hidrógeno tienen lugar entre el anión y el catión se observa una ralentización en la dinámica de los sistemas En la figura B.6 puede observarse una muestra de este comportamiento, la presencia del catión colina (Fig. B.6b) compite con el agua por las posiciones aceptoras del anión acetato, dificultando la absorción del agua en el LI e incrementando la viscosidad del sistema. También se han medido las energías de interacción entre los diferentes iones y el solvente. Los valores obtenidos explican parcialmente la dinámica de los diferentes sistemas, si bien, es difícil establecer una relación cuantitativa entre la viscosidad y las interacciones ión-ión e ión-solvente.

A.4 Conclusiones

El primer criterio que ha de tenerse en cuenta es la capacidad de absorción que el absorbente tiene sobre el refrigerante. Si bien no existe una única propiedad que determine la capacidad de absorción, la afinidad entre ambos compuestos puede determinarse midiendo la presión de vapor de refrigerante en una disolución para unas condiciones dadas o bien a partir de la energía

libre del proceso de solvatación. En esta tesis, este aspecto se ha abordado utilizando dinámica molecular, concretamente, el algoritmo free energy perturbation (FEP), los resultados indican que la clave para una elevada capacidad de absorción se encuentra en el anión, que deberá ser un aceptor fuerte de protones para formar enlaces de hidrógeno con el agua. Por otra parte, los cationes no deberán competir por las posiciones aceptoras con el agua, por lo que deberán evitarse aquellas estructuras químicas que contengan hidrógenos ácidos.

En segundo lugar, y relacionado con la capacidad de absorción, es necesario considerar las propiedades dinámicas de los sistemas absorbente-refrigerante. En esta tesis, se ha abordado la capacidad de los sistemas agua + líquido iónico para transportar cantidad de movimiento, es decir, su viscosidad y difusividad. En menor medida, se ha estudiado también la conductividad eléctrica de algunos sistemas y el efecto que la temperatura y la concentración de agua tienen sobre ellas. Los resultados obtenidos muestran como una mayor organización interna en los líquidos iónicos aumenta drásticamente la viscosidad y por tanto dificulta la aplicación de estos sistemas en sistemas de bomba de calor. Además, los efectos del agua y la temperatura son muy importantes, provocando un descenso acusado de la viscosidad. Es difícil establecer un límite cuantitativo de viscosidad para esta aplicación puesto que dependería de otros muchos factores. En la bibliografía pueden encontrarse algunas referencias, si bien, en ellas existe un componente de arbitrariedad.

Por último, es fundamental que las mezclas agua + LI se encuentren en estado líquido entre las temperaturas mínima (absorbedor) y máxima (regenerador) del ciclo de absorción. Al igual que sucede con las propiedades dinámicas, es importante tener en cuenta que el LI no se encontrará nunca puro en el interior del sistema. En principio esto es una ventaja, puesto que la temperatura de solidificación de la mezcla será inferior en la mayor parte de los casos a la del líquido iónico puro. En cualquier caso, y utilizando un criterio restrictivo, se han determinado las transiciones de fase de los líquidos iónicos puros encontrándose una gran dispersión entre los resultados obtenidos. En cuanto al límite superior, si bien es cierto que la temperatura de degradación que se ha encontrado supera los requisitos del ciclo de absorción, es importante señalar que los periodos de tiempo empleados para su determinación son sensiblemente inferiores al tiempo que el absorbente debe permanecer en el ciclo. Asimismo, el análisis termogravimétrico no tiene en cuenta la degradación química o los efectos mecánicos derivados de los cambios de presión en el sistema.

Appendix B

Résumé de la thèse de doctorat

B.1 Contexte de la thèse de doctorat

La thèse de doctorat *Caractérisation thermophysique de nouveaux absorbants basés sur des liquides ioniques pour le réfrigérant naturel, l'eau* dirigée par la Dr Josefa García Sánchez et le Dr Agílio A. H. Pádua s'inscrit dans le cadre du projet *Développement de nouveaux fluides de travail, composants et configurations pour les bombes à chaleur d'absorption de grandes prestations - AHP2* financé par le Ministère d'Économie et de Compétitivité et porte sur l'étude de propriétés physico-chimiques de liquides ioniques.

Pour la réalisation de l'objectif global du projet, le développent de nouvelles paires de travail eau+liquide ionique (LI) pour son application dans des systèmes de bombes à chaleur par absorption, il est nécessaire de définir les propriétés essentielles que doit posséder un absorbant afin d'assurer un rendement adéquat dans la production de froid/chaleur. À partir de ces propriétés l'élaboration de LIs devra être réalisée comme de potentiels absorbants pour des bombes à chaleur par absorption en utilisant l'eau comme réfrigérant.

Avant de définir les propriétés que nous considérerons critiques pour le développement du processus, il est nécessaire de décrire brièvement une bombe à chaleur par absorption (voirB.1).

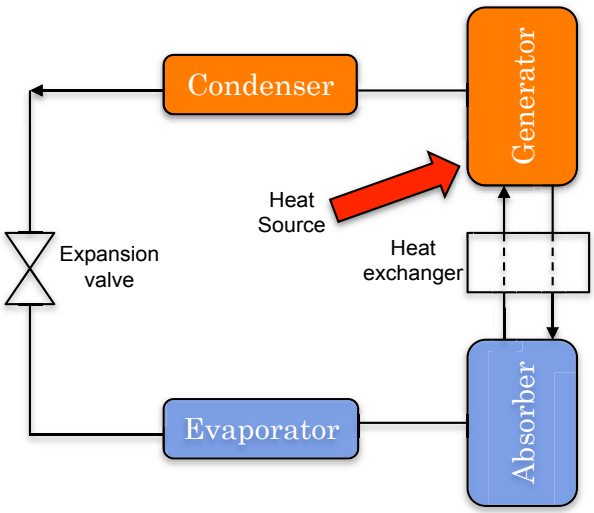

Figure B.1: Schéma du fonctionnent d'une bombe à chaleur par absorption.

Une bombe à chaleur par absorption est un dispositif thermodynamique capable de propor-

tionner du froid et de la chaleur en consommant, principalement, de l'énergie thermique en contraste avec les systèmes de bombes à chaleur traditionnels aussi appelés bombes à compression mécaniques, qui nécessitent une importante consommation d'énergie électrique. Dans les systèmes d'absorption ou systèmes de compression chimique, un processus absorption /desabsorption est utilisé afin d'augmenter la pression du réfrigérant, en profitant de la réduction drastique dans le volume spécifique qui se produit dans le changement de phase vapeur-liquide. Une fois absorbé le réfrigérant (en état liquide), l'augmentation de la pression se fait au travers du pompage du mélange réfrigérant/absorbant, étant sa consommation énergétique très inférieure à celle du compresseur utilisé dans les systèmes traditionnels. Une fois la pression élevée, l'absorbant se régénère à travers l'application de l'énergie thermique avant d'entrer dans le condensateur. Dans le but de mener à bout le processus d'absorption d'une manière efficiente il faut garantir que le pair de travail respecte les conditions:

1. Capacité d'absorption. Le changement de phase du réfrigérant se réalise au travers d'un processus d'absorption. Il est difficile de déterminer une unique propriété proportionnant une mesure de la capacité d'absorption étant donné que les facteurs qui influent sur la mise en marche de ce processus sont nombreux. On identifie souvent les déviations négatives de la loi de Raoult comme le principal facteur pour une absorption adéquate du réfrigérant, néanmoins, les propriétés de transport ou les enthalpies de mélange sont des facteurs qui en moindre mesure affectent aussi le processus d'absorption qui, en général, est associé à des dissolutions exothermiques, par conséquent, il est nécessaire d'utiliser une canalisation de chaleur afin de maintenir et d'éviter l'augmentation de la température durant l'absorption du réfrigérant

2. Grande volatilité relative. La régénération du réfrigérant se réalise à travers la distillation. Dans le générateur, une source thermique s'applique dans le mélange réfrigérant/absorbant, une grande volatilité relative favorise la séparation des deux fluides en une seule étape, en améliorant l'efficience du processus. Dans le cas de paires de travail H2O/LI cet aspect ne représente pas un problème puisque l'une des caractéristiques fondamentales des LIs est leur basse pression de vapeur, facilitant ainsi leur séparation d'autres dissolvants ayant de plus grande volatilité.

3. Intervalle liquide. Bien qu'il dépendra de la configuration choisie pour le cycle thermodynamique, la différence entre les températures d'absorption (température inférieure) et la régénération (température supérieure) du réfrigérant peut être élevée. Dans tous les cas, il est nécessaire que le mélange réfrigérant/ absorbant se trouve dans un état liquide dans cet intervalle de températures et soit stable aussi bien thermiques que chimiquement dans toute l'intervalle de températures durant de longues périodes de temps.

4. Viscosité. Dans ce paragraphe la viscosité a été sélectionnée comme la propriété de transport la plus pertinente pour cette application, bien que le transfert de chaleur comme celui de matière jouent aussi un rôle important dans ce processus. Des absorbants ayant une faible viscosité facilitent l'absorption du réfrigérant, de plus, étant donné que l'augmentation de la pression du réfrigérant se fait dans un état liquide au travers d'un pompage du mélange réfrigérant/absorbant, une viscosité moindre diminuera le coût du processus de pompage.

D'autres aspects, tels que la capacité de corrosion, liée à la conductivité électrique et le pH de la dissolution, ou la toxicité des composants utilisés, ainsi que la viabilité économique du

processus doivent être pris en compte au moment d'élaborer de nouvelles paires de travail pour des bombes à chaleur par absorption.

L'ensemble de ces facteurs déterminera l'efficacité du processus, qui se définit d'une manière générale à partir de deux paramètres fondamentaux, le COP (eq. B.1) et le ratio de recirculation (eq. B.2).

$$COP = \frac{calor\ útil\ (evap.)}{calor\ consumido\ (gen.)} \tag{B.1}$$

$$Ratio\ recirculación = \frac{flujo\ vapor}{flujo\ disolución} \tag{B.2}$$

Le COP est un indicateur de l'efficacité générale de la bombe à chaleur, défini comme l'énergie utile que le système est capable de proportionner entre l'énergie thermique consommée dans le générateur (eq. B.1), de ce fait, un COP plus élevé impliquera une plus grande efficacité énergétique. D'un autre côté, le ratio de recirculation est un indicateur de l'efficacité du cycle d'absorption, puisque plus la quantité d'absorbant est moindre afin de produire une quantité déterminée de vapeur et plus faible sera la demande thermique du générateur, un ratio de recirculation plus élevé (ec. B.2) sera aussi avantageux pour l'efficacité du système, en plus de permettre un design adéquat des équipements.

B.2 Approche de la thèse de doctorat et techniques utilisées

L'étude des propriétés citées antérieurement a été abordée aussi bien d'un point de vue expérimental que d'un point de vue théorique. Tout au long de cette thèse de doctorat diverses techniques expérimentales, modèles semi-théoriques pour la prédiction et la corrélation des propriétés prises et l'analyses atomistiques ont été utilisés au travers de simulations moléculaires afin de comprendre plus en profondeur les différents facteurs qui influent sur les propriétés étudiées.

1. Prétraitement des échantillons. Dans le but d'éliminer les impuretés et de caractériser les échantillons, les liquides ioniques ont été déposés durant au moins 24 heures au vide. Dans le cas de liquides ioniques purs le contenu en eau a été déterminé avec un Karl Fischer (KF) avant chaque mesure. De cette manière, dans un des articles de cette thèse, le contenu en sels provenant de la synthèse du liquide ionique, a été déterminé avec des techniques chromatographiques.

2. Détermination de l'échelle liquide. Afin de déterminer l'échelle liquide, on a utilisé l'analyse thermogravimétrique (TGA) pour la stimulation du liquide supérieur et l'analyse calorimétrique différentielle (DSC) pour la limite inférieure. Dans le premier cas, des études dynamiques et isothermiques ont été réalisées, en utilisant un critère conservateur à l'heure d'établir la température maximum d'opération, du fait de la longue période de temps où l'absorbant restera dans le circuit. Dans le cas du DSC, las transitions de phase d'état ont été étudiées dans le but de déterminer la température de solidification qui définira la limite inférieure de l'échelle liquide.

3. Détermination expérimentale et modélisation de propriétés physiques. La détermination de la densité des liquides ioniques et leurs mélanges avec de l'eau a été réalisée au moyen d'un densimètre de tube vibrant. Les données obtenues ont été modélisées en fonction de la température au travers de modèles linéaires et en utilisant l'équation d'état PC-SAFT.

La viscosité a été mesurée avec un viscosimètre du type "rolling ball" et un viscosimètre rotationnel (Stabinger) alors que les modèles utilisés pour leur corrélation et prédiction ont été l'équation Vogel-Fulcher-Tamman (VFT) ainsi que le modèle Hard-Sphere (HS). De plus, la conductivité électrique du mélange eau + liquide ionique a été mesuré pour deux systèmes concrets, en analysant l'effet de la concentration de l'eau sur cette propriété, les données obtenues se sont ajustées à l'équation Casteel-Amis.

4. Étude atomistique de systèmes eau /LI. En plus du travail expérimental et de la modélisation des résultats, l'étude d'un point de vue atomistique du mélange eau+ liquide ionique informe sur la dynamique et l'énergie de solvatation de l'eau en liquide ionique. Les études de dynamique moléculaire incluent plusieurs liquides ioniques purs ainsi que des mélanges avec de l'eau. Le logiciel LAMMPS et les paramètres publiés par Pádua et Canongia Lopes en ce qui concerne des liquides ioniques ont été utilisés pour cette analyse. Les propriétés calculées par simulations moléculaires sont la densité, utilisée pour la validation du modèle, des propriétés dynamiques comme la viscosité et les coefficients de diffusion des substances présentes dans chaque mélange. Les effets de la température et de la concentration d'eau ont été analysés. De plus, l'énergie libre de Gibbs à dilution infinie pour l'absorption d'eau dans le liquide ionique s'est calculée en utilisant l'algorithme FEP appliqué dans LAMMPS. La dépendance des propriétés citées a été analysée en se basant sur les fonctions de distribution spatiale des ions et sur la formation de liaisons d'hydrogène entre ceux-ci et l'eau.

B.3 Résumé des résultats

Étant donné que cette thèse de doctorat se présente comme une recompilation d'articles, le résumé des résultats obtenus se présente suivant le même schéma.

Dans l'article *Liquid range temperature of ionic liquids as potential working fluids for absorption heat pumps* l'analyse thermogravimétrique (TGA, sigles en anglais) et le scan calorimétrique différentiel (DSC, sigles en anglais) ont été utilisés afin de déterminer l'échelle liquide de six liquides ioniques. Alors que le DSC permet d'obtenir les transitions de phase, et de cette manière, la température de solidification ou de transition vitreuse, les résultats proportionnés durant l'analyse TGA permet d'établir une limite maximum, à partir de laquelle c'est LI qui se dégrade par action de la température, néanmoins il est nécessaire d'avoir présent que des facteurs comme la stabilité chimique ou mécanique du liquide ionique n'ont pas été pris en compte durant ces mesures.

Les ILs étudiés ne montrent pas de patron clair dans leurs transitions de phase en fonction des ions qui le conforment. La complexité des leurs interactions provoque que se produisent différents changements de phase, aussi bien exothermique qu'endothermiques, ainsi comme il est fréquent dans des fluides complexes, les transactions de phase se produisent à différentes températures en fonction du secteur de température. Dans certains cas, on a trouvé que l'énergie ne correspond pas à une transition solide-liquide, ce qui suggère un échange énergétique dû à une réorganisation dans la structure interne des LIs. Les six LIs liquides étudiés ont des températures de solidification qui vont de -14 °C du $[C_2C_1Im][OTf]$ à 62 °C du $[C_2Py][MeSO_3]$.

En ce qui concerne la détermination de la limite supérieure de l'échelle liquide, il est fondamental de différencier entre deux types d'analyses complémentaires, la dynamique et l'isotherme. Dans la première, la température augmente à une vitesse constante jusqu'à provoquer la dégradation thermique de l'échantillon, à partir de la courbe masse face à temps on calculera la température onset. Dans l'analyse isotherme, les échantillons sont maintenus à une température constante durant un temps déterminé, en fonction de la vitesse de dégradation de l'échantillon.

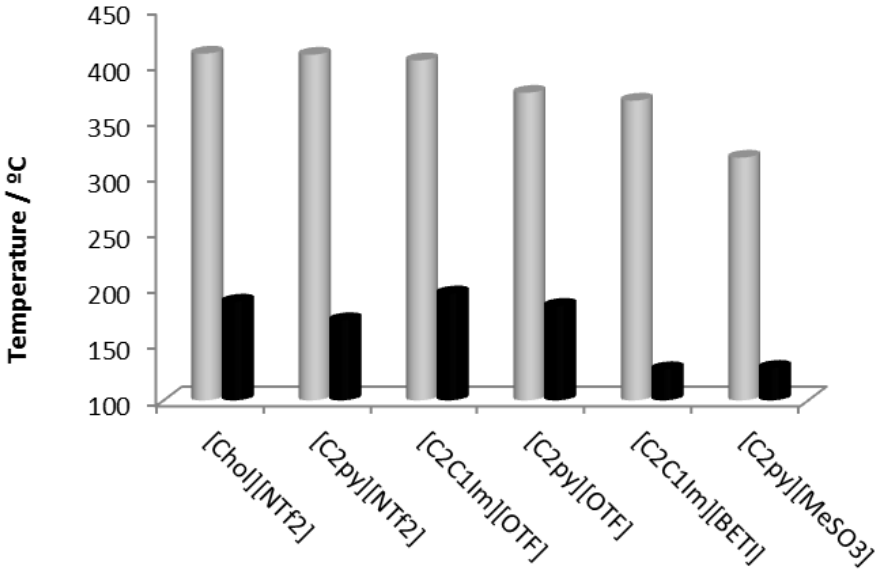

Figure B.2: Températures onset (gris) et température en accord avec le critère $t_{0.01/10h}$ (noir) pour les six LIs étudiés.

Dans cette deuxième analyse, on commencera à partir de la température onset, en la réduisant jusqu'à ce que la perte de masse soit considérée négligeable. Avec ce critère, il existe une dose arbitraire dans notre cas on a opté pour un critère restrictif, s'agissant d'une application où le liquide ionique passera une longue période de temps soumis à des températures élevées. Dans la figure B.2, on peut observer la différence entre la température onset et la température de dégradation, une perte de masse de 1% étant devenue un critère après 10 heures.

Dans l'article *Density and viscosity study of pyridinium based ionic liquids as potential absorbents for natural refrigerants: Experimental and modelling* la densité et la viscosité de deux liquides ioniques ont été étudiées: 1-ethylpyridinium bis(trifluoromethylsulfonyl)imide, $[C_2Py][NTf_2]$ et 1-ethylpyridinium triflate, $[C_2Py][OTf]$. De plus, avec la détermination expérimentale de ces propriétés, la version Perturbed Chain de l'équation d'état Statistical Fluid Theory (PC-SAFT) et le modèle Hard Sphere (HS) ont été appliqués pour la prédiction de la densité et la viscosité, respectivement. Il est important de souligner que pour le modèle HS, les paramètres actualisés par Ciotta et collaborateurs supposent une nette majorité dans la capacité du modèle à décrire de manière adéquate la viscosité de fluides denses comme l'indique la figure B.3b. Dans tous les cas, les modèles, PC-SAFT et HS, ont produit des résultats satisfaisants en l'appliquant à des liquides purs.

Il a également été vérifié de manière expérimentale la différence de solubilité de l'eau dans les deux liquides ioniques. De ces résultats, l'hydrophobie du groupe trifluorometil peut se conclure. En effet, alors que le LI formé par l'anion $[OTf]^-$ et l'eau sont miscibles dans toutes les échelles de concentrations, l'anion $[NTf_2]^-$ donne lieu à des composés d'une plus grande hydrophobie. Par conséquent, son utilisation comme absorbant dans des bombes à chaleur doit être exclue. Au contraire, dans le même article, la densité et la viscosité pour les mélanges $[C_2Py][OTf] + H_2O$ a été déterminé et les modèles utilisés pour les composants purs ont été appliqués, dans ce cas, sa capacité prédictive diminue notablement par rapport aux liquides ioniques purs.

Dans l'article *Studies of Volumetric and Transport Properties of Ionic Liquid-Water Mixtures and Its Viability To Be Used in Absorption Systems*, également d'un point de vue expérimental, différentes propriétés dans des systèmes d'eau/liquide ionique ont été explorés. Une des particularités des

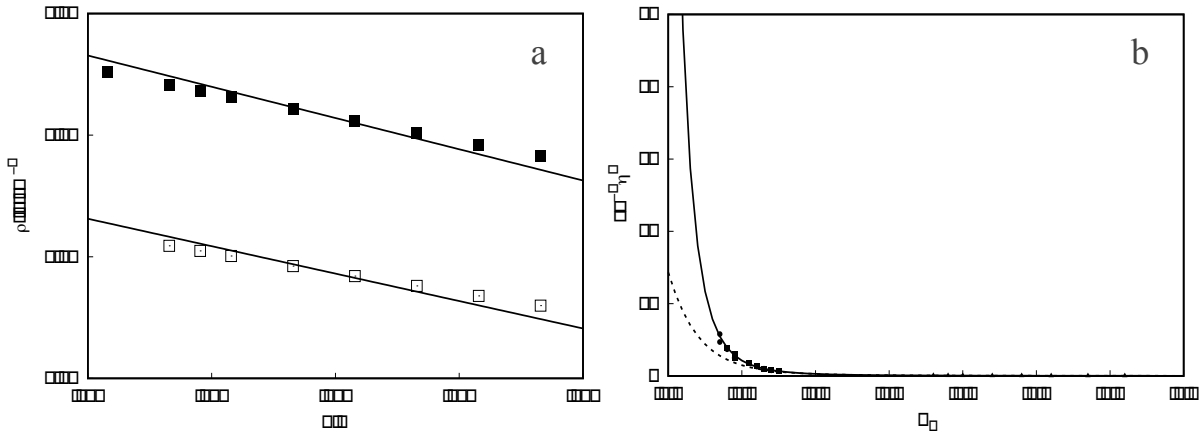

Figure B.3: (a). Prédictions de PC-SAFT pour la densité des liquides ioniques purs $[C_2Py][NTf_2]$ (carrés noirs) et $[C_2Py][OTf]$ (carrés blancs) (b) Ajustement des systèmes étudiés à la courbe universelle (viscosité réduite face au volume réduit) proposition faite par Ciotta et collaborateurs (ligne continue) face aux valeurs proposées par Assael et collaborateurs (lignes discontinue)

systèmes étudiés est que les deux LIs sont solides à température ambiante. Par conséquent, nous avons exclu l'étude des LIs purs et nous avons analysé les systèmes binaires ($LI + H_2O$), puisque dans un système de bombe à chaleur par absorption le fluide de travail sera toujours un système binaire, le point de fusion de l'absorbant pur ne suppose pas un problème pour son application dans des cycles d'absorption.

Les mélanges étudiés sont ethylpyridinium methanesulfonate $[C_2Py][MeSO_3]$ et choline dihydrogen phosphate $[Chol][H_2PO_4]$, dans les deux cas avec de l'eau. En plus de la densité et de la viscosité, avec leur ajustement respectifs en accord avec des équations polynomiales, dans le cas de la densité et de la décroissante exponentielle (VFT) pour la viscosité ; dans cet article, des données du pH ont été publiées et la conductivité électrique en fonction de la température et de la concentration de l'eau. Comme il est indiqué dans la figure **??**, l'effet de la concentration de LI provoque une augmentation de la conductivité électrique dans la dissolution. Néanmoins, à partir d'une valeur déterminée (approximativement $X_{LI} = 0.06$) la conductivité descend de manière significative, du fait en partie de la baisse de la mobilité des ions provoquée par l'augmentation dans la viscosité du mélange.

Dans l'article *Molecular Understanding of Pyridinium Ionic Liquids as Absorbents with Water as Refrigerant for Use in Heat Pumps* le comportement des LIs $[C_2Py][NTf_2]$ et $[C_2Py][OTf]$ a été étudié à partir de techniques de dynamique moléculaire. Cette approche permet une analyse à échelle atomique des facteurs qui influent sur les propriétés physico-chimiques de chaque fluide. En utilisant des valeurs paramétrées de manière spécifique pour ces composants, nous avons appliqué un champ de force de type OPLS. En se basant sur les données expérimentales de densité publiées antérieurement 1, le modèle a été validé. De cette manière et en accord avec d'autres références bibliographiques nous avons opté pour réduire les charges partielles des substances ioniques en un facteur de 0.8.

À partir du modèle décrit, nous avons exploré les possibilités que la dynamique moléculaire offre pour la sélection de liquides ioniques comme absorbants potentiels. D'une part, les facteurs qui influent sur la dynamique du système ont été étudiés à partir des coefficients de diffusion des différents ions et de l'eau. Nous avons aussi exploré l'effet de la température sur la diffusion de chaque ion et du système dans son ensemble. Avec les coefficients de diffusion, nous avons

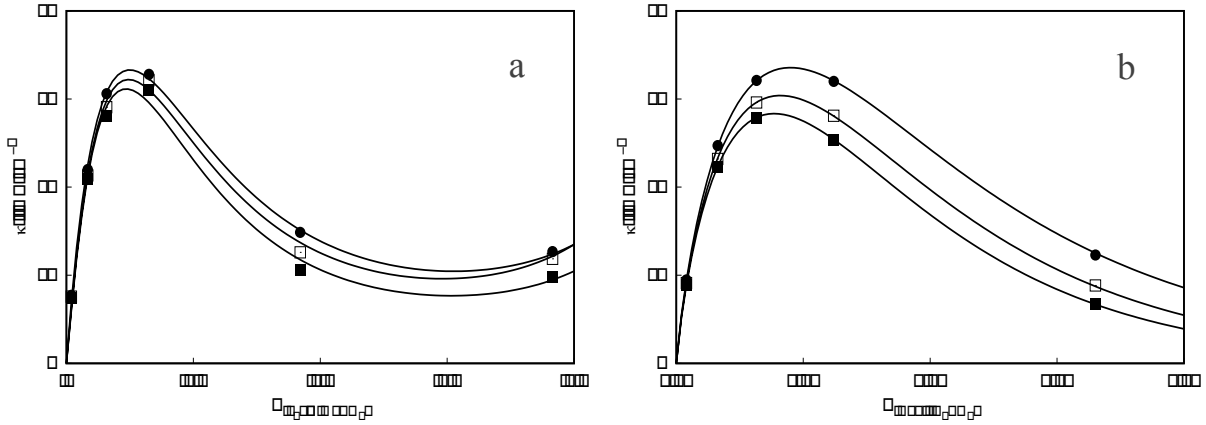

Figure B.4: Conductivité électrique en fonction de la température, 298.15 K (carré noir), 315.15 (carré blanc), 333.15 (cercle noir) et la fraction molaire de LI pour les systèmes $[C_2Py][MeSO_3]$ + H_2O (a) et $[Chol][H_2PO_4]$ + H_2O (b).

calculé la viscosité de chaque système, et nous avons obtenu des résultats consistants grâce aux données expérimentales

Une autre des propriétés critiques pour cette application est la capacité absorption de l'eau dans le liquide ionique, elle a été absorbée en calculant l'énergie libre de Gibbs de la solvatation de l'eau dans le liquide ionique. Dans ce but, nous avons appliqué l'algorytme *free energy perturbation* (FEP), dont nous avançons les résultats dans la figure B.5 et dont la description détaillée se trouve dans les travaux de Chipot et collaborateurs. De la même manière que pour les propriétés dynamiques, les résultats sont cohérents avec ceux des données expérimentales. De ce fait, dans l'organisation à échelle atomique des ions et de l'eau, on observe les causes provoquant une plus ou moins grande affinité entre le liquide ionique et l'eau. Le facteur déterminant est l'affinité entre les positions accepteuses de protons de l'anion et l'eau.

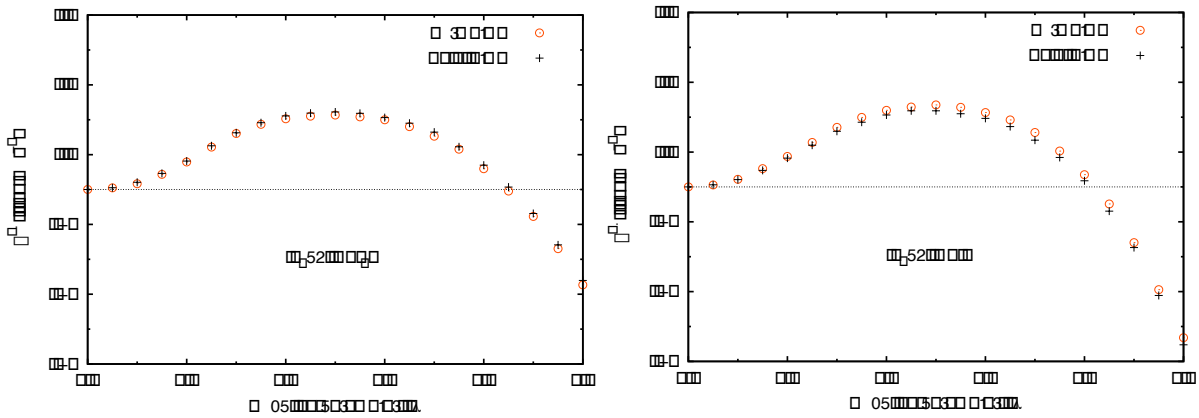

Figure B.5: Routes de formation et anéantissement d'une molécule d'eau dans deux liquides ioniques purs, $[C_2Py][NTf_2]$ et $[C_2Py][OTf]$. La différence entre $\lambda = 0$ (l'eau n'interagit pas avec le milieu) et $\lambda = 1$ (l'interaction entre l'eau et le milieu est complète) détermine le potentiel chimique mis en jeu durant la solvatation de l'eau.

Dans l'article *Structural effects on dynamic and energetic properties of mixtures of ionic liquids and*

water on développe plus longuement et avec un plus grand nombre de systèmes les techniques employées dans l'article antérieur. Concrètement, nous avons sélectionné deux cations $[C_2Py]^+$ et $[Chol]^+$ ainsi que trois anions $[MeSO_3]^-$, $[DCA]^-$ y $[Ac]^-$ et nous avons étudié les six combinaisons possibles. Dans tous les cas, nous avons sélectionné deux mélanges avec de l'eau, avec des fractions molaires de x_{H_2O} = 0.104 et x_{H_2O} = 0.900, dans le but de simuler les conditions qui peuvent apparaître dans l'application étudiée.

Les propriétés dynamiques du mélange ont été analysées en suivant une procédure analogue à celle de l'article antérieur. En plus, nous avons inclus l'analyse de l'effet qui sur les mélanges doit augmenter la concentration d'eau. Une fois de plus, les résultats sont cohérents avec les données expérimentales et proportionnent une information pertinente sur les principaux facteurs qui influent sur la dynamique des mélanges eau + liquide ionique. De la même manière, l'affinité entre l'eau et les différents LIs a été simulée à travers FEP. Les résultats permettent de faire une sélection préalable en fonction de la capacité d'absorption.

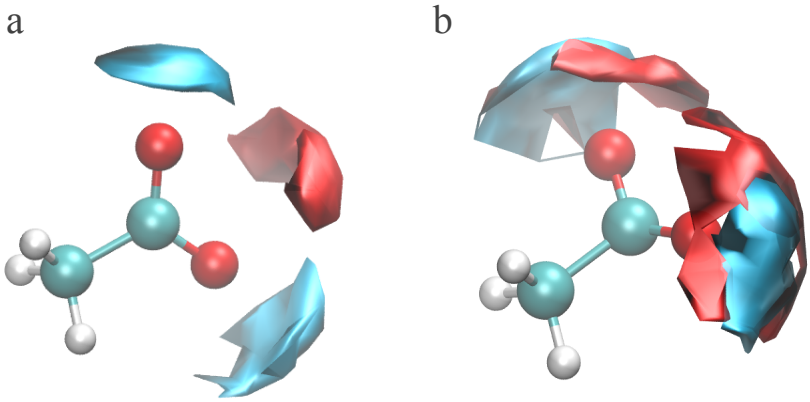

Figure B.6: Compétences pour les positions accepteuses de protons dans des systèmes avec un ion commun, l'acétate $[Ac]^-$ et deux cations, le $[C_2Py]^+$ (a) et $[Chol]^+$ (b). En bleu, on peut voir l'hydrogène de l'eau alors qu'en rouge se trouve l'hydrogène plus acide de chaque cation.

En plus de la simulation des propriétés critiques pour les bombes à chaleur par absorption, nous avons également étudié minutieusement les facteurs à échelle atomique qui affectent ces propriétés. Concrètement, nous avons quantifié les liaisons d'hydrogène entre les différents groupes fonctionnels de ce système, aussi bien leur fréquence comme leur intensité ont été prises en compte et dans les deux cas, les résultats montrent la grande influence que les ponts d'hydrogène ont sur la solvatation de l'eau dans le liquide ionique. Ainsi, lorsque ces liaisons d'hydrogène ont lieu entre l'anion et le cation on a observé un ralentissement dans la dynamique des systèmes. Dans la figure B.6, on peut observer un échantillon de ce comportement, la présence du cation colina (Fig. B.6b) rivalise avec l'eau par les positions accepteuses de l'anion acétate, rendant difficile l'absorption de l'eau dans le LI et augmente la viscosité du système. Ainsi, les énergies d'interaction entre les différents ions et le solvant ont été mesurées. Valeurs obtenues expliquent partiellement la dynamique des différents systèmes, de cette manière, il est difficile d'établir une relation quantitative entre la viscosité et l'interaction ion-ion et ion-solvant.

B.4 Conclusions

Après avoir étudié de manière théorique et expérimentale les propriétés fondamentales des liquides ioniques pour leur application dans des systèmes de bombes à chaleur nous en sommes arrivés à ces conclusions.

Le premier critère qui doit être pris en compte est la capacité d'absorption que l'absorbant possède sur le réfrigérant. Malgré le fait qu'il n'existe pas de propriété unique qui détermine la capacité absorption, l'affinité entre les deux composés peut se déterminer au travers de la pression à vapeur de réfrigérant en une dissolution pour des conditions données ou bien à partir de l'énergie libre du processus de solvatation. Dans cette thèse, cet aspect a été abordé en utilisant une dynamique moléculaire, concrètement, l'algorithme free energy perturbation (FEP), les résultats indiquent que la clé pour une capacité élevée d'absorption se trouve dans l'anion, qui devra être un accepteur fort de protons afin de former des liaisons d'hydrogène avec l'eau. D'un autre coté, les cations ne devront pas rivaliser du fait des positions accepteuse avec l'eau, il faudra donc éviter les structures chimiques contenant des hydrogènes acides.

Deuxièmement, pour ce qui est de la capacité d'absorption, il est nécessaire de considérer les propriétés dynamiques des systèmes absorbant-réfrigérant. Dans cette thèse, nous avons abordé la capacité des systèmes eau + liquide ionique afin de transporter une quantité de mouvement, c'est à dire, sa viscosité et diffusivité. Dans une moindre mesure, nous avons aussi étudié la conductivité électrique de certains systèmes et l'effet que les températures et la concentration d'eau ont sur elles. Les résultats obtenus montrent comment une plus grande organisation interne dans des liquides ioniques augmente de manière drastique la viscosité et rend donc difficile l'application de ces systèmes en systèmes de bombe à chaleur. De plus, les effets de l'eau et la température sont très importants, provoquant une forte baisse de la viscosité. Il est difficile d'établir une limite quantitative de viscosité pour cette application étant donné que cela dépendra d'autres facteurs. Dans la bibliographie nous trouverons certaines références bien qu'il y ait un composant arbitraire.

Finalement, Il est fondamental que les mélanges eau + LI se trouve dans un état liquide entre les températures minimales (absorbeur) et maximales (régénérateur) du cycle absorption. De la même manière qu'avec les propriétés dynamiques, il est important de prendre en compte que le LI ne se trouvera jamais pur à l'intérieur du système. En principe, cela est un avantage puisque la température de solidification du mélange sera inférieure dans la plupart des cas à celle du liquide ionique pur. Dans tout les cas, et en utilisant un critère restrictif, nous avons déterminé les transitions de phase des liquides ioniques purs, en constatant une grande dispersion entre les résultats obtenus. Pour ce qui est de la limite supérieure, bien qu'il soit vrai que la température de dégradation trouvée dépasse les conditions du cycle d'absorption, il est important de signaler que les périodes de temps employées afin de déterminer sont légèrement inférieures au temps où l'absorbant doit rester dans le cycle. De ce fait, l'analyse thermogravimétrique ne prend pas compte de la dégradation chimique ou des effets mécaniques dérivés des changements de pression dans le système.